HYBRID COHERENT LIGHT

Modeling light-emitting quantum dot superluminescent diodes

TECHNISCHE
UNIVERSITÄT
DARMSTADT

Dem Fachbereich Physik
der Technischen Universität Darmstadt

zur Erlangung des Grades
eines Doktors der Naturwissenschaften (Dr. rer. nat.)

genehmigte Dissertation von
M. Sc. Franziska Friedrich
aus Weiterstadt

1. Gutachten: Prof. Dr. Reinhold Walser
2. Gutachten: Prof. Dr. Wolfgang Elsäßer

Darmstadt 2019
D 17

Hybrid coherent light – Modeling light-emitting quantum dot superluminescent diodes
Hybrid-kohärentes Licht – Modellierung von lichtemittierenden Quantenpunkt-Superlumineszenzdioden

Genehmigte Dissertation von Franziska Friedrich aus Weiterstadt

1. Gutachten: Prof. Dr. Reinhold Walser
2. Gutachten: Prof. Dr. Wolfgang Elsäßer

Tag der Einreichung: 17. Dezember 2018
Tag der Prüfung: 19. Februar 2019

Darmstadt – D17

Bitte zitieren Sie dieses Dokument als:
URN: urn:nbn:de:tuda-tuprints-85278
URI: https://tuprints.ulb.tu-darmstadt.de/id/eprint/8527

ABSTRACT

Commercial devices for optical coherence tomography greatly benefit from the exceptional features of broadband light-emitting quantum dot superluminescent diodes (QDSLDs). Here, light generation occurs at the transition from spontaneous to stimulated emission, the regime of the amplified spontaneous emission. In this context, initially spontaneously emitted photons are amplified by stimulated emission processes when traversing through the QDSLD, which leads to strong light amplification. The suitable choice of the waveguide geometry and the gain medium formed by quantum dots, enables large spectral widths of some terahertz combined with a rather higher degree of spatial coherence. Modern measurement methods based on two-photon absorption processes provide a temporal resolution of some femtoseconds and thus allow correlation studies of the emitted QDSLD light. Also from a theoretical point of view, the characterization of the amplified spontaneous emission generated by QDSLDs and their associated photon statistics represents an interesting and challenging research topic. Especially in a particular temperature regime these devices exhibit uncommon properties with regard to the temporal field and intensity correlations $g^{(1)}(\tau)$ and $g^{(2)}(\tau)$: While $g^{(1)}(\tau)$ reflects the rather highly incoherent nature of light emitted by QDSLDs due to its spectral width of several THz, a reduction of $g^{(2)}(0)$ from 2 to 1.33 at a temperature of $T = 190$ K was observed in the Semiconductor Optics group of Prof. W. Elsäßer at the Technical University of Darmstadt in 2011 [1]. The understanding of the occurrence of these hybrid coherent light states, which are simultaneously incoherent in $g^{(1)}(\tau)$ and coherent in $g^{(2)}(\tau)$ is the subject of this thesis.

In a first step we find the quantum mechanical light state associated with the QDSLD to be well described by a multimode phase-randomized Gaussian state by comparison with experimental results. In the second step we present a microscopic theory of the amplified spontaneous emission, which allows an explanation of the temperature-dependent noise suppression of broadband QDSLDs. For this purpose we consider distinguishable quantum dots, which are embedded in a strongly absorptive bulk material that defines a waveguide. Tilted and anti-reflection coated output facets, leading to a suppression of longitudinal modes, are modeled by beam splitters that couple the internal field to the surroundings. Regarding the spectral properties of QDSLDs, the broadband light generated inside the diode is described by a multimode electric field. This multimode quantum field theory yields rate equations for the optical power densities and the level occupation of the inhomogeneous ensemble of quantum dots within the diode. With the help of the input-output formalism, we determine the optical power spectrum. As a main result, we find the broadband external power spectrum to be a convolution of the intra-diode photon spectrum with a Lorentzian response. This finding corresponds with experimentally available spectra. Furthermore, based on the quantum theory of QDSLDs we determine the central second-order degree of coherence $g^{(2)}(0)$. It reveals a reduction within a special detuning regime and therefore allows the interpretation of the hybrid coherent light phenomenon from a quantum optical point of view.

ZUSAMMENFASSUNG

Kommerzielle Messapparaturen für die optische Kohärenztomographie profitieren von den einzigartigen Eigenschaften von breitbandigen Quantenpunkt-Superlumineszenzdioden (engl. quantum dot superluminescent diodes (QDSLDs)). Die Lichterzeugung tritt hier am Übergang von spontaner zu stimulierter Emission auf, welches dem Bereich der verstärkt-spontanen Emission entspricht. Die zu Beginn spontan emittierten Photonen werden bei ihrer Propagation im Wellenleiter durch stimulierte Emissionsprozesse verstärkt. Mittels geeigneter Wahl von Wellenleitergeometrie und Gewinnmedium, hier Quantenpunkte, werden große spektrale Breiten von einigen Terahertz mit gleichzeitig hoher, räumlicher Kohärenz realisiert. Der Einsatz von sogenannten Zwei-Photonen Absorptionsdetektoren zur Messung von zeitlichen Korrelationen ermöglicht Auflösungen von einigen Femtosekunden und erlaubt somit auch Korrelationsstudien von terahertz-breiten QDSLDs. Aber auch aus theoretischer Sicht stellt die Charakterisierung der verstärkt spontanen Emission von QDSLDs und deren photon-statistischen Eigenschaften ein interessantes und herausforderndes Forschungsprojekt dar. Gerade im Hinblick auf einen ganz bestimmten Temperaturbereich zeigen diese Bauelemente ein ungewöhnliches Verhalten bzgl. der zeitlichen Feld- und Intensitätskorrelation, $g^{(1)}(\tau)$ und $g^{(2)}(\tau)$. Während $g^{(1)}(\tau)$ hochgradig inkohärent mit einer spektralen Breite von einigen THz ist, lässt sich eine Reduktion von $g^{(2)}(0)$ von 2 nach 1.33 bei einer Temperatur von $T = 190$ K im Labor beobachten. Dieses Experiment wurde in der AG Halbleiteroptik von Prof. W. Elsäßer an der Technischen Universität Darmstadt durchgeführt. Das Auffinden einer physikalischen Erklärung für die Beobachtung dieses hybrid-kohärenten Lichtes, welches gleichzeitig inkohärent in $g^{(1)}(\tau)$ und kohärent in $g^{(2)}(\tau)$ ist, stellt das Ziel dieser Dissertation dar.

Im ersten Schritt postulieren wir zunächst einen Quantenzustand des emittierten Lichts einer QDSLD und vergleichen die theoretischen mit den experimentellen Ergebnissen. Es zeigt sich, dass der multimodige, phasenverschmierte, gaußsche Zustand die experimentellen Daten sehr gut wiederspiegelt. Im zweiten Schritt stellen wir eine mikroskopische Theorie der verstärkt-spontanen Emission vor um eine Erklärung für die temperaturabhängige Rauschunterdrückung von breitbandigen QDSLDs zu finden. Diese berücksichtigt unterscheidbare Quantenpunkte, die sich in einem stark absorbierenden Bulk-Material, dem Wellenleiter, befinden. Geneigte und antireflexbeschichtete Austrittsfacetten sorgen für eine Unterdrückung longitudinaler Moden. Sie werden durch Strahlteiler modelliert, welche das interne Feld an die äußere Umgebung koppeln. Aufgrund der spektralen Eigenschaften von QDSLDs wird das breitbandige Licht innerhalb des Wellenleiters durch ein multimodales, elektrisches Feld beschrieben. Diese multimodale Quantentheorie liefert Ratengleichungen für die optischen Leistungsdichten sowie Niveaubesetzungen des inhomogenen Ensembles der Quantenpunkte. Mit Hilfe des Input-Output Formalismus bestimmen wir das optische Spektrum, welches durch eine Faltung des internen Photonenspektrums mit einer Lorentz'schen Antwort gegeben ist. Ein Vergleich dieses wichtigen Ergebnisses mit den experimentellen Daten zeigt gute Übereinstimmung. Des Weiteren untersuchen wir den zentralen Kohärenzgrad zweiter Ordnung, $g^{(2)}(0)$, mit Hilfe unserer Quantentheorie. Dabei wird eine Reduktion innerhalb eines bestimmten Bereiches der Verstimmung beobachtet. Die gewonnenen Ergebnisse lassen die Interpretation des Phänomens von hybrid-kohärenten Licht aus einer rein quantenoptischen Perspektive zu.

CONTENTS

1

INTRODUCTION

The concept of ’coherence’ is inevitably associated with the concept of the laser (light amplification by stimulated emission of radiation). The invention of the laser in 1960 by *T. Maiman* [2] represents a milestone in modern physics and provides novel opportunities in the field of research and development until this day. A complete description of its working principle can only be ensured by a quantum theory, which allows to differentiate between a light bulb and a laser. The theoretical foundations were laid by *R. Glauber* in his optical coherence theory [3–6] for which he was awarded the Nobel Prize in 2005 [7]. Detailed laser theories were established i.a. by the schools of *M. Lax* [8, 9], *H. Haken* [10–12] and *W. Lamb* [13, 14]. In the context of Glauber’s theory of coherence, correlations play a central role. Especially, field and intensity correlations are relevant, since they provide statements about the power spectral density and the photon statistics of light sources. The first experiment that measured intensity correlations was performed by *R. Hanbury Brown* and *R. Q. Twiss* in 1956 [15] with the goal to measure the size of stars. The observed bunching effect of these thermal light sources could be explained by classical considerations. However, based on Glauber’s theory there exists a further, pure quantum optical phenomenon, today known as antibunching, which was theoretically predicted by *H. J. Carmichael* and *D. F. Walls* [16] and experimentally confirmed by *L. Mandel*, *H. J. Kimble* and *M. Dagenais* in atomic resonance fluorescence [17]. Until this day, antibunching was observed in further single-photon emitters like quantum dots [18–20], single dye molecules trapped in a solid [21] or single nitrogen-vacancy centers in diamonds [22]. Currently, the structural engineering of such single-photon sources operating as qubits, that form the basis of quantum information, represents a big challenge [23].

While this field of research is addressed to such a single- or few-body problem for building a quantum computer, further groups are primary concerned with light sources composed of many degrees of freedom. Among other things, optical properties of semiconductor devices play an important role due to their wide applicability in research and development but also in commercial technologies. Especially, broadband superluminescent diodes with light emission characteristics that are spatially directed and additionally possess a considerable spectral width are relevant for industrial applications – for fiber-sensor technologies [24–27], medical diagnostics [28], to only name a few. But also from the aspect of fundamental research, these semiconductor devices are of major interest regarding their coherence properties in first- and second-order. Their broad bandwidths are accompanied by femtosecond coherence times, that are too short for usual detectors with a temporal resolution of some picoseconds. Thus, measuring intensity correlations of such broadband light sources was long time not possible until *F. Boitier* developed a novel detector, based on the two-photon absorption process [29, 30]. This pioneering progress in the detection process offered new insights to the quantum nature of light-emitting broadband sources.

In this context a key experiment was performed in 2011 by *M. Blazek* and *W. Elsäßer* at the Technical University of Darmstadt [1]. Their investigation of field and intensity correlations of the amplified spontaneous emission of quantum dot superluminescent diodes highlighted a new class of light states. These novel states of light exhibit an optical spectrum with a spectral width of about several THz. This means that the radiation is incoherent in first-order of correlation.

Simultaneously, a reduction of the equal-time, second-order degree of coherence from 2 to 1.33 within a special temperature regime of about $T = 190$ K was observed, which in return implies that the amplified spontaneous emission became coherent in second-order. The formulation of a theory of the so-called hybrid coherent light, which is incoherent in first- and coherent in second-order of correlation function represents an interesting and simultaneously challenging topic of research. The following thesis is dedicated to this phenomenon and is structured as follows:

In chapter 2 we study some basics of quantum electrodynamics, which are relevant to clarify the concept of correlations. Starting with the quantization procedure in isotropic media, we end up in an expression for the quantized electric field inside the diode system. With regard to hybrid coherent light, coherent and thermal states are studied in more detail. Subsequently, we summarize fundamental aspects of Glauber's coherence theory, in particular the definition of correlations of first- and second-order which allows a classification of light in terms of their coherence properties.

Chapter 3 is addressed to the working principle and the main characteristics of a quantum dot superluminescent diode. Special attention is paid to the gain medium formed by quantum dots as well as the geometry of the waveguide. Furthermore, the main facts of the central hybrid coherent light experiment is shortly summarized. Accordingly, chapter 2 and chapter 3 lay the necessary foundations to characterize the amplified spontaneous emission of the broadband semiconductor device.

For modeling light emission of the diode under investigation, we postulate a quantum state described in chapter 4. It turns out that the multimode phase-randomized Gaussian state is an excellent choice. In this connection, we determine first- and second-order correlations. The theoretical results are compared with two experiments conducted by *S. Blumenstein* from the Semiconductor Optics group at the Technical University of Darmstadt. Both, a feedback and a mixed light experiment, in which the emitted radiation of the quantum dot superluminescent diode is superimposed with the emission of a single-mode laser, fits the experimental data remarkably well.

In chapter 5 we propose a microscopic theory of the amplified spontaneous emission of the diode system. This model considers inhomogeneously broadened quantum dots forming the gain medium. In addition, the special geometry of the waveguide is taken into account. Based on stochastic equations of the system operators we find rate equations which allow a detailed study of the intrawaveguide system. In this context, we concentrate on the special cases of a transversal single-mode as well as a multimode quantum dot superluminescent diode composed of identical quantum dots.

By the help of the input-output formalism, we calculate the output spectrum measured by a single photon-detector and compare it with the experimental data in chapter 6.

Due to the unusual light behavior of broadband quantum dot superluminescent diodes we investigate their photon statistics in chapter 7. Starting from our microscopic, multimode theory we examine the equal-time, also called central, second-order correlation. The special case of a single-mode diode highlights a reduction of this measure as a function of detuning, which again permits an explanation of the occurrence of hybrid coherent light from a theoretical perspective.

A summary of the results as well as an outlook is provided in chapter 8.

2

QUANTUM ELECTRODYNAMICS

Hybrid coherent light reveals unusual behavior when studying its temporal correlation functions. In a particular temperature regime, a reduction of the temporal central second-order degree of coherence from 2 to 1.33 was observed in the lab whereas the optical power spectrum remains broadband with a spectral width of some THz [1]. How can we interpret these measurement data? And how do first- and second-order correlations provide information about the coherence or incoherence of light sources in general? Is it possible to fully characterize radiation fields by considering their spectral and statistical characteristics? This chapter is devoted to these questions.

Motivated by the experimental results of hybrid coherent light emitted by a quantum dot superluminescent diode, we choose a pure quantum mechanical description of the emitted light and consider correlations in the quantum world. In doing so, we first quantize the electromagnetic field in the presence of an isotropic, inhomogeneous, dielectric medium for investigating the radiation field inside the diode system composed of semiconductor materials of high refractive index. After that, two classes of quantum states, coherent and thermal states, are characterized to classify hybrid coherent light as a coherent and simultaneously incoherent radiation source with regard to their first- and second-order correlation function. The chapter closes with a short overview of classical and non-classical light sources and clarifies the concept of photon bunching and antibunching.

2.1 QUANTIZATION IN AN INHOMOGENEOUS DIELECTRIC

Quantum effects can be strongly modified by the presence of macroscopic dielectric bodies. E.g. optical instruments in which the electromagnetic field under study propagates or the surrounding semiconductor material of quantum dot superluminescent diodes, in which the gain media (quantum dots) are embedded, influence the emission and photon statistical properties. In such cases it is necessary to consider the quantization of the electromagnetic field in presence of a polarizable medium. In the following we study a non-relativistic quantum description of the electromagnetic field in a linear, isotropic, nonmagnetic, nondispersive, nonabsorptive and inhomogeneous dielectric medium with frequency-independent polarizability and position dependent dielectric constant. This section about the quantization in the presence of dielectric matter is based on the theory of *R. Glauber* and *M. Lewenstein* [31–33], which is a generalization of the familiar canonical field quantization concepts.

MACROSCOPIC MAXWELL EQUATIONS The starting point are the classical, source-free (i.e. no free charges $\rho = 0$ and displacement currents $\mathbf{j} = \mathbf{0}$) macroscopic *Maxwell equations* in vector calculus formulation[1] that read in SI units [35, 36]

$$\begin{aligned}
\nabla \cdot \mathbf{D}(\mathbf{r},t) &= 0 \qquad &&\text{(Gauss's law of electricity)}, &&(2.1a)\\
\nabla \cdot \mathbf{B}(\mathbf{r},t) &= 0 \qquad &&\text{(Gauss's law of magnetism)}, &&(2.1b)\\
\nabla \times \mathbf{E}(\mathbf{r},t) &= -\partial_t \mathbf{B}(\mathbf{r},t) \qquad &&\text{(Faraday's law)}, &&(2.1c)\\
\nabla \times \mathbf{H}(\mathbf{r},t) &= \partial_t \mathbf{D}(\mathbf{r},t) \qquad &&\text{(Ampére's law)}. &&(2.1d)
\end{aligned}$$

Here, **E** and **H** are the electric and magnetic field and **D** and **B** are the electric displacement and the magnetic induction field.

Generally, the dielectric medium is described by the phenomenological quantity ε known as dielectric function. For an isotropic, linear, nonabsorptive [2] and nondispersive dielectric, ε becomes a real, frequency independent scalar and the dielectric displacement is related to the electric field according to [32]

$$\mathbf{D}(\mathbf{r},t) = \varepsilon(\mathbf{r})\mathbf{E}(\mathbf{r},t). \tag{2.2}$$

Assuming a nonmagnetic medium, the magnetic induction field **B**,

$$\mathbf{B}(\mathbf{r},t) = \mu_0 \mathbf{H}(\mathbf{r},t), \tag{2.3}$$

is proportional to the magnetic field **H** with vacuum permeability μ_0.

The quantization procedure of the canonical field theory includes (1) the definition of a scalar and a vector potential as well as the choice of an appropriate gauge, (2) the formulation of a Lagrangian density for the dynamical variables and finally (3) the quantization process by replacing the canonical variables by operators.

VECTOR POTENTIAL AND CHOICE OF GAUGE We define a vector potential, which is related to the electric field and the magnetic induction field by

$$\mathbf{B}(\mathbf{r},t) = \nabla \times \mathbf{A}(\mathbf{r},t), \tag{2.4}$$

$$\mathbf{E}(\mathbf{r},t) = -\partial_t \mathbf{A}(\mathbf{r},t). \tag{2.5}$$

In general, one expects an additional contribution in (2.5) arising from a scalar potential Φ. However, due to the assumption of absent charges, we set this scalar potential equal to zero and choose the **generalized Coulomb gauge**[3],

$$\nabla \cdot (\varepsilon(\mathbf{r})\mathbf{A}(\mathbf{r},t)) = 0, \tag{2.6}$$

which is obviously in agreement with the Gauss law (2.1a) or rather the generalized transversality condition, $\nabla \cdot (\varepsilon(\mathbf{r})\partial_t \mathbf{A}(\mathbf{r},t)) = 0$. We can rewrite the Maxwell equation (2.1d) in terms of the vector potential **A** under consideration of the definition (2.4). As a main result, we find an equation of motion for the vector potential,

$$\nabla \times (\nabla \times \mathbf{A}(\mathbf{r},t)) + \frac{\varepsilon(\mathbf{r})}{\varepsilon_0 c_0^2} \partial_t^2 \mathbf{A}(\mathbf{r},t) = 0, \tag{2.7}$$

that depends on the vacuum permittivity ε_0 and the speed of light in vacuum

$$c_0 = (\mu_0 \varepsilon_0)^{-1/2}. \tag{2.8}$$

---

[1] The vector calculus formulation of the original Maxwell equations was introduced by *O. Heaviside* [34].

[2] Clearly, for modeling a quantum dot superluminescent diode, the assumption of a nonabsorptive medium sounds doubtful. However, the absorption effect of the semiconductor is included in our quantum theory by coupling the gain medium to a large reservoir, leading to damping effects in the diode system.

[3] Equation (2.6) is a generalization of the well-known Coulomb gauge $\nabla \cdot \mathbf{A} = 0$ in free space.

LAGRANGIAN FORMALISM Clearly, equation (2.7) can also be derived by the help of the Lagrangian formalism. The Lagrangian for the electromagnetic field propagating in an inhomogeneous dielectric in terms of the dynamical variables [4] $(\mathbf{A}, \partial_t \mathbf{A})$ and the position dependent permittivity $\varepsilon(\mathbf{r})$ is specified by [31]

$$\mathscr{L} = \frac{1}{2}\int \mathrm{d}^3r \Big[\varepsilon(\mathbf{r})\mathbf{E}^2(\mathbf{r},t) - \frac{\mathbf{B}^2(\mathbf{r},t)}{\mu_0}\Big] = \frac{1}{2}\int \mathrm{d}^3r \Big[\varepsilon(\mathbf{r})(\partial_t \mathbf{A}(\mathbf{r},t))^2 - \frac{(\nabla \times \mathbf{A}(\mathbf{r},t))^2}{\mu_0}\Big]. \tag{2.9}$$

The vector potential $\mathbf{A}$ represents the canonical field variable and its corresponding canonically conjugate, the canonical momentum $\mathbf{\Pi}$, is defined by the functional derivative of the Lagrangian (2.9) according to

$$\mathbf{\Pi}(\mathbf{r},t) = \frac{\delta \mathscr{L}}{\delta(\partial_t \mathbf{A})} = \varepsilon(\mathbf{r})\partial_t \mathbf{A}(\mathbf{r},t) = -\varepsilon(\mathbf{r})\mathbf{E}(\mathbf{r},t) = -\mathbf{D}(\mathbf{r},t). \tag{2.10}$$

Because the canonical momentum is the negative electric displacement, the divergence of $\mathbf{\Pi}$ is zero as a consequence of the Gauss's law of electricity (2.1a), i.e.

$$\nabla \cdot \mathbf{\Pi} = -\nabla \cdot \mathbf{D} = 0, \tag{2.11}$$

and therefore purely transversal.

The Hamilton function of the classical electromagnetic field in the presence of an inhomogeneous dielectric reads

$$\mathscr{H}[\mathbf{A},\mathbf{\Pi}] = \int \mathrm{d}^3r\, \mathbf{\Pi}(\mathbf{r},t)\partial_t \mathbf{A}(\mathbf{r},t) - \mathscr{L} = \frac{1}{2}\int \mathrm{d}^3r \left[\frac{\mathbf{\Pi}^2(\mathbf{r},t)}{\varepsilon(\mathbf{r})} + \frac{(\nabla \times \mathbf{A}(\mathbf{r},t))^2}{\mu_0}\right] \tag{2.12}$$

$$= \frac{1}{2}\int \mathrm{d}^3r \left[\varepsilon(\mathbf{r})\mathbf{E}^2(\mathbf{r},t) + \frac{1}{\mu_0}\mathbf{B}^2(\mathbf{r},t)\right] \tag{2.13}$$

and the Hamilton field equations or rather the canonical equations are defined by the derivative of the Hamilton function in terms of the canonical variables, that is

$$\partial_t \mathbf{A}(\mathbf{r},t) = \frac{\delta \mathscr{H}}{\delta \mathbf{\Pi}} = \frac{\mathbf{\Pi}(\mathbf{r},t)}{\varepsilon(\mathbf{r})}, \tag{2.14}$$

$$\partial_t \mathbf{\Pi}(\mathbf{r},t) = -\frac{\delta \mathscr{H}}{\delta \mathbf{A}} = -\frac{\nabla \times (\nabla \times \mathbf{A}(\mathbf{r},t))}{\mu_0}. \tag{2.15}$$

Taking the time derivative of (2.14), the solution can be directly inserted into the Hamilton equation (2.15) which again yields to the predicted equation of motion (2.7).

2.1.1 Homogeneous dielectric medium

This more general consideration of an inhomogeneous medium, in which the dielectric function depends on position $\mathbf{r}$ simplifies in case of a bulk material with dielectric function

$$\varepsilon(\mathbf{r}) = \varepsilon. \tag{2.16}$$

A quantum dot superluminescent diode in absence of a gain material corresponds to such a bulk medium. Therefore, we restrict the quantization process of the electromagnetic field to the

---

[4] In classical physics, a system is described by a set of dynamical variables. Knowing their equations of motion as well as their initial values, the system's evolution is uniquely defined.

more simple problem of a homogeneous dielectric. In this case equation (2.7) reduces to the well-known wave equation

$$\left[\Delta - \frac{1}{c^2}\partial_t^2\right]\mathbf{A}(\mathbf{r},t) = 0, \qquad c = \frac{c_0}{n}, \qquad n = \sqrt{\frac{\varepsilon}{\varepsilon_0}}, \tag{2.17}$$

with refractive index n and speed of light c in a bulk medium [5]. Equation (2.17) looks quite similar to a wave equation of the field **A** propagating in vacuum [32]. The only difference between them is a refractive index $n \neq 1$ in the speed of light c in the bulk material.

MODE EXPANSION In order to solve the wave equation (2.17) we make the separation ansatz for the vector potential,

$$\mathbf{A}(\mathbf{r},t) = \frac{1}{\sqrt{\varepsilon}}\sum_j q_j(t)\mathbf{f}_j(\mathbf{r}) = \frac{1}{\sqrt{\varepsilon}}\sum_j q_j^*(t)\mathbf{f}_j^*(\mathbf{r}) = \mathbf{A}^*(\mathbf{r},t), \tag{2.18}$$

where $\varepsilon^{-1/2}$ has been chosen as an appropriate normalization factor. Here, $\mathbf{A} \in \mathbb{R}^3$ is given by a discrete set of monochromatic mode functions $\mathbf{f}_j(\mathbf{r}) \in \mathbb{C}^3$ and dynamical coordinates $q_j(t) \in \mathbb{C}$ which are allowed to be complex by convenience [32]. The index j numerates the different modes of the multimode field **A**. In case of a field propagating freely in an infinitely large, linear, isotropic, homogeneous medium, j labels the set of indices $(\mathbf{k}, \lambda)$ with wave vector **k** and polarization λ of a plane wave [31]. The mode functions $\mathbf{f}_j(\mathbf{r})$ depend on the boundary conditions of the corresponding physical volume and are chosen in such a way that they satisfy the orthonormality relation

$$\int \mathrm{d}^3 r\, \mathbf{f}_i(\mathbf{r}) \cdot \mathbf{f}_j^*(\mathbf{r}) = \delta_{ij} \tag{2.19}$$

and form a complete set in the space of the transverse vector functions with completeness condition [32],

$$\sum_j \mathbf{f}_j(\mathbf{r}) \otimes \mathbf{f}_j^*(\mathbf{r}') = \delta^\perp(\mathbf{r} - \mathbf{r}'). \tag{2.20}$$

$\delta^\perp(\mathbf{r})$ is the transverse tensor-valued delta function in three dimensions with components [31,37]

$$\delta^\perp_{\alpha\beta}(\mathbf{r} - \mathbf{r}') = \frac{1}{(2\pi)^3}\int \mathrm{d}^3 k \left(\delta_{\alpha\beta} - \frac{k_\alpha k_\beta}{k^2}\right) e^{\mathrm{i}\mathbf{k}(\mathbf{r}-\mathbf{r}')}. \tag{2.21}$$

This transverse delta function $\delta^\perp_{\alpha\beta}$ acts as a projection operator, which projects out the transverse part of the total vector field. This becomes quite obvious when considering the Helmholtz decomposition theorem of an arbitrary vector field, $\mathbf{V}(\mathbf{r}) = \mathbf{V}^\parallel(\mathbf{r}) + \mathbf{V}^\perp(\mathbf{r})$, with longitudinal and transverse part, $\mathbf{V}^\parallel$ and $\mathbf{V}^\perp$, obeying [37, 38]

$$\sum_\beta \int \mathrm{d}^3 r'\, \delta^\perp_{\alpha\beta}(\mathbf{r} - \mathbf{r}') V^\perp_\beta(\mathbf{r}') = V^\perp_\alpha(\mathbf{r}), \qquad \sum_\beta \int \mathrm{d}^3 r'\, \delta^\perp_{\alpha\beta}(\mathbf{r} - \mathbf{r}') V^\parallel_\beta(\mathbf{r}') = 0. \tag{2.22}$$

According to the Coulomb gauge (2.6) for a bulk material, the mode functions satisfy the transversality condition [39]

$$\nabla \cdot \mathbf{f}_j(\mathbf{r}) = 0. \tag{2.23}$$

---

[5] Please note, that the refractive index n is real as a consequence of a nondispersive and nonabsorptive medium.

Considering the completeness condition (2.20), the complex conjugate mode function $\mathbf{f}_i^*(\mathbf{r})$ is related with the mode function itself by

$$\mathbf{f}_i^*(\mathbf{r}) = \int \mathrm{d}^3 r' \; \delta^{\perp}(\mathbf{r}-\mathbf{r}') \cdot \mathbf{f}_i^*(\mathbf{r}') = \sum_j U_{ij}^* \mathbf{f}_j(\mathbf{r}), \tag{2.24}$$

with expansion coefficients given by the integral of the scalar product of mode function $\mathbf{f}_i$ and $\mathbf{f}_j$,

$$U_{ij} = \int \mathrm{d}^3 r \; \mathbf{f}_i(\mathbf{r}) \cdot \mathbf{f}_j(\mathbf{r}). \tag{2.25}$$

Obviously, the matrix U is symmetric [31],

$$U_{ij} = U_{ji}. \tag{2.26}$$

Furthermore, U is a unitary matrix, which can be shown by utilizing the orthonormality condition (2.19) as well as the relation between the mode function and its corresponding complex conjugate (2.24). There holds

$$\begin{aligned} \sum_k U_{ik} U_{jk}^* &= \sum_{k,l} U_{ik} U_{jl}^* \int \mathrm{d}^3 r \; \mathbf{f}_k^*(\mathbf{r}) \cdot \mathbf{f}_l(\mathbf{r}) = \int \mathrm{d}^3 r \sum_{k,l} U_{ik} \mathbf{f}_k^*(\mathbf{r}) \cdot U_{jl}^* \mathbf{f}_l(\mathbf{r}) \\ &= \int \mathrm{d}^3 r \; \mathbf{f}_i(\mathbf{r}) \cdot \mathbf{f}_j^*(\mathbf{r}) = \delta_{ij}. \end{aligned} \tag{2.27}$$

Inserting the separation ansatz (2.18) into the dielectric wave equation (2.17) results in a Helmholtz equation for each mode function $\mathbf{f}_j(\mathbf{r})$ as well as a harmonic oscillator equation for the time-dependent canonical variable $q_j(t)$ with separation constant ω_j,

$$\Delta \mathbf{f}_j(\mathbf{r}) + \frac{\omega_j^2}{c^2} \mathbf{f}_j(\mathbf{r}) = 0, \tag{2.28}$$

$$\ddot{q}_j(t) + \omega_j^2 q_j(t) = 0. \tag{2.29}$$

The corresponding canonical momenta p_i, induced by the Lagrangian (2.9) in terms of the canonical coefficients q_i are directly specified by utilizing the relation (2.10) and by inserting the ansatz of the vector potential (2.18) into the Lagrangian. One finds

$$\mathscr{L} = \frac{1}{2} \int \mathrm{d}^3 r \left[\left(\sum_j \dot{q}_j(t) \mathbf{f}_j(\mathbf{r}) \right)^2 - \frac{1}{\varepsilon \mu_0} \left(\sum_j q_j(t) (\nabla \times \mathbf{f}_j(\mathbf{r})) \right)^2 \right]. \tag{2.30}$$

Partial derivative of this Lagrangian with respect to $\dot{q}_i$ specifies the canonical momentum

$$p_i = \frac{\partial \mathscr{L}}{\partial \dot{q}_i} = \sum_j U_{ij} \dot{q}_j. \tag{2.31}$$

Clearly, equation (2.31) together with the characteristics (2.26)-(2.27) of the matrix U allow to determine the temporal derivative $\dot{q}_i$ as a function of p_i,

$$\dot{q}_i = \sum_j U_{ij}^* p_i, \tag{2.32}$$

and therefore the field variable $\mathbf{\Pi}$ (see equation (2.10)) in terms of p_i

$$\mathbf{\Pi}(\mathbf{r},t) = \varepsilon \dot{\mathbf{A}} = \sqrt{\varepsilon} \sum_j \dot{q}_j(t) \mathbf{f}_j(\mathbf{r}) = \sqrt{\varepsilon} \sum_j p_j(t) \mathbf{f}_j^*(\mathbf{r}). \tag{2.33}$$

QUANTIZATION PROCESS A quantization in Coulomb gauge is based on a set of canonical variables which exhibit operator character after quantization,

$$q_j(t) \quad \rightarrow \quad \hat{q}_j(t), \qquad p_j(t) \quad \rightarrow \quad \hat{p}_j(t), \tag{2.34}$$

and whose commutators are given by

$$[\hat{q}_i, \hat{p}_j] = \mathrm{i}\hbar\delta_{ij}, \quad [\hat{q}_i, \hat{q}_j] = [\hat{p}_i, \hat{p}_j] = 0. \tag{2.35}$$

Furthermore, we can calculate the hermitian conjugated variables $\hat{q}_j^\dagger$ and $\hat{p}_j^\dagger$ by taking into account that the canonical field operators are hermitian, i.e. $\hat{\mathbf{A}} = \hat{\mathbf{A}}^\dagger$ and $\hat{\mathbf{\Pi}} = \hat{\mathbf{\Pi}}^\dagger$. Utilizing the orthonormality relation (2.19) we end up with the expressions

$$\hat{q}_i^\dagger = \sum_j U_{ij}\hat{q}_j, \qquad \hat{p}_i^\dagger = \sum_j U_{ij}^*\hat{p}_j, \tag{2.36}$$

which allow to evaluate the commutators

$$[\hat{q}_i, \hat{q}_j^\dagger] = [\hat{p}_i, \hat{p}_j^\dagger] = 0, \qquad [\hat{q}_i, \hat{p}_j^\dagger] = \mathrm{i}\hbar U_{ij}^*. \tag{2.37}$$

HAMILTONIAN AND GENERAL FIELD EXPRESSIONS With Hamilton function (2.12) in terms of the vector potential and canonical momentum, we can specify the Hamilton operator of the total electromagnetic field in terms of the canonical operators $\hat{q}_j$ and $\hat{p}_j$ by using equations (2.18) and (2.33), respectively. The resulting Hamilton operator of the electromagnetic field, which propagates freely in a bulk medium with speed of light c reads

$$\hat{H} = \frac{1}{2}\sum_j \left(\hat{p}_j\hat{p}_j^\dagger + \omega_j^2\hat{q}_j\hat{q}_j^\dagger\right). \tag{2.38}$$

This result is in close analogy to the Hamiltonian of a set of uncoupled harmonic oscillators with frequency ω_j and unit mass. Next, we express the operators $\hat{q}_j$ and $\hat{p}_j$ as linear combinations of annihilation and creation operators $\hat{a}_j$ and $\hat{a}_j^\dagger$ by applying the linear, canonical transformation

$$\hat{q}_j = \sqrt{\frac{\hbar}{2\omega_j}}\left(\hat{a}_j + \hat{a}_{-j}^\dagger\right), \quad \hat{p}_j = \mathrm{i}\sqrt{\frac{\hbar\omega_j}{2}}\left(\hat{a}_j^\dagger - \hat{a}_{-j}\right) \quad \text{with} \quad \hat{a}_{-j} \equiv \sum_i U_{ij}\hat{a}_i. \tag{2.39}$$

Inserting (2.39) into (2.37) allows to specify the bosonic commutation relations of $\hat{a}_j$ and $\hat{a}_j^\dagger$,

$$\left[\hat{a}_i, \hat{a}_j^\dagger\right] = \delta_{ij}, \quad \left[\hat{a}_i, \hat{a}_j\right] = \left[\hat{a}_i^\dagger, \hat{a}_j^\dagger\right] = 0. \tag{2.40}$$

Generally, an annihilation (creation) operator acting on a number state $|...,n_j,...\rangle$ annihilates (creates) a photon in mode j and therefore decreases (increases) the number of quanta by one according to

$$\hat{a}_j\,|...,n_j,...\rangle = \sqrt{n_j}\,|...,n_j-1,...\rangle, \quad \hat{a}_j^\dagger\,|...,n_j,...\rangle = \sqrt{n_j+1}\,|...,n_j+1,...\rangle. \tag{2.41}$$

Inserting (2.39) into (2.38) and utilizing the commutation relations (2.40) yields the Hamilton operator (2.38) in terms of the annihilation and creation operators

$$\hat{H} = \sum_j \hbar\omega_j\left(\hat{a}_j^\dagger\hat{a}_j + \hat{a}_j\hat{a}_j^\dagger\right) = \sum_j \hbar\omega_j\left(\hat{n}_j + \frac{1}{2}\right). \tag{2.42}$$

Here,

$$\hat{n}_j = \hat{a}_j^\dagger \hat{a}_j \tag{2.43}$$

denotes the photon number operator of the j^{th} mode. The last term in equation (2.42) corresponds to an infinite sum of zero point energies of the harmonic oscillators. However, this vacuum energy distribution can be omitted by an appropriate renormalization so that the Hamiltonian reduces to

$$\hat{H} = \sum_j \hbar\omega_j \hat{a}_j^\dagger \hat{a}_j. \tag{2.44}$$

Inserting (2.39) into the general ansatz of the vector potential (2.18) as well as into the electric and magnetic field (cf. equation (2.4) and (2.5)) directly leads to the general field expressions

$$\hat{\mathbf{A}}(\mathbf{r},t) = \sum_j \sqrt{\frac{\hbar}{2\omega_j\varepsilon}}\mathbf{f}_j(\mathbf{r})\hat{a}_j(t) + \text{h.c.}, \tag{2.45}$$

$$\hat{\mathbf{E}}(\mathbf{r},t) = \mathrm{i}\sum_j \sqrt{\frac{\hbar\omega_j}{2\varepsilon}}\mathbf{f}_j(\mathbf{r})\hat{a}_j(t) + \text{h.c.}, \tag{2.46}$$

$$\hat{\mathbf{B}}(\mathbf{r},t) = \sum_j \sqrt{\frac{\hbar}{2\omega_j\varepsilon}}(\nabla \times \mathbf{f}_j(\mathbf{r}))\hat{a}_j(t) + \text{h.c.}. \tag{2.47}$$

They depend on the mode function $\mathbf{f}_j(\mathbf{r})$ and the time-dependent quantized field amplitudes $\hat{a}_j(t)$. The precise expression of $\mathbf{f}_j(\mathbf{r})$ is specified by particular boundary conditions determined by the volume geometry in which the field propagates. For example, reflecting walls have boundary conditions which lead to standing waves. This assumption is applicable for the description of laser systems. Optical devices which are designed in such a way that back reflections at the output facets are suppressed obey to periodic boundary conditions. The last case is of great significance in the study of light-emitting quantum dot superluminescent diodes.

PERIODIC BOUNDARY CONDITIONS Here, the electromagnetic field is assumed to propagate in a finite rectangular box of volume $V = L_xL_yL_z$ with lengths L_i $(i = x,y,z)$ in all three spatial directions. Periodic boundary conditions require that

$$\mathbf{f}_j(\mathbf{r}) = \mathbf{f}_j(\mathbf{r}+\mathbf{L}) \quad \text{with} \quad \mathbf{L} = (n_xL_x, n_yL_y, n_zL_z)^T,\ n_i \in \mathbb{Z}. \tag{2.48}$$

The solution of the Helmholtz equation (2.28) under consideration of the boundary condition (2.48) are traveling waves

$$\mathbf{f}_j(\mathbf{r}) = \frac{1}{\sqrt{V}}\mathbf{e}_{\mathbf{k},\lambda}e^{\mathrm{i}\mathbf{kr}}, \quad j \mapsto (\mathbf{k},\lambda), \tag{2.49}$$

with the polarization vector $\mathbf{e}_{\mathbf{k},\lambda}$. The wave vector,

$$\mathbf{k} = 2\pi\left(\frac{n_x}{L_x}, \frac{n_y}{L_y}, \frac{n_z}{L_z}\right)^T, \tag{2.50}$$

satisfies the linear dispersion relation

$$\omega_{\mathbf{k}} = c|\mathbf{k}| \tag{2.51}$$

with the speed of light c within the bulk material. Please note, that $\mathbf{e}_{\mathbf{k},\lambda}$ and $\mathbf{k}$ are perpendicular to each other due to the transversality condition (2.23) according to $\mathbf{k}\cdot\mathbf{e}_{\mathbf{k},\lambda} = 0$. Therefore, there exist two independent, generally complex, polarization vectors $\mathbf{e}_{\mathbf{k},\lambda}$ $(\lambda = 1,2)$, which again are perpendicular to each other, that is $\mathbf{e}_{\mathbf{k},\lambda}\cdot\mathbf{e}_{\mathbf{k},\lambda'} = \delta_{\lambda\lambda'}$. Thus, the set of unit vectors $\{\mathbf{k}/|\mathbf{k}|, \mathbf{e}_{\mathbf{k},1}, \mathbf{e}_{\mathbf{k},2}\}$ forms a trihedron. In this context, inserting equation (2.49) into (2.46), the electric field in a bulk medium of permittivity ε can be written as

$$\hat{\mathbf{E}}(\mathbf{r},t) = \hat{\mathbf{E}}^{(+)}(\mathbf{r},t) + \hat{\mathbf{E}}^{(-)}(\mathbf{r},t) \tag{2.52}$$

with positive frequency part

$$\hat{\mathbf{E}}^{(+)}(\mathbf{r},t) = \left[\hat{\mathbf{E}}^{(-)}(\mathbf{r},t)\right]^{\dagger} = \sum_{j} v_{\mathbf{k}}(\mathbf{r})\hat{a}_{\mathbf{k},\lambda}(t)\mathbf{e}_{\mathbf{k},\lambda} \tag{2.53}$$

and mode function

$$v_{\mathbf{k}}(\mathbf{r}) = \mathscr{E}_{\mathbf{k}} e^{\mathrm{i}\mathbf{k}\mathbf{r}}, \quad \mathscr{E}_{\mathbf{k}} = \mathrm{i}\sqrt{\frac{\hbar\omega_{\mathbf{k}}}{2\varepsilon V}}. \tag{2.54}$$

Analogical considerations yield a similar expression for the magnetic flux

$$\hat{\mathbf{B}}(\mathbf{r},t) = \hat{\mathbf{B}}^{(+)}(\mathbf{r},t) + \hat{\mathbf{B}}^{(-)}(\mathbf{r},t), \quad \hat{\mathbf{B}}^{(+)}(\mathbf{r},t) = \sum_{j} w_{\mathbf{k}}(\mathbf{r})\hat{a}_{\mathbf{k},\lambda}(t)(\mathbf{k}\times\mathbf{e}_{\mathbf{k},\lambda}) \tag{2.55}$$

with mode function

$$w_{\mathbf{k}}(\mathbf{r}) = \mathscr{B}_{\mathbf{k}} e^{\mathrm{i}\mathbf{k}\mathbf{r}}, \quad \mathscr{B}_{\mathbf{k}} = \mathrm{i}\sqrt{\frac{\hbar}{2\varepsilon\omega_{\mathbf{k}} V}}. \tag{2.56}$$

2.1.2 Poynting vector and intensity

In analogy to classical electrodynamics, the quantum Poynting vector describes the energy flux density with dimension (energy/area×time) and is defined by [40]

$$\hat{\mathbf{S}} = \hat{\mathbf{E}}\times\hat{\mathbf{H}} = \frac{1}{\mu_0}\hat{\mathbf{E}}\times\hat{\mathbf{B}}. \tag{2.57}$$

Neglecting the fast oscillating terms in (2.57), the (normal-ordered) Poynting vector operator reduces to

$$\hat{\mathbf{S}} \approx \frac{1}{\mu_0}\left(\hat{\mathbf{E}}^{(-)}\times\hat{\mathbf{B}}^{(+)} - \hat{\mathbf{B}}^{(-)}\times\hat{\mathbf{E}}^{(+)}\right). \tag{2.58}$$

For an electromagnetic field describable by traveling waves (2.52) and (2.55) with corresponding mode functions (2.54) and (2.56) and wave vectors pointing in common direction, $\mathbf{k} = |\mathbf{k}|\mathbf{n}$, the poynting vector magnitude (or intensity operator) parallel to the propagation direction $\mathbf{n}$ of the electromagnetic field is

$$\hat{S}(\mathbf{r},t) = \mathscr{C} n \hat{\mathbf{E}}^{(-)}(\mathbf{r},t)\cdot\hat{\mathbf{E}}^{(+)}(\mathbf{r},t), \qquad \mathscr{C} = 2\varepsilon_0 c_0. \tag{2.59}$$

Its ensemble average defines the optical intensity[6]

$$I(\mathbf{r},t) = \langle\hat{S}(\mathbf{r},t)\rangle = \mathscr{C} n\langle\hat{\mathbf{E}}^{(-)}(\mathbf{r},t)\cdot\hat{\mathbf{E}}^{(+)}(\mathbf{r},t)\rangle. \tag{2.60}$$

The bracket symbolizes the quantum mechanical expectation value, $\langle ... \rangle = \mathrm{Tr}\{...\hat{\rho}\}$, which is an ensemble average with density operator $\hat{\rho}$.

---

[6] There exist other well-established definitions of an intensity which neglect the factor of $2n\varepsilon_0 c_0$ [37].

LINEAR POLARIZED LIGHT In case of an electromagnetic field with a single linear polarization parallel to the unit vector $\mathbf{e}$[7],

$$\hat{\mathbf{E}}(\mathbf{r},t) = \hat{E}(\mathbf{r},t)\mathbf{e}, \tag{2.61}$$

the intensity is determined by the equal space-time, ensemble average

$$I(\mathbf{r},t) = \mathscr{C}n\langle \hat{E}^{(-)}(\mathbf{r},t)\hat{E}^{(+)}(\mathbf{r},t)\rangle \tag{2.62}$$

with the scalar field $\hat{E}(\mathbf{r},t)$. Please note (2.62) corresponds to the intensity inside the bulk medium with refractive index n. Clearly, an intensity of a radiation field under study is measured outside the light source and the refractive index in equation (2.62) is set equal to one.

Up to now, we quantized the electromagnetic field in the presence of a bulk medium. This description is more general compared to the quantization process in vacuum and in particular relevant for an accurate description of the electric field propagating inside the considered semiconductor device of a superluminescent diode, which represents the central object of this thesis. In the following we study some important quantum states of the electromagnetic field which are relevant in the context of the hybrid coherent light phenomenon.

2.2 QUANTUM STATES OF LIGHT

Generally, there exist numerous classes of important quantum states, which form a quantum mechanical basis for relevant observables like correlation functions [32]. Especially in the context of hybrid coherent light, so-called coherent and thermal states play a fundamental role as we will see later in this thesis. In the following, we briefly summarize the main characteristics of both light states. For more information we refer the reader to standard quantum optics textbooks [32,41–43].

2.2.1 Coherent states

Coherent states were invented by *E. Schrödinger* [44] in 1926 as the most "classical" quantum states [41] with a minimum allowed uncertainty in amplitude and phase. Their physical meaning becomes apparent in the context of laser physics: the radiation field emitted by a stabilized laser operating well above its threshold is in a coherent state.

There exist a number of possible options to introduce coherent states. Here, we follow the definition by *R. Glauber* [4] in 1963, in which a coherent state $|\alpha\rangle$ is described by an unitary displacement operator $\hat{D}(\alpha)$ [45] acting on the vacuum state $|0\rangle$,

$$|\alpha\rangle = \hat{D}(\alpha)\,|0\rangle\,, \quad \text{with} \quad \hat{D}(\alpha) = e^{\alpha\hat{a}^\dagger - \alpha^*\hat{a}}. \tag{2.63}$$

Simultaneously, from equation (2.63) it follows that $|\alpha\rangle$ is an eigenstate of the annihilation operator $\hat{a}$ with complex eigenvalue $\alpha = |\alpha|e^{\mathrm{i}\phi}$,

$$\hat{a}\,|\alpha\rangle = \alpha\,|\alpha\rangle\,. \tag{2.64}$$

Applying the Baker-Campbell Hausdorff formula [46] to the definition (2.63) allows to determine the coherent state in Fock representation $\{|n\rangle\}$,

$$|\alpha\rangle = \sum_{n=0}^{\infty} \frac{\alpha^n}{\sqrt{n!}} e^{-\frac{|\alpha|^2}{2}}\,|n\rangle\,. \tag{2.65}$$

---

[7] Practically, a radiation of type (2.61) can be realized by implementing a polarization filter into the detection setup.

The probability to measure n photons in state α,

$$P_n(\alpha) = |\langle n|\alpha\rangle|^2 = \frac{|\alpha|^{2n}}{n!} e^{-|\alpha|^2}, \tag{2.66}$$

corresponds to a Poissonian distribution with mean photon number $\bar{n} = |\alpha|^2$ as depicted in figure 2.1 for $|\alpha = 2\rangle$ (blue), $|\alpha = 4\rangle$ (red) and $|\alpha = 6\rangle$ (green).

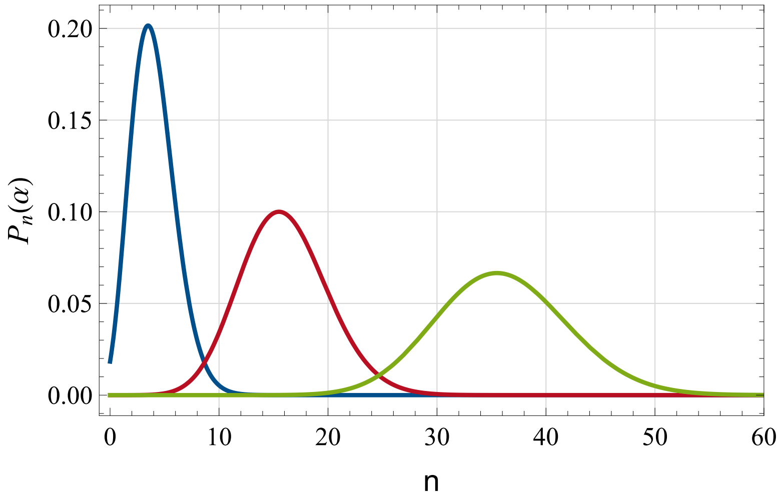

Figure 2.1: Poissonian distribution of a coherent state $|\alpha\rangle$ describing the probability to measure n photons in state $|\alpha = 2\rangle$ (blue), $|\alpha = 4\rangle$ (red) and $|\alpha = 6\rangle$ (green).

Coherent states are not orthogonal. They form an overcomplete set and satisfy the completeness relation

$$\frac{1}{\pi}\int \mathrm{d}^2\alpha \; |\alpha\rangle\langle\alpha| = \hat{\mathbb{1}}. \tag{2.67}$$

An illustration of quantum states provides the *one-dimensional Wigner function* invented by *E. Wigner* [47] in 1932. It refers to a phase-space distribution of an arbitrary quantum state with density operator $\hat{\rho}$ [47,48] and is defined by the ordinary two-dimensional integral ($\mathrm{d}^2\xi = \mathrm{d}\xi_r \mathrm{d}\xi_i$ with $\xi = \xi_r + \mathrm{i}\xi_i$)

$$W(\alpha) = \langle \delta^{(s=0)}(\hat{a}^\dagger - \alpha^*, \hat{a} - \alpha)\rangle \quad \text{with} \quad \delta^{(s)}(\hat{a}^\dagger, \hat{a}) = \int_{-\infty}^{\infty} \frac{\mathrm{d}^2\xi}{\pi^2} e^{\xi\hat{a}^\dagger - \xi^*\hat{a} + \frac{s}{2}|\xi|^2}. \tag{2.68}$$

In case of a coherent state with density operator $\hat{\rho} = |\beta\rangle\langle\beta|$ the Wigner function,

$$W(\alpha) = \frac{2}{\pi} e^{-2|\alpha-\beta|^2}, \tag{2.69}$$

is a Gaussian. Figure 2.2 and 2.3 show a contour plot of the Wigner function for a vacuum state $|\beta = 0\rangle$ and a pure coherent state $|\beta = 3 + 3\mathrm{i}\rangle$. Obviously, a coherent state corresponds to a displaced vacuum state in phase space.

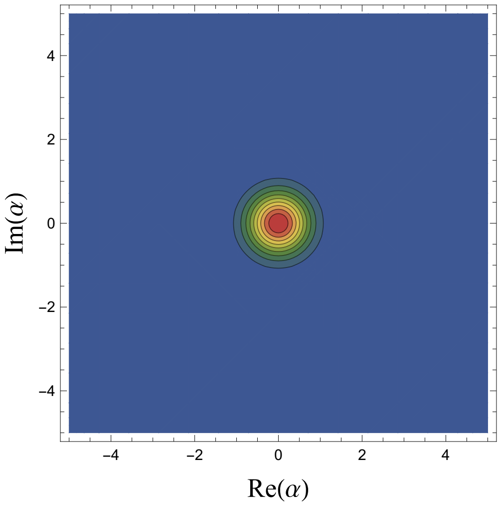

Figure 2.2: Wigner function of a vacuum state $|\beta = 0\rangle$ in phase space.

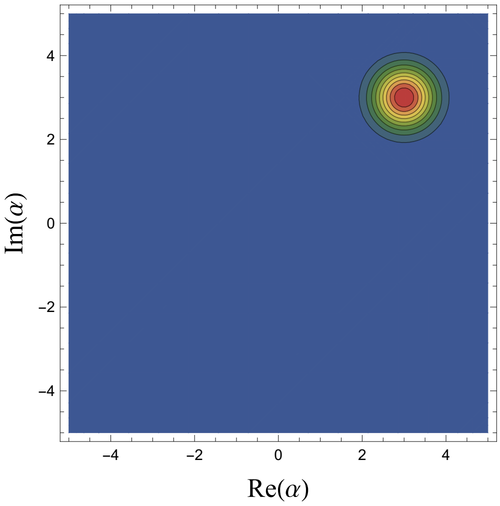

Figure 2.3: Wigner function of a coherent state $|\beta = 3 + 3\mathrm{i}\rangle$ in phase space.

2.2.2 Thermal states

We consider an arbitrary system with Hamilton operator $\hat{H}$ which is in thermal equilibrium with a large reservoir at temperature T. The density operator of such a thermal state is described by the Boltzmann distribution [32, 49],

$$\hat{\rho}_t = \frac{e^{-\beta \hat{H}}}{Z}, \qquad Z = \mathrm{Tr}\{\exp(-\beta \hat{H})\}, \qquad \beta = \frac{1}{k_B T}. \tag{2.70}$$

Here, Z represents the canonical partition function and β is inverse proportional to the Boltzmann constant $\mathrm{k_B} = 1.38 \times 10^{-23}\ \mathrm{J/K}$. In case of a multimode quantized field with angular frequency ω_i, the Hamiltonian,

$$\hat{H} = \hbar \sum_i \omega_i \hat{a}_i^\dagger \hat{a}_i\,, \tag{2.71}$$

is given by the sum of many harmonic oscillators of frequencies ω_i. Inserting equation (2.71) into the thermal density operator (2.70), we find that [49]

$$\hat{\rho}_t = \frac{1}{Z} e^{-\beta\hbar \sum_i \omega_i \hat{a}_i^\dagger \hat{a}_i} = \frac{1}{Z} e^{-\beta\hbar \sum_i \omega_i \hat{n}_i} = \prod_i (1 - e^{-\beta\hbar\omega_i}) e^{-\beta\hbar\omega_i \hat{n}_i} = \prod_i \hat{\rho}_i \tag{2.72}$$

factorizes into a product of independent density operators for each mode of the multimode field with photon number operator $\hat{n}_i$ (cf. equation (2.43)). In the Fock representation with states $\{|n_i\rangle\}$, which obey the completeness relation

$$\sum_{n_i} |n_i\rangle \langle n_i| = \hat{\mathbb{1}}, \tag{2.73}$$

the density operator (2.72) is given by [49]

$$\hat{\rho}_t = \prod_i \sum_{n_i} P(n_i)\, |n_i\rangle \langle n_i| \tag{2.74}$$

with

$$P(n_i) = (1 - e^{-\beta\hbar\omega_i}) e^{-\beta\hbar\omega_i n_i} = \frac{1}{(1 + n_T(\omega_i))(1 + 1/n_T(\omega_i))^{n_i}}. \tag{2.75}$$

In the last step we introduced the first moment of $\hat{n}_i$ or rather the mean thermal occupation number of mode i,

$$n_T(\omega_i) = \langle \hat{n}_i \rangle = \left(e^{\beta\hbar\omega_i} - 1\right)^{-1}, \tag{2.76}$$

which again is the well-known Planck thermal excitation function [8]. Obviously, thermal states are mixed states with probability $P(n_i)$ for finding n_i photons in mode i of the thermal state. Figure 2.4 illustrates $P(n_i)$ with mean thermal occupation numbers $n_T(\omega_i) = 0.1$ (red), $n_T(\omega_i) = 1$ (blue) and $n_T(\omega_i) = 10$ (green).

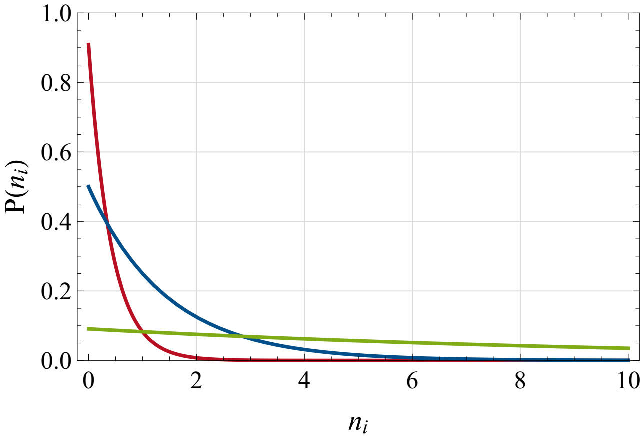

Figure 2.4: Probability $P(n_i)$ for finding n_i photons in mode i with mean thermal occupation numbers $n_T(\omega_i) = 0.1$ (red), $n_T(\omega_i) = 1$ (blue) and $n_T(\omega_i) = 10$ (green).

The joint probability $P(\{n\})$ of a set of photon occupation numbers $\{n\}$ is a product of Bose-Einstein distributions [49],

$$P(\{n\}) = \prod_i P(n_i) = \prod_i \frac{1}{(1+n_T(\omega_i))(1+1/n_T(\omega_i))^{n_i}}, \tag{2.77}$$

and the density operator (2.74) in terms of this joint probability reads

$$\hat{\rho}_t = \sum_{\{n\}} P(\{n\}) \left|\{n\}\right\rangle \left\langle\{n\}\right|. \tag{2.78}$$

The Wigner function of a single mode harmonic oscillator of frequency ω reads [50]

$$W(\alpha) = \frac{2}{\pi}\tanh(\eta)e^{-2\tanh(\eta)|\alpha|^2} \quad \text{with} \quad \eta = \frac{\hbar\omega}{2k_\mathrm{B}T}. \tag{2.79}$$

Figure 2.5 shows the corresponding phase space representation of a harmonic oscillator in thermodynamic equilibrium described by the Wigner function (2.79) for $\eta = 1$ (left) as well as $\eta = 0.1$ (right). It corresponds to a broadened vacuum state.

---

[8] Please note, $n_T(\omega_i)$ is only a function of frequency ω_i and temperature T. This measure becomes negligibly small for near-infrared photons at room temperature with $n_T(\omega_i) \sim 10^{-17}$.

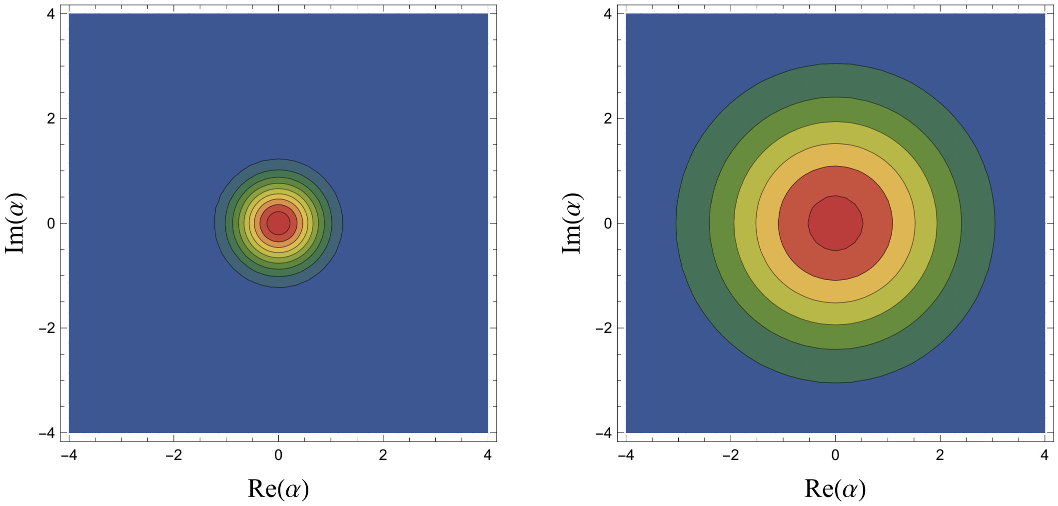

Figure 2.5: Contour plot of the Wigner function (2.79) for a single mode harmonic oscillator in thermodynamical equilibrium with $\eta = 1$ (left) and $\eta = 0.1$ (right).

2.3 SPECTRAL AND STATISTICAL PROPERTIES OF LIGHT

Quantum correlations provide information about the characteristics of light under study. The theoretical background was formulated by *R. Glauber* in 1963 [3–7], laying the foundation of modern quantum optics. Especially, temporal correlations in terms of first- and second-order are significant within this thesis, which yield information about optical power spectra and photon statistics. Therefore, we focus on Glauber's coherence theory and study in more detail first- and second-order correlation functions, which are crucial for a theoretical description of hybrid coherent light. With regard to the measured intensity correlation of a quantum dot superluminescent diode as a function of temperature, which offers characteristics of both, a light bulb and a laser (cf. reference [1] or chapter 3), we discuss relevant correlation functions of coherent and thermal light states.

Clearly, an ideal broadband photon counting detector [51] relies on absorption processes of single photons and is therefore sensitive to the positive frequency part of the electric field $\hat{\mathbf{E}}^{(+)}(\mathbf{r},t)$ which executes a transition from the initial state $|i\rangle$ to the final state $|f\rangle$ with transition probability [41, 52, 53]

$$T_{if} = |\langle f|\,\hat{\mathbf{E}}^{(+)}(x)\,|i\rangle\,|^2, \qquad x = (\mathbf{r},t). \tag{2.80}$$

Here, an ideal photon detector is assumed to have negligibly small size with transition probability independent of frequency. Summing over all final states, which satisfy the completeness relation $\sum_f |f\rangle\langle f| = \hat{\mathbb{1}}$, defines the total counting rate,

$$R_i = \sum_f T_{if} = \langle i|\,\hat{\mathbf{E}}^{(-)}(x)\cdot\hat{\mathbf{E}}^{(+)}(x)\,|i\rangle\,, \tag{2.81}$$

of an electric field in a pure state $|i\rangle$. More generally, in case of a mixed state with density operator $\hat{\rho} = \sum_i P_i\,|i\rangle\langle i|$, the total counting rate or rather the probability of photodetection $w(x)$ is given by

$$w(x) = \sum_i P_i R_i = \mathrm{Tr}\{\hat{\mathbf{E}}^{(-)}(x)\cdot\hat{\mathbf{E}}^{(+)}(x)\hat{\rho}\} = \langle\hat{\mathbf{E}}^{(-)}(x)\cdot\hat{\mathbf{E}}^{(+)}(x)\rangle. \tag{2.82}$$

This result can be extended to a more general expression in which the electric field is evaluated at different space time events in the sense

$$G^{(1)}(x;x') = \langle \hat{\mathbf{E}}^{(-)}(x) \cdot \hat{\mathbf{E}}^{(+)}(x') \rangle. \tag{2.83}$$

It defines the so-called first-order correlation function that is relevant and sufficient to interpret classical interference setups. In order to characterize the nature of light sources [42], the difference between classical and quantum fields [40] or experiments which measure intensity correlations [15], higher-order correlations have to be taken into account.

AUTOCORRELATION FUNCTIONS We consider autocorrelation functions which describe correlations between the same electric field $\hat{\mathbf{E}}$. Correlations between different electrical fields are not relevant within this thesis due to common experimental setups to measure optical spectra or photon statistics which again are related to first- and second-order autocorrelations. For this reason, we always mean autocorrelation functions when talking about correlation functions.

Generally, the n^{th}-order autocorrelation function (tensor) with space-time event $x = (\mathbf{r}, t)$ is defined by the tensor product [4, 6]

$$G^{(n)}(x_1,...,x_n;x_{n+1},...,x_{2n}) = \langle \hat{\mathbf{E}}^{(-)}(x_1) \otimes ... \otimes \hat{\mathbf{E}}^{(-)}(x_n) \otimes \hat{\mathbf{E}}^{(+)}(x_{n+1}) \otimes ... \otimes \hat{\mathbf{E}}^{(+)}(x_{2n}) \rangle. \tag{2.84}$$

It is a normally ordered function, which means that all creation operators lie on the left-hand side of all annihilation operators. The general normalized n^{th}-order correlation function [40],

$$g^{(n)}(x_1,...,x_n;x_{n+1},...,x_{2n}) = \frac{G^{(n)}(x_1,...,x_n;x_{n+1},...,x_{2n})}{\prod_{i=1}^{2n} \sqrt{\mathrm{Tr}\{G^{(1)}(x_i;x_i)\}}}, \tag{2.85}$$

is called the n^{th}-order degree of coherence. It characterizes the measured response in experiments, in which n photons are detected, simultaneously [40].

Both, first- and second-order correlation functions play essential roles in the study of hybrid coherent light and will be analyzed in more detail in the following section. In this context we get more specific and consider in the following traveling electric fields $\hat{\mathbf{E}}(\mathbf{r}, t) = \hat{E}(\mathbf{r}, t)\mathbf{e}$ with a single linear polarization $\mathbf{e}$ of type (2.61), which allows to describe correlation functions in terms of scalar-valued ensemble averages

$$G^{(n)}(x_1,...,x_n;x_{n+1},...,x_{2n}) = \langle \hat{E}^{(-)}(x_1)...\hat{E}^{(-)}(x_n)\hat{E}^{(+)}(x_{n+1})...\hat{E}^{(+)}(x_{2n}) \rangle. \tag{2.86}$$

Clearly, the correlation function itself becomes a scalar, physical measure.

2.3.1 First-order autocorrelation and power spectrum

According to equation (2.84), the first-order correlation function is defined by the ensemble average of the electric field at different space-time events x_1 and x_2 (cf. equation (2.83)) [54],

$$G^{(1)}(x_1;x_2) = \langle \hat{E}^{(-)}(x_1)\hat{E}^{(+)}(x_2) \rangle. \tag{2.87}$$

The first-order degree of coherence is specified by this first-order correlation normalized by the square root of the electric field product at equal events (cf. equation (2.85)) with

$$g^{(1)}(x_1;x_2) = \frac{G^{(1)}(x_1;x_2)}{\sqrt{G^{(1)}(x_1;x_1)G^{(1)}(x_2;x_2)}}. \tag{2.88}$$

With the help of the Cauchy-Schwarz inequality[9] one can show that the absolute value of $g^{(1)}(x_1;x_2)$ has an upper and lower bound,

$$0 \leq |g^{(1)}(x_1;x_2)| \leq 1, \tag{2.89}$$

and is fully matching classical considerations [10] [40]. According to equation (2.62), the first-order correlation function for equal space-time events, $G^{(1)}(x;x)$, is proportional to the intensity

$$I(x) = \mathscr{C} n G^{(1)}(x;x). \tag{2.90}$$

As an application, we consider a multimode electric field of type (2.61) with scalar positive frequency component

$$\hat{E}^{(+)}(\mathbf{r},t) = \sum_j v_j(\mathbf{r}) \hat{a}_j(t). \tag{2.91}$$

Inserting (2.91) into the definition of the first-order correlation function ends up in an expression,

$$G^{(1)}(\mathbf{r}_1,t_1;\mathbf{r}_2,t_2) = \sum_{ij} v_i^*(\mathbf{r}_1) v_j(\mathbf{r}_2) \langle \hat{a}_i^\dagger(t_1) \hat{a}_j(t_2) \rangle, \tag{2.92}$$

that is proportional to the two-time expectation value of creation and annihilation operator of modes i and j. Thus, knowing this expectation value and the mode function, we can specify the first-order correlation function.

Within this thesis, only temporal correlations of stationary fields, describing the correlations at the same position but at different time events, t_1 and t_2, are relevant.

POWER SPECTRUM Consider again an electric field of type (2.61), $\hat{\mathbf{E}}(\mathbf{r},t) = \hat{E}(\mathbf{r},t)\mathbf{e}$, described by a plane wave propagating parallel to the z-direction, which is measured by a photodetector at position z_d with cross-section area A perpendicular to z. Its Fourier transform as well as its inverse Fourier transform is defined by

$$\underline{\hat{\mathbf{E}}}(\mathbf{r},\omega) = \frac{1}{2\pi} \int_{-\infty}^{\infty} \mathrm{d}t \, \hat{\mathbf{E}}(\mathbf{r},t) e^{\mathrm{i}\omega t}, \quad \hat{\mathbf{E}}(\mathbf{r},t) = \int_{-\infty}^{\infty} \mathrm{d}\omega \, \underline{\hat{\mathbf{E}}}(\mathbf{r},\omega) e^{-\mathrm{i}\omega t}. \tag{2.93}$$

The power spectral density is proportional to the square of the absolute value of the electric field in frequency space,

$$S(\omega) = \mathscr{C} \langle \underline{\hat{E}}^{(-)}(\omega) \underline{\hat{E}}^{(+)}(\omega) \rangle \propto n^s(\omega), \quad \underline{\hat{E}}^{(+)}(\omega) = \int \mathrm{d}x \mathrm{d}y \, \underline{\hat{E}}^{(+)}(\mathbf{r},\omega), \tag{2.94}$$

and therefore directly related to the stationary photon number $n^s(\omega)$ of the light field. The Fourier transform of the temporal first-order correlation function $G^{(1)}(\mathbf{r},t;\mathbf{r},t+\tau)$ with time delay $\tau = t_2 - t_1 > 0$ is related to the power spectral density of the stationary electric field $\hat{\mathbf{E}}$ at position $\mathbf{r} = (x,y,z)$ according to the *Wiener-Khintchine theorem* [55,56],

$$\mathscr{S}(\mathbf{r},\omega) = \lim_{t\to\infty} \frac{\mathscr{C}}{2\pi} \mathrm{Re} \int\limits_{-\infty}^{\infty} \mathrm{d}\tau \, e^{\mathrm{i}\omega\tau} G^{(1)}(\mathbf{r},t;\mathbf{r},t+\tau) = \frac{\mathscr{C}}{\pi} \mathrm{Re} \int\limits_{0}^{\infty} \mathrm{d}\tau \, e^{\mathrm{i}\omega\tau} G^{(1)}(\mathbf{r},\tau). \tag{2.95}$$

---

[9] The Cauchy Schwarz inequality for a scalar product $\langle x,y \rangle$ with $x,y \in \mathrm{C}$ reads $|\langle x,y \rangle|^2 \leq \langle x,x \rangle \langle y,y \rangle$.

[10] As the classical and the quantum first-order degree of coherence exhibit the same range of values, first-order interference experiments are not suitable to measure quantum effects. Thus, higher-order correlations have to be taken into account.

In the last step, we utilized that the first-order temporal correlation function of the free stationary field possesses time-symmetry

$$G^{(1)}(\mathbf{r},\tau) = \lim_{t\to\infty}\langle \hat{E}^{(-)}(\mathbf{r},t)\hat{E}^{(+)}(\mathbf{r},t+\tau)\rangle = G^{(1)}(\mathbf{r},-\tau)^{*}. \tag{2.96}$$

Integration of equation (2.95) over the total detector area A provides the experimentally available **power spectral density** (PSD) or **power spectrum**

$$S(\omega) = \int_A \mathrm{d}x\,\mathrm{d}y\, \mathscr{S}(\mathbf{r},\omega) = \frac{\mathscr{C}}{\pi}\,\mathrm{Re}\int_0^{\infty}\mathrm{d}\tau\, e^{\mathrm{i}\omega\tau}\, G^{(1)}(\tau), \tag{2.97}$$

with the spatially averaged temporal first-order correlation function

$$G^{(1)}(\tau) \equiv \lim_{t\to\infty}\int_A \mathrm{d}x\,\mathrm{d}y\, G^{(1)}(\mathbf{r},t;\mathbf{r},t+\tau). \tag{2.98}$$

Please note, $G^{(1)}(\tau)$ is only a function of time delay τ, that is independent of position $\mathbf{r}$ and time t, due to the assumption of a stationary electromagnetic field described by traveling waves.

Usually, an optical power spectrum is measured by an optical spectrum analyzer. In chapter 6, we will see that the power spectrum of a quantum dot superluminescent diode is Gaussian shaped with a central frequency in the near-infrared regime and a broad spectral width of several THz.

For stationary fields, the temporal first-order degree of coherence as a function of time delay $\tau > 0$ is determined by

$$g^{(1)}(\mathbf{r},\tau) = \lim_{t\to\infty}\frac{\langle \hat{E}^{(-)}(\mathbf{r},t)\hat{E}^{(+)}(\mathbf{r},t+\tau)\rangle}{\langle \hat{E}^{(-)}(\mathbf{r},t)\hat{E}^{(+)}(\mathbf{r},t)\rangle} = g^{(1)}(\mathbf{r},-\tau)^{*}, \tag{2.99}$$

In general, $g^{(1)}(\mathbf{r},\tau)$ is complex. Its absolute value describes the correlation strength between the same electric field measured at different times with time delay τ and is therefore a quantitative measure of coherence. For $g^{(1)}(\mathbf{r},\tau) = 1$ the light field is said to be temporal coherent, whereas $g^{(1)}(\mathbf{r},\tau\to\infty) = 0$ it looses coherence at some point in time. The light field is called incoherent [57]. As a consequence of the inequality (2.89), the temporal first-order degree of coherence is bounded by

$$0 \leq |g^{(1)}(\mathbf{r},\tau)| \leq |g^{(1)}(\mathbf{r},\tau=0)| = 1. \tag{2.100}$$

CHARACTERIZING SHAPES OF DISTRIBUTIONS A power spectral density is characterized by some essential quantities: the central frequency, bandwidth and coherence time. In this context, we define the probability normalized power spectral density

$$s(\omega) = \frac{S(\omega)}{\int_{-\infty}^{\infty}\mathrm{d}\omega\, S(\omega)}. \tag{2.101}$$

The resulting first and second moments,

$$\bar{\omega} = \int_{-\infty}^{\infty}\mathrm{d}\omega\;\omega\; s(\omega), \tag{2.102}$$

and

$$\sigma^2 = \int_{-\infty}^{\infty}\mathrm{d}\omega\;(\omega-\bar{\omega})^2\; s(\omega), \tag{2.103}$$

define the central angular frequency and the variance of $s(\omega)$.

An unambiguously definition of the spectral width and the coherence time does not exist. One can find a number of different specifications, depending on the shape of $S(\omega)$ [49,58]. It becomes apparent that the spectral profile determines the validity of the single definitions. For example, a well-established definition of the spectral width $\tilde{b}$ is given by the twofold standard deviation

$$\tilde{b} = 2\sigma. \tag{2.104}$$

However, for fat-tailed distributions like Lorentzian spectra, the definition of a width written in equation (2.104) is not applicable. Therefore, we use an alternative definition for the frequency **spectral width**

$$b = \frac{1}{\int_{-\infty}^{\infty} \mathrm{d}\omega \, s^2(\omega)}, \tag{2.105}$$

introduced by *L. Mandel*[11] [59] and also known as Süssmann measure [48]. Based on the relation between frequency and wavelength, $\nu = c/\lambda$, the frequency spectral width b in terms of the wavelength spectral width $\Delta\lambda$ and central wavelength $\bar{\lambda}$ is given by [49]

$$b = 2\pi\Delta\nu \simeq \frac{2\pi c}{\bar{\lambda}^2}\Delta\lambda. \tag{2.106}$$

Clearly, a strict declaration of the definition of a spectral width is necessary [12], which becomes quite obvious in case of a single normalized Gaussian spectrum $s(\omega)$ with standard deviation σ. According to definition (2.105) the spectral width for the light beam is

$$b_{\text{gauss}} = 2\sqrt{\pi}\sigma. \tag{2.107}$$

A direct comparison with the definition (2.104) reveals a discrepancy of a factor $\sqrt{\pi} \approx 1.77$.

The **coherence time** is defined by the integral

$$\tau_c = \int_{-\infty}^{\infty} \mathrm{d}\tau \, |g^{(1)}(\tau)|^2, \tag{2.108}$$

which reflects the timescales at which $|g^{(1)}(\tau)|$ vanishes. To be specific, on timescales $\tau < \tau_c$ the correlation of the fluctuations is strong, whereas for $\tau > \tau_c$ the correlation becomes weak. In addition, the spectral width and the coherence time are related by [49]

$$\tau_c \sim \frac{1}{b}. \tag{2.109}$$

---

[11] The definition (2.105) of a spectral width by *L. Mandel* was firstly introduced in the context of a study of the extent of a unit cell of the photon phase space.

[12] A superluminescent diode spectrum described by equation (4.5) and parameters listed in table 4.1 shows a spectral width of about $b = 2\pi \cdot 13$ THz according to the definition (2.105). A comparison with the spectral width definition in equation (2.104), $\tilde{b} = 2\pi \cdot 7.5$ THz exhibits a significant systematic bias.

2.3.2 Second-order autocorrelation

The second-order autocorrelation function provides information about the photon statistics of light under consideration. It describes the photon counting probability to detect a photon at space-time event $x_1 = (\mathbf{r}_1,t_1)$ and a second one at $x_2 = (\mathbf{r}_2,t_2)$. This corresponds to the expectation value

$$G^{(2)}(x_1;x_2) = \langle \hat{E}^{(-)}(x_1)\hat{E}^{(-)}(x_2)\hat{E}^{(+)}(x_2)\hat{E}^{(+)}(x_1)\rangle. \tag{2.110}$$

The second-order degree of coherence is defined by

$$g^{(2)}(x_1;x_2) = \frac{G^{(2)}(x_1;x_2)}{G^{(1)}(x_1;x_1)G^{(1)}(x_2;x_2)}. \tag{2.111}$$

We consider again the general electric field described by equation (2.91). Obviously, $G^{(2)}(x_1;x_2)$ is proportional to the fourth-order moment of annihilation and creation operators,

$$G^{(2)}(x_1;x_2) = \sum_{ijlm} v_i^*(\mathbf{r}_1)v_j^*(\mathbf{r}_2)v_l(\mathbf{r}_2)v_m(\mathbf{r}_1)\langle \hat{a}_i^\dagger(t_1)\hat{a}_j^\dagger(t_2)\hat{a}_l(t_2)\hat{a}_m(t_1)\rangle, \tag{2.112}$$

evaluated at different space-time events $(\mathbf{r}_1,t_1)$ and $(\mathbf{r}_2,t_2)$. Again, we only need to specify the mode functions and the quantum expectation value of annihilation and creation operators to determine the temporal second-order autocorrelation function of a radiation field described by an arbitrary quantum state.

Generally, the temporal second-order degree of coherence with time delay $\tau > 0$ is given by

$$g^{(2)}(\mathbf{r},\tau) = \lim_{t\to\infty} \frac{\langle \hat{E}^{(-)}(\mathbf{r},t)\hat{E}^{(-)}(\mathbf{r},t+\tau)\hat{E}^{(+)}(\mathbf{r},t+\tau)\hat{E}^{(+)}(\mathbf{r},t)\rangle}{\langle \hat{E}^{(-)}(\mathbf{r},t)\hat{E}^{(+)}(\mathbf{r},t)\rangle\langle \hat{E}^{(-)}(\mathbf{r},t+\tau)\hat{E}^{(+)}(\mathbf{r},t+\tau)\rangle}, \quad g^{(2)} \in \mathbb{R}. \tag{2.113}$$

This experimentally available measure is real, symmetric and has no upper bound [57],

$$g^{(2)}(\mathbf{r},\tau) = g^{(2)}(\mathbf{r},-\tau), \qquad 0 \leq g^{(2)}(\mathbf{r},\tau) \leq \infty, \tag{2.114}$$

in contrast to the first-order degree of coherence (cf. equation (2.100)). An equal-time, second-order degree of coherence defines the central second-order degree of coherence $g^{(2)}(0)$. This physical quantity plays a central role in the context of hybrid coherent light as we will see later in this thesis.

2.3.3 Temporal autocorrelation of coherent states

Regarding the general expression for a multimode, transverse electric field in equation (2.91), the n^{th}-order degree of coherence of a coherent state is [60]

$$|g^{(n)}(x_1,...,x_n;x_n,...,x_1)| = 1, \quad \forall n \in \mathbb{N}\backslash\{0\}. \tag{2.115}$$

In general, the state of a radiation field is said to be n^{th}-order coherent, if

$$|g^{(j)}(x_1,...,x_j;x_j,...,x_1)| = 1, \quad \forall j \leq n. \tag{2.116}$$

In particular, first- and second-order temporal correlations in terms of coherent states with time delay τ satisfy

$$|g^{(1)}(\tau)| = g^{(2)}(\tau) = 1. \tag{2.117}$$

2.3.4 *Temporal autocorrelation of thermal states*

2.3.4.1 *Temporal first-order autocorrelation*

We consider a free radiation field $\hat{\mathbf{E}}$ of type (2.91) with $\hat{a}_i(t) = \hat{a}_i e^{-\mathrm{i}\omega_i t}$, described by a thermal state with density operator (2.72). As already shown in equation (2.92), the first-order correlation function $G^{(1)}(\mathbf{r},t;\mathbf{r},t+\tau)$ depends on

$$\langle \hat{a}_i^\dagger(t)\hat{a}_j(t+\tau)\rangle = \langle \hat{a}_i^\dagger \hat{a}_j\rangle e^{\mathrm{i}(\omega_i-\omega_j)t} e^{-\mathrm{i}\omega_j\tau}. \tag{2.118}$$

The average on the right-hand side of equation (2.118) is given by the mean thermal occupation number already defined in equation (2.76),

$$\langle \hat{a}_i^\dagger \hat{a}_j\rangle = \mathrm{Tr}\{\hat{a}_i^\dagger \hat{a}_j \hat{\rho}_t\} = n_T(\omega_i)\delta_{ij}. \tag{2.119}$$

Therefore, the temporal first-order correlation function and the first-order degree of coherence of a free thermal radiation field reduces to

$$G^{(1)}(\mathbf{r},t;\mathbf{r},t+\tau) = \sum_i |v_i(\mathbf{r})|^2 e^{-\mathrm{i}\omega_i\tau} n_T(\omega_i), \quad g^{(1)}(\mathbf{r},\tau) = \frac{\sum_i |v_i(\mathbf{r})|^2 n_T(\omega_i) e^{-\mathrm{i}\omega_i\tau}}{\sum_i |v_i(\mathbf{r})|^2 n_T(\omega_i)}. \tag{2.120}$$

1D WAVEGUIDE In the following, we assume that the considered radiation field is linearly polarized in y-direction with running waves propagating along the z-axis which are subjected to periodic boundary conditions (cf. section 2.1.1). The mode function of the electric field in equation (2.91) is written by

$$v_j(\mathbf{r}) = \mathrm{i}\sqrt{\frac{\hbar\omega_j}{2\varepsilon V}}\chi(x,y)e^{\mathrm{i}k_j z}. \tag{2.121}$$

Here, V is the physical volume and $\chi(x,y)$ is an additional spatial component. With such a specific mode function, the normalized first-order correlation (2.120) reads

$$g^{(1)}(\tau) = \frac{\sum_i \omega_i n_T(\omega_i) e^{-\mathrm{i}\omega_i\tau}}{\sum_i \omega_i n_T(\omega_i)}, \qquad g^{(1)}(0) = 1. \tag{2.122}$$

Please note, $g^{(1)}(\tau)$ is independent of position z and has a maximum at vanishing time delay. In [60] (see also [49]), we already discussed temporal correlations of thermal light sources. By calculating the real part of the first-order correlation function in the continuum limit, it turned out that the first-order degree of coherence is specified by

$$g^{(1)}(\tau) = -3\,\mathrm{csch}^2\left(\frac{\pi k_\mathrm{B} T\tau}{\hbar}\right) + 3\left(\frac{\hbar}{\pi k_\mathrm{B} T}\right)^2 \frac{1}{\tau^2}. \tag{2.123}$$

Furthermore, in case of time delays much smaller (bigger) than the thermal coherence time

$$\tau_c = \frac{\hbar}{2\pi k_B T}, \tag{2.124}$$

the absolute value $|g^{(1)}(\tau)|$ is determined by

$$|g^{(1)}(\tau)| = \begin{cases} 1, & \tau \ll \tau_c \\ 0, & \tau \gg \tau_c \end{cases}. \tag{2.125}$$

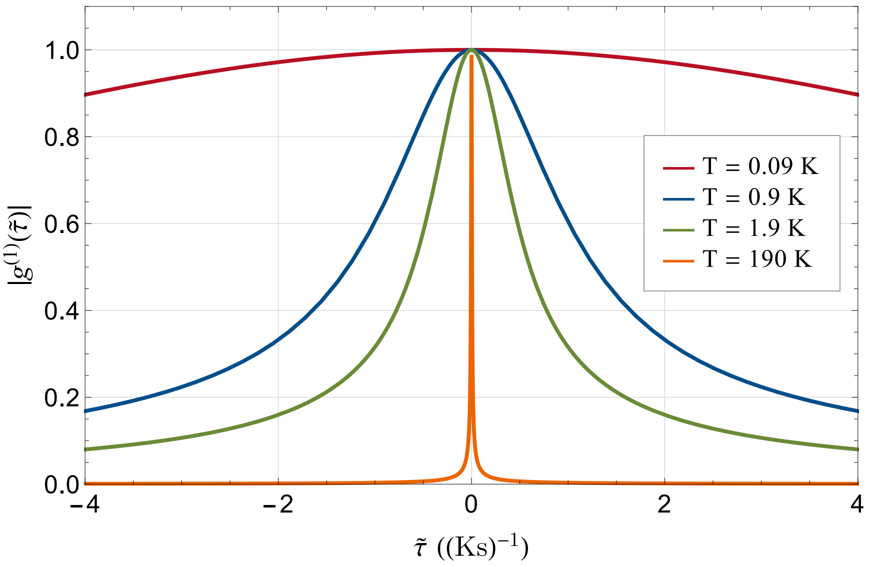

Figure 2.6: Absolute value of the first-order degree of coherence of a thermal state at temperature $T = 0.09$ K (red), $T = 0.9$ K (blue), $T = 1.9$ K (green) and $T = 190$ K (orange) as a function of scaled time delay $\tilde{\tau}$.

Figure 2.6 visualizes this behavior of the absolute value of the first-order degree of coherence for a thermal light state at temperatures $T = 0.09$ K (red), $T = 0.9$ K (blue), $T = 1.9$ K (green) and $T = 190$ K (orange) in terms of

$$\tilde{\tau} = \frac{\pi k_B}{\hbar}\tau = \frac{1}{2T}\frac{\tau}{\tau_c} \tag{2.126}$$

which is of unit (K^{-1}s^{-1}). Obviously, for increasing temperature, the correlation time becomes shorter, that is the radiation field in thermal equilibrium described by a thermal state decorrelates more rapidly for higher temperatures.

2.3.4.2 *Temporal second-order correlation function*

To calculate the second-order correlation of the free propagating thermal radiation field $\hat{\mathbf{E}}$ with mode functions described by equation (2.121),

$$G^{(2)}(\mathbf{r},t;\mathbf{r},t+\tau) = \sum_{ijkl} v_i^*(\mathbf{r})v_j^*(\mathbf{r})v_k(\mathbf{r})v_l(\mathbf{r})e^{-\mathrm{i}(\omega_k+\omega_l-\omega_i-\omega_j)t}e^{-\mathrm{i}(\omega_k-\omega_j)\tau}\langle\hat{a}_i^\dagger\hat{a}_j^\dagger\hat{a}_k\hat{a}_l\rangle, \tag{2.127}$$

we have to calculate equal-time averages of annihilation and creation operators. Such averages are easily determined by utilizing the result (2.119) and *Wick's theorem* (see appendix A), which is applicable for Gaussian states. Thereby, the fourth-order moment factorizes into products of second-order moments according to

$$\begin{aligned}\langle\hat{a}_i^\dagger\hat{a}_j^\dagger\hat{a}_k\hat{a}_l\rangle &= \langle\hat{a}_i^\dagger\hat{a}_j^\dagger\rangle\langle\hat{a}_k\hat{a}_l\rangle + \langle\hat{a}_i^\dagger\hat{a}_k\rangle\langle\hat{a}_j^\dagger\hat{a}_l\rangle + \langle\hat{a}_i^\dagger\hat{a}_l\rangle\langle\hat{a}_j^\dagger\hat{a}_k\rangle \\ &= n_T(\omega_i)n_T(\omega_j)(\delta_{ik}\delta_{jl} + \delta_{il}\delta_{jk}).\end{aligned} \tag{2.128}$$

Inserting this solution into the second-order autocorrelation function (cf. equation (2.127)) allows to determine the second-order degree of coherence of a thermal state given by

$$g^{(2)}(\tau) = 1 + \frac{|\sum_i \omega_i n_T(\omega_i)e^{-\mathrm{i}\omega_i\tau}|^2}{(\sum_i \omega_i n_T(\omega_i))^2} = 1 + |g^{(1)}(\tau)|^2, \tag{2.129}$$

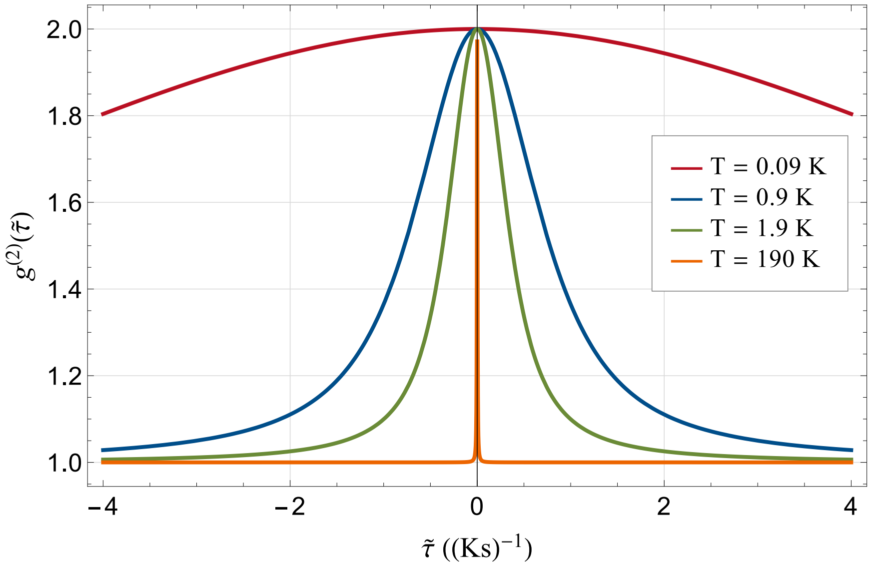

Figure 2.7: Second-order degree of temporal coherence of a thermal state at the temperatures $T = 0.09$ K (red), $T = 0.9$ K (blue), $T = 1.9$ K (green) and $T = 190$ K (orange) as a function of scaled time delay $\tilde{\tau}$.

with a maximum value of $g^{(2)}(0) = 2$ as depicted in figure 2.7. Here, we have chosen the same temperature values as already considered for the first-order correlation in figure 2.6.

Equation (2.129) is known as *Siegert relation* [61] and relates the second-order to the first-order correlation. This relation together with the condition (2.89) reveal an upper and lower bound for the second-order correlation of thermal states,

$$g^{(2)}(0) \geq g^{(2)}(\tau), \tag{2.130}$$

which is fully in line with classical optics [40] and therefore permits an unambiguous interpretation of the occurrence of an increased $g^{(2)}(0) = 2$ value. For thermal light sources, the probability to detect equal-time photon coincidences is greater than measuring coincidences of photons at different times. In other words: the probability to detect a photon at time $t + \tau$ after detection of a photon at time t increases for decreasing time delay τ. From the photon concept of light, this means that photons of classical thermal light sources have the tendency to arrive at the detector much closer together, that is in form of photon *bunches*. This phenomenon was observed for the first time by *R. Hanbury Brown* and *R. Q. Twiss* (HBT). They measured intensity-intensity correlations to analyze the size of astronomic objects by using a special interferometer setup which is depicted in figure 2.8 [15]. Here, radiation emitted by the light source is split into two partial beams, each one measured by a photomultiplier detector. One of theses detectors possesses a variable time delay τ, experimentally realized by a movable mount. Within a correlator, both fields are multiplied and averaged. This experiment represents one of the most important milestones of modern quantum optics and becomes a standard method in interferometry.

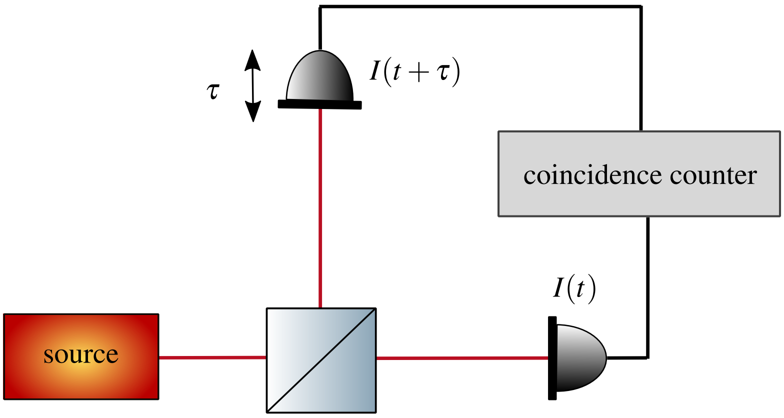

Figure 2.8: A Hanbury Brown & Twiss interferometer.

2.4 PHOTON STATISTICS OF LIGHT SOURCES

Photons of classical light sources have a tendency to strike the detector in pairs, which is reflected by an increasing value of the second-order correlation function for decreasing time delay. Thermal light sources show such classical intensity fluctuations with a central second-order degree of coherence of $g^{(2)}(0) = 2$. Coherent light sources with $g^{(2)}(\tau) = g^{(2)}(0) = 1$ form the limiting case of the condition (2.130). Here, photon counts are measured randomly separated [40]. As already demonstrated in section 2.3.3 and 2.3.4, radiation described by a thermal state is incoherent and obeys a Bose-Einstein statistics, whereas coherent states exhibit Poissonian photon statistics. This presents an evidence of an inherent difference in the photon emission process itself: While the radiation of truly thermal light sources is based on spontaneous emission, coherent light is dominated by stimulated emission processes.

From classical considerations, the temporal second-order degree of coherence obeys the inequality $g^{(2)}(0) > g^{(2)}(\tau)$, which can be easily verified by applying the Cauchy-Schwarz inequality [62]. Thus, a raising slope of the classical temporal second-order degree of coherence is forbidden. However, from a quantum mechanical point of view, this behavior is quite observable. Photons of non-classical light sources tend to arrive well-separated from each other [32]. Here, the probability to detect a photon at a finite time $t+\tau$ after detecting a second photon at time t is higher than detecting two photons, simultaneously. This pure quantum effect is called *antibunching*. Therefore, measuring a $g^{(2)}(0) < g^{(2)}(\tau)$ represents a direct proof of the quantum nature of light. Photon antibunching is observable in resonance fluorescence of single two-level atoms [17,63,64], in a beam of definite photon number [65] and also in single quantum dots at room temperature [18,66]. Obviously, the temporal second-order degree of coherence allows to categorize light in terms of its quantum nature by studying the slope for varying time delay τ, resulting in three different cases:

$$\begin{aligned} &g^{(2)}(0) > g^{(2)}(\tau) && \text{classical light (bunching)} \\ &g^{(2)}(\tau) = g^{(2)}(0) && \text{coherent light} \\ &g^{(2)}(0) < g^{(2)}(\tau) && \text{non-classical light (antibunching)} \end{aligned} \tag{2.131}$$

Regarding the concept of hybrid coherent light, showing both coherent and incoherent characteristics in terms of $g^{(2)}(0)$, we have a closer look at the central second-order degree of coherence. Again, light sources are classified in the following categories [40]:

$$\begin{aligned} &g^{(2)}(0) > 2 && \text{superbunched light} \\ &g^{(2)}(0) = 2 && \text{incoherent (thermal) light} \\ &1 < g^{(2)}(0) < 2 && \text{partially coherent light} \\ &g^{(2)}(0) = 1 && \text{coherent light} \\ &0 \leq g^{(2)}(0) < 1 && \text{antibunched light} \end{aligned} \tag{2.132}$$

Figure 2.9 sketches the different coherence regimes of light sources with regard to the second-order coherence degree for varying time delay τ in arbitrary units. Please note that we distinguish between incoherent (orange) and partially coherent (green) light sources in the sense that purely incoherent light corresponds to thermal light or blackbody radiation with a central degree of coherence of $g^{(2)}(0) = 2$, whereas partial coherent light denotes classical (bunched) light with $1 < g^{(2)}(0) < 2$. Coherent radiation with a constant $g^{(2)}$-value of 1 is reflected by the blue line. The red curve shows non-classical emission in which the antibunching phenomenon is observable. The limiting case of $g^{(2)}(0) = 0$ in the classification (2.132) represents a vanishing probability to measure two photons simultaneously which is the case for temporal, equidistant photon emission.

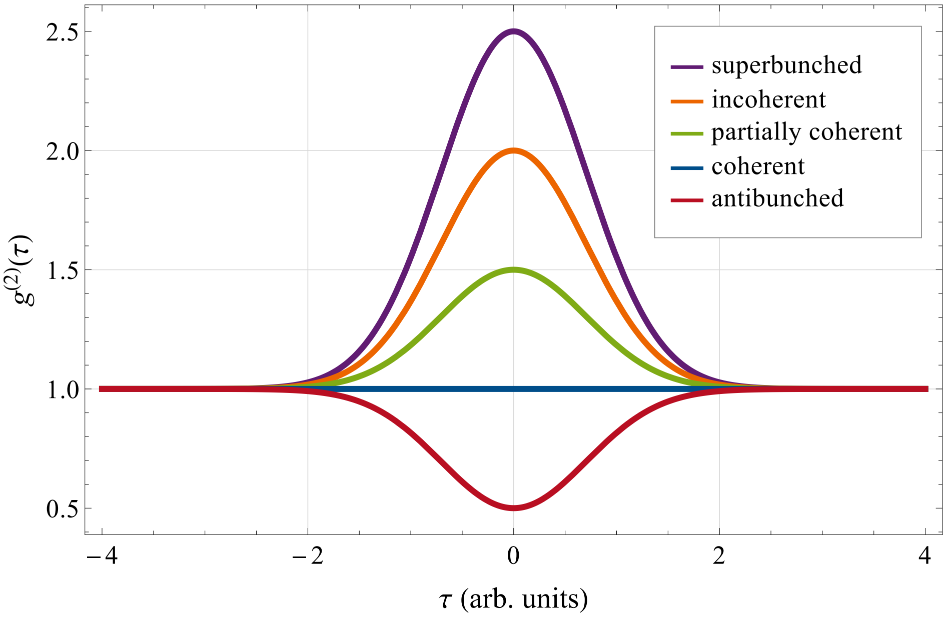

Figure 2.9: Sketch of the temporal second-order degree of coherence $g^{(2)}(\tau)$ as a function of time delay τ in arbitrary units for superbunched (purple), incoherent (orange), partially coherent (green), coherent (blue) and antibunched (red) light sources.

Subject to the enumeration (2.132), classical (bunched) light sources with a second-order degree of coherence of $g^{(2)} > 2$ exhibit *superbunching* [67] observable e.g. for displaced-squeezed states [68], in twin beams created by the nonlinear optical effect of parametric down conversion [69] or for two-photon path interference [70].

Special attention is dedicated to the limiting case of infinitely long time delay. In all mentioned cases summarized in (2.131), the second-order correlation tends to one, $g^{(2)}(\tau) \rightarrow 1$. That is, photon separations are randomly distributed for infinitely large time delay τ and no correlation between emitted photons is observable. Thus, each light source becomes uncorrelated for $\tau \rightarrow \infty$.

In this section, we determined the quantized electric field in the presence of a dielectric medium and introduced temporal correlations. We mentioned the main characteristics of coherent and thermal states and analyzed their temporal first- and second-order correlations. Furthermore, we studied the photon statistics of light sources by having a closer look at the central second-order degree of coherence. For the sake of completeness, one should mention the other feasible counterpart, namely the spatial autocorrelations, e.g. relevant for ghost imaging techniques[13] [71–73]. In the context of hybrid coherent light, these spatial correlations are irrelevant from a theoretical as well as an experimental point of view. Therefore, the whole thesis is dedicated entirely to the description of temporal first-and second-order autocorrelation functions of light emitted by a quantum dot superluminescent diode. However, this becomes quite challenging without the knowledge of the working principle, structure and performance of the special semiconductor device. The next chapter deals with these open questions and outlines the key characteristics of quantum dot superluminescent diodes.

---

[13] Here, an arbitrary object is imaged by spatially correlating information of two detectors. One detector measures a light beam which passes the object, the other one detects light which never interacts with the object.

3

HYBRID COHERENT LIGHT

A detailed experimental study of the light characteristics of quantum dot superluminescent diodes in terms of first- and second-order temporal autocorrelations by *M. Blazek* and *W. Elsäßer* [1] in 2011 highlighted a new class of light states, neither observed in natural photon sources nor in experimentally manipulated systems so far. These novel states of light are incoherent in first and simultaneously coherent in second-order correlation function. Understanding the generation of this hybrid coherent light represents an interesting and challenging field of research, giving more insights to the quantum nature of light-emitting semiconductor devices. This thesis is dedicated to find an explanation for the hybrid coherent light phenomenon. Therefore, this chapter is of high importance as it delivers a brief summary of the significant characteristics of quantum dot superluminescent diodes as well as all relevant information about the hybrid-coherent light experiment, necessary to study the occurrence of these novel states of light from a theoretical point of view. More details of the correlation measurements can be found in reference [1, 74, 75].

3.1 QUANTUM DOT SUPERLUMINESCENT DIODES

Superluminescent diodes (SLDs) are opto-electronic, edge-emitting semiconductor devices, which emit spatial directed light with spectral widths of several THz [74, 76–78]. Figure 3.1 shows such a diode.

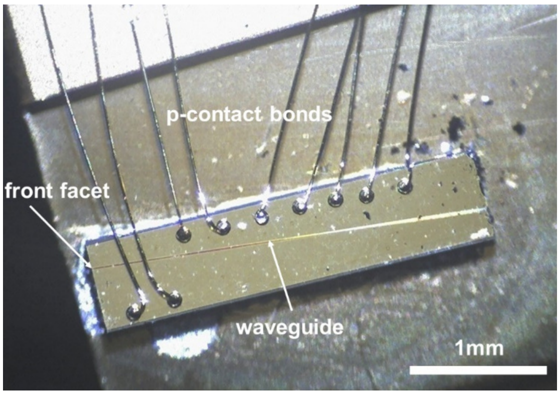

Figure 3.1: Image of a quantum dot superluminescent diode. With kind permission of *S. Blumenstein* [75].

The setup of the device is comparable with standard laser diodes (LDs). The active medium inside the optical waveguide is embedded in a forward biased p-n junction [76, 78]. Electrons of the n-doped and holes of the p-doped material relax in the active region due to diffusion processes and recombine under the emission of photons. But in contrast to typical laser diodes or light-emitting diodes (LEDs), a SLDs exhibits neither purely spontaneous nor purely stimulated emission; it generates amplified spontaneous emission (ASE). Here, initially spontaneous emitted photons receive light amplification by stimulated emission processes during their propagation through the waveguide. Table 3.1 summarizes the major differences of LEDs, SLDs and LDs.

Properties	Light Emitting Diode	Superluminescent Diode	Laser Diode
Optical bandwidth	Large	Large	Small
Optical power	Low	Medium	High
Coherence length	Small	Small	Large
Light emission	Spontaneous emission	Amplified spontaneous emission	Stimulated emission

Table 3.1: Comparison of the main optical characteristics of LEDs, SLDs and LDs [78].

Accordingly, a SLD combines the spatial coherence features of typical laser diodes with the remarkable broadband spectrum of light-emitting diodes. To guarantee broadband ASE, some requirements need to be satisfied regarding the waveguide geometry and of course the gain medium itself.

There are different kinds of waveguide configurations providing some advantages or disadvantages, depending on the system of interest. In the hybrid coherent light experiment of *M. Blazek* and *W. Elsäßer* [1], a SLD with a tilted, both-sided emitting waveguide was used, that will be described more detailed within the next section.

QUANTUM DOTS The gain medium are quantum dots (QDs) or nano-crystallites. QDs are semiconductor heterostructures [1] of about $1 - 10$ nm [79] and are composed of $10^3 - 10^9$ atoms. Here, a semiconductor with a large band gap encloses a lower band gap semiconductor, in which the charge carriers are localized in all three spatial directions in the region of their de Broglie wavelength. The quantum mechanical problem of a particle in a box models this three-dimensional confinement of the charge carriers [80] and therefore verifies in a very simple way the occurrence of discrete energy levels in QDs. Needless to say, this model has been improved during the last decades by integrating more and more physical phenomena and material specific properties for instance electron-hole Coulomb interaction, valence band structure and so on, leading to eventually drastic modifications of the energy states [81]. Nevertheless, the prediction of discrete structures in energy is correct and experimentally confirmed by considering identical QD gain systems realized by lithographic etching techniques [82]. The energy spectra of QDs are comparable with the spectra of ordinary atoms but with one significant difference: while the quantized energy levels of atoms are well defined in their localization, the energy bands of QDs depend strongly on intrinsic parameters like size, shape, material and material composition as well as on the external temperature [83–86]. Thus, it is possible to tune the energy band gap over a long range merely by changing the mentioned parameters. This is the reason why a quantum dot is also called *artificial atom*. Similar to the case of atoms, an external excitation, realized by applying an electric current, leads to photon emission of definite wavelengths. But here, the generation of photons is based on radiative recombination processes of electrons from the conduction band with holes from the valence band. Clearly, the photon energies are equal to the corresponding quantum dot transitions. The lowest optical interband transition is called ground state (GS). Higher transitions are called the first excited state (ES), second excited state (SES) and so on. Figure 3.2 depicts the energy band structure of a quantum dot. Charge carrier

---

[1] "For developing semiconductor heterostructures used in high-speed- and opto-electronics" H. Kroemer and Z. I. Alferov had been awarded the nobel prize in physics in 2000.

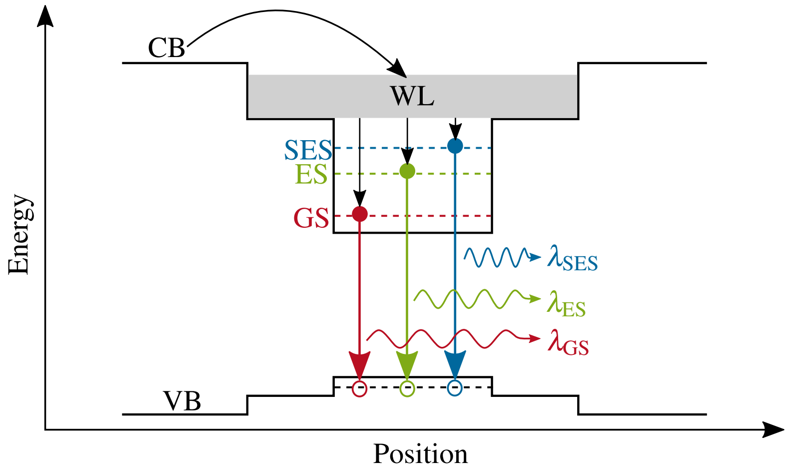

Figure 3.2: Energy band structure of a quantum dot in position space. Electrons from the conduction band (CB) of the bulk medium relax into the wetting layer (WL) and from the WL to the ground (GS), first excited (ES) and second excited state (SES). The GS, ES and SES electrons recombine with holes from the valence band (VB) and simultaneously emit photons of wavelength λ_{GS}, λ_{ES} and λ_{SES}.

relaxation from the conduction band of the bulk medium into the wetting layer (WL) and from the wetting layer into the energy levels (GS, ES, SES) are symbolized by black arrows. The recombination process of the lowest, first and second excited state and the simultaneously emitted photons of wavelength $\lambda_{\text{GS}} \geq \lambda_{\text{ES}} \geq \lambda_{\text{SES}}$ are visualized by red, green and blue arrows. The possibility to produce such artificial atoms with desired opto-electronic properties opens a wide field of applications for commercial purposes like solar cells [87] or biological diagnostic tools for discerning cellular function at the molecular level [88]. But also for the field of quantum information, QDs became indispensable as single-photon emitters [89] or qubits [90, 91].

A widely-used fabrication technique of self-assembled QD gain media is epitaxially grown based on the *Stranski-Krastanow method* [92, 93]. This technique is much cheaper and more rapid compared to lithographic techniques [94]. The QDs nucleate spontaneously on the growth surface driven by the strain of lattice mismatch between epitaxial layer and the substrate when using molecular beam epitaxy or metal-organic vapor phase epitaxy techniques [78]. Due to this self-organized growth, the dots are not identical but rather show an approximately Gaussian distribution in their sizes [95]. Therefore, the single energy levels of the complete set of QDs are broadened. This inhomogeneous broadening of the gain medium is utilized in a **quantum dot superluminescent diode (QDSLD)** which is the central object of this thesis.

Figure 3.3 shows a typical measured optical power spectrum of a QDSLD with purely GS emission (black line). The green line is a Gaussian fit,

$$S(\omega) = \frac{S_0}{\sqrt{2\pi\sigma^2}}\, e^{-(\omega-\bar{\omega})^2/(2\sigma^2)}, \tag{3.1}$$

of central frequency $\bar{\omega} = 2\pi \cdot 0.24$ PHz ($\bar{\lambda}$ =1249.14 nm), standard deviation $\sigma = 2\pi \cdot 1.16$ THz and amplitude $S_0 = 0.113/\sqrt{2\pi\sigma^2}$. The spectral width is given by $b = 2\pi \cdot 4.11$ THz or in terms of wavelength $\Delta\lambda$ =21.39 nm.

In order to obtain such smooth THz broad radiation spectra and spatial directed ASE, more than one layer of the gain medium are used [96]. Typically, $5 - 15$ layers guarantee the desirable light behavior. They are spatially separated by another semiconductor material, the so-called buffer layers.

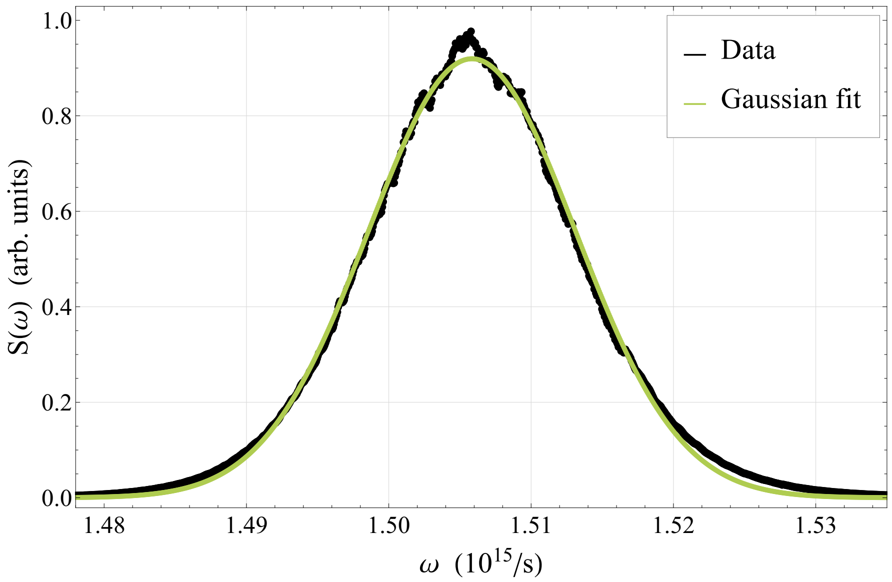

Figure 3.3: The measured optical power spectrum $S(\omega)$ of a QDSLD in arbitrary units shows GS emission. The experimental data (black) are fitted with a Gaussian function (green) with a central frequency $\bar{\omega} = 2\pi \cdot 0.24$ PHz ($\bar{\lambda}$ =1249.14 nm), a standard deviation $\sigma = 2\pi \cdot 1.16$ THz and an amplitude $S_0 = 0.113/\sqrt{2\pi\sigma^2}$. The spectral width is given by $b = 2\pi \cdot 4.11$ THz ($\Delta\lambda$ =21.39 nm).

In summary, the delicate choice of waveguide geometry and gain medium results in high output powers, high efficiency, spatial coherence and a very broad spectral width. These features of the emitted radiation field together with the remarkable fabrication characteristics of an adaptable, compact and robust semiconductor device, are in great demand for industrial applications like optical coherence tomography (OCT) [28, 97–100], telecommunication [101], fiber-optic sensors and gyroscopes [24, 25, 102], etc. Also fundamental research such as ghost imaging techniques [73, 103–105] or the analysis of fundamental quantum optical questions on the photon statistics of broadband emitting semiconductor devices [1, 106, 107] takes advantage of these semiconductor devices. The last mentioned experiment performed by *M. Blazek* and *W. Elsäßer* measured temporal hybrid coherent light for the first time with the help of a QDSLD.

3.2 FIRST OBSERVATION OF HYBRID COHERENT LIGHT

The QDSLD, studied by *M. Blazek* and *W. Elsäßer* [1], was commercially fabricated by the University of Sheffield and the III-V Labs in Palaiseau (series VN1035). This diode possessed a gain medium containing indium arsenide (InAs) quantum dots embedded in indium gallium arsenide (InGaAs) quantum wells (dot-in-well structure). The optical waveguide had a length of $L = 6$ mm and was slightly tilted under an angle of $5-8°$ with respect to the longitudinal axes. In addition, the emission facets where anti-reflection coated to suppress the formation of longitudinal modes [108]. To obtain high efficient light amplifications with broad spectral ranges six layers of the gain medium were utilized, whereas each layer consisted of about 400 quantum dots per μm^2. They were spatially separated by buffer layers with refractive index $n_m \approx 3.5$ slightly smaller than the index of the single gain layers $n_c \approx 3.505$. The diode emitted on both sides.

The emitted light of the QDSLD had an optical output power of $P = 50$ mW and a central wavelength of $\bar{\lambda}$= 1220 ± 110 nm at room temperature. The device emitted transverse-electric

(TE) linear polarized light with a polarization degree of $90-95\%$. To allow temperature measurements in the range of $T = 90-290$ K, the diode was embedded in a liquid-nitrogen cooled cryostat. The power spectrum $S(\lambda) = P_{\mathrm{Opt}}(\lambda)$ was measured with an optical spectrum analyzer and is depicted in figure 3.4 for a fix pump current $I = 1$ A and different temperatures $T = 90$ K (red, dotted line), $T = 190$ K (light blue, dashed line) and $T = 290$ K (dark blue, solid line) [1].

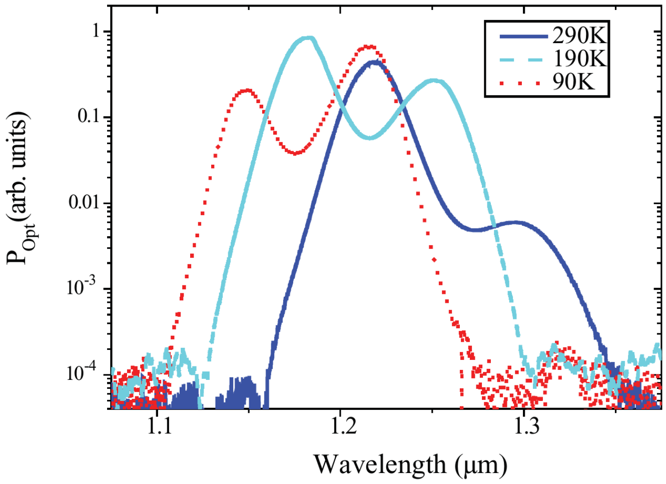

Figure 3.4: Semi-log plot of the optical power spectrum $S(\lambda) = P_{\mathrm{Opt}}$ versus wavelength λ at pump current I =1 A and various temperature $T = 90$ K (red, dotted line), 190 K (light blue, dashed line) and 290 K (dark blue line). Dominated GS emission at 90 K and dominated ES emission at 290 K is observable. Requested figure with permission from M. Blazek and W. Elsäßer, Coherent and thermal light: Tunable hybrid states with second-order coherence without first-order coherence, **84**, 063840, 2011. Copyright 2018 by the American Physical Society.

Obviously, at $T = 290$ K the ES emission dominates with central wavelength $\bar{\lambda}_{\mathrm{ES}} = 1219$ nm in contrast to the rather weak GS emission ($\bar{\lambda}_{\mathrm{GS}} = 1300$ nm). This proportion changes drastically with a decreasing temperature. At $T = 190$ K the ES contribution with central wavelength $\bar{\lambda}_{\mathrm{ES}} = 1181$ nm is still larger that the GS emission ($\bar{\lambda}_{\mathrm{GS}} = 1252$ nm), but the ratio becomes appreciably weaker. Further reduction of the temperature to $T = 90$ K reveals a dominant GS emission with central wavelength $\bar{\lambda}_{\mathrm{GS}} = 1215$ nm larger than the central wavelength of the ES contribution ($\bar{\lambda}_{\mathrm{ES}} = 1146$ nm). In addition, a raising output power P_{Opt} with decreasing temperature is observable. However, we suppose that the generation of hybrid coherent light does not originate from a special ratio of GS and ES emission. The most important result which we should keep in mind is that the spectral width is still of the order of THz and no significant spectral narrowing is visible. That is, the radiation emitted by the QDSLD operated at $T = 190$ K remains highly incoherent in the first-order temporal correlation.

MEASUREMENT OF $g^{(2)}(0)$ Generally, light of mean wavelength $\bar{\lambda}$ with a large spectral width $\Delta\lambda$ has a short coherence time τ_c according to equations (2.109) and (2.106) [49, 58],

$$\tau_c \sim \frac{\bar{\lambda}^2}{2\pi c \Delta\lambda}, \tag{3.2}$$

requested in cases where undesired interference effects prohibit high resolutions. Especially THz-wide optical power spectra of QDSLDs give rise to a coherence time of the order of femtoseconds, $\tau_c \sim$ fs. As already mentioned, usual photon statistical intensity correlation measurements are based on HBT setups [15] (see figure 2.8) comparable with standard Michelson interferometer, in which the mirrors are replaced by detectors. Here, the two light beams, formed by a beam splitter, are measured independently by the particular detectors, in contrast to the Michelson interferometers, where a combination of the light fields before detection is essential. Therefore, only intensity fluctuations are measurable and all information about their relative phase is lost. However, typical photo detectors have temporal resolutions of picoseconds [109], obviously not high enough to detect the ASE of broadband QDSLDs with standard HBT interferometry. In 2009 *F. Boitier et al.* [29] introduced a new kind of photon correlation measurement technique based on the so called two-photon absorption (TPA), a non-linear effect already predicted in 1931 by *M. Goeppert-Mayer* [110] and studied theoretically in terms of field correlation functions by *B. R. Mollow* [111] in 1968. In a semiconductor, two-photon absorption is based on a transition from the valence band to the conduction band by two instantaneously single-photon transitions of energy $\hbar\omega_1$, $\hbar\omega_2$ via an intermediate virtual state (see figure 3.5).

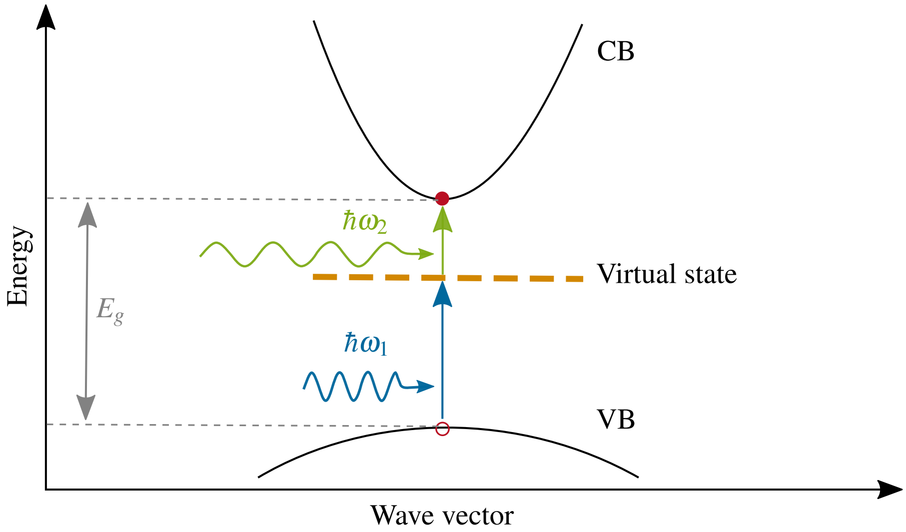

Figure 3.5: Sketch of the two-photon process in a semiconductor quantum dot. It is based on a transition from the valence band (VB) to the conduction band (CB) via two instantaneously single-photon transitions of frequency $\hbar\omega_1$ and $\hbar\omega_2$ via an intermediate virtual state. The band gap energy is $E_g \leq \hbar(\omega_1 + \omega_2)$.

The energies of the single-photon transitions are smaller than the band gap energy E_g whereas the sum of both transition energies is at least the band gap energy E_g, that is $E_g \leq \hbar(\omega_1 + \omega_2)$. The lifetime of the virtual state is limited by $\tau \leq \hbar/E_g$ due to the Heisenberg uncertainty relation [61, 112]. Two-photon absorption is detectable within this ultrashort time regime of τ which is of some femtoseconds in case of near-infrared photons. Thus, within this method it is possible to detect photon bunching in the femtosecond regime, indispensable for the observation of hybrid coherent light.

The experimental setup [1] for measuring the second-order autocorrelation function of broadband QDSLDs corresponded to a Michelson-interferometer in which a TPA signal was generated inside a TPA photomultiplier tube (PMT). The emitted light entered a beam splitter (BS) which generated two partial beams. Each of them striked a mirror, in which one of them was movable with displacement Δx and therefore induced a time shift τ, necessary to extract $g^{(2)}(\tau)$ from the measured PMT interferogram [1, 29, 113]. The entire setup was insulated from the environment by a black box due to the PMT sensitivity to visible light. The QDSLD was cooled inside the liquid-nitrogen cryostat in order to measure temperature dependent central second-order correlations. A more detailed explanation of the experiment is found in ref. [1, 74].

Figure 3.6 shows the experimental result of the central second-order degree of coherence as a function of temperature.

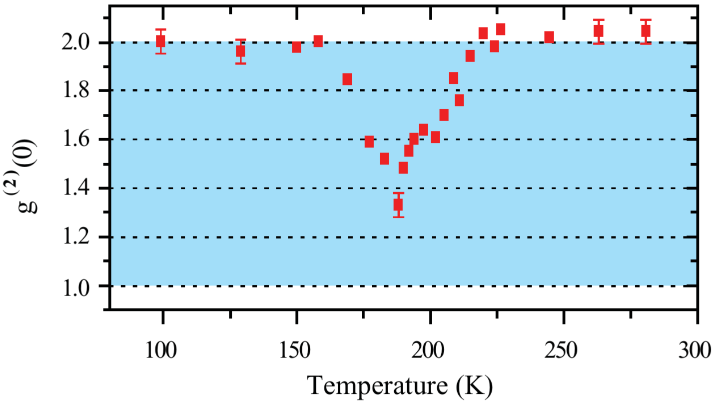

Figure 3.6: Second-order degree of coherence as a function of temperature. A clear reduction from $g^{(2)}(0) = 2$ to $g^{(2)}(0) = 1.33$ at a temperature of $T = 190$ K is visible. Requested figure with permission from M. Blazek and W. Elsäßer, Coherent and thermal light: Tunable hybrid states with second-order coherence without first-order coherence, **84**, 063840, 2011. Copyright 2018 by the American Physical Society.

Clearly, for QDSLD emission a reduction of $g^{(2)}(0)$ from 2 to 1.33 is observable at a temperature of $T = 190$ K, whereas its spectral property of a broadband THz emission is preserved (see light blue, dashed line in figure 3.4). In other words, at $T = 190$ K light emitted by a QDSLD is incoherent in first and simultaneously coherent in second-order of temporal correlation. The direct observation of so-called **hybrid coherent light** is in conflict with Glauber's coherence theory (cf. section 2.3). Please remember, an incoherent, thermal light state with broadband radiation spectrum exhibits a central second-order degree of coherence of $g^{(2)}(0) = 2$, whereas coherent states are coherent in all orders of the correlation function with $|g^{(n)}(0)| = 1$ for all $n \in \mathrm{N}$ (cf. equation (2.116)). From the perspective of fundamental physics, the violation of this paradigm is of particular interest.

An explanation for the occurrence of these novel states of light represents the aim of this thesis. For this reason, a theory of broadband ASE of QDSLDs is particularly relevant, which of course has to reflect the main device specific characteristics as well as the experimental hybrid coherent light conditions highlighted in this chapter. As a first step, we study in the following chapter the light already emitted by a QDSLD in terms of first- and second-order correlations.

4

LIGHT STATES OF QUANTUM DOT SUPERLUMINESCENT DIODES

The analysis of hybrid coherent light enforces a detailed study on the photon statistics of the amplified spontaneous emission which was first studied by *L. Allen* and *G. I. Peters* classically [114–117]. However, photon statistics is the footprint of the quantum nature of light, which is directly related to the emission spectral density and mathematically quantified by the central second-order degree of coherence (see chapter 2). Therefore, already existing, well-established theories of SLD emission, based on rate equations or traveling wave approaches [118–120], have to be extended to the quantum world, which has not been done yet to the best of our knowledge. The high complex material semiconductor structure can be directly embedded within a quantum field theoretical ansatz. However, this leads to many degrees of freedom.

As a first step, we want to postulate a quantum state describing ASE of the diode system, allowing us to implement the emission and photon statistical properties by disregarding additional material or geometric specific characteristics of the device. Thus, at this point of the thesis, we claim that it is so far unnecessary to study the light creation and propagation in the semiconductor waveguide structure.

In this chapter, first- and second-order correlation functions of the chosen light state are studied in detail, the validity which is proven by two experiments [121, 122] at room temperature conducted by *S. Blumenstein* (name of birth Hartmann) *et al.*. All pictures showing measurements are adapted or taken from ref. [122], generated in a collaborative way. The first measurement is based on optical feedback, whereas the second one considers the convolution of coherent light with the SLD broadband radiation. We will see that both experiments exhibit remarkable agreement with our theoretical predictions.

4.1 PHASE-RANDOMIZED GAUSSIAN STATE

In order to model a THz broadband radiation spectrum of a QDSLD, we choose a quantized transversal electric field $\hat{\mathbf{E}}(\mathbf{r},t)$ evaluated at position $\mathbf{r} = (x,y,z)^T$ and time t. The observed radiation field outside the quantum dot superluminescent diode is highly multimode. Therefore, we consider a free electric field given by a superposition of a large number of N longitudinal modes with positive frequency part

$$\hat{\mathbf{E}}^{(+)}(\mathbf{r},t) = \hat{\mathbf{E}}^{(+)}(x,y,t-\frac{z}{c_0}) = \hat{E}^{(+)}(\mathbf{r},t)\mathbf{e}_y, \quad \hat{E}^{(+)}(\mathbf{r},t) = \sum_{j=1}^{N} u_j(\mathbf{r},t)\hat{a}_j. \tag{4.1}$$

We require a linear polarization in *y*-direction due to the structural composition of the device (see chapter 3.2) [123]. Although the diode system emits both-sided, we consider a mono-directional theory for right traveling waves in equation (4.1), motivated by experimental setups. Therefore, we study mode functions of type

$$u_j(\mathbf{r},t) = \mathscr{E}_j \chi(x,y) e^{\mathrm{i}(k_j z - \omega_j t)}, \qquad k_j = \frac{2\pi j}{L}, \quad j \in \mathbb{N}, \tag{4.2}$$

formed by a single transverse wave function $\chi(x,y)$ and N longitudinal plane waves with wave numbers k_j and optical system's length L. The radiation field (4.1) is an approximate solution of the free Maxwell equations which satisfies the one-dimensional wave equation (cf. section 2.1) and shows a linear dispersion relation,

$$\omega_j = c_0 k_j > 0. \tag{4.3}$$

The spatio-temporal field modes are normalized according to

$$\int_V \mathrm{d}^3 r \, |u_j(\mathbf{r},t)|^2 = V, \tag{4.4}$$

with system volume $V = LA$ and cross-section area A. The normalization term $\mathscr{E}_j$ originates from the choice of periodic boundary conditions during the quantization process and was already introduced in (2.54) with $\varepsilon = \varepsilon_0$.

PARAMETERIZING THE QUANTUM STATE For parameterizing the quantum state, we interpret the optical power spectrum of the QDSLD shown in figure 4.1, measured within the mixed light experiment, which will be explained in section 4.5.

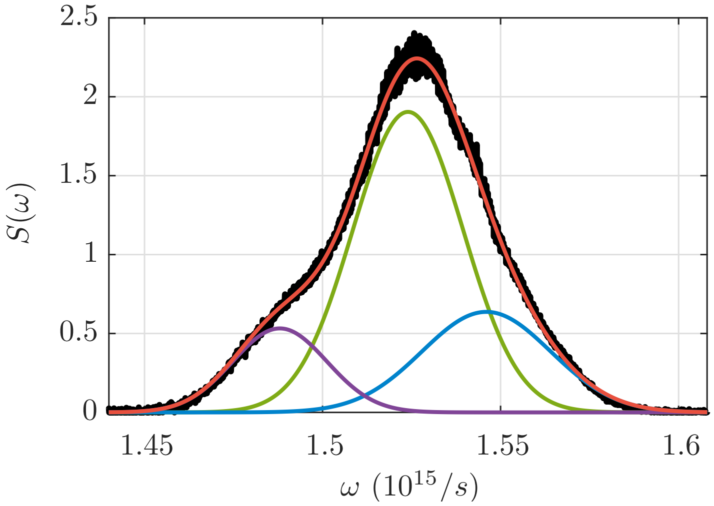

Figure 4.1: Measured optical power spectrum $S(\omega)$ (black) as a function of angular frequency ω of a QDSLD used in the mixed-light experiment (cf. section 4.5). The diode emits at a central frequency of $\bar{\omega} = 2\pi \cdot 242.6$ THz ($\bar{\lambda} = 1236.0$ nm) with a spectral width of $b = 2\pi \cdot 13$ THz ($\Delta\lambda$ 66.25 nm). A three-term Gaussian fit (red) possesses a dominant central emission (green dashed line) as well as upper (blue) and lower (purple) side-bands with fit parameters, listed in table 4.1.

The diode shows broadband GS and higher-order emission with Gaussian-shaped distributions. It emits on a central frequency of about $\bar{\omega} = 2\pi \cdot 242.6$ THz ($\bar{\lambda}$=1236.0 nm) with a spectral width of $b = 2\pi \cdot 13$ THz ($\Delta\lambda = 66.25$ nm). Furthermore, there are upper and lower side-bands, whose strength are determined by a thee-term Gaussian fit of the optical power spectrum

$$S(\omega) = \sum_{i=1}^{3} S_i^0 e^{-\frac{(\omega - \bar{\omega}_i)^2}{2\sigma_i^2}}. \tag{4.5}$$

The numerical data of the fitted amplitudes S_i^0, the central frequencies $\bar{\omega}_i$ and standard deviations σ_i are listed in table 4.1.

i	1 (green)	2 (blue)	3 (purple)
$\bar{\omega}_i$ (THz)	$2\pi \cdot 242.55$	$2\pi \cdot 246.05$	$2\pi \cdot 236.82$
$\bar{\lambda}_i$ (nm)	1236.0	1218.42	1265.91
σ_i (THz)	$2\pi \cdot 2.468$	$2\pi \cdot 2.875$	$2\pi \cdot 2.105$
S_i^0 (arbitrary units)	1.904	0.637	0.532

Table 4.1: Fit parameters of the Gaussian interpolation (cf. equation (4.5)) of the mixed-light spectral density shown in figure 4.1.

Obviously, this illustrates that the quantum state is highly incoherent, which is measured by the first-order temporal autocorrelation function $g^{(1)}(\tau)$. However, the shape of the power spectrum is rather a Gaussian than a Planck distribution. Therefore, the light state is not describable by a thermal state.

In addition, in the context of hybrid coherent light generation, a reduction of the second-order degree of coherence to $g^{(2)}(0) = 1.33$ at a temperature of $T = 190\,\mathrm{K}$ is observable, which is clearly a significant discrepancy from ideal thermal photon statistics with $g^{(2)}(0) = 2$. This can be interpreted as a delicate balance between spontaneous and stimulated emission processes.

This experimental observation is compatible with the multimode **phase-randomized Gaussian (PRAG) state**

$$\hat{\rho}_s = \frac{1}{(2\pi)^N} \int_0^{2\pi} \mathrm{d}^N\phi \; \hat{D}(\gamma)\hat{\rho}_t\hat{D}^\dagger(\gamma). \tag{4.6}$$

Here, the multimode displacement operator

$$\hat{D}(\gamma) = \exp\left[\sum_{i=1}^{N} \gamma_i \hat{a}_i^\dagger - \gamma_i^* \hat{a}_i\right] \tag{4.7}$$

acts on the canonical thermal state

$$\hat{\rho}_t = \frac{e^{-\beta\hat{H}}}{Z}, \qquad Z = \mathrm{Tr}\{e^{-\beta\hat{H}}\}, \qquad \beta = \frac{1}{k_\mathrm{B}T}, \tag{4.8}$$

with partition function Z, Hamilton operator $\hat{H}$ given by equation (2.44) and β, which is inversely proportional to the temperature T. Please note the explicit temperature dependency of the quantum state, relevant for a potential description of the hybrid coherent light phenomenon within a certain temperature regime. The phase-space representation of the PRAG state for one single-mode i is depicted in figure 4.2. Here, a Gaussian state which is initially centered at the origin, is shifted by a complex amplitude $\gamma_i = |\gamma_i|e^{\mathrm{i}\phi_i}$, where the phase ϕ_i is randomized by integration.

PRAG STATE OF ZERO TEMPERATURE Let us investigate a single-mode of vanishing temperature, $T \to 0$. The probability to find n photons in mode i,

$$p(n) = \langle \delta(n-\hat{n}) \rangle = \mathrm{Tr}\{\delta(n-\hat{n})\hat{\rho}_s\} = \frac{|\gamma|^{2n}}{n!} e^{-|\gamma|^2}, \tag{4.9}$$

corresponds to a Poissonian distribution of the coherent state $|\gamma\rangle = \hat{D}(\gamma)\,|0\rangle$ in spite of randomization all phases of the PRAG state with density operator defined in equation (4.6).

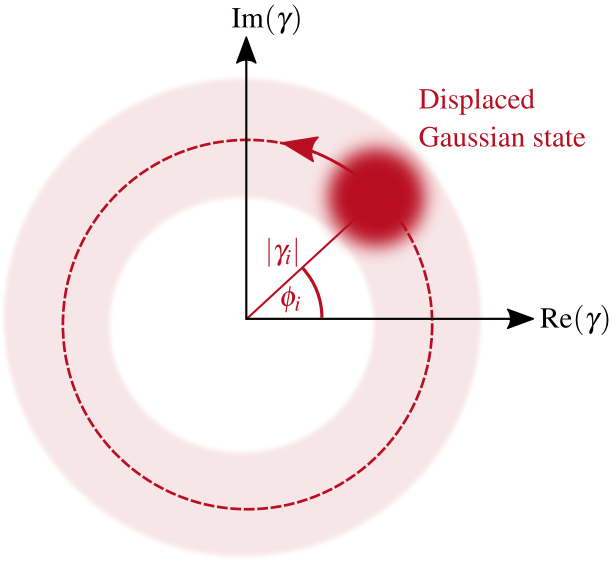

Figure 4.2: Phase-space representation of the PRAG state. We depict the mode i, which is prepared in a Gaussian (thermal) state, displaced by $\gamma_i = |\gamma_i|e^{i\phi_i}$, and the phase angle is randomized (cf. equation (4.6)).

Field and intensity correlations are evaluable using beneficial Lie algebraic similarity transformations, more precisely the harmonic oscillator algebra [124] with

$$\hat{D}^{\dagger}(\gamma)\hat{a}_j\hat{D}(\gamma) = \hat{a}_j + \gamma_j. \tag{4.10}$$

As a relevant result, we find first and second moments of the PRAG state, given by

$$\langle \hat{a}_i \rangle = 0, \quad \langle \hat{a}_j^{\dagger}\hat{a}_i \rangle = n_S(\omega_i)\delta_{ij} \quad \text{with} \quad n_S(\omega_i) = n_C(\omega_i) + n_T(\omega_i), \quad n_C(\omega_i) = |\gamma_i|^2. \tag{4.11}$$

A detailed derivation of equation (4.11) is elaborated in appendix B. Furthermore, higher-order moments are expressible by these lowest moments using Wick's theorem (see appendix A), which is a powerful tool to facilitate the determination of the second-order autocorrelation function. One should notice that the mean thermal occupation number n_T (cf. equation (2.76)) explicitly arises in the second moment (see equation (4.11)) which corresponds to a Bose-Einstein distribution referred in section 2. Therefore, in case of near-infrared (NIR) photons at room temperature possessing a central angular frequency of $\bar{\omega} = 2\pi \cdot 0.24$ PHz, the thermal occupation $n_T(\omega) \approx 10^{-17}$ is negligibly small. However, we are dealing with a driven semiconductor system, so that the temperature of the photons must not be the same as the environmental temperature.

As shown in section 2.1.2, a common definition of the field intensity $I(\mathbf{r},t)$ (see equation (2.62)) of the emitted QDSLD light is proportional to the expectation value of the electric field at equal space-time events,

$$I(\mathbf{r},t) = I(x,y) = \mathscr{C}\langle \hat{E}^{(-)}(\mathbf{r},t)\hat{E}^{(+)}(\mathbf{r},t)\rangle, \tag{4.12}$$

and therefore directly related to the second-order moment (4.11). Obviously, $I(x,y)$ is independent of time t and position z, resulting from the stationarity of the state itself as well as the translational invariance of the traveling radiation field described by equation (4.1). This physical variable is of unit W m^{-2} in fully agreement to the radiometric definition of an intensity [125].

The optical power P, measured by a standard single-photon detector at a fix position z is given by this intensity integrated over the full detector area A,

$$P = \int_A \mathrm{d}x\,\mathrm{d}y\, I(x,y) = \sum_{i=1}^{N} p_i^s = \sum_{i=1}^{N} p_i^c + p_i^t \equiv P^c + P^t \quad \text{with} \tag{4.13}$$

$$p_i^c = p^c(\omega_i) \equiv \frac{\hbar\omega_i c_0}{L} n_C(\omega_i), \qquad p_i^t = p^t(\omega_i) \equiv \frac{\hbar\omega_i c_0}{L} n_T(\omega_i), \qquad p_i^s = p_i^c + p_i^t. \tag{4.14}$$

As shown in figure 4.1, the optical power spectrum $S(\omega)$ is Gaussian distributed over the frequency bandwidth $[\omega_1, \omega_N]$. Clearly, integration of $S(\omega)$ over this bandwidth corresponds to the optical power itself,

$$\int_{\omega_1}^{\omega_N} \mathrm{d}\omega\, S(\omega) = P. \tag{4.15}$$

Thus, a definition of frequency averages and variances,

$$\langle\langle p \rangle\rangle \equiv \frac{1}{N} \sum_{i=1}^{N} p_i, \qquad \Delta^2 p \equiv \sum_{i=1}^{N} \frac{(p_i - \langle\langle p \rangle\rangle)^2}{N}, \tag{4.16}$$

is inevitable for the interpretation of spectra. The total optical power in terms of power averages and variances (4.16), is given by the sum of the average of the incoherent field $\langle\langle p^c \rangle\rangle$ and the average of the thermal field $\langle\langle p^t \rangle\rangle$ multiplied by the number of modes N,

$$P = P^c + P^t = N \left(\langle\langle p^c \rangle\rangle + \langle\langle p^t \rangle\rangle \right). \tag{4.17}$$

In the following, we will show that field and intensity correlations are expressible by these physical quantities.

4.2 FIRST-ORDER CORRELATION FUNCTION

We already showed that, by definition of Glauber's coherence theory, the first-order autocorrelation function of the QDSLD emission is given by the average value of the positive and negative frequency parts of the electric field (4.1) for different space-time events $x \equiv (\mathbf{r}, t)$ (cf. equation (2.87)). Scale invariant properties can be achieved by introducing the normalized first-order autocorrelation function described by (2.88), in which the denominator corresponds to a product of intensities (see equation (2.90)). The Wiener-Khintchine theorem (cf. equation (2.95)) relates the temporal field correlation to the optical power spectrum by a Fourier-transformation, which is experimentally accessible using a spectrum analyzer. The measured signal is proportional to the spatially averaged temporal first-order correlation function (cf. equation (2.98)). The integral over the total detector area A can be evaluated by utilizing the normalization condition (4.4) and the solution of the second moment given in equation (4.11). The corresponding calculation can be found in appendix B. As a main result we find that the temporal first-order autocorrelation function of PRAG states is given by

$$G^{(1)}(\tau) = \frac{1}{\mathscr{C}} \sum_{i=1}^{N} e^{-\mathrm{i}\omega_i \tau} p_i^s. \tag{4.18}$$

In case of vanishing time delay, $\tau = 0$, the correlation function is proportional to the total optical power P,

$$G^{(1)}(0) = \frac{P}{\mathscr{C}}. \tag{4.19}$$

The spatially averaged normalized temporal first-order degree of coherence, $g^{(1)}(\tau)$, is approximately specified by the ratio of the spatially averaged temporal first-order correlation function (2.98) and $G^{(1)}(0)$, that is

$$g^{(1)}(\tau) \simeq \frac{G^{(1)}(\tau)}{G^{(1)}(0)} = \frac{\mathscr{C}}{P} G^{(1)}(\tau) = \frac{1}{P} \sum_{i=1}^{N} e^{-\mathrm{i}\omega_i \tau} p_i^s. \tag{4.20}$$

Obviously, the absolute value of $g^{(1)}(\tau)$ achieves its maximum value of 1 for $\tau = 0$ and consequently satisfies the Cauchy-Schwarz inequality (2.100).

POWER SPECTRAL DENSITY Experimentally available field correlation spectra at a fix position $\mathbf{r}$ are specified in the stationary limit by the Wiener-Khintchine theorem (2.95). Integration over the cross-section area of the single-photon detector results in a discrete power spectrum, due to the sum in equation (4.18). This sum is compatible with the first term of the Euler-Maclaurin series (see appendix C), by considering equal frequency separation between adjacent modes,

$$\Delta\omega = \frac{\omega_N - \omega_1}{N-1}, \tag{4.21}$$

as well as assuming a finite support in the frequency band $[\omega_1, \omega_N]$ of the spectrum and a spectral width, $\sigma \ll |\omega_N - \omega_1|$, being much less than the bandwidth. Finally, we arrive at the continuous optical power spectrum at position z,

$$S(\omega) = \frac{\mathscr{C}}{2\pi} \mathrm{Re} \int_{-\infty}^{\infty} \mathrm{d}\tau \, e^{\mathrm{i}\omega\tau} G^{(1)}(\tau) = \frac{p^s(\omega)}{\Delta\omega}, \qquad p^s(\omega) = (p^c(\omega) + p^t(\omega)), \tag{4.22}$$

of unit W · s. A derivation of this measure is given in appendix B.1.2. Thus, $S(\omega)$ is independent of position and is given by a superposition of the incoherent and thermal contributions, $n_C(\omega_i)$ and $n_T(\omega)$. Their values can be directly extracted from the measured optical power spectrum in figure 4.1.

As expected, the integral of the continuous optical frequency spectrum $S(\omega)$ over the total bandwidth is exactly the total optical power, in agreement to (4.15).

4.3 SECOND-ORDER CORRELATION FUNCTION

Due to the experimental setup for measuring the second-order autocorrelation function of highly broadband light sources by the help of a single two-photon detector, we have to evaluate the temporal second-order degree of coherence (cf. equation (2.113)) in terms of time delay τ. This physical quantity is approximately given by

$$g^{(2)}(\tau) \simeq \left(\frac{\mathscr{C}}{P}\right)^2 \int_A \mathrm{d}x\mathrm{d}y \, G^{(2)}(\mathbf{r},t;\mathbf{r},t+\tau). \tag{4.23}$$

To evaluate the integrand, a fourth-order moment of type $\langle \hat{a}_i^\dagger \hat{a}_j^\dagger \hat{a}_l \hat{a}_m \rangle$ has to be determined, which can be done by utilizing Wick's theorem for Gaussian states (see appendix A). A detailed derivation of $g^{(2)}(\tau)$ can be found in appendix B.1.3. Here, we only indicate the result of the temporal second-order correlation function of a PRAG state

$$g^{(2)}(\tau) = 1 + |g^{(1)}(\tau)|^2 - \sum_{i=1}^{N} \left(\frac{p_i^c}{P}\right)^2. \tag{4.24}$$

The second term in equation (4.24) has an upper and lower bound (see equation (2.100)), while the last term takes values between 0 and 1. Therefore, $g^{(2)}(\tau)$ is limited by $0 \leq g^{(2)}(\tau) \leq 2$. In addition, we find that this normalized correlation satisfies the inequalities

$$g^{(2)}(0) \geq g^{(2)}(\tau), \qquad g^{(2)}(0) \geq 1, \tag{4.25}$$

in agreement to classical considerations of the ASE (cf. equation (2.131)). This central second-order degree of coherence is an experimentally available quantity and determined by

$$g^{(2)}(0) = 2 - \frac{1}{N} \frac{1 + \frac{\Delta^2 p^c}{\langle\langle p^c \rangle\rangle^2}}{\left(1 + \frac{\langle\langle p^t \rangle\rangle}{\langle\langle p^c \rangle\rangle}\right)^2}, \tag{4.26}$$

with mean values $\langle\langle p^c \rangle\rangle$, $\langle\langle p^t \rangle\rangle$ and variance $\Delta^2 p^c$. In case of a single-mode radiation field, $N = 1$, and negligible thermal occupation number ($\langle\langle p^t \rangle\rangle = 0$), this variance vanishes, $\Delta^2 p^c = 0$, and $g^{(2)}(0)$ corresponds to the limiting value of 1. For infinitely large number of modes, $N \to \infty$, the second term of equation (4.26) tends to zero and $g^{(2)}(0) = 2$ as in the case of purely thermal light sources.

For varying number of modes N and negligible thermal contributions, $n_T(\omega) = 0$, at room temperature $g^{(2)}(0)$ shows steep trajectories for increasing values of the power ratio $\Delta^2 p^c / \langle\langle p^c \rangle\rangle^2$, leading to a considerable shift towards higher values of N (see figure 4.3).

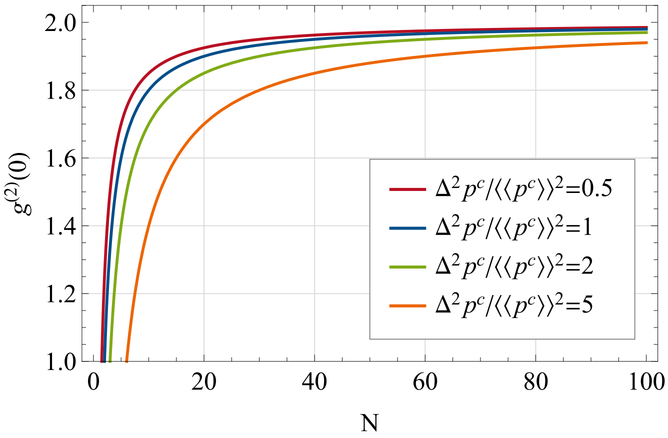

Figure 4.3: Central second-order degree of coherence $g^{(2)}(0)$ as a function of the number of modes N for different values of the power ratio $\Delta^2 p^c / \langle\langle p^c \rangle\rangle^2$ and negligible thermal contribution, $\langle\langle p^t \rangle\rangle = 0$.

We have to point out that the photon statistics of PRAG states depends on the number of modes N and their distributions $n_C(\omega)$ and $n_T(\omega)$, meaning that $g^{(2)}(0)$ depends on the nature of each individual QDSLD. This is an astonishing statement, as it obviously demonstrates that material structural composition of diodes highly influences the light character of these devices. In the same way, varying the number of modes results in tunable photon statistics, ranging continuously from Poissonian ($g^{(2)}(0) = 1$ for $N = 1$) to Gaussian ($g^{(2)}(0) = 2$ for $N \to \infty$) statistics. In experiment, this is realizable by applying optical feedback, as reducing the number of modes N corresponds to narrowing the spectral width. This technique is utilized in a first experiment, successfully performed by the Semiconductor optics group of *W. Elsäßer* at TU Darmstadt. For the sake of completeness, we want to give a brief overview of the experimental results to compare it with our theory and therefore to proof the validity of the chosen light state.

4.4 COMPARISON WITH A FEEDBACK EXPERIMENT

A first test for proofing the quality of our chosen light state is a feedback experiment conducted by *S. Blumenstein et al.*. The setup and experimental details can be found in the publications [121, 122]. Here, we only want to summarize briefly the working principle of this feedback technique for measuring $g^{(2)}(0)$ of broadband QDSLDs in terms of varying number of modes N.

The gain medium of the QDSLD under study was formed by six InAs QD layers embedded in InGaAs quantum wells with a device length of about 3 mm. The output facets were anti-reflection coated and slightly tilted under an angle of 5°. The diode operated at a voltage up to 900 mA at room temperature. For measuring the second-order correlations of the QDSLD emission as a function of the number of modes N, they used a TPA detector. This detector was implemented in a Michelson interferometer, in which a motorized translation stage enforces a time delay τ, necessary to measure TPA interferograms. Using low-pass filtering, $G^{(2)}(\tau)$ was directly evaluated from these interferograms [29, 113]. The emitted light of the QDSLD entered a 50 : 50 beam splitter, which generated two partial light beams. The reflected beam, striking a mirror, achieved optical feedback back into the QDSLD system with a total feedback distance of about 600 mm. It should be noted, that we are not interested in dynamical regions, in which optical feedback on semiconductor emitters enables the entry of nonlinear effects or chaotic behavior [126, 127], especially they are also not included in our theory. Furthermore, only $g^{(2)}(0)$ data with optical spectra showing controlled emission during the measurement process were considered in order to eliminate disturbing optical feedback effects.

Figure 4.4 shows the normalized second-order autocorrelation function for zero time delay $g^{(2)}(0)$ versus number of modes N. The blue dots with the error bars are the experimental data, presented in reference [121] with number of modes N calculated from the measured spectra p_i^c. In particular, contributions of thermal photons $n_T(\omega)$ as well as peaks below 13 dB of the maximum power value were ignored. Otherwise, the latter would distort the statistics of the

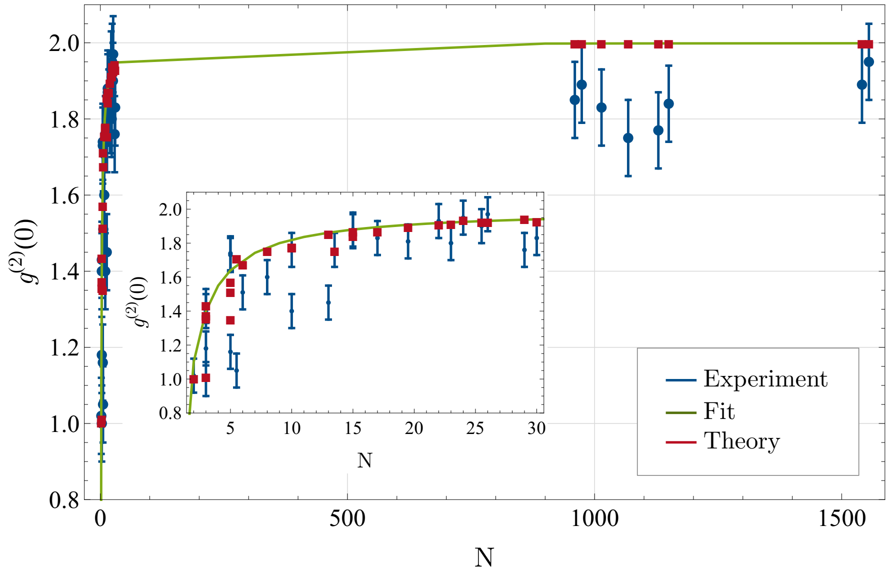

Figure 4.4: Second-order degree of coherence $g^{(2)}(0)$ for varying number of modes N, measured within the optical feedback experiment (blue dots with error bars) [122] and theoretically determined using equation (4.26) (red squares). The green line shows a guide-to-the-eye fit for illustrating the decreasing tendency in the range of small N (with kind permission of S. Blumenstein).

light state. The red squares are the theoretical values, specified by equation (4.26) for the given experimental values of N, $\langle\langle p^c \rangle\rangle$ and $\Delta^2 p^c$, to reflect experimental requirements of the coherence transition. In addition, table 4.2 lists some theoretical and experimental values for $g^{(2)}(0)$ with experimentally determined number of modes N and power ratio $\Delta^2 p^c / \langle\langle p^c \rangle\rangle^2$. To avoid confusion, we denote the temporal second-order correlation function, determined experimentally by $g^{(2)}_{\text{exp}}(\tau)$ and theoretically by $g^{(2)}_{\text{th}}(\tau)$.

N	$\frac{\Delta^2 p^c}{\langle\langle p^c \rangle\rangle^2}$	$g^{(2)}_{\text{exp}}(0)$	$g^{(2)}_{\text{th}}(0)$
3	1.31	1.18	1.23
10	1.12	1.78	1.74
30	1.08	1.83	1.931
1945	0.57	1.84	1.999

Table 4.2: Experimental and theoretical values of $g^{(2)}(0)$ with experimentally determined parameters N and $\Delta^2 p^c / \langle\langle p^c \rangle\rangle^2$. The number of modes N were varied by applying optical feedback. The experimental data were kindly supplied by S. Blumenstein.

A comparison between theory and experiment highlights an overall good agreement. For a large number of modes, $N > 1000$, i.e. weak optical feedback, the QDSLD shows ultra-broadband emission with a second-order correlation function of about $g^{(2)}_{\text{th}}(0) \approx 1.999$ in theory. From the experimental point of view, $g^{(2)}_{\text{exp}}(0)$ can not be determined within this regime simply by counting the number of spectral peaks, due to the formation of smooth Gaussian power spectra as shown in figure 4.1.

In the experiment, N was determined by fitting modes with spacing according to the free spectral range in terms of angular frequency,

$$\Delta\omega = \frac{2\pi c_0}{2 n_{\text{GaAs}} L} \approx 2\pi \cdot 1.465 \cdot 10^{10}\ \text{Hz}, \qquad n_{\text{GaAs}} \approx 3.41, \tag{4.27}$$

representing a lower-bound estimate [122]. Within this mode regime, a second-order correlation around $g^{(2)}_{\text{exp}}(0) = 1.85$ was measured, which reveals an appreciable deviation from the calculated value of 1.999. This discrepancy between theory and experiment is caused by technical challenges during the measurement process (see ref. [122]) leading to experimental data lying below the predicted theoretical values for large number of modes, $N > 1000$. With increasing optical feedback, spectral peaks became more and more visible, so that N are experimentally determined by just counting the peaks. In the range of $N = 30$ down to $N = 15$ we observe a slight decreasing tendency of $g^{(2)}(0)$ both in experiment ($g^{(2)}_{\text{exp}}(0) = 1.83$ for $N = 30$) as well as in theory ($g^{(2)}_{\text{th}}(0) = 1.931$ for $N = 30$). For $N < 15$ a fast transition in coherence is observable due to a reduction of $g^{(2)}(0)$ from 1.8 to 1 in both theory and experiment.

Indeed, optical feedback offers a dramatic change of the statistical behavior of photons emitted by QDSLDs. However, a coherence transition is observable even for small number of modes, where the smooth THz-wide Gaussian character disappear. Therefore, the precision of our theory, especially formulated for broadband QDSLD emission, has to be confirmed by a further experiment, retaining the broadband character of emitting QDSLDs. It becomes apparent that a mixed-light experiment, in which coherent light is superimposed with the radiation of a QDSLD, represents an ideal candidate for this challenging examination of the PRAG state quality for describing light emitted by these semiconductor devices.

4.5 MIXING LIGHT FROM TWO SOURCES

In this section we analyze the result of a mixed-light experiment in which light of the QDSLD was superimposed with light from a single-mode laser of angular frequency ω_k (see figure 4.5). More details about this mixed-light experiment is given in reference [122].

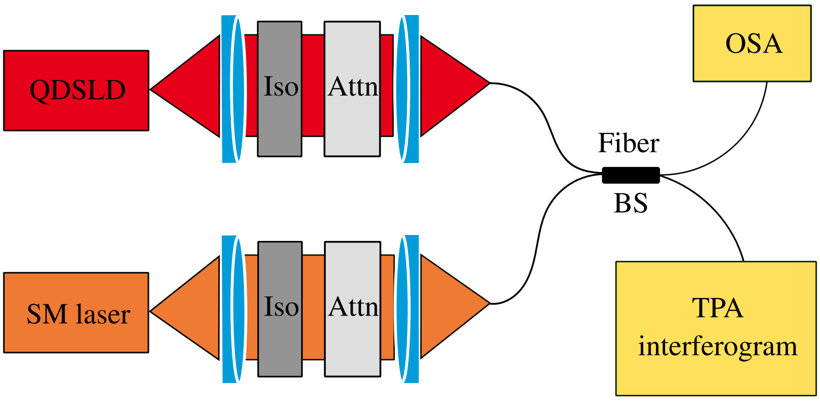

Figure 4.5: Sketch of the setup for the mixed-light experiment [122]. The emitted radiations of two light sources, the QDSLD and the single-mode laser (SM laser), pass through optical isolators (Iso) and attenuators (Attn) and are subsequently superimposed in a fiber-based beam splitter. An optical spectrum analyzer (OSA) and a TPA interferometer measure the desired temporal first- and second-order correlation function of the mixed light.

Generally, the total electric field $\hat{\mathbf{E}}$ of a superposition of a quantized radiation field $\hat{\mathbf{E}}_{\mathrm{Q}}$ and a classical electric field $\boldsymbol{\mathscr{E}}_{\mathrm{cl}} = \mathscr{E}_{\mathrm{cl}}(\mathbf{r},t)\mathbf{e}$ with polarization $\mathbf{e}$ reads

$$\hat{\mathbf{E}}(\mathbf{r},t) = \hat{\mathbf{E}}_{\mathrm{Q}}(\mathbf{r},t) + \mathscr{E}_{\mathrm{cl}}(\mathbf{r},t)\mathbf{e} = \hat{D}^{\dagger}(\mathscr{E}_{\mathrm{cl}}(\mathbf{r},t))\hat{\mathbf{E}}_{\mathrm{Q}}(\mathbf{r},t)\hat{D}(\mathscr{E}_{\mathrm{cl}}(\mathbf{r},t)), \tag{4.28}$$

which is directly applicable the the considered mixed light experiment, where $\hat{\mathbf{E}}_{\mathrm{Q}}$ and $\boldsymbol{\mathscr{E}}_{\mathrm{cl}}$ correspond to the emission of the QDSLD and the single-mode laser. The QDSLD light is again specified by our PRAG state's density operator $\hat{\rho}_s$ defined in equation (4.6) and the single-mode laser is described by a coherent state of amplitude α_k with

$$|\alpha_k\rangle = \hat{D}(\alpha_k)\,|0\rangle = e^{\alpha_k \hat{a}_k^{\dagger} - \alpha_k^* \hat{a}_k}\,|0\rangle\,. \tag{4.29}$$

Therefore, the mixed-light state is given by the operator product (see appendix B)

$$\hat{\rho}_m = \hat{D}(\alpha_k)\hat{\rho}_s\hat{D}^{\dagger}(\alpha_k), \tag{4.30}$$

of displacement and density operator, $\hat{D}(\alpha_k)$ and $\hat{\rho}_s$. Roughly speaking, we add the coherent amplitude α_k to the mode k as a consequence of the beam splitter causing a mixture of the two independent radiation fields of coherent single-mode laser and highly incoherent QDSLD. First- and second-order temporal correlation functions can be determined in an equivalent way as shown in the previous section. Their calculations can be found in appendix B. It turns out that the normalized field correlation $g^{(1)}(\tau)$ as well as the total power P^m for the mixed-light state,

$$g^{(1)}(\tau) = \frac{1}{P^m}\sum_{i=1}^{N} e^{-i\omega_i\tau} p_i^m = \frac{\mathscr{C}}{P^m} G^{(1)}(\tau) \tag{4.31}$$

$$\text{with} \quad P^m = \sum_{i=1}^{N} p_i^m \equiv P^l + P^c + P^t, \quad p_i^m = p_i^l + p_i^c + p_i^t = p_i^l + p_i^s, \tag{4.32}$$

shows the same result as in case of pure QDSLD emission (cf. equation (4.20)), but with an additional term, which describes the contribution of the laser field with optical power,

$$P^l \equiv \sum_{i=1}^{N} p_i^l \quad \text{with} \quad p_i^l = \frac{\hbar\omega_i c_0}{L}|\alpha_i|^2\delta_{ik}. \tag{4.33}$$

Obviously, p_i^l of mode $i = k$ is proportional to the square of the absolute value of the amplitude α_k, while modes $i \neq k$ do not receive amplification by the laser source in agreement to the assumption of purely single-mode emission. The total power is the sum over all single powers of each mode.

POWER SPECTRUM The optical spectrum, given by the Fourier transform of the first-order autocorrelation function $G^{(1)}(\tau)$ can again be expressed in terms of the continuous angular frequency ω (see appendix B) by applying the Euler-Maclaurin approximation. In case of the mixed-light state, the power spectrum[1]

$$S(\omega) = P^l\delta(\omega-\omega_k) + \frac{p^s(\omega)}{\Delta\omega} \tag{4.34}$$

consists of three single spectral distributions, arising from the laser, the QDSLD and the thermal photons. Figure 4.6 shows a sketch of the single contributions. Here, the optical power of the laser light state (green) corresponds to a delta distribution at frequency ω_k, the QDSLD has a Gaussian shape (red) and thermal photons exhibit a Planck distribution (blue).

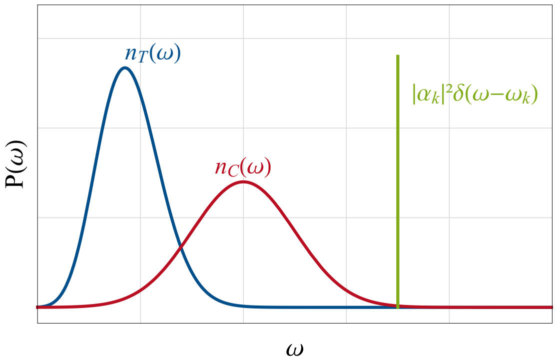

Figure 4.6: Sketch of the spectral distribution for mixed-light. The laser shows a delta distribution (green) and the QDSLD emission is formed by a Gaussian distribution (red) and a thermal Planck distribution (blue).

The normalized second-order temporal autocorrelation function of the superimposed electric field,

$$g^{(2)}(\tau) = 1 + |g^{(1)}(\tau)|^2 - \frac{P^{l2} + \sum_{i=1}^{N} p_i^{c2}}{P^{m2}}, \tag{4.35}$$

described by the density operator in equation (4.30), depends explicitly on the square of the absolute value of the temporal field correlation function

$$|g^{(1)}(\tau)|^2 = \frac{1}{P^{m2}}\Big[P^{l2} + |\sum_{i=1}^{N} p_i^c e^{-i\omega_i\tau}|^2 + |\sum_{i=1}^{N} p_i^t e^{-i\omega_i\tau}|^2 \\ + 2\sum_{i,j=1}^{N} p_j^c p_i^t \cos(\Delta_{ij}\tau) + 2P^l \sum_{i=1}^{N} p_i^s \cos(\Delta_{ik}\tau)\Big] \tag{4.36}$$

---

[1] See also equation (B.29).

with frequency difference $\Delta_{ij} = \omega_i - \omega_j$. Clearly, the last term in equation (4.36) oscillates with beat frequency $\Delta_{ik} = \omega_i - \omega_k$, resulting from the frequency difference of the QDSLD mode i and the laser frequency. This leads to the occurrence of sidebands in the spectrum and finally in the second-order degree of coherence $g^{(2)}(\tau)$.

SPECIAL CASE: SINGLE-MODE MIXED-LIGHT EMISSION ($N = 1$) It is interesting to study the intensity correlation for the special case of a single-mode mixed-light state. Here, the last term in equation (4.35) is equal to one and the square of the absolute value of the first-order degree of coherence (4.36) reduces to $|g^{(1)}(\tau)| = 1$. Therefore, the second-order degree of coherence of a single-mode mixed-light state is

$$g^{(2)}(\tau) = 1, \tag{4.37}$$

in agreement to purely coherent light sources.

SPECIAL CASE: THERMAL MIXED-LIGHT EMISSION For negligible laser and QDSLD emission, that is we are dealing with a purely thermal light source, the last term in (4.35) vanishes and $g^{(2)}(\tau)$ reduces to

$$g^{(2)}(\tau) = 1 + |g^{(1)}(\tau)|^2, \tag{4.38}$$

which is the well-known Siegert relation (cf. equation (2.129)). Equation (4.38) shows a maximum value of 2 for time delay $\tau = 0$, which provides an evidence for the occurrence of bunching as expected.

The second-order correlation function of the mixed-light state for zero time delay is given by

$$g^{(2)}(0) = 2 - \frac{P^{l2} + \sum_{i=1}^{N} p_i^{c2}}{P^{m2}}, \tag{4.39}$$

or alternative in terms of variances and mean values using equation (4.14), (4.16) and (4.33),

$$g^{(2)}(0) = 2 - \frac{1}{N} \frac{1 + \frac{\Delta^2 p^c}{\langle\langle p^c \rangle\rangle^2} + \frac{P^{l2}}{N\langle\langle p^c \rangle\rangle^2}}{\left(1 + \frac{\langle\langle p^t \rangle\rangle}{\langle\langle p^c \rangle\rangle} + \frac{P^l}{N\langle\langle p^c \rangle\rangle}\right)^2}. \tag{4.40}$$

The photon statistics depends on the number of modes N, as in case of pure QDSLD emission, but is also affected by the optical power of the laser.

4.5.1 *Example of a Gaussian shaped diode spectrum*

Regarding the spectral shape of typical measured spectral densities, a single Gaussian spectrum of type

$$p^c(\omega) = P_0^c \frac{\omega \Delta\omega}{\sqrt{2\pi}\sigma\bar{\omega}} e^{-\frac{(\omega-\bar{\omega})^2}{2\sigma^2}} \tag{4.41}$$

with mean frequency $\bar{\omega}$, standard deviation σ and frequency separation $\Delta\omega$ (cf. equation (4.21)) represents obviously an interesting and informative example. The normalization constant P_0^c is specified by the discrete summation of the powers,

$$P^c = \sum_{i=1}^{N} p^c(\omega_i) \simeq \frac{1}{\Delta\omega} \int_{\omega_1}^{\omega_N} \mathrm{d}\omega\, p^c(\omega) = P_0^c. \tag{4.42}$$

which is satisfied by (4.41) under the assumption of the applicability of the Euler-Maclaurin formula. Again, we utilize that NIR photons at room temperature are negligible small so that $p^t(\omega_i) = 0$. After introducing new dimensionless variables $\tilde{\tau} = \sigma\tau$, $\tilde{\bar{\omega}} = \bar{\omega}/\sigma$, $\Delta\tilde{\omega} = \Delta\omega/\sigma$ as well as $\delta\tilde{\omega}_k = \delta\omega_k/\sigma = (\bar{\omega} - \omega_k)/\sigma$, we find the second-order degree of coherence for Gaussian shaped QDSLD emission in terms of the power ratio ε

$$g^{(2)}(\tilde{\tau}) = 1 + \frac{e^{-\tilde{\tau}^2}\left(1 + (\tilde{\tau}/\tilde{\bar{\omega}})^2\right) - \eta + 2e^{-\frac{\tilde{\tau}^2}{2}}\varepsilon\left[\cos\left(\delta\tilde{\omega}_k\tilde{\tau}\right) - \frac{\tilde{\tau}}{\tilde{\bar{\omega}}}\sin\left(\delta\tilde{\omega}_k\tilde{\tau}\right)\right]}{(1+\varepsilon)^2}, \tag{4.43}$$

with

$$\eta = \frac{\Delta\tilde{\omega}}{2\sqrt{\pi}}\left(1 + \frac{1}{2\tilde{\bar{\omega}}^2}\right), \qquad \varepsilon = \frac{P^l}{P^c}. \tag{4.44}$$

The first term in the enumerator of equation (4.43) exhibits an exponentially decreasing behavior, while the second term is a constant offset, which is proportional to the frequency difference $\Delta\tilde{\omega}$ and depends on the mean scaled frequency $\tilde{\bar{\omega}}$. The last term in the enumerator oscillates with beat frequency $\delta\tilde{\omega}_k$ with additional damping behavior. The red line in figure 4.7 shows the intensity correlation of the mixed-light state with a power ratio $\varepsilon = 3/2$ and parameters $\Delta\tilde{\omega} = 10^{-3}$, $\tilde{\bar{\omega}} = 100$ and $\delta\tilde{\omega}_k = 4$. The blue and green line represent pure QDSLD or rather pure laser emission.

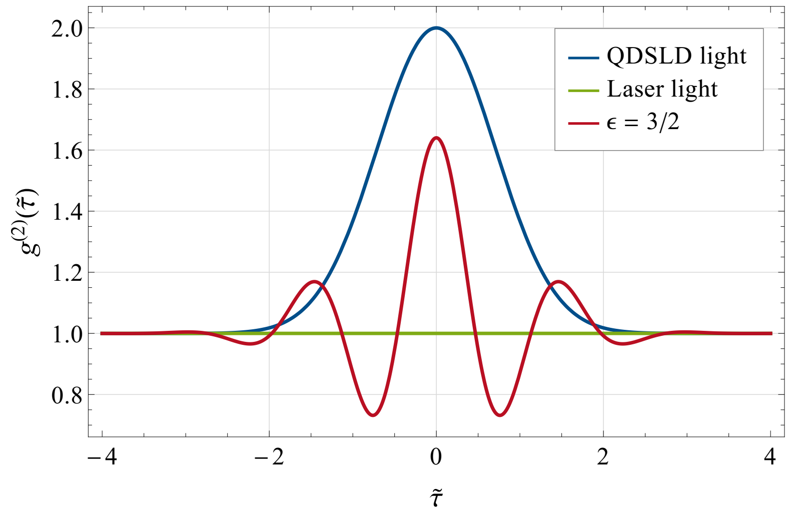

Figure 4.7: Temporal intensity correlation as a function of dimensionless time delay $\tilde{\tau}$ (see equation (4.43)) for a Gaussian-shaped photon number $n_C(\omega_i)$ with parameters $\Delta\tilde{\omega} = 10^{-3}$, $\tilde{\bar{\omega}} = 100$ and $\delta\tilde{\omega}_k = 4$. The red solid line represents mixed-light with $\varepsilon = 3/2$. The blue and green line show emission in absence of laser and QDSLD light, respectively.

For equal space-time events, equation (4.43) reduces to the simple expression

$$g^{(2)}(0) = 2 - \frac{\eta + \varepsilon^2}{(1+\varepsilon)^2}, \tag{4.45}$$

depending significantly on the power ratio ε as well as the frequency width $\Delta\omega$ and the standard deviation σ.

4.5.2 Comparison with experimental results

The considered QDSLD used in the mixed-light experiment consisted of a 4 mm long waveguide with InAs/InGaAs dot-in-well structure. This diode possessed ten active QD layers as well as a high reflective facet on the backside and an anti-reflection coated front facet and produced an optical power spectrum already shown in figure 4.1 with parameters listed in table 4.1. The coherence time was of about $\tau_c = 100$ fs. For the coherent part of the mixed-light superposition, a single-mode quantum-well ridge waveguide Fabry-Pérot laser with central wavelength $\bar{\lambda} = 1300$ nm and spectral width of $b < 2\pi \cdot 1.75 \cdot 10^6$ Hz was used. Both light sources operated at a constant temperature of $T = 20\,^\circ$C and constant DC-pump currents. Thus, thermal contributions are negligible, $n_T(\omega_i) = 0$.

In order to compare our theory with the experimental results in a best way, we introduce a new variable

$$\zeta = \frac{P^l}{P^l + P^c} = \frac{\varepsilon}{1+\varepsilon}, \tag{4.46}$$

considering the different power contribution of laser and SLD in a sense, that only values between 0 and 1 are possible, corresponding to the limiting cases of purely QDSLD ($\zeta = 0$ for $P^l = 0$) and purely single-mode ($\zeta = 1$ for $P^c = 0$) emission. In addition, we utilize the definition of mean value and variance introduced in equation (4.16) and finally we arrive at a new expression for the normalized second-order temporal correlation function (cf. equation (4.35)) in terms of ζ,

$$g^{(2)}(\tau,\zeta) = 1 + |g^{(1)}(\tau)|^2 - \zeta^2 - \frac{1}{N}\left[1 + \frac{\Delta^2 p^c}{\langle\langle p^c \rangle\rangle^2}\right](1-\zeta)^2, \tag{4.47}$$

with first-order correlation (cf. equation (4.31))

$$g^{(1)}(\tau) = \frac{1}{P^l + P^c}\sum_{i=1}^{N} e^{-i\omega_i\tau}(p_i^l + p_i^c) = \frac{\mathscr{C}}{P^l + P^c} G^{(1)}(\tau). \tag{4.48}$$

In the following, we study $g^{(2)}(\tau,\zeta)$ for different values of ζ.

Figure 4.8 shows the result of the second-order correlation as a function of time delay and the corresponding TPA counts for perfect QDSLD light with $\zeta = 0$ (left) and for single-mode emission with $\zeta = 1$ (right). The blue line represents the theoretical model and the red curve reflects the measurements. The theoretical values were calculated using equation (4.47), in which the occurring parameters N and p_i^c were extracted from the measured TPA interferograms in the same way as in the feedback experiment, described in the section before. In the single-mode emission and the broadband QDLSD emission, theory and experiment show an overall good agreement. The broadband character of the QDSLD ($\zeta = 0$) reproduced by the theoretical model exhibits a maximum value of $g^{(2)}_{\text{th}}(0,\zeta = 0) = 1.999$ at $\tau = 0$. This incoherence is verified by the experiment, which provides a value of $g^{(2)}_{\text{exp}}(0,\zeta = 0) = 1.91 \pm 0.05$. A constant second-order autocorrelation function of $g^{(2)}_{\text{th}}(\tau,\zeta = 1) = 1$ predicted by theory is also confirmed by the experimental measurement with $g^{(2)}_{\text{exp}}(\tau,\zeta = 1) = 1.01 \pm 0.04$.

Figure 4.9 shows $g^{(2)}(\tau,\zeta)$ (top) and the corresponding TPA-interferogram (bottom) in arbitrary TPA-count units for $\zeta = 0.6$. Clearly, the interferogram reveals the mixture of the two light sources: for $\tau \gg \tau_c$ the laser emission dominates, however with reduced constructive and destructive interference maxima, which is an apparent indication for the superposition of the two emitters. In the regime of $\tau < \tau_c$, an enhanced correlation arises from the QDSLD emission together with a modulation of the envelope. This behavior reflects again the mixing of the two light sources. The theoretical trajectories (blue) of $g^{(2)}(\tau,\zeta = 0.6)$ (top) show good agreement

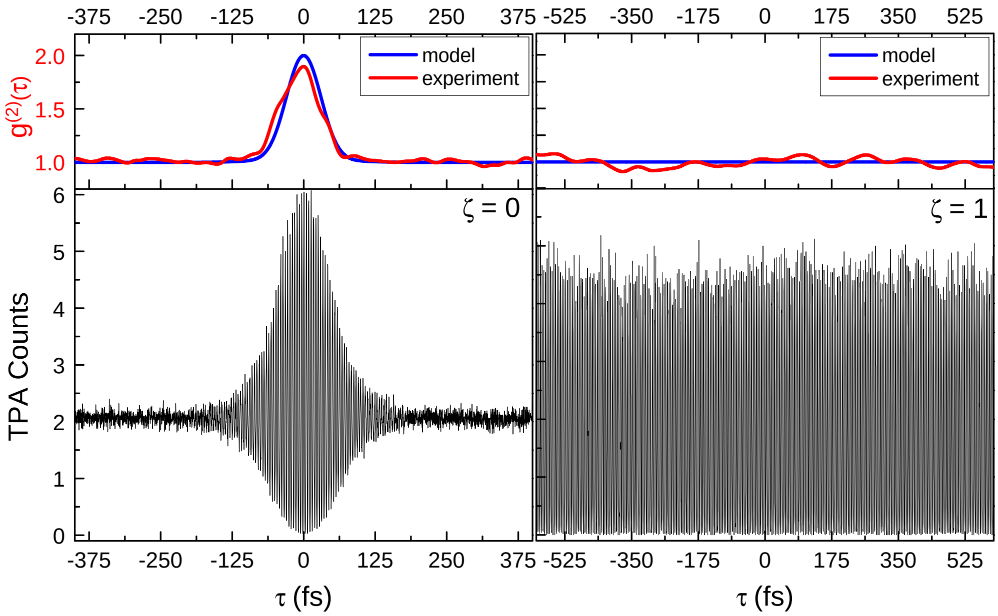

Figure 4.8: Temporal second-order degree of coherence $g^{(2)}(\tau,\zeta)$ as a function of time delay τ (top) and the corresponding TPA interferograms in arbitrary TPA-counts units (bottom) for purely QDSLD light $\zeta = 0$ (left) and purely single-mode emission $\zeta = 1$ (right). The blue lines show the theoretical and the red lines the experimental results of $g^{(2)}(\tau,\zeta)$ [122].

with the experiment (red). A maximum value of $g^{(2)}_{\text{exp}}(0,\zeta = 0.6) = 1.64$ at $\tau = 0$ in the experiment is measured, clearly deviating from the single emissions of the two light sources shown in figure 4.8, but in good agreement with the theoretical prediction of $g^{(2)}_{\text{th}}(0,\zeta = 0.6) = 1.63$.

Additionally, secondary maxima $g^{(2)}(\pm\tau,\zeta = 0.6)$ are observable. These maxima coincide with the spread of the central wavelength of both light sources $\Delta\lambda \approx 64$ nm, leading to a beat frequency of $\tau_{\text{beat}} = \tau_2 \approx 76$ fs, in which our theory reproduces the values τ_2 and $-\tau_2$ as well as the corresponding second-order correlation $g^{(2)}_{\text{th}}(\pm\tau_2,\zeta = 0.6) = 1.1$. Nevertheless, small deviations between theory and experiment are visible, especially in the time regime $0 < |\tau| < |\tau_2|$, where theoretical values smaller than one, $g^{(2)}_{\text{th}}(\tau,\zeta = 0.6) < 1$, are postulated, which are experimentally not accessible due to limited resolution.

Regarding the coherence classification of light sources summarized in (2.132), the central second-order degree of coherence should be studied in more detail in terms of the power ratio ζ, given by

$$g^{(2)}(0,\zeta) = 2 - \zeta^2 - \frac{1}{N}\left[1 + \frac{\Delta^2 p^c}{\langle\langle p^c\rangle\rangle^2}\right](1-\zeta)^2. \tag{4.49}$$

Obviously, varying ζ between the allowed boundary values of $\zeta \in [0,1]$, we achieve a continuous tunability of $g^{(2)}(0,\zeta)$ ranging from Gaussian ($g^{(2)}(0,\zeta) = 2$) to Poissonian ($g^{(2)}(0,\zeta) = 1$) photon statistics. This prediction is experimentally confirmed, as shown in figure 4.10, where the central second-order degree of coherence is plotted as a function of the power ratio ζ. The red linked dots show the calculated theoretical values using equation (4.49) with experimentally determined parameters ζ, N, $\Delta^2 p^c$ and $\langle\langle p^c\rangle\rangle$ (see also table 4.3).

The blue dots with the error bars are the experimental results, exhibiting values between $g^{(2)}(0,\zeta) = 1.91$ and $g^{(2)}(0,\zeta) = 1$ with a parabola-like trajectory. The error bars were determined by applying standard deviation of five averaged experimental values. It should be pointed

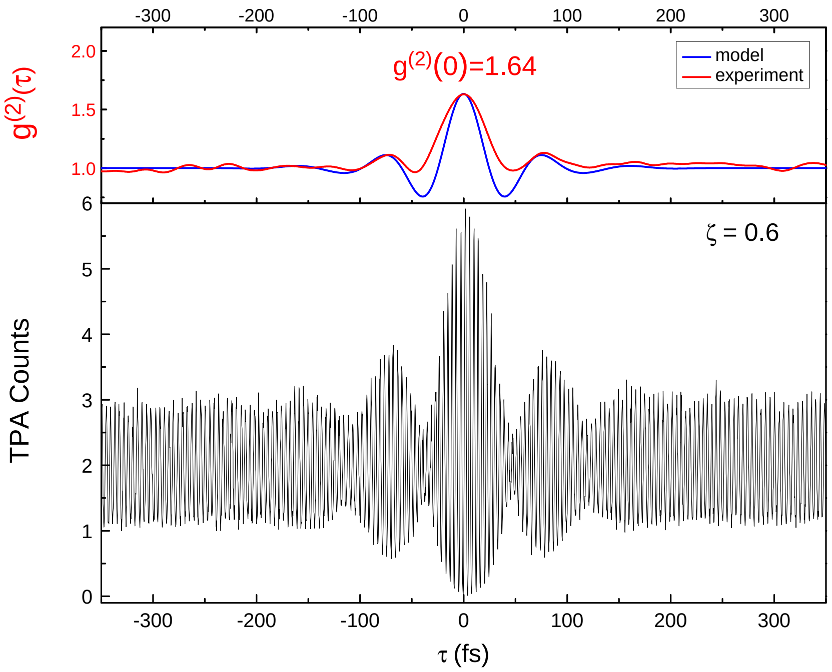

Figure 4.9: Temporal second-order autocorrelation function $g^{(2)}(\tau,\zeta)$ as a function of time delay τ (top) and the corresponding TPA-interferogram in arbitrary units (bottom) for power ratio $\zeta = 0.6$ [122].

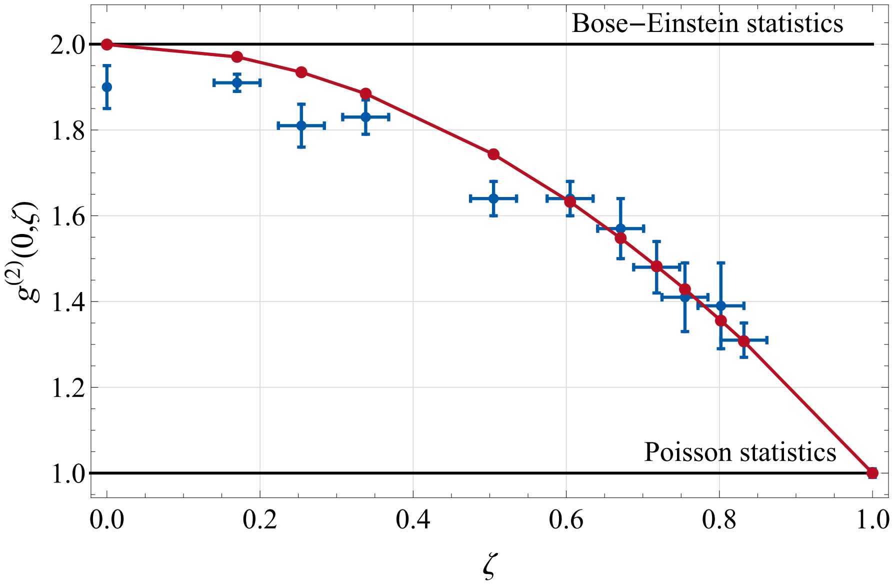

Figure 4.10: Central second-order degree of coherence $g^{(2)}(0,\zeta)$ as a function of ζ [122]. The blue dots with the arrow bars are the experimental data and the red linked dots represents $g^{(2)}(0,\zeta)$ for a mixed-light state described by the density operator (4.30) (with kind permission of S. Blumenstein).

out, that this is the first demonstration of the mixed-light phenomenon using an ultra-broadband emitter [122]. A comparison between the red and blue dots reveals a very good agreement especially for $\zeta \geq 0.6$, where the theoretical values are lying within the statistical uncertainties. With increasing correlation or rather $\zeta < 0.6$, deviations between theory and experiment become apparent, caused by the same technical challenges representing a disturbing factor in the optical

ζ	N	$\frac{\Delta^2 p^c}{\langle\langle p^c \rangle\rangle^2}$	$g^{(2)}_{\mathrm{exp}}(0,\zeta)$	$g^{(2)}_{\mathrm{th}}(0,\zeta)$
0.83 ± 0.03	1990	0.83	1.28 ± 0.03	1.276
0.34 ± 0.03	1990	0.83	1.79 ± 0.04	1.862

Table 4.3: Experimental and theoretical values of $g^{(2)}(0,\zeta)$ for mixed-light with experimentally determined parameters ζ, N and $\Delta^2 p^c / \langle\langle p^c \rangle\rangle^2$.

feedback experiment discussed in the section before [122]. Within this ζ regime, the resulting parabola trend lies below the trajectory of the model. Nevertheless, our model fits the experimental data remarkably well.

In summary, it was demonstrated that our chosen PRAG state is well suited to describe ASE light emitted by a QDSLD at room temperature, as it considers the broadband spectral character and reflects correct intensity correlations, verified by an optical feedback and mixed-light experiment. However, a reduction of $g^{(2)}(0)$ at a special temperature regime around 190 K is not captured by this ansatz, and thus not really applicable to describe the phenomenon of hybrid coherent light. The results of the chapter also shows, that we are not able to avoid the introduction of a detailed description of ASE generated by the semiconductor device itself on a microscopic level. This model has to consider both, the special geometry of the device itself and of course the influence of the gain medium on the emission process. Within this analysis, it should be possible to reconstruct the broadband power spectrum in a straightforward way, which is demonstrated in the following chapter.

5

MICROSCOPIC THEORY OF QUANTUM DOT SUPERLUMINESCENT DIODES

In the last chapter we showed that the postulated quantum state, the PRAG state, describes experimental measurements with QDSLD emission applied to optical feedback and superpositions with coherent light sources in an excellent way. At least at room temperature, this model works quite well which implicates substantial benefits for further studies. However, the fact that a reduction of the second-order correlation function in a specific temperature regime could not be observed within this ansatz, shows that the PRAG states are unsuitable for an explanation of the occurrence of hybrid coherent light emission. Thus we need to study light generation inside the semiconductor device in more detail. In this context, a field theory has to be formulated which considers the specific geometry of the waveguide structure. Also, a realistic model of the gain medium has to be implemented into the total QDSLD system under study. In this chapter we present such a model of the superluminescent diode and study the amplified spontaneous emission on a microscopic level.

Figure 5.1 shows our diode model.

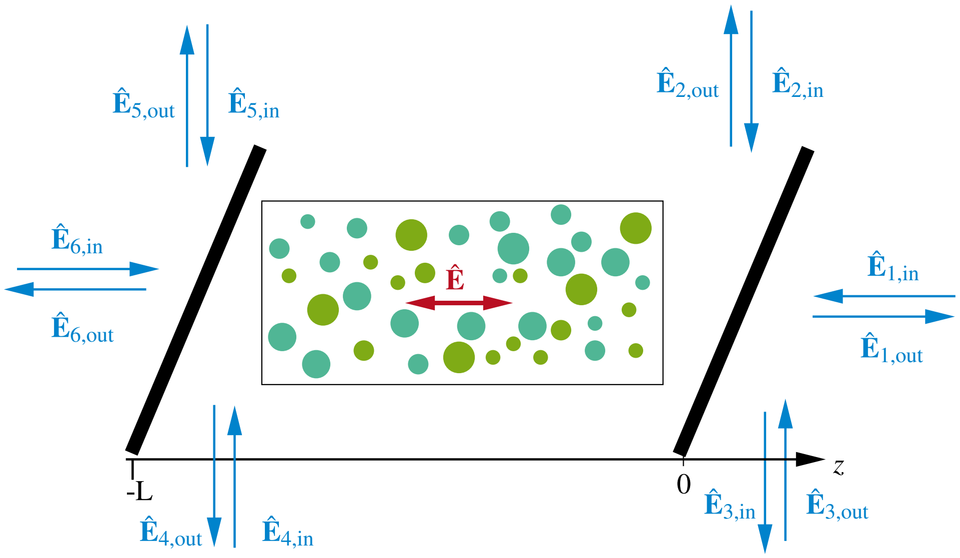

Figure 5.1: Model of a QDSLD. Absorptive bulk material defines a rectangular waveguide, which hosts M QDs (green dots). The tilted end facets of the QDSLD prevent reflection back into the medium and are formally represented by beam splitters. In principle, six discrete, external quantum channels $\hat{\mathbf{E}}_{1\leq i\leq 6}$ couple into the waveguide and interact with the ASE field $\hat{\mathbf{E}}$.

A typical SLD consists of a set of layers (generally of about 6-10) which are spatially separated by another semiconductor material. These layers do not influence each other, they only give rise to an even more inhomogeneously broadened gain medium visible in the optical power spectrum (see figure 3.3). Therefore, for simplicity we only consider one layer of the gain medium. The gain medium is composed of M QDs, which are embedded in a strongly absorptive bulk material that defines a waveguide. This waveguide is assumed to be rectangular, which results in a linear dispersion relation [60].

INTRAWAVEGUIDE RADIATION Clearly, the light generated inside the diode is broadband and must be described by a multimode electrical field [37,51],

$$\hat{\mathbf{E}}(\mathbf{r},t) = \hat{\mathbf{E}}^{(+)}(\mathbf{r},t) + \hat{\mathbf{E}}^{(-)}(\mathbf{r},t). \tag{5.1}$$

For the positive frequency part we consider a superposition of waves propagating along the z-direction,

$$\hat{\mathbf{E}}^{(+)}(\mathbf{r},t) = \hat{E}^{(+)}(\mathbf{r},t)\mathbf{e}_y = \sum_{\{k_i\}} u_i(\mathbf{r})\hat{a}_i(t)\mathbf{e}_y, \tag{5.2}$$

formed by a superposition of N polarized modes

$$u_i(\mathbf{r}) = \mathscr{E}_i \chi(x,y) e^{\mathrm{i}k_i z} \tag{5.3}$$

which factorize into a single transverse wave function $\chi(x,y)$ and longitudinal plane waves with wave vector $\mathbf{k}_i = k_i\mathbf{e}_z$. Here, $k_i = 2\pi i/L$ with $i \in [-N/2, N/2-1]$ and $N/2 \in \mathbb{N}$ depends on the length of the waveguide L. Due to the rectangular geometry of the QDSLD [123], the field is linearly polarized. Without loss of generality, we chose a linear polarization $\mathbf{e}_y$ in y-direction. The transverse mode function is normalized to the cross section area of the waveguide $A = \int_A \mathrm{d}x\mathrm{d}y\,|\chi|^2$. If the system's volume is $V = AL$, then the normalization factor of the electric fields reads $\mathscr{E}_i = \mathrm{i}\sqrt{\hbar\omega_i/2\varepsilon V}$. There is a linear intrawaveguide dispersion relation between frequency ω and wave number $|k_z|$,

$$\omega = c\,|k_z|, \qquad c = c_0/n_c, \tag{5.4}$$

with the speed of light c in the bulk medium of refractive index n_c. This is in contrast to the consideration of chapter 4 where we studied propagation in free space with vacuum velocity c_0.

As we want to pursue a quantum theory, we need to consider bosonic amplitudes $\hat{a}_i$, which satisfy the commutation relations (2.40). Due to energy conservation, a non-vanishing coupling between left- and right-propagating modes of the same k_i inside the diode system is conceivable. However, the presence of a bulk material suppresses possible interference effects between any field modes inside the waveguide system, in fact also between modes of the same frequency, but with opposite propagation direction. Therefore, in good approximation we can neglect this intrawaveguide coupling.

WAVEGUIDE GEOMETRY Tilted end facets on the left- and right-hand side prevent back reflections, experimentally realized by tilting the emission facets as well as using anti-reflection coatings (cf. chapter 3). These end facets are modeled by beam splitters enclosing the active medium. In theory, a lossless beam splitter can be considered as a device which couples a particular set of input modes to a set of particular output modes. As shown in figure 5.2 the beam splitter has four input and four output ports with corresponding bosonic annihilation vector operator $\hat{\mathbf{b}}_{\text{in/out}} = (\hat{b}_{1,\text{in/out}}, \hat{b}_{2,\text{in/out}}, \hat{b}_{3,\text{in/out}}, \hat{b}_{4,\text{in/out}})^T$ being related by the S-matrix [32,128–131],

$$\hat{\mathbf{b}}_{\text{out}} = S\,\hat{\mathbf{b}}_{\text{in}}. \tag{5.5}$$

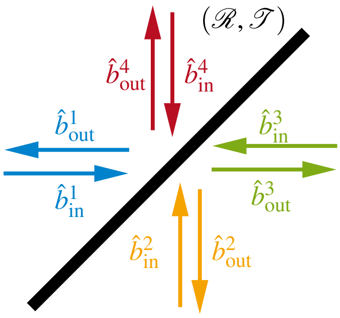

Figure 5.2: Lossless beam splitter with four input and output ports.

S depends on the reflection and transmission amplitudes, $\mathscr{R}$ and $\mathscr{T}$. Here, effects resulting from polarization mismatch as well as imperfect beam collimation [131] are neglected, two important assumptions within our quantum model of a QDSLD. A detailed deviation of the exact form of the scattering matrix will be presented later in this chapter.

As an effective method to describe dissipation, we introduce external fields $\hat{\mathbf{E}}^\alpha$ which couple to the inside. To be specific, six channels[1] labeled by the channel number α (see figure 5.1) enter the waveguide from the left- and right-hand side leading to damping effects of the system. For simplicity, we assume (quasi) one-dimensional electromagnetic fields,

$$\hat{\mathbf{E}}^{\alpha(+)}(\mathbf{r},t) = \sum_{\{k_q\}} v_q^\alpha(\mathbf{r})\hat{b}_q^\alpha(t)e^{-\mathrm{i}\mathbf{k}_q^\alpha\mathbf{r}}\mathbf{e}_y, \tag{5.6}$$

linearly polarized in y-direction with single modes of type [2]

$$v_q^\alpha(\mathbf{r}) = \mathrm{i}\sqrt{\frac{\hbar\omega_q}{2\varepsilon_0 V}}\varsigma^\alpha(\mathbf{r}). \tag{5.7}$$

The transverse mode function $\varsigma^\alpha(\mathbf{r})$ is normalized to the system volume

$$V = \int \mathrm{d}^3r|\varsigma^\alpha(\mathbf{r})|^2 \tag{5.8}$$

and the field amplitudes obey the bosonic commutation relation

$$\left[\hat{b}_q^\alpha(t), \hat{b}_p^{\beta\dagger}(t)\right] = \delta_{\alpha\beta}\delta_{qp}. \tag{5.9}$$

Here, correlations between the channel fields are excluded from our theoretical considerations. However, we permit external channel fields coupling to the inside, to excite waveguide photons moving to both the left and right direction.

To be specific, we consider the electric field from channel 1 propagating along the z-direction (see figure 5.1). The positive frequency part of the total channel field outside the diode is given by

$$\hat{\mathbf{E}}^{1(+)}(\mathbf{r},t) = \hat{\mathbf{E}}_{\text{in}}^{1(+)}(x,y,t+\frac{z}{c_0}) + \hat{\mathbf{E}}_{\text{out}}^{1(+)}(x,y,t-\frac{z}{c_0}), \quad z>0. \tag{5.10}$$

Equation (5.10) states that the total electric field of channel 1 is determined by the sum of the incoming and outgoing field, $\hat{\mathbf{E}}_{\text{in}}^{1(+)}(x,y,t+z/c_0)$ and $\hat{\mathbf{E}}_{\text{out}}^{1(+)}(x,y,t-z/c_0)$ in terms of advanced and retarded time. This result is not quite obvious. A proof of this statement is given in [50] and

---

[1] As the tilted end facets are modeled by beam splitters, we need at least six channels.

[2] In practice, channels of type (5.6) can be realized when the electric fields outside the diode are immediately captured by single-mode fibers which support linearly polarized, single modes specified by (5.7).

summarized in appendix E. Thus, there exist two kinds of field modes; incoming and outgoing. The former influences the dynamics of the internal system of the QDSLD by producing random noise effects and providing an amount of energy, carried away by the outgoing modes leading to damping effects. Therefore, we are dealing with radiation damping which is usually the case whenever a field interpretation of the bath is possible and this is again always possible according to reference [50]. Please note, in contrast to the ASE field inside the waveguide of the QDSLD (see equation (5.1)), the single electromagnetic channel fields outside the diode propagate in vacuo with dispersion relation $\omega_i = c_0|k_i|$. The other optical channels $\hat{\mathbf{E}}^\alpha$ of figure 5.1 can be described in an analogous fashion, but are not required for this discussion. Nevertheless, we will give a detailed expression for each individual channel field later in this chapter.

GAIN MEDIUM The active gain medium is formed by an ensemble of M QDs embedded in an opaque semiconductor material. Due to their spectral properties, each dot can be modeled by a multi-level system. In order to receive light amplification, we need to consider at least three energy levels [18]. Each quantum dot interacts with the multimode ASE field (5.2) and is incoherently pumped with rate R due to the injected current. As we are dealing with a solid, the emitted light experiences a high rate of absorption loss. Therefore, the generated light which is amplified by the dots is absorbed, profoundly. This can be modeled by coupling each transition s of the quantum dot j to a one-dimensional reservoir,

$$\hat{H}^j_\mathrm{b} = \sum_{\{s\}}\sum_{\{k\}} \hbar\omega^j_{sk}\hat{b}^{j\dagger}_{sk}\hat{b}^j_{sk}, \quad s \in \{(21),(20),(10)\,|\,(mn) : |m\rangle \to |n\rangle\}. \tag{5.11}$$

They satisfy the bosonic commutation relation

$$\left[\hat{b}^i_{sk}(t), \hat{b}^{j\dagger}_{sk'}(t)\right] = \delta_{ij}\delta_{kk'}. \tag{5.12}$$

As a further consequence of a high absorption coefficient of solids, interactions between QDs are assumed to be negligible.

5.1 QUANTUM DOTS

Up to now, we have sketched the main ingredients for our microscopic model of a quantum dot superluminescent diode. In the following we have to elaborate this model by having a closer look at the quantum mechanical formulation of the gain medium and the geometry of the waveguide structure, separately. The resulting equations of motion allow to determine emission and photon statistical properties or rather first- and second-order moments, which will be studied in chapter 6 and 7.

Before calculating the electrical output field measured by the detector to determine first- and second-order autocorrelation functions, we have a look at the generation and amplification processes of light inside the gain medium of a quantum dot superluminescent diode. First we examine the interaction of the ASE field with the gain medium inside the QDSLD system. Figure 5.3 shows one of the quantum dot systems under consideration with energy $\hbar\omega_m$ of the m^th level and transition frequency $\omega_{mn} = \omega_m - \omega_n$ between level m and n and corresponding decay rates γ_{mn}. Here, the ASE field (5.2) acts on the transition $|1\rangle \leftrightarrow |2\rangle$ leading to a broad Gaussian power spectrum (see figure 3.3) arising from purely ground state (GS) emission. Higher-order radiation (excited state (ES), second excited state (SES), etc.) is easily implemented within this theoretical model by just incorporating additional levels forming the quantum dot. However, as a first step we want to keep our theory as simple as possible and as we do not believe that

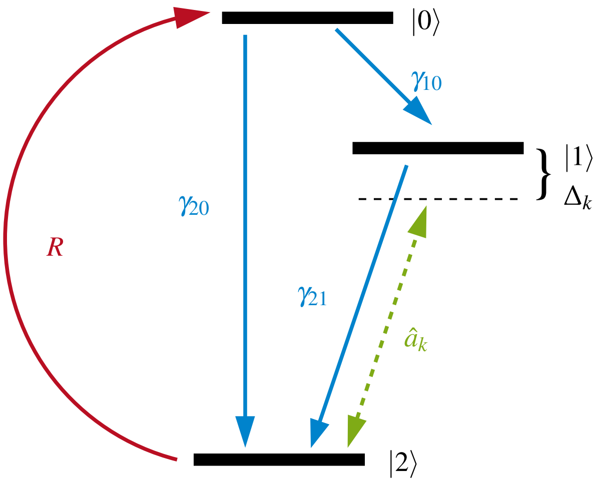

Figure 5.3: Three-level quantum dot energy diagram with decay rates γ_{mn} $(m,n \in \{0,1,2\})$, driven by the ASE radiation field with amplitudes $\hat{a}_k$ and incoherently pumped with rate R.

higher-order emission is a substantial, primary cause for observing hybrid coherent light, we restrict the following discussion to three energy levels.

Due to the experimental observation of an increased decorrelation in a certain temperature regime of $g^{(2)}(0)$, we assume that the radiation field need to be described quantum mechanically. Thus, the Hamilton operator in the Schrödinger picture,

$$\hat{\mathscr{H}}_s = \hat{\mathscr{H}}_r + \hat{\mathscr{H}}_a + \hat{\mathscr{H}}_{\text{int}}, \tag{5.13}$$

is given by the Hamilton operator of the quantized N-mode ASE field,

$$\hat{\mathscr{H}}_r = \sum_{\{k_i\}} \hbar\omega_i \hat{a}_i^\dagger \hat{a}_i, \tag{5.14}$$

the Hamilton operator of the M QDs with transition operators $\hat{\sigma}_{mn}^j = |m\rangle\langle n|$ of the j^{th} QD,

$$\hat{\mathscr{H}}_a = \sum_{j=1}^{M} \sum_{i=0}^{2} \hbar\omega_i^j \hat{\sigma}_{ii}^j, \tag{5.15}$$

and their dipole interaction with the broadband light field in the rotating wave approximation,

$$\hat{\mathscr{H}}_{\text{int}} = -\mathrm{i} \sum_{\{k_i\}} \sum_{j=1}^{M} \hbar g_i^j \hat{\sigma}_{21}^{j\dagger} \hat{a}_i + \text{h.c.}. \tag{5.16}$$

The coupling constant,

$$g_i^j = -\mathrm{i}\mathbf{d}_{21}^{j*} u_i(\mathbf{r}_j)\mathbf{e}_y/\hbar, \tag{5.17}$$

is proportional to the dipole matrix element $\mathbf{d}_{21}^j$ and depends on frequency ω_i[3].

It is useful to switch into a convenient interaction picture in which explicit time-dependent terms are eliminated and in which the radiation field oscillates with a detuning Δ_i of the order of

---

[3] Generally, the dipole operator $\hat{\mathbf{d}} = \sum_{i,j} \mathbf{d}_{ij} |i\rangle\langle j| = \sum_\alpha q_\alpha \hat{\mathbf{r}}_\alpha$ depends on the quantized coordinates $\hat{\mathbf{r}}_\alpha$ of the bound charges q_α relative to the classical center-of-mass position $\mathbf{r}_0$ of the QD. The dipole matrix element in position representation is given by the integral $\mathbf{d}_{ij} = \sum_\alpha q_\alpha \int \mathrm{d}^3 r_\alpha\, \mathbf{r}_\alpha \psi_i^*(\mathbf{r}_\alpha)\psi_j(\mathbf{r}_\alpha)$ over all charge coordinates $\mathbf{r}_\alpha$. For electron states of definite parity, $\psi_i(-\mathbf{r}) = \pm\psi_i(\mathbf{r})$, the matrix element is zero for equal parity, that is $\mathbf{d}_{ii} = \mathbf{0}$.

THz. Here, the interaction state $|\psi(t)\rangle_{\mathrm{I}}$ is related with the state vector in the Schrödinger picture $|\psi(t)\rangle_{\mathrm{S}}$,

$$|\psi(t)\rangle_{\mathrm{I}} = \hat{U}^{\dagger}(t)\,|\psi(t)\rangle_{\mathrm{S}}, \tag{5.18}$$

by the transformation operator

$$\hat{U}(t) = e^{-\mathrm{i}\hat{G}t}, \qquad \hat{G} = \sum_{\{k_i\}} \bar{\omega}_{12}\hat{a}_i^{\dagger}\hat{a}_i + \sum_{j=1}^{M}\left[\omega_0^j\hat{\sigma}_{00}^j + (\omega_1^j - \delta\omega_{12}^j)\hat{\sigma}_{11}^j + \omega_2^j\hat{\sigma}_{22}^j\right]. \tag{5.19}$$

Thus, the system Hamilton operator in the interaction picture reads

$$\begin{aligned} \hat{H}_s &= \mathrm{i}\hbar\dot{\hat{U}}^{\dagger}\hat{U} + \hat{U}^{\dagger}\hat{\mathscr{H}}_s\hat{U} \\ &= \sum_{\{k_i\}} \hbar\Delta_i\hat{a}_i^{\dagger}\hat{a}_i + \sum_{j=1}^{M}\hbar\delta\omega_{12}^j\hat{\sigma}_{11}^j - \sum_{\{k_i\}}\sum_{j=1}^{M}\left[\mathrm{i}\hbar g_i^j(\Delta_i)\hat{\sigma}_{21}^{j\dagger}\hat{a}_i + \mathrm{h.c.}\right]. \end{aligned} \tag{5.20}$$

In this interaction picture, the ASE field oscillates with detuning Δ_i and depends on the mean transition frequency $\bar{\omega}_{12}$ of the QDs defined by

$$\Delta_i = \omega_i - \bar{\omega}_{12}, \qquad \bar{\omega}_{12} = \frac{1}{N}\sum_{\{k_i\}}\omega_i. \tag{5.21}$$

Accordingly, the frequency $\delta\omega_{12}^j = \omega_{12}^j - \bar{\omega}_{12}$ occurring in equation (5.20) represents a small deviation of the j^{th} quantum dot from the mean value $\bar{\omega}_{12}$.

To generate light amplification, the dots are incoherently pumped. In theory, this can be implemented by introducing a pumping rate R acting on transition $|2\rangle \rightarrow |0\rangle$ as shown in figure 5.3. This represents an accurate description for the pumping mechanism inside semiconductor diodes, receiving light amplification by applying a voltage I on the pn-junction. As already mentioned, each driven quantum dot system inside the superluminescent diode is strongly damped due to the surrounding semiconductor material, which can be described by a coupling to a large reservoir. The next subsection is dedicated to this relevant aspect.

5.1.1 Pumping of quantum dots at room temperature

Dissipation processes play a significant role in the context of QDs embedded in a semiconductor bulk material, which we have to take into account when describing light generation in QDSLDs. For the sake of simplicity, we first consider a single quantum dot, $M = 1$, inside the QDSLD driven by the ASE radiation field, specified by the Hamiltonian (5.20). Obviously, the energy correction term in this Hamiltonian in the interaction picture, describing small deviations from the mean frequency of several QDs vanishes in case of a single dot and equation (5.20) reduces to

$$\hat{H}_s = \sum_{\{k_i\}} \hbar\Delta_i\hat{a}_i^{\dagger}\hat{a}_i - \sum_{\{k_i\}}\left[\mathrm{i}\hbar g_i\hat{\sigma}_{21}^{\dagger}\hat{a}_i + \mathrm{h.c.}\right]. \tag{5.22}$$

Naturally, also the index j in equation (5.20), labeling the single QD systems, becomes superfluous and was therefore eliminated. In order to describe a damped, incoherently driven quantum dot, the microscopic model has to be extended by adding an external incoherent pumping rate R as well as coupling the small system to the environment specified by many harmonic oscillators with Hamilton operator introduced in equation (5.11).

In general, for describing a damped quantum system, we consider a small system (S) of operators $\{\hat{S}, \hat{S}^{\dagger}\}$ with Hamilton operator $\mathscr{H}_S$, weakly coupled to a large reservoir (R) with a huge number of unobserved degrees of freedom, described by a Hamiltonian composed of many harmonic oscillators (see equation (5.11)). Please note, that we are only interested in the dynamics of the small system (S) so that the exact form of both, the environment and the coupling constant, is not relevant. This physical problem can be studied in detail in the Schrödinger or Heisenberg picture. The resulting equations of motion are called *master equation* or *quantum Langevin equation*, respectively. The former describes the dynamics of the reduced density operator of the small system whereas the quantum Langevin equations specify the time evolution of the dynamical variables of this subsystem. Here, we concentrate on the description of damping in the Schrödinger picture in which all operators possess at most an explicit time dependency. A detailed derivation of the master equation is given in appendix D[4]. In the following we just highlight the main assumptions and approximations necessary to achieve this density operator equation of motion.

MASTER EQUATION The dynamics of a quantum system described by the temporal derivative of the density operator $\hat{\rho}$ is determined by the Liouville von Neumann equation,

$$\dot{\hat{\rho}}(t) = -\frac{i}{\hbar}\left[\hat{\mathsf{H}}, \hat{\rho}\right], \tag{5.23}$$

given by the commutator of $\hat{\rho}$ and the total system Hamiltonian

$$\hat{\mathsf{H}} = \hat{\mathsf{H}}_{\mathrm{S}} + \hat{\mathsf{H}}_{\mathrm{R}} + \hat{\mathsf{H}}_{\mathrm{I}} \tag{5.24}$$

in the Schrödinger picture. Here, $\hat{\mathsf{H}}_{\mathrm{S}}$ is the Hamiltonian of the small system whose interaction is described by the system's deexcitation and excitation operators $\{\hat{S}^\dagger, \hat{S}\}$[5]. $\hat{\mathsf{H}}_{\mathrm{R}}$ is the reservoir Hamilton operator and the interaction between system and environment is described by $\hat{\mathsf{H}}_{\mathrm{I}}$. At the initial time $t = 0$, the environment, consisting of many harmonic oscillators with Hamiltonian $\hat{\mathsf{H}}_{\mathrm{R}}$, is assumed to be in a stationary state and decorrelated with the small system. The coupling energy between the system and its environment is supposed to be weak, so that the system's action on the dynamics of the environment is negligible. The state of the total system approximately factorizes into a tensor product of the time-dependent system's density operator and the stationary density operator of the reservoir (Born approximation). Taking the trace over the reservoir degrees of freedom and applying the iteration method to the Liouville equation results in an integro-differential equation for the reduced system's density operator $\hat{\rho}_{\mathrm{S}}(t) = \mathrm{Tr}_{\mathrm{R}}\{\hat{\rho}(t)\}$. The time scales over which the correlation functions of the environment decay, are assumed to be much smaller than the evolution time scales of the system. The environment loses its memory on time scales larger than the correlation time of the reservoir fluctuations. Within the Markov approximation reservoir correlation functions are replaceable by delta distributions. Taking into account all mentioned assumptions and approximations we end up in a **master equation** for the density matrix of the open system in Lindblad form [132]

$$\frac{\mathrm{d}}{\mathrm{d}t}\hat{\rho}_{\mathrm{S}}(t) = (\mathfrak{L}_{\mathrm{S}} + \mathfrak{L}_{\mathrm{R}})\hat{\rho}_{\mathrm{S}}(t). \tag{5.25}$$

---

[4] The derivation of the master equation in appendix D considers a continuum version of the reservoir Hamiltonian (5.11). A formulation in terms of discrete modes is analogous.

[5] E.g. the operators $\hat{S}, \hat{S}^\dagger$ could be annihilation and creation operators of a cavity mode or the excitation and deexcitation operators of a two-level system.

Here, the system Liouville operator $\mathfrak{L}_{\mathrm{S}}\,\hat{\rho}_{\mathrm{S}}(t) = -\frac{\mathrm{i}}{\hbar}\left[\hat{\mathsf{H}}_{\mathrm{S}}, \hat{\rho}_{\mathrm{S}}\right]$, describes the unperturbed system and the damping Liouvillian,

$$\begin{aligned} \mathfrak{L}_{\mathrm{R}}\,\hat{\rho}_{\mathrm{S}}(t) =& \Gamma(\underbrace{\bar{N}(0)}_{\text{stim. emission}} + \underbrace{1}_{\text{spon. emission}})(2\hat{S}\hat{\rho}_{\mathrm{S}}(t)\hat{S}^{\dagger} - \hat{S}^{\dagger}\hat{S}\hat{\rho}_{\mathrm{S}}(t) - \hat{\rho}_{\mathrm{S}}(t)\hat{S}^{\dagger}\hat{S}) \\ &+ \underbrace{\Gamma\bar{N}(0)}_{\text{stim. absoption}}\,(2\hat{S}^{\dagger}\hat{\rho}_{\mathrm{S}}(t)\hat{S} - \hat{S}\hat{S}^{\dagger}\hat{\rho}_{\mathrm{S}}(t) - \hat{\rho}_{\mathrm{S}}(t)\hat{S}\hat{S}^{\dagger}) \\ &- \mathrm{i}\left[\delta\omega\hat{S}^{\dagger}\hat{S} + \delta\omega_{\mathrm{th}}\left[\hat{S}^{\dagger}, \hat{S}\right], \hat{\rho}_{\mathrm{S}}(t)\right], \quad \delta\omega_{\mathrm{th}} = \mathscr{P}\int \mathrm{d}\Delta\,|W(\Delta)|^{2}\bar{N}(\Delta)/\Delta, \end{aligned} \tag{5.26}$$

considers the coupling between environment and system, leading to dissipation captured by a relaxation rate Γ, energy shift $\delta\omega$ as well as thermal energy shift $\delta\omega_{\mathrm{th}}$ depending on the thermal occupation number $\bar{N}(\Delta)$. The first term in the damping Liouvillian (cf. equation (5.26)) characterizes spontaneous and stimulated emission whereas the second one specifies stimulated absorption processes. The last term includes the mentioned energy shifts which can be eliminated by appropriate renormalization.

More generally, for a set of system operators $\{\hat{S}_i, \hat{S}_i^{\dagger}\}$ the master equation is extendable by summing over all these system operators with corresponding damping rates Γ_i and occupation numbers $\bar{N}_i$. For adaptable renormalization of the energy shifts, the **multicomponent master equation** for the reduced density operator reads

$$\begin{aligned} \frac{\mathrm{d}}{\mathrm{d}t}\hat{\rho}_{\mathrm{S}}(t) =& -\frac{\mathrm{i}}{\hbar}\left[\hat{\mathsf{H}}_{\mathrm{S}}, \hat{\rho}_{\mathrm{S}}\right] + \sum_i \Gamma_i(\bar{N}_i + 1)(2\hat{S}_i\hat{\rho}_{\mathrm{S}}(t)\hat{S}_i^{\dagger} - \hat{S}_i^{\dagger}\hat{S}_i\hat{\rho}_{\mathrm{S}}(t) - \hat{\rho}_{\mathrm{S}}(t)\hat{S}_i^{\dagger}\hat{S}_i) \\ &+ \sum_i \Gamma_i\bar{N}_i(2\hat{S}_i^{\dagger}\hat{\rho}_{\mathrm{S}}(t)\hat{S}_i - \hat{\rho}_{\mathrm{S}}(t)\hat{S}_i\hat{S}_i^{\dagger} - \hat{S}_i\hat{S}_i^{\dagger}\hat{\rho}_{\mathrm{S}}(t)). \end{aligned} \tag{5.27}$$

This important equation of motion for the system's density operator $\hat{\rho}_{\mathrm{S}}$ can be directly applied to our problem of a single quantum dot embedded in the isolated semiconductor waveguide depicted in figure 5.1. What we find is nothing else but Bloch equations, characterizing the temporal dynamics of the quantum dot populations and coherences which will be explicitly demonstrated in the next section.

5.1.2 Response, gain and inversion of a quantum dot at room temperature

Regarding the results of the two mentioned experiments in chapter 4 performed at room temperature, the temporal autocorrelation properties in first- and second-order of QDSLDs are very similar to usual diodes, showing broad Gaussian shaped spectral densities as well as incoherent photon statistics with a central second-order correlation function of approximately 2. Thus, at a first glance it does not seem to be necessary to treat the ASE light field quantum mechanically. In order to analyze optimal response and gain of a driven single quantum dot with classical center-of-mass position $\mathbf{r}_0$ in the diode system at room temperature, we first investigate a single-mode, time-harmonic ASE field with space dependent amplitude $\mathbf{E}(\mathbf{r})$ and angular frequency ω

$$\mathbf{E}(\mathbf{r},t) = \mathbf{E}(\mathbf{r})e^{-\mathrm{i}\omega t} + \text{c.c.}. \tag{5.28}$$

Please remember, usual atoms moving with a certain velocity induce a Doppler-shift in the classical single-mode field frequency. However, a QD is a static system and the dependency of the position variable in the general expression of field amplitude in (5.28) can be eliminated. Thus, $\mathbf{E}(\mathbf{r})$ only depends on the constant center-of-mass position $\mathbf{r}_0$ of the considered QD, $\mathbf{E}(\mathbf{r}) = \mathbf{E}(\mathbf{r}_0)$.

The total Hamilton operator of this three-level system interacting with a classical light field in rotating wave approximation is given by

$$\hat{\mathsf{H}}_{\mathrm{cl}} = \sum_{i=0}^{2} \hbar\omega_i \hat{\sigma}_{ii} - \hbar\Omega e^{-\mathrm{i}\omega t} \hat{\sigma}_{21}^{\dagger} - \hbar\Omega^* e^{\mathrm{i}\omega t} \hat{\sigma}_{21}. \tag{5.29}$$

Here, we introduced the characteristic physical quantity known as Rabi frequency,

$$\Omega(\mathbf{r}_0) = \frac{\mathbf{d}_{21}^* \mathbf{E}(\mathbf{r}_0)}{\hbar}, \tag{5.30}$$

depending on the dipole matrix element $\mathbf{d}_{21}$ and the field amplitude $\mathbf{E}(\mathbf{r}_0)$ at the QD's position $\mathbf{r}_0$. Again, we switch into a suitable interaction picture according to equation (5.18) with transformation operator

$$\hat{U}(t) = e^{-\mathrm{i}\hat{G}t}, \qquad \hat{G} = \hbar\omega_0\hat{\sigma}_{00} + \hbar(\omega_1 + \Delta)\hat{\sigma}_{11} + \hbar\omega_2\hat{\sigma}_{22}, \quad \Delta = \omega - \omega_{12}. \tag{5.31}$$

Thus, the Hamiltonian in this interaction picture oscillating with frequency detuning Δ is determined by

$$\hat{H}_{\mathrm{cl}}(t) = -\hbar\Delta\hat{\sigma}_{11}(t) - \hbar\Omega^*\hat{\sigma}_{21}(t) - \hbar\Omega\hat{\sigma}_{21}^{\dagger}(t). \tag{5.32}$$

Applying the multicomponent master equation (5.27), we find the equation of motion for the reduced density operator considering coherent evolution of the system described by the commutator of the density operator with the system Hamiltonian (5.32) and irreversible damping effects. The sum in equation (5.27) extends over all possible quantum dot transitions $i \in \{(21),(20),(10)\}$ with system operators corresponding to the quantum dot lowering operators, $\hat{S}_i = \hat{\sigma}_i$. Introducing an incoherent pumping rate [133–135] $R = \gamma_{20}\bar{N}_{20}$ proportional to the photon number $\bar{N}_{20}$, we find *optical Bloch equations* [51] for a driven quantum dot interacting with a single-mode classical radiation field

$$\dot{\rho}_{00}(t) = -2(R + \gamma_{20} + \gamma_{10})\rho_{00} + 2R\rho_{22}, \tag{5.33}$$

$$\dot{\rho}_{11}(t) = -\mathrm{i}\Omega^*\rho_{12} + \mathrm{i}\Omega\rho_{11} - 2\gamma_{21}\rho_{11} + 2\gamma_{10}\rho_{00}, \tag{5.34}$$

$$\dot{\rho}_{22}(t) = -2R\rho_{22} + \mathrm{i}\Omega^*\rho_{12} - \mathrm{i}\Omega\rho_{21} + 2\gamma_{21}\rho_{11} + 2(R + \gamma_{20})\rho_{00}, \tag{5.35}$$

$$\dot{\rho}_{10}(t) = (\mathrm{i}\Delta - \gamma_{21} - R - \gamma_{20} - \gamma_{10})\rho_{10} + \mathrm{i}\Omega\rho_{20}, \tag{5.36}$$

$$\dot{\rho}_{12}(t) = (\mathrm{i}\Delta - \gamma_{21} - R)\rho_{12} + \mathrm{i}\Omega(\rho_{22} - \rho_{11}), \tag{5.37}$$

$$\dot{\rho}_{20}(t) = -(2R + \gamma_{20} + \gamma_{10})\rho_{20} + \mathrm{i}\Omega^*\rho_{10}, \tag{5.38}$$

with $\rho_{ij} = \langle i|\,\hat{\rho}_{\mathrm{S}}\,|j\rangle$, $\rho_{ij} = \rho_{ji}^*$, $\gamma_{ij} = \gamma_{ji}$ and vanishing thermal occupation numbers, $\bar{N}_{21} = \bar{N}_{10} = 0$. Figure 5.4 visualizes the time evolution of the populations for a QD system initially in its ground state with zero coherences ($\rho_{22}(0) = 1$, $\rho_{00}(0) = \rho_{11}(0) = 0$ and $\rho_{ij}(0) = 0$ with $i \neq j$).

The quantum dot is incoherently pumped with rate $R = 5\gamma_{21}$, driven by a single-mode radiation field of Rabi frequency $\Omega = \gamma_{21}$ and zero detuning, $\Delta = 0$. The damping rate from the highest to the lowest state in both cases is assumed to be negligibly small, $\gamma_{20} = 0$. In figure 5.4 (left) we have chosen an upper decay rate of $\gamma_{10} = 0.1\gamma_{21}$. The ground state population indeed decreases but is always higher than the population for the upper energy states, that is no inversion between level $|1\rangle$ and $|2\rangle$ ($w = \rho_{11} - \rho_{22} < 0$) or no amplification of the system is observable, respectively. For $\gamma_{10} = 10\gamma_{21}$ depicted in figure 5.4 (right), the population of the ground state decreases much faster. Furthermore, for $\gamma_{21}t > 0.14$ the ground state population is below the population of the intermediate level $|1\rangle$, that is inversion ($w > 0$) arises.

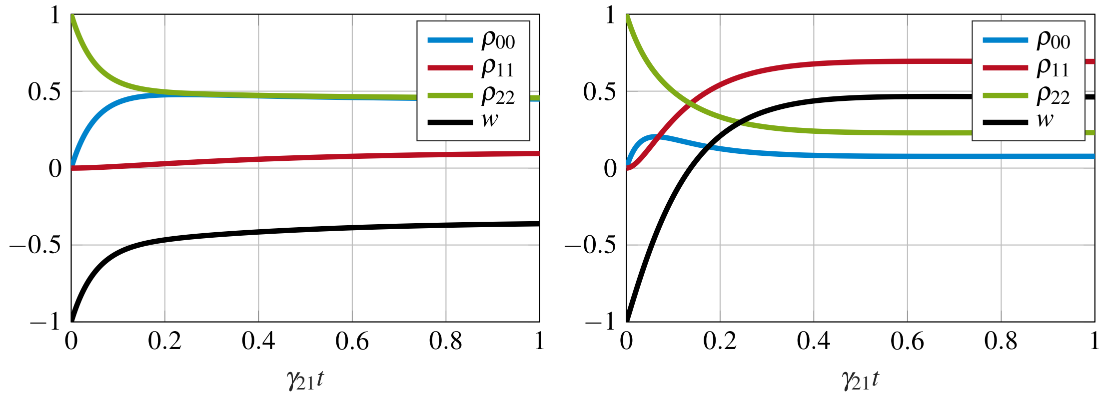

Figure 5.4: Time evolution of the populations from a single QD initially in its ground state, incoherently pumped with $R = 5\gamma_{21}$, driven by a single-mode radiation field of Rabi frequency $\Omega = \gamma_{21}$ and zero detuning, $\Delta = 0$, as well as a radiation damping $\gamma_{20} = 0$. Different damping rates of the upper transition exhibit negative inversion between level $|1\rangle$ and $|2\rangle$ ($w = \rho_{11} - \rho_{22} < 0$) for $\gamma_{10} = 0.1\gamma_{21}$ (left) and positive inversion ($w = \rho_{11} - \rho_{22} > 0$) for $\gamma_{10} = 10\gamma_{21}$ (right).

The polarization density **P**, that is the number of dipole moment per unit volume, induced by the external electric field (5.28) is given by the expectation value of the dipole operator $\hat{\mathbf{d}}$ times the quantum dot density $\mathcal{N}$ [136],

$$\mathbf{P} = \mathcal{N}\,\mathrm{Tr}\{\hat{\mathbf{d}}\hat{\rho}_S\}. \tag{5.39}$$

On the other hand, in case of an isotropic medium and linear response [137, 138], the polarization density is related with the electric field via

$$\mathbf{P}(\omega) = \varepsilon_0 \chi^{(1)}(\omega)\mathbf{E}(\omega), \tag{5.40}$$

which defines a linear susceptibility $\chi^{(1)}$. In terms of the QD off-diagonal element of the density matrix ρ_{21}, the susceptibility reads

$$\boxed{\chi^{(1)} = \chi' + \mathrm{i}\chi'' = \frac{\mathcal{N}\,|\mathbf{d}_{21}|^2}{\hbar\varepsilon_0\Omega}\rho_{21} = \frac{1}{\alpha}\rho_{21}, \quad \alpha = \frac{\hbar\varepsilon_0\Omega}{\mathcal{N}\,|\mathbf{d}_{21}|^2}}. \tag{5.41}$$

The real part χ' describes the dispersion whereas the imaginary part χ'' characterizes loss (for $\chi'' > 0$) or rather gain (for $\chi'' < 0$) depending on the sign of χ''. Figure 5.5 shows the stationary, real (blue dashed line) and imaginary (red solid line) part of ρ_{21} as a function of scaled frequency detuning Δ/γ_{21} for $R = 5\gamma_{21}$, $\Omega = \gamma_{21}$ and $\gamma_{20} = 0$. Again, we have chosen the upper decay rates $\gamma_{10} = 0.1\gamma_{21}$ (left) and $\gamma_{10} = 10\gamma_{21}$ (right). The red curve progression in figure 5.5 (left) reveals a negative Lorentzian shaped imaginary ρ_{21} for varying detuning, an indication for an absorbing system in contrast to figure 5.5 (right), where positive $\mathrm{Im}(\rho_{21})$ assures amplification of the radiation field propagating in the medium under consideration. At zero detuning, the absorption (left) and amplification (right) reach their minimum and maximum value, respectively, whereas the dispersion simultaneously vanishes.

For modeling a QDSLD, the single QD system embedded in a bulk medium of high refractive index has to be extended to a many-body system consisting of a huge set of slightly different QDs randomized in the waveguide. Therefore, these nano-structures have to be treated as being distinguishable and located at different positions. The results of a driven quantum dot system can be directly picked up by just summarizing over all M QDs. The assumption of absent correlations

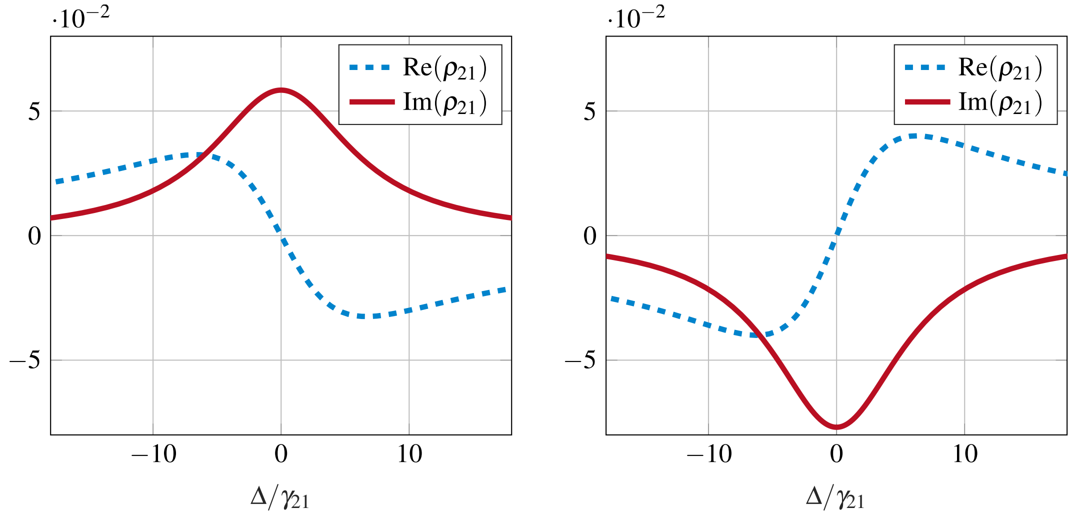

Figure 5.5: Real (blue dashed line) and imaginary (red solid line) part of ρ_{21} as a function of scaled detuning Δ/γ_{21} for a three-level quantum dot incoherently pumped with rate $R = 5\gamma_{21}$, driven by a single-mode radiation field of Rabi frequency $\Omega = \gamma_{21}$ with damping rates $\gamma_{20} = 0$. The case $\gamma_{10} = 0.1\gamma_{21}$ shows absorption (left) whereas $\gamma_{10} = 10\gamma_{21}$ corresponds to an amplified system (right).

between the dots strongly simplifies further investigations. However, as already mentioned before, we suppose that quantum effects cause the observed coherence in the second-order correlation. Therefore, we have to replace the classical single-mode field by a multimode quantized radiation field in the sense of equation (5.1). However, as this is again straightforward we will directly implement this assumption to the total superluminescent diode model including all mentioned important device characteristics like e.g. the geometry of the output facets considered in the following.

5.2 WAVEGUIDE GEOMETRY

A broadband emission spectrum observable for quantum dot superluminescent diodes originates not only from distinguishable, inhomogeneous broadened QDs, but also from a special structure of the waveguide. Here, the output facets are slightly tilted and anti-reflection coated in order to suppress the formation of longitudinal modes. As motivated before, this geometrical feature can be modeled by two beam splitters enclosing the active medium. In the following, this beam splitter configuration will be discussed in detail. Subsequently, we consider the emission of the empty superluminescent diode meaning that any quantum dot or similar gain medium as well as any intrawaveguide absorption losses are absent.

5.2.1 Empty superluminescent diode

We investigate the output field of an empty superluminescent diode under consideration of the facet geometry measured by a single photon detector located at the right-hand side of the diode. Figure 5.6 illustrates the empty diode with the two beam splitters modeling the output facets. The electrical fields $\hat{\mathbf{E}}^{\alpha}(\mathbf{r},t)$ of amplitudes $\hat{b}^{\alpha}_{i,\mathrm{in}}$ and $\hat{\tilde{b}}^{\alpha}_{i,\mathrm{out}}$ striking these facets from the left- and right-hand side are enumerated by the channel number $\alpha = 1,...,8$. They interact with an N-mode electric field of amplitudes $\hat{a}_i$ inside a virtual cavity.

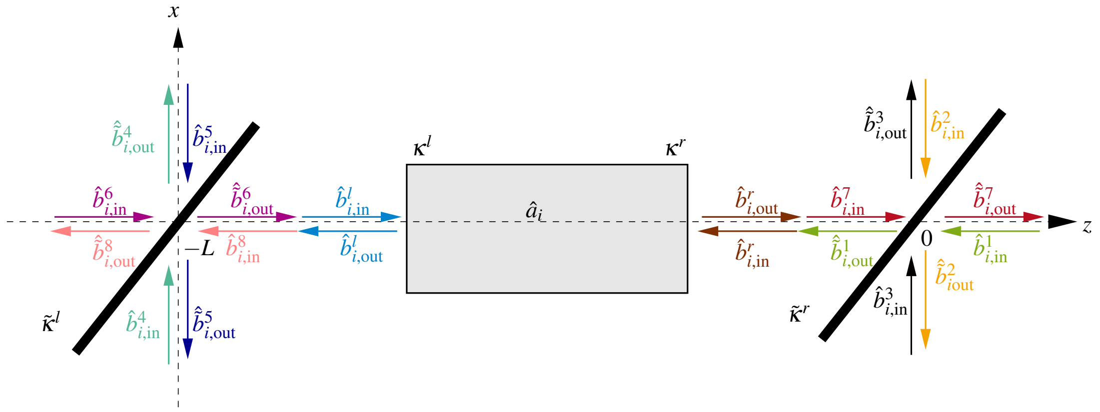

Figure 5.6: Sketch of the field channels $\hat{\mathbf{E}}^\alpha(\mathbf{r},t)$ of amplitudes $\hat{b}^\alpha_{i,\mathrm{in}}$ and $\hat{b}^\alpha_{i,\mathrm{out}}$ ($\alpha = 1,...,8$) which strike the output facets of the QDSLD from the left- and right-hand side and interact with a multimode field of amplitude $\hat{a}_i$ inside.

CASCADED SYSTEM As an important simplification, we subdivide the tilted device in figure 5.6 into three separable physical regimes (see figure 5.7): beam splitter (system *I*), virtual cavity (system *II*) and beam splitter (system *III*), which corresponds to a so called cascaded system, a standard tool in signal theory, that was introduced to the quantum world by *C. W. Gardiner* and *P. Zoller* [139] in the context of quantum communications [50, 140]. A similar formalism was developed by *H. J. Carmichael* [141] as well as *M. I. Kolobov* and *I. V. Sokolov* [142].

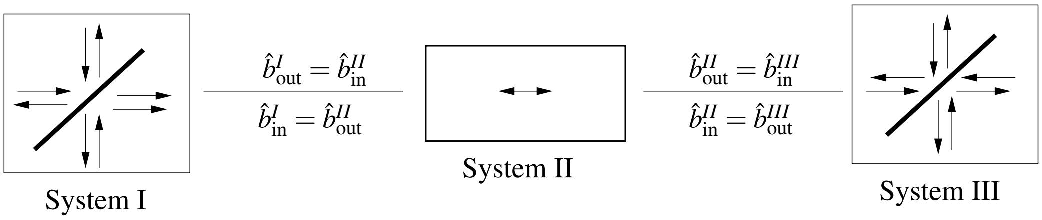

Figure 5.7: QDSLD model represented as a cascaded system composed of three subsystems, two beam splitters (system I and system III) and a cavity (system II). For negligible propagation times between the subsystems, the output of one system is instantaneously the input of the subsequent system.

In general, the output of one system *I* is the input of the second system *II* shifted by time delay τ (the same holds for the output of system *II* being the input of system *III*) according to

$$\hat{b}^{II}_{\mathrm{in}}(t) = \hat{b}^{I}_{\mathrm{out}}(t-\tau) \approx \hat{b}^{I}_{\mathrm{out}}(t), \quad \text{for} \quad \tau \to 0^+, \tag{5.42}$$

$$\hat{b}^{III}_{\mathrm{in}}(t) = \hat{b}^{II}_{\mathrm{out}}(t-\tau) \approx \hat{b}^{II}_{\mathrm{out}}(t), \quad \text{for} \quad \tau \to 0^+. \tag{5.43}$$

Please note, in our simplified empty diode model, the reverse scenario is also admissible, that is

$$\hat{b}^{II}_{\mathrm{in}}(t) = \hat{b}^{III}_{\mathrm{out}}(t-\tau) \approx \hat{b}^{I}_{\mathrm{out}}(t), \quad \text{for} \quad \tau \to 0^+, \tag{5.44}$$

$$\hat{b}^{I}_{\mathrm{in}}(t) = \hat{b}^{II}_{\mathrm{out}}(t-\tau) \approx \hat{b}^{II}_{\mathrm{out}}(t), \quad \text{for} \quad \tau \to 0^+, \tag{5.45}$$

in contrast to [50]. Figure 5.7 sketches the cascaded quantum system for the case of negligible propagation time τ between the single systems.

Two sub-systems are given by beam splitters, which couple the external field modes to the inside with corresponding coupling constants $\tilde{\kappa}^l$ and $\tilde{\kappa}^r$. The output fields of the beam splitters with amplitudes $\hat{\hat{b}}^6_{i,\text{out}}$ and $\hat{\hat{b}}^1_{i,\text{out}}$ interact with radiation field $\hat{\mathbf{E}}$ of amplitudes $\hat{a}_i$ (see equations (5.1)-(5.2)), which in turn propagates inside a virtual cavity with coupling strength κ^l and κ^r. Both mirrors of this cavity are assumed to be semi-transparent and satisfy frequency conservation so that every photon striking the mirrors is reflected and transmitted without changing the absolute value of the wave vector. With respect to the entire QDSLD model including gain and absorption processes, we disregard any coupling between left- and right-propagating internal modes of the same k_i. As already mentioned, this assumption is quite appropriate in presence of a bulk material suppressing any interference effects between field modes. Nevertheless, we allow that external radiation fields which couple into the cavity from the left- and right-hand side respectively, excite cavity photons moving forwards and backwards. At first glance, it seems to be unnecessary to introduce a virtual cavity instead of a dielectric slab, especially in the context of the existent mode suppression caused by the special end facet's geometry modeled by beam splitters. However, regarding the phenomenon of hybrid coherent light highlighting an increasing coherence in terms of the second-order correlation at a particular temperature regime, the choice of a fictitious cavity is reasonable.

In addition, the mentioned spatial separation between the cavity and the output facets does not exist in reality. It is rather a simplification by separating it into a set of simple problems. This means that the spatial distances between the beam splitters and the fictive cavity and therefore the free propagation time from the first system to the second one and so on is equal to zero. Therefore, the output fields of the enclosing systems propagating in cavity direction parallel to the z-axis, coincide with the input fields of the cavity system and no time delay is observable in agreement to the approximation made in equation (5.42). Regarding the chosen notation used in figure 5.6, this predication implies the equivalence of the field amplitudes

$$\begin{aligned}\hat{\hat{b}}^6_{i,\text{out}}(t) &= \hat{b}^l_{i,\text{in}}(t),\\ \hat{\hat{b}}^1_{i,\text{out}}(t) &= \hat{b}^r_{i,\text{in}}(t),\\ \hat{b}^l_{i,\text{out}}(t) &= \hat{b}^8_{i,\text{in}}(t),\\ \hat{b}^r_{i,\text{out}}(t) &= \hat{b}^7_{i,\text{in}}(t).\end{aligned} \tag{5.46}$$

WELL RESOLVED LINES Before formulating the total Hamilton operator of the cascaded system we first make some restrictions with regard to the coupling of the external fields with the internal one. Each of the many modes of the ASE field is assumed to couple only to a certain range of frequencies, so-called coupling bandwidth [139], from each field outside without overlapping with neighboring frequency ranges. Figure 5.8 illustrates this hypothesis.

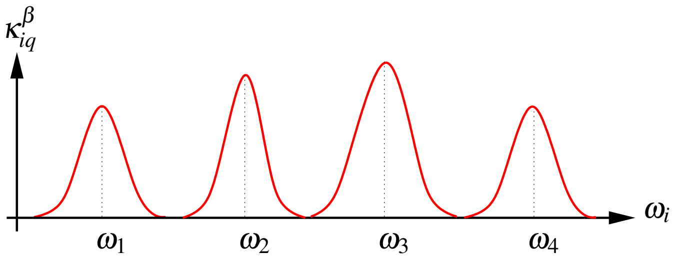

Figure 5.8: Sketch of the mode coupling constant κ^β_{iq} as a function of ω_i. The ASE field modes couple only to a certain range of frequencies outside without overlapping with neighboring frequency ranges.

In atomic spectroscopy this corresponds to a spectrum of many well resolved lines. Therefore, the external fields which couple to the i^{th} ASE modes, consist of a unique set of modes $\hat{b}^{\alpha}_{iq}(t)$ with frequencies ω_q,

$$q \in M_i^{\alpha}, \quad M_i^{\alpha} = \{q(k_i) \in \mathbb{Z} : q^{\alpha}_{\min}(k_i) \leq q(k_i) \leq q^{\alpha}_{\max}(k_i)\},$$

centering around the frequency ω_i of field mode i. They are very close to each other, so that each bath separately consists of many harmonic oscillators. To be specific, we specify the set of modes which couple an ASE mode i to $\hat{b}^{\alpha}_{iq}(t)$, $q \in M_i^{\alpha}$, and which satisfy the bosonic commutation relation

$$\left[\hat{b}^{\alpha}_{iq}(t), \hat{b}^{\beta\dagger}_{jp}(t)\right] = \delta_{\alpha\beta}\delta_{qp}\delta_{ij}. \tag{5.47}$$

HAMILTON OPERATOR OF THE EMPTY DIODE SYSTEM The total Hamiltonian of the three-component system in the Heisenberg picture,

$$\hat{H} = \hat{H}_{\mathrm{r}} + \hat{H}_{\mathrm{B}} + \hat{H}_{\mathrm{I}} + \hat{H}_{\mathrm{b}} + \hat{H}_{\mathrm{lr}} + \hat{H}_{\mathrm{i}}, \tag{5.48}$$

is given by the field Hamiltonian of the intra-cavity field,

$$\hat{H}_{\mathrm{r}} = \sum_{\{k_i\}} \hbar\omega_i \hat{a}_i^{\dagger}\hat{a}_i\,, \tag{5.49}$$

the Hamiltonian of the external reservoirs corresponding to each channel α,

$$\hat{H}_{\mathrm{B}} = \sum_{\alpha=1}^{8} \hat{H}^{\alpha}_{\mathrm{B}}, \quad \hat{H}^{\alpha}_{\mathrm{B}} = \sum_{\{k_i\}} \sum_{q \in M_i^{\alpha}} \hbar\omega_q \hat{b}^{\alpha\dagger}_{iq}\hat{b}^{\alpha}_{iq}, \tag{5.50}$$

and the interaction Hamiltonian of the channel fields at the position of the beam splitters given by

$$\hat{H}_{\mathrm{I}} = \mathrm{i}\hbar \sum_{\{k_i\}} \Big(\sum_{q\in M_i^5} \tilde{\kappa}^{l}_{iq}\hat{b}^{5\dagger}_{iq}\hat{b}^{8}_{iq} + \sum_{q\in M_i^4} \tilde{\kappa}^{l}_{iq}\hat{b}^{4\dagger}_{iq}\hat{b}^{6}_{iq} + \sum_{q\in M_i^1} \tilde{\kappa}^{r}_{iq}\hat{b}^{1\dagger}_{iq}\hat{b}^{2}_{iq} + \sum_{q\in M_i^3} \tilde{\kappa}^{r}_{iq}\hat{b}^{3\dagger}_{iq}\hat{b}^{7}_{iq}\Big) + \text{h.c.} \tag{5.51}$$

with coupling strength $\tilde{\kappa}^{\beta}_{iq}$, ($\beta \in \{l, r\}$). The Hamiltonian of the reservoirs, which couple into the virtual cavity system from the outside on the left- and right-hand side reads

$$\hat{H}_{\mathrm{b}} = \sum_{\beta\in\{l,r\}} \sum_{\{k_i\}} \sum_{q\in M_i^{\beta}} \hbar(\omega_q + \xi_{iq})\hat{b}^{\beta\dagger}_{iq}\hat{b}^{\beta}_{iq}. \tag{5.52}$$

Here, we introduced a common energy shift ξ_{iq}. Additionally, we permit the interaction between the left and right channel of coupling strength η_{iq} according to

$$\hat{H}_{\mathrm{lr}} = \mathrm{i}\hbar \sum_{\{k_i\}} \sum_{q\in M_i} \eta_{iq}\hat{b}^{l\dagger}_{iq}\hat{b}^{r}_{iq} + \text{h.c.}, \qquad M_i = M_i^{\beta}, \quad \beta \in \{l, r\}. \tag{5.53}$$

As we will see later, this term is essential for a correct characterization of the empty diode system as it gives rise to an input-output relation which is consistent with the relation derived from the corresponding boundary value problem.

The interaction of the external fields with the virtual cavity radiation field is captured by the Hamilton operator,

$$\hat{H}_{\mathrm{i}} = \mathrm{i}\hbar \sum_{\{k_i\}} \sum_{\beta\in\{l,r\}} \sum_{q\in M_i^{\beta}} \kappa^{\beta}_{iq}\hat{b}^{\beta\dagger}_{iq}\hat{a}_i + \text{h.c.}, \quad \kappa^{\beta}_{iq} = |\kappa^{\beta}_{iq}|e^{\mathrm{i}\phi_i^{\beta}}, \tag{5.54}$$

depending on the coupling constant κ_{iq}^{β} sketched in figure 5.8. It characterizes the coupling strength between the multimode inside ASE field and the external electrical field channels which couple into the waveguide from the left- and the right-hand side [6]. Please remember that we permit a conversion of photons of the same frequency propagating in opposite direction inside the bulk medium.

The three sub-systems forming the cascaded system can be discussed separately. In the following section we formulate a quantum description of a single beam splitter first. Subsequently, the theory will be extended to the total beam splitter system, composed of system *I* and *III* (cf. figure 5.7). System *II* corresponds to a two-sided open virtual cavity, which will be investigated in detail. The subsection ends with an evaluation of the entire cascaded system depicted in figure 5.7 resulting into a complete theory of the QDSLD waveguide.

5.2.2 Output coupling through tilted end facets

At the beginning of section 5 we directly specified the result of the output vector amplitude $\hat{\mathbf{b}}_{\text{out}}$ of a single beam splitter which is given by the S-matrix applied to the input vector operator $\hat{\mathbf{b}}_{\text{in}}$, that is (cf. equation (5.5))

$$\hat{\mathbf{b}}_{\text{out}} = S\hat{\mathbf{b}}_{\text{in}}. \tag{5.55}$$

The entries of the matrix are given by reflection and transmission amplitudes, $\mathscr{R}$ and $\mathscr{T}$, which is easily verified by simple considerations regarding the propagation of the single channel ports. However, with this more heuristic method for finding a relation between the input and output channels, we can not make any statement about the exact form of the reflection and transmission amplitudes especially not in terms of coupling strengths between two different channels at the position of the beam splitter. Therefore, in this chapter we study the coupling of external channel fields to a single beam splitter system first, that is relevant to model tilted facets of QDSLDs introduced before. Subsequently, we directly specify the entire beam splitter system, composed of system *I* and *III* in figure 5.7.

SINGLE END FACET We consider a single beam splitter depicted in figure 5.9 located at position $\mathbf{r} = (x, y, z = 0)^T$ with four inputs and four outputs.

The channel fields,

$$\hat{\mathbf{E}}^{\alpha(+)}(\mathbf{r},t) = \sum_{q\in M^{\alpha}} v_q^{\alpha}(\mathbf{r})\hat{b}_q^{\alpha}(t)e^{-\mathrm{i}\mathbf{k}_q^{\alpha}\mathbf{r}}\mathbf{e}_y, \quad \alpha \in \{1,2,3,4\}, \tag{5.56}$$

compose of $q \in M^{\alpha}$ modes with mode function specified in (5.7). Here, M^{α} labels a set of modes with wave vectors

$$\mathbf{k}_q^{\alpha} = \begin{cases} k_q\mathbf{e}_z, & \alpha = 1,3 \\ k_q\mathbf{e}_x, & \alpha = 2,4 \end{cases}, \quad k_q = \frac{2\pi q}{L}, \quad q \in \mathbb{Z}, \tag{5.57}$$

in which k_q depends on the system length L. Please note, k_q can take both positive and negative values. The wave number $|k_q|$ obeys the linear dispersion relation, $|k_q| = \omega_q/c_0$ (cf. equation (5.4)), with vacuum speed of light c_0. As already introduced at the beginning of this chapter, we claim that the radiation channel fields are again linear polarized in y-direction and satisfy Maxwell's equations with corresponding periodic boundary conditions. The transverse wave functions

$$\varsigma^{\alpha}(\mathbf{r}) = \begin{cases} \varsigma(x,y), & \alpha = 1,3 \\ \varsigma(y,z), & \alpha = 2,4 \end{cases} \tag{5.58}$$

---

[6] Note, that we have replaced necessary boundary conditions for describing the physical problem by effective interactions, a well established method in quantum field theory.

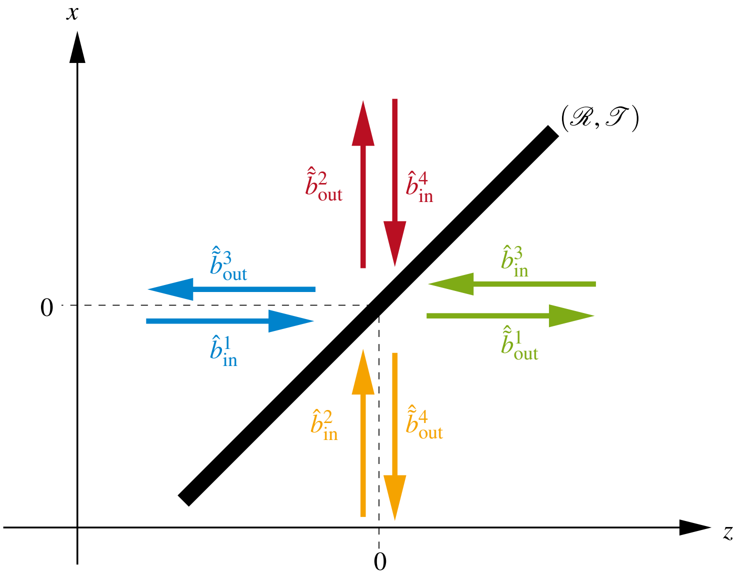

Figure 5.9: Sketch of a lossless beam splitter with four inputs and four outputs.

are normalized to the system volume V (cf. equation (5.8)) and the annihilation and creation operators $\hat{b}_q^\alpha$ and $\hat{b}_q^{\alpha\dagger}$ satisfy the bosonic commutation relation (5.9).

In general, a beam splitter couples a particular input field mode to a particular output mode. Thus, the Hamilton operator of this system is given by

$$\hat{H} = \sum_{\alpha=1}^{4}\sum_{q\in M^\alpha} \hbar\omega_q \hat{b}_q^{\alpha\dagger}\hat{b}_q^{\alpha} + \mathrm{i}\hbar \sum_{q\in M^I} \tilde{\kappa}_q \hat{b}_q^{1\dagger}\hat{b}_q^{2} + \text{h.c.} + \mathrm{i}\hbar \sum_{q\in M^{II}} \tilde{\kappa}_q \hat{b}_q^{3\dagger}\hat{b}_q^{4} + \text{h.c.}. \tag{5.59}$$

Due to energy conservation, we required $M^1 = M^2 \equiv M^I$ and $M^3 = M^4 \equiv M^{II}$.

The Heisenberg equations of motion for the channel field's amplitudes,

$$\dot{\hat{b}}_q^1 = -\frac{\mathrm{i}}{\hbar}\left[\hat{b}_q^1, \hat{H}\right] = -\mathrm{i}\omega_q \hat{b}_q^1 + \tilde{\kappa}_q \hat{b}_q^2, \tag{5.60}$$

$$\dot{\hat{b}}_q^2 = -\frac{\mathrm{i}}{\hbar}\left[\hat{b}_q^2, \hat{H}\right] = -\mathrm{i}\omega_q \hat{b}_q^2 - \tilde{\kappa}_q^* \hat{b}_q^1, \tag{5.61}$$

$$\dot{\hat{b}}_q^3 = -\frac{\mathrm{i}}{\hbar}\left[\hat{b}_q^3, \hat{H}\right] = -\mathrm{i}\omega_q \hat{b}_q^3 + \tilde{\kappa}_q \hat{b}_q^4, \tag{5.62}$$

$$\dot{\hat{b}}_q^4 = -\frac{\mathrm{i}}{\hbar}\left[\hat{b}_q^4, \hat{H}\right] = -\mathrm{i}\omega_q \hat{b}_q^4 - \tilde{\kappa}_q^* \hat{b}_q^3, \tag{5.63}$$

are given by their free evolution with oscillation frequency ω_q and their interaction with the corresponding channel field at the same side of the beam splitter system with coupling strength $\tilde{\kappa}_q = |\tilde{\kappa}_q| e^{\mathrm{i}\tilde{\phi}_q}$. The solutions of this coupled equation system in terms of initial and final time, $t_0 < t$ and $t_f > t$, are given by

$$\hat{\mathbf{b}}_q(t) = e^{-\mathrm{i}\omega_q(t-t_0)} S_q(t-t_0)\hat{\mathbf{b}}_q(t_0), \tag{5.64}$$

$$\hat{\mathbf{b}}_q(t) = e^{-\mathrm{i}\omega_q(t-t_f)} S_q(t-t_f)\hat{\mathbf{b}}_q(t_f), \tag{5.65}$$

with the vector operator $\hat{\mathbf{b}}_q = (\hat{b}_q^1, \hat{b}_q^2, \hat{b}_q^3, \hat{b}_q^4)^T$ and the time-dependent, unitary matrix

$$S_q(\tau) = \begin{pmatrix} \mathscr{T}_q & \mathscr{R}_q & 0 & 0 \\ -\mathscr{R}_q^* & \mathscr{T}_q & 0 & 0 \\ 0 & 0 & \mathscr{T}_q & \mathscr{R}_q \\ 0 & 0 & -\mathscr{R}_q^* & \mathscr{T}_q \end{pmatrix} \tag{5.66}$$

with matrix elements

$$\mathscr{R}_q(\tau) = e^{\mathrm{i}\tilde{\phi}_q} \sin(|\tilde{\kappa}_q|\tau), \qquad \mathscr{T}_q(\tau) = \cos(|\tilde{\kappa}_q|\tau). \tag{5.67}$$

Please note, a sharply localized coupling constant in space results in an approximately flat frequency independent coupling strength which is valid for Markovian systems. Therefore, we make the approximation $\tilde{\kappa}(\omega_q) \approx \tilde{\kappa}$, so that S_q is independent of frequency ω_q, that is $S_q(t) \approx S(t)$.

Next, we define input and output operators in terms of initial and final time respectively,

$$\hat{b}^{\alpha}_{\mathrm{in}}(t) = \sqrt{\Delta\nu} \sum_{q\in M^{\alpha}} e^{-\mathrm{i}\omega_q(t-t_0)} \hat{b}^{\alpha}_q(t_0), \tag{5.68}$$

$$\hat{\hat{b}}^{\alpha}_{\mathrm{out}}(t) = \sqrt{\Delta\nu} \sum_{q\in M^{\alpha}} e^{-\mathrm{i}\omega_q(t-t_f)} \hat{b}^{\alpha}_q(t_f), \quad \Delta\nu = \frac{\Delta\omega}{2\pi}, \tag{5.69}$$

with equally spaced frequency interval $\Delta\omega = \omega_{i+1} - \omega_i$. They satisfy the commutation relation

$$\begin{aligned} \left[\hat{b}^{\alpha}_{\mathrm{in}}(t), \hat{b}^{\beta\dagger}_{\mathrm{in}}(t')\right] &= \Delta\nu \sum_{q\in M^{\alpha}} \sum_{p\in M^{\beta}} e^{-\mathrm{i}\omega_q(t-t_0)} e^{\mathrm{i}\omega_p(t'-t_0)} \left[\hat{b}^{\alpha}_q(t_0), \hat{b}^{\beta\dagger}_p(t_0)\right] \\ &= \delta_{\alpha\beta}\delta_{qp}\Delta\nu \sum_{q\in M^{\alpha}} e^{-\mathrm{i}\omega_q(t-t')}. \end{aligned} \tag{5.70}$$

In the continuum limit, $\Delta\omega \to 0$, the sum approaches a delta distribution

$$\lim_{\Delta\omega\to 0} \frac{\Delta\omega}{2\pi} \sum_{q\in M^{\alpha}} e^{-\mathrm{i}\omega_q(t-t')} = \delta(t-t'). \tag{5.71}$$

Therefore, we find the central commutation relation of the input noise

$$\boxed{\left[\hat{b}^{\alpha}_{\mathrm{in}}(t), \hat{b}^{\beta\dagger}_{\mathrm{in}}(t')\right] = \delta_{\alpha\beta}\delta(t-t')}. \tag{5.72}$$

The same holds for the output amplitudes $\hat{\hat{b}}^{\alpha}_{i,\mathrm{out}}$. Obviously, the field amplitudes have the dimension of $s^{-1/2}$ in contrast to the dimensionless field operators $\hat{b}^{\alpha}_q(t)$ (cf. commutation relation (5.9)). Equating the right-hand side of equation (5.64) and (5.65), summing both sides over all modes q, multiplying by $\sqrt{\Delta\nu}$ and finally utilizing the unitarity of the matrix (5.66), we find a relation between the input and output operators

$$\boxed{\hat{\mathbf{b}}_{\mathrm{out}}(t) = S(t_f - t_0)\, \hat{\mathbf{b}}_{\mathrm{in}}(t)}, \tag{5.73}$$

with $\hat{\mathbf{b}}_{\mathrm{in}} = (\hat{b}^1_{\mathrm{in}}, \hat{b}^2_{\mathrm{in}}, \hat{b}^3_{\mathrm{in}}, \hat{b}^4_{\mathrm{in}})^T$ and $\hat{\mathbf{b}}_{\mathrm{out}} = (\hat{b}^1_{\mathrm{out}}, \hat{b}^2_{\mathrm{out}}, \hat{b}^3_{\mathrm{out}}, \hat{b}^4_{\mathrm{out}})^T \equiv (\hat{\hat{b}}^3_{\mathrm{out}}, \hat{\hat{b}}^4_{\mathrm{out}}, \hat{\hat{b}}^1_{\mathrm{out}}, \hat{\hat{b}}^2_{\mathrm{out}})^T$. Please note, to allow for the concept of channel fields in analogy to scattering theory, in which the total electromagnetic field of each channel is given by in- and outgoing electromagnetic fields with opposite propagation direction in the sense of figure 5.10, we applied an appropriate permutation of the output vector operator.

UNITARY S-MATRIX Equation (5.73) shows that the input and output operators are connected by the S-matrix, (cf. equation (5.66))

$$S \equiv \lim_{\substack{t_f - t_0 \to \infty \\ \tilde{\kappa}\to 0 \\ \tilde{\kappa}(t_f - t_0) = \mathrm{const.}}} S(t_f - t_0) = \begin{pmatrix} 0 & 0 & \mathscr{T} & \mathscr{R} \\ 0 & 0 & -\mathscr{R}^* & \mathscr{T} \\ \mathscr{T} & \mathscr{R} & 0 & 0 \\ -\mathscr{R}^* & \mathscr{T} & 0 & 0 \end{pmatrix} \tag{5.74}$$

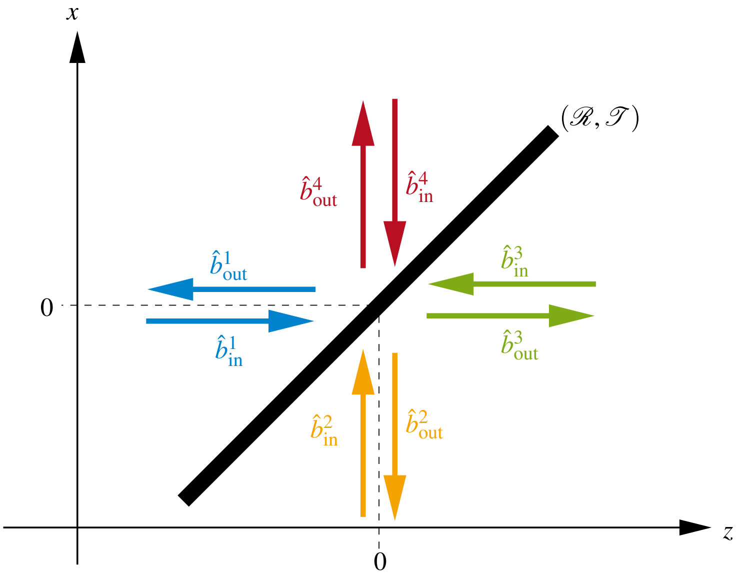

Figure 5.10: Sketch of a lossless beam splitter with corresponding channel field notation.

which only depends on the constant time delay between the final and initial time, $t_f - t_0$. Its important characteristics of unitary,

$$SS^\dagger = S^\dagger S = \mathbb{1}, \tag{5.75}$$

is synonymous to energy conservation [143]. In analogy to scattering theory, we can interpret the matrix elements $\mathscr{R}$ and $\mathscr{T}$ as reflection and transmission amplitudes, respectively. In the limiting case $t_f - t_0 \to \infty$ and $|\tilde{\kappa}| \to 0$, reflection and transmission amplitudes remain constant as well,

$$\mathscr{R} = e^{\mathrm{i}\tilde{\phi}} \sin(|\tilde{\kappa}|(t_f - t_0)) = \text{const.}, \qquad \mathscr{T} = \cos(|\tilde{\kappa}|(t_f - t_0)) = \text{const.}. \tag{5.76}$$

The sum of reflection and transmission coefficients is constant with $|\mathscr{T}|^2 + |\mathscr{R}|^2 = 1$ in agreement with classical considerations of a lossless beam splitter system. In case of a symmetric beam splitter, $\tilde{\phi} = \pi/2$, we find that $\mathscr{R}^* \mathscr{T} + \mathscr{R}\mathscr{T}^* = 0$.

SPECIAL CASE: VANISHING EFFECTIVE INTERACTION For zero coupling $\tilde{\kappa} = 0$ between the input and output ports of the single end facet and finite constant time delay $t_f - t_0$,

$$\lim_{\tilde{\kappa} \to 0} \mathscr{R}(t_f - t_0) = 0, \qquad \lim_{\tilde{\kappa} \to 0} \mathscr{T}(t_f - t_0) = 1, \tag{5.77}$$

no reflecting part of the input field emerges and the transmittance reaches its maximum value. Thus, in this special case of vanishing coupling the beam splitter becomes transparent and the output is exactly the input, that is $\hat{b}^\alpha_{\mathrm{out}}(t) = \hat{b}^\alpha_{\mathrm{in}}(t)$.

As an example, we consider the channel $\alpha = 3$ (cf. figure 5.10) outside the diode system for $z > 0$. This field is a superposition of the input and the output electric fields with positive frequency part

$$\hat{\mathbf{E}}^{3(+)}(x,y,z,t) = \hat{\mathbf{E}}^{3(+)}_{\mathrm{in}}\left(x,y,t + \frac{z}{c_0}\right) + \hat{\mathbf{E}}^{3(+)}_{\mathrm{out}}\left(x,y,t - \frac{z}{c_0}\right), \quad z > 0. \tag{5.78}$$

The input and output electric fields are given by

$$\hat{\mathbf{E}}_{\text{in}}^{3(+)}\left(x,y,t+\frac{z}{c_0}\right) = \sum_{q\in M^3} v_q^3(\mathbf{r})\hat{b}_q^3(t_0)e^{-\mathrm{i}\omega_q\left(t+\frac{z}{c_0}-t_0\right)}\mathbf{e}_y, \tag{5.79}$$

$$\hat{\mathbf{E}}_{\text{out}}^{3(+)}\left(x,y,t-\frac{z}{c_0}\right) = \sum_{q\in M^3} v_q^3(\mathbf{r})\hat{b}_q^3(t_f)e^{-\mathrm{i}\omega_q\left(t-\frac{z}{c_0}-t_f\right)}\mathbf{e}_y. \tag{5.80}$$

As we want to assume that the reservoir frequencies are centered around a single frequency ω, which is justified for Markovian systems, we can replace these frequencies ω_q in the exponents of (5.79)-(5.80) by the central frequency ω, that is $\omega_q \approx \omega$. Therefore, the mode functions $v_q^\alpha(\mathbf{r})$ (see equation (5.7)) become equal for all modes according to

$$v_q^\alpha(\mathbf{r}) = \mathrm{i}\sqrt{\frac{\hbar\omega_q}{2\varepsilon_0 V}}\varsigma^\alpha(\mathbf{r}) \approx \Delta\nu^{-\frac{1}{2}}\,\tilde{v}^\alpha(\mathbf{r}) \quad \text{with} \quad \tilde{v}^\alpha(\mathbf{r}) = \mathrm{i}\sqrt{\frac{\hbar\omega\pi}{\varepsilon_0 V\Delta\omega}}\varsigma^\alpha(\mathbf{r}). \tag{5.81}$$

This approximation allows to express the input- and output fields (5.79)-(5.80) in terms of the input- and output operators defined in equations (5.68)-(5.69). We find for the channel 3

$$\hat{\mathbf{E}}_{\text{in}}^{3(+)}\left(x,y,t+\frac{z}{c_0}\right) \approx \tilde{v}^3(\mathbf{r})\,\hat{b}_{\text{in}}^3\left(t+\frac{z}{c_0}\right)\mathbf{e}_y, \tag{5.82}$$

$$\hat{\mathbf{E}}_{\text{out}}^{3(+)}\left(x,y,t-\frac{z}{c_0}\right) \approx \tilde{v}^3(\mathbf{r})\hat{b}_{\text{out}}^3\left(t-\frac{z}{c_0}\right)\mathbf{e}_y. \tag{5.83}$$

Analogously, we can determine the other channel fields of the four port beam splitter,

$$\hat{\mathbf{E}}^{1(+)}(x,y,z,t) = \hat{\mathbf{E}}_{\text{in}}^{1(+)}\left(x,y,t-\frac{z}{c_0}\right) + \hat{\mathbf{E}}_{\text{out}}^{1(+)}\left(x,y,t+\frac{z}{c_0}\right), \quad z<0, \tag{5.84}$$

$$\hat{\mathbf{E}}^{2(+)}(x,y,z,t) = \hat{\mathbf{E}}_{\text{in}}^{2(+)}\left(y,z,t-\frac{x}{c_0}\right) + \hat{\mathbf{E}}_{\text{out}}^{2(+)}\left(y,z,t+\frac{x}{c_0}\right), \quad x<0, \tag{5.85}$$

$$\hat{\mathbf{E}}^{4(+)}(x,y,z,t) = \hat{\mathbf{E}}_{\text{in}}^{4(+)}\left(y,z,t+\frac{x}{c_0}\right) + \hat{\mathbf{E}}_{\text{out}}^{4(+)}\left(y,z,t-\frac{x}{c_0}\right), \quad x>0. \tag{5.86}$$

BEAM SPLITTER CONFIGURATION OF THE WAVEGUIDE The general considerations of the input and output ports of a single beam splitter can be directly extended to the beam splitter system enclosing the virtual cavity (system *I* plus system *III*) depicted in figure 5.6. This system is described by the Hamiltonian (5.51) [7]. Here, the set of coupled Heisenberg equations of motion for all mode amplitudes is given by

$$\frac{\mathrm{d}}{\mathrm{d}t}\hat{\mathbf{b}}_q = A_q\hat{\mathbf{b}}_q, \qquad A_q = \begin{pmatrix} -\mathrm{i}\omega_q & \tilde{\kappa}_q^r & 0 & 0 & 0 & 0 & 0 & 0 \\ -\tilde{\kappa}_q^{r*} & -\mathrm{i}\omega_q & 0 & 0 & 0 & 0 & 0 & 0 \\ 0 & 0 & -\mathrm{i}\omega_q & 0 & 0 & 0 & \tilde{\kappa}_q^r & 0 \\ 0 & 0 & 0 & -\mathrm{i}\omega_q & 0 & \tilde{\kappa}_q^l & 0 & 0 \\ 0 & 0 & 0 & 0 & -\mathrm{i}\omega_q & 0 & 0 & \tilde{\kappa}_q^l \\ 0 & 0 & 0 & -\tilde{\kappa}_q^{l*} & 0 & -\mathrm{i}\omega_q & 0 & 0 \\ 0 & 0 & -\tilde{\kappa}_q^{r*} & 0 & 0 & 0 & -\mathrm{i}\omega_q & 0 \\ 0 & 0 & 0 & 0 & -\tilde{\kappa}_q^{l*} & 0 & 0 & -\mathrm{i}\omega_q \end{pmatrix}, \tag{5.87}$$

---

[7] Please note, that we only consider the waveguide's facet geometry in absent of a virtual cavity. Therefore, we skip the index *i* enumerating the single intracavity modes.

with $A_q = -A_q^\dagger$, $\hat{\mathbf{b}}_q = (\hat{b}_q^1, \hat{b}_q^2, \hat{b}_q^3, \hat{b}_q^4, \hat{b}_q^5, \hat{b}_q^6, \hat{b}_q^7, \hat{b}_q^8)^T$ as well as coupling strengths $\tilde{\kappa}_q^\beta = |\tilde{\kappa}_q^\beta| e^{\mathrm{i}\tilde{\phi}_q^\beta}$, $\beta \in \{l, r\}$. In analogy to the study of the single beam splitter, we can determine the solution of equation (5.87) in terms of initial time $t_0 < t$ and in terms of final time $t_f > t$ according to

$$\hat{\mathbf{b}}_q(t) = e^{-\mathrm{i}\omega_q(t-t_0)} S_q(t - t_0) \hat{\mathbf{b}}_q(t_0), \tag{5.88}$$

$$\hat{\mathbf{b}}_q(t) = e^{-\mathrm{i}\omega_q(t-t_f)} S_q(t - t_f) \hat{\mathbf{b}}_q(t_f), \tag{5.89}$$

with unitary matrix (cf. equation (5.66))

$$S_q(\tau) = \begin{pmatrix} \mathscr{T}_q^r & \mathscr{R}_q^r & 0 & 0 & 0 & 0 & 0 & 0 \\ -\mathscr{R}_q^{r*} & \mathscr{T}_q^r & 0 & 0 & 0 & 0 & 0 & 0 \\ 0 & 0 & \mathscr{T}_q^r & 0 & 0 & 0 & -\mathscr{R}_q^{r*} & 0 \\ 0 & 0 & 0 & \mathscr{T}_q^l & 0 & -\mathscr{R}_q^{l*} & 0 & 0 \\ 0 & 0 & 0 & 0 & \mathscr{T}_q^l & 0 & 0 & -\mathscr{R}_q^{l*} \\ 0 & 0 & 0 & \mathscr{R}_q^l & 0 & \mathscr{T}_q^l & 0 & 0 \\ 0 & 0 & \mathscr{R}_q^r & 0 & 0 & 0 & \mathscr{T}_q^r & 0 \\ 0 & 0 & 0 & 0 & \mathscr{R}_q^l & 0 & 0 & \mathscr{T}_q^l \end{pmatrix} \tag{5.90}$$

and time-dependent parameters

$$\mathscr{R}_q^\beta(\tau) = e^{\mathrm{i}\tilde{\phi}_q^\beta} \sin(|\tilde{\kappa}_q^\beta| \tau), \qquad \mathscr{T}_q^\beta(\tau) = \cos(|\tilde{\kappa}_q^\beta| \tau), \quad \beta \in \{l, r\}. \tag{5.91}$$

Again, we utilize that for Markovian systems the coupling constant is approximately frequency independent, so that the coupling strength $\tilde{\kappa}_q^\beta \simeq \tilde{\kappa}^\beta = |\tilde{\kappa}^\beta| e^{\mathrm{i}\tilde{\phi}^\beta}$ as well as $S_q(t) \simeq S(t)$. Furthermore, we consider the in- and output operator definition of the single channel fields (cf. equation (5.68)-(5.69)). To allow the interpretation of channel fields in the sense of figure 5.11, we apply an appropriate permutation of the output field amplitudes and introduce the vector operators

$$\hat{\mathbf{b}}_{\text{in}}^T = (\hat{b}_{\text{in}}^1, \hat{b}_{\text{in}}^2, \hat{b}_{\text{in}}^3, \hat{b}_{\text{in}}^4, \hat{b}_{\text{in}}^5, \hat{b}_{\text{in}}^6, \hat{b}_{\text{in}}^7, \hat{b}_{\text{in}}^8), \tag{5.92}$$

$$\begin{aligned} \hat{\mathbf{b}}_{\text{out}}^T &= (\hat{\tilde{b}}_{\text{out}}^7, \hat{\tilde{b}}_{\text{out}}^3, \hat{\tilde{b}}_{\text{out}}^2, \hat{\tilde{b}}_{\text{out}}^5, \hat{\tilde{b}}_{\text{out}}^4, \hat{\tilde{b}}_{\text{out}}^8, \hat{\tilde{b}}_{\text{out}}^1, \hat{\tilde{b}}_{\text{out}}^6) \\ &= (\hat{b}_{\text{out}}^1, \hat{b}_{\text{out}}^2, \hat{b}_{\text{out}}^3, \hat{b}_{\text{out}}^4, \hat{b}_{\text{out}}^5, \hat{b}_{\text{out}}^6, \hat{b}_{\text{out}}^7, \hat{b}_{\text{out}}^8). \end{aligned} \tag{5.93}$$

Therefore, the input-output relation of the tilted end facets in the new channel notation reads

$$\hat{\mathbf{b}}_{\text{out}} = S \hat{\mathbf{b}}_{\text{in}}, \tag{5.94}$$

with S-matrix

$$S \equiv \lim_{\substack{t_f - t_0 \to \infty \\ \tilde{\kappa} \to 0 \\ \tilde{\kappa}(t_f - t_0) = \text{const.}}} S(t_f - t_0) = \begin{pmatrix} 0 & 0 & \mathscr{R}^r & 0 & 0 & 0 & \mathscr{T}^r & 0 \\ 0 & 0 & \mathscr{T}^r & 0 & 0 & 0 & -\mathscr{R}^{r*} & 0 \\ -\mathscr{R}^{r*} & \mathscr{T}^r & 0 & 0 & 0 & 0 & 0 & 0 \\ 0 & 0 & 0 & 0 & \mathscr{T}^l & 0 & 0 & -\mathscr{R}^{l*} \\ 0 & 0 & 0 & \mathscr{T}^l & 0 & -\mathscr{R}^{l*} & 0 & 0 \\ 0 & 0 & 0 & 0 & \mathscr{R}^l & 0 & 0 & \mathscr{T}^l \\ \mathscr{T}^r & \mathscr{R}^r & 0 & 0 & 0 & 0 & 0 & 0 \\ 0 & 0 & 0 & \mathscr{R}^l & 0 & \mathscr{T}^l & 0 & 0 \end{pmatrix}, \tag{5.95}$$

in terms of reflection and transmission amplitude

$$\mathscr{R}^\beta = e^{\mathrm{i}\tilde{\phi}^\beta} \sin(|\tilde{\kappa}^\beta|(t_f - t_0)), \qquad \mathscr{T}^\beta = \cos(|\tilde{\kappa}^\beta|(t_f - t_0)), \quad \beta \in \{l, r\}. \tag{5.96}$$

Equation (5.94) relates the output field modes to the input field operators by the S-matrix in direct analogy to scattering theory. The S-matrix is determined by the transmission or reflection amplitudes defined in (5.96).

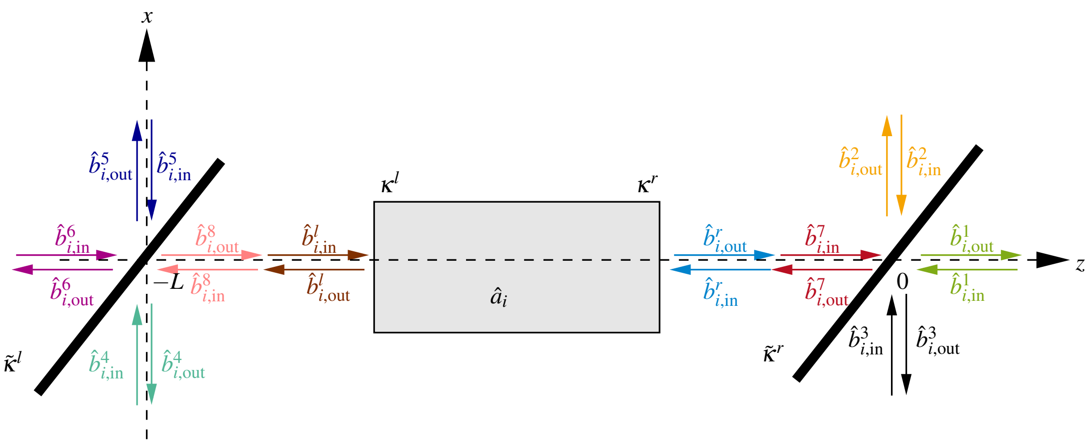

Figure 5.11: Sketch of the empty superluminescent diode system including the concept of channels in analogy to scattering theory.

5.2.3 *Virtual cavity system*

Up to now, we have studied system *I* and system *III* of the total cascaded model shown in figure (5.6). This sketch of an empty diode system reveals that the output fields with amplitudes $\hat{\hat{b}}^6_{\text{out}}$ and $\hat{\hat{b}}^1_{\text{out}}$ enter the virtual cavity (system *II*) resulting in a quasi one-dimensional field propagation inside the cavity parallel to the z-direction. In the following we study in more detail this two-sided open cavity sketched in figure 5.12.

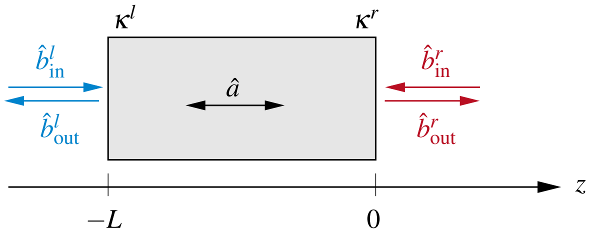

Figure 5.12: Sketch of a two-sided open, virtual cavity (system *II* in figure 5.7).

We are searching for an expression of the output modes $\hat{b}^{l/r}_{\text{out}}$ in terms of the input $\hat{b}^{l/r}_{\text{in}}$ and their coupling with the multimode radiation field of amplitudes $\hat{a}$ inside the cavity of coupling constants $\kappa^{l/r}$. It turns out that the input-output formalism developed by *C. W. Gardiner* and *M. J. Collett* [144] in 1985 provides response to this issue in a very simple and elegant way. It is based on the quantum network theory of *B. Yurke* and *J. S. Denker* [145] and is directly applicable to our cascaded system straightforwardly. However, in this quantum noise theory the input and output field modes are defined in terms of initial and final time (see appendix E) leading to a relation which does not include information about reflection and transmission processes always arising when studying boundary conditions at a semi-transparent mirror in standard quantum electrodynamics (QED) derivation. Accordingly, the quantum noise formalism has to be extended by an implementation of these coefficients.

To be consistent, we study first the boundary value problem of a virtual cavity similar to reference [146]. Here, reflection and transmission amplitudes are identified and an input-output relation is formulated. After that, we replace the boundary conditions by effective interactions according to reference [144].

5.2.3.1 *Input-output formalism from scattering theory*

Let us study a Fabry-Pérot cavity modeled by two *imperfect mirrors* located at position $z = -L$ and $z = 0$ perpendicular to the z-direction and described by dielectric slabs of thickness l^l and l^r (see figure 5.13) [146]. The slabs are formed by homogeneous, isotropic, non-absorbing and passive media resulting in constant, real-valued refractive indices $n^l \in \mathbb{R}$ and $n^r \in \mathbb{R}$. We assume vacuum between both semi-transparent mirrors. Thus, the relative dielectric function $\varepsilon_r = \varepsilon / \varepsilon_0$ reads

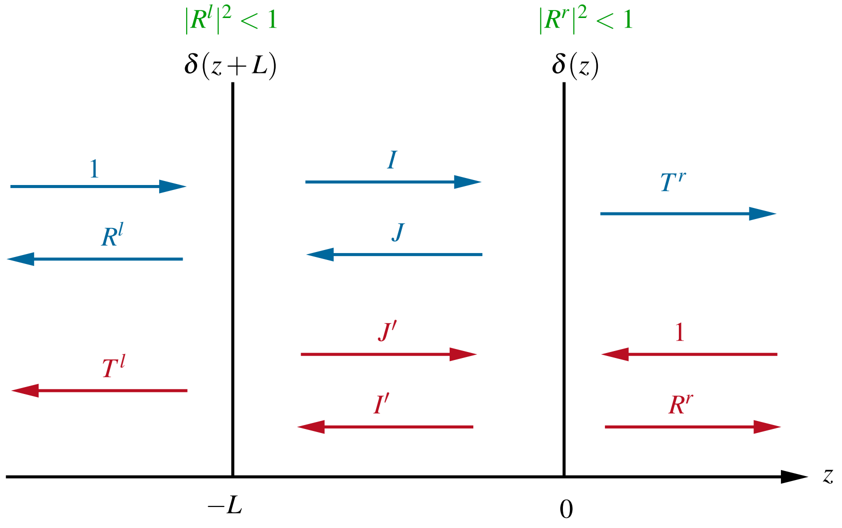

Figure 5.13: Sketch of a two-sided open, empty cavity. The semi-transparent mirrors located at $z = -L$ and $z = 0$ are modeled by delta potentials.

$$\varepsilon_r(z) = n^2(z) = \frac{\varepsilon(z)}{\varepsilon_0} = 1 + \nu^l \delta(z+L) + \nu^r \delta(z), \quad \nu^i = n^{i2} l^i, \quad \nu^l, \nu^r \in \mathbb{R}. \tag{5.97}$$

SINGLE-MODE EMISSION OF A FABRY-PÉROT CAVITY For simplicity, we study the case of a single-mode electric field propagating parallel to the z-axes with a linear polarization in y-direction described by the positive frequency part,

$$\mathbf{E}^{(+)}(\mathbf{r},t) = E^{(+)}(z,t)\varkappa(x,y)\mathbf{e}_y, \tag{5.98}$$

in which the transverse mode function is normalized to the cross-section area

$$\int_{-\infty}^{\infty} \mathrm{d}x\, \mathrm{d}y\, |\varkappa(x,y)|^2 = A. \tag{5.99}$$

According to the Maxwell's equation, the electric field $E(z,t)$ is a solution of the wave equation (cf. equation (2.17))

$$\left[\partial_z^2 - \frac{n^2(z)}{c_0^2}\partial_t^2\right] E^{(+)}(z,t) = 0. \tag{5.100}$$

The classical electromagnetic field of type

$$E^{(+)}(z,t) = \alpha u(z) e^{-\mathrm{i}\omega t}, \quad \omega > 0 \tag{5.101}$$

yields a Helmholtz equation for the mode function $u(z)$,

$$\left(\partial_z^2 + \frac{\omega^2}{c_0^2} n^2(z)\right) u(z) = 0. \tag{5.102}$$

Thus, outside the semitransparent mirrors plane waves are solutions ($u(z) \sim e^{\pm \mathrm{i}kz}$) and the vacuum dispersion $\omega = |k|c_0$ follows. Please note, that the wave vector magnitude k can be both positive and negative. For each k there exist two solutions of equation (5.102). Here, $u(z)$ labels the purely outgoing mode on the right-hand side of the cavity at $z > 0$ whereas $u'(z)$ corresponds to the mode purely outgoing on the left-hand side at $z < -L$. The mode solutions for $k > 0$ read:

OUTGOING MODES ON THE RIGHT $(k > 0)$

$$u(z) = \begin{cases} e^{\mathrm{i}kz} + R^l e^{-\mathrm{i}kz} & z < -L \\ I e^{\mathrm{i}kz} + J e^{-\mathrm{i}kz} & -L < z < 0\,, \\ T^r e^{\mathrm{i}kz} & z > 0 \end{cases} \tag{5.103}$$

OUTGOING MODES ON THE LEFT $(k > 0)$

$$u'(z) = \begin{cases} T^l e^{-\mathrm{i}kz} & z < -L \\ I' e^{-\mathrm{i}kz} + J' e^{\mathrm{i}kz} & -L < z < 0\,. \\ e^{-\mathrm{i}kz} + R^r e^{\mathrm{i}kz} & z > 0 \end{cases} \tag{5.104}$$

The amplitudes R^l, I, J, T^r as well as R^r, I', J', T^l are determined by the boundary conditions at the mirror surfaces at $z = -L$ and $z = 0$. Continuity of the electric field tangential component as well as discontinuity of the magnetic field tangential component require

$$u(-L^-) = u(-L^+), \qquad \partial_z u(-L^-) - \partial_z u(-L^+) = k^2 \nu^l u(-L), \tag{5.105}$$

$$u(0^-) = u(0^+), \qquad \partial_z u'(-L^-) - \partial_z u'(-L^+) = k^2 \nu^l u'(-L), \tag{5.106}$$

$$u'(-L^-) = u'(-L^+), \qquad \partial_z u(0-) - \partial_z u(0^+) = k^2 \nu^r u(0), \tag{5.107}$$

$$u'(0^-) = u'(0^+), \qquad \partial_z u'(0^-) - \partial_z u'(0^+) = k^2 \nu^r u'(0). \tag{5.108}$$

Here, the plus or minus sign in the arguments of equation (5.105)-(5.108) refers to the abbreviations $L^\pm = \lim_{\varepsilon \to 0}(L \pm \varepsilon)$ and $0^\pm = \lim_{\varepsilon \to 0} \pm\varepsilon$. With this set of boundary conditions, the amplitudes can be calculated, leading to the following expressions

$$T^r = \frac{t^l t^r}{\lambda}, \qquad T^l = T^r, \tag{5.109}$$

$$R^l = \frac{r^l e^{-2\mathrm{i}kL} + r^r e^{2\mathrm{i}Arg(t^l)}}{\lambda}, \qquad R^r = \frac{r^l e^{2\mathrm{i}kL + 2\mathrm{i}Arg(t^r)} + r^r}{\lambda}, \tag{5.110}$$

$$I = \frac{t^l}{\lambda}, \qquad I' = \frac{t^r}{\lambda}, \tag{5.111}$$

$$J = \frac{t^l r^r}{\lambda}, \qquad J' = \frac{t^r r^l e^{2\mathrm{i}kL}}{\lambda}, \tag{5.112}$$

in terms of the definitions

$$\lambda \equiv 1 - \frac{\nu^l \nu^r k^2 e^{2\mathrm{i}kL}}{(2\mathrm{i} + k\nu^l)(2\mathrm{i} + k\nu^r)} = 1 - r^l r^r e^{2\mathrm{i}kL}, \quad t^\beta = \frac{2}{2 - \mathrm{i}k\nu^\beta}, \quad r^\beta = \frac{\mathrm{i}k\nu^\beta}{2 - \mathrm{i}k\nu^\beta}. \tag{5.113}$$

Here, R^l and T^r as well as R^r and T^l correspond to reflection and transmission amplitudes of the Fabry-Pérot cavity. They satisfy the conditions, [8]

$$|R^l|^2 + |T^r|^2 = |R^r|^2 + |T^l|^2 = 1, \tag{5.114}$$

$$R^{l*} T^l + R^r T^{r*} = 0, \tag{5.115}$$

---

[8] In case of an absorbing mirror equation (5.114) becomes an inequality of type $|R^l|^2 + |T^r|^2 \leq 1$.

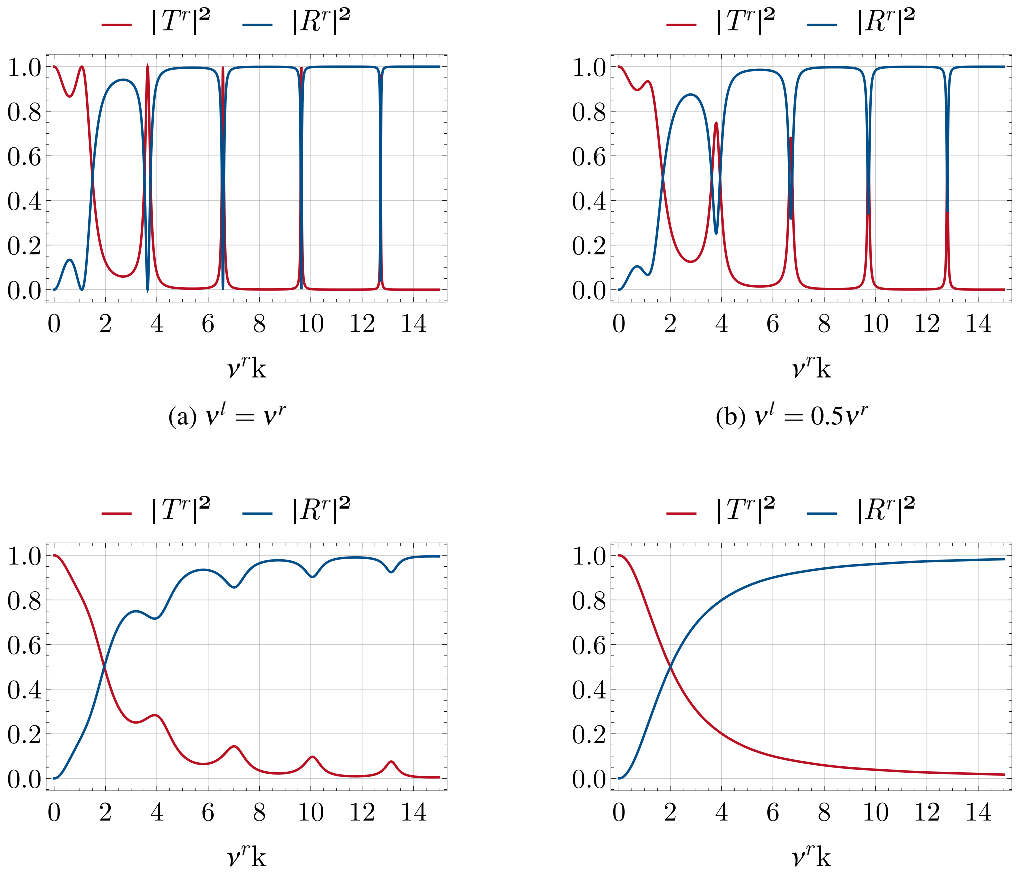

(a) $\nu^l = \nu^r$

(b) $\nu^l = 0.5\nu^r$

(c) $\nu^l = 0.1\nu^r$

(d) $\nu^l = 0.001\nu^r$

Figure 5.14: Reflection and transmission coefficient, $|R^r|^2$ and $|T^r|^2$, of an open cavity of length $L = \nu^r$ as a function of the scaled wave number $\nu^r k$ for characteristic function (a) $\nu^l = \nu^r$, (b) $\nu^l = 0.5\nu^r$, (c) $\nu^l = 0.1\nu^r$, (d) $\nu^l = 0.001\nu^r$.

due to energy conservation. Figure 5.14 shows the transmission $|T^r|^2$ (red) and the reflection $|R^r|^2$ (blue) coefficient on the right-hand side of the cavity of length $L = \nu^r$ as a function of scaled wave number $\nu^r k$. For a smaller ratio ν^l/ν^r, reflection and transmission reveal resonances observable in figure 5.14(a) for $\nu^l = \nu^r$ and figure 5.14(b) for $\nu^l = 0.5\nu^r$. These resonances are smeared out with decreasing ratio ν^l/ν^r visible in figure 5.14(c) and figure 5.14(d) for $\nu^l = 0.1\nu^r$ and $\nu^l = 0.001\nu^r$, respectively. In addition, for decreasing the ratio ν^l/ν^r, an increasing reflection and a decreasing transmission coefficient are observable until they reach their maximum and minimum value of 1 and 0, respectively [9]. At the same time, the sum of both coefficients remains constant according to condition (5.114).

The mode function (5.103) is normalized by [146]

$$\int \mathrm{d}z\, n^2(z) u(k,z) u^*(k',z) = 2\pi\delta(k-k'). \tag{5.116}$$

The same is valid for the mode function $u'(z)$. Furthermore, the mode functions obey the orthogonality condition [146]

$$\int \mathrm{d}z\, n^2(z) u(k,z) u'^*(k',z) = 0. \tag{5.117}$$

---

[9] Figure 5.14(d) corresponds to the bad cavity limit.

Thus, a general solution of the z-component of the positive frequency part of the electromagnetic field is given by the linear combination

$$E^{(+)}(z,t) = \left(\alpha u(z) + \alpha' u'(z)\right) e^{-\mathrm{i}\omega t}. \tag{5.118}$$

Taking into account the separation ansatz (5.98), the classical electric field is specified by

$$\mathbf{E}^{(+)}(\mathbf{r},t) = \varkappa(x,y) \left(\alpha u(z) + \alpha' u'(z)\right) e^{-\mathrm{i}\omega t} \mathbf{e}_y. \tag{5.119}$$

QUANTIZED ELECTROMAGNETIC FIELD Following the same quantization procedure described in section 2.1 we are able to determine the total electric field on the left- and right-hand side of the cavity. They are composed of the left- and right-propagating part of the radiation field on the appropriate location of the cavity with positive frequency part according to

$$\hat{\mathbf{E}}^{\beta(+)}(\mathbf{r},t) = \hat{\mathbf{E}}^{\beta(+)}_{\text{in}}(\mathbf{r},t) + \hat{\mathbf{E}}^{\beta(+)}_{\text{out}}(\mathbf{r},t), \qquad \beta = l, r, \tag{5.120}$$

$$= \mathscr{E} \varkappa(x,y) \left(u(z)\hat{a} + u'(z)\hat{a}'\right) e^{-\mathrm{i}\omega t} \mathbf{e}_y, \quad \mathscr{E} = \mathrm{i}\sqrt{\frac{\hbar\omega}{2\varepsilon_0 V}}. \tag{5.121}$$

Due to equations (5.103)-(5.104), the positive frequency part of the input and the output quantized electric field on the left-hand side of the cavity with $z < -L$ (see figure 5.13) can be written as

$$\hat{\mathbf{E}}^{l(+)}_{\text{in}}(\mathbf{r},t) = \hat{\mathbf{E}}^{l(+)}_{\text{in}}(x,y,t - \frac{z}{c_0}) = \mathscr{E} \varkappa(x,y) \hat{a} e^{-\mathrm{i}(\omega t - kz)} \mathbf{e}_y, \tag{5.122}$$

$$\hat{\mathbf{E}}^{l(+)}_{\text{out}}(\mathbf{r},t) = \hat{\mathbf{E}}^{l(+)}_{\text{out}}(x,y,t + \frac{z}{c_0}) = \mathscr{E} \varkappa(x,y) \left(R^l \hat{a} + T^l \hat{a}'\right) e^{-\mathrm{i}(\omega t + kz)} \mathbf{e}_y. \tag{5.123}$$

Here, we introduced the annihilation and creation operators $\hat{a}$, $\hat{a}^\dagger$ of mode u and $\hat{a}'$, $\hat{a}'^\dagger$ of mode u' which satisfy the commutation relations

$$[\hat{a}, \hat{a}] = \left[\hat{a}^\dagger, \hat{a}^\dagger\right] = [\hat{a}', \hat{a}'] = \left[\hat{a}'^\dagger, \hat{a}'^\dagger\right] = 0, \tag{5.124}$$

$$\left[\hat{a}, \hat{a}'^\dagger\right] = \left[\hat{a}', \hat{a}^\dagger\right] = 0, \tag{5.125}$$

$$\left[\hat{a}, \hat{a}^\dagger\right] = \left[\hat{a}', \hat{a}'^\dagger\right] = 1. \tag{5.126}$$

Defining the mode function

$$v(x,y) = \mathrm{i}\sqrt{\frac{\hbar\omega\pi}{\varepsilon_0 V \Delta\omega}} \varkappa(x,y), \tag{5.127}$$

as well as left and right **output operators**

$$\hat{b}^l_{\text{out}}(t) = \sqrt{\Delta\nu} \left(R^l \hat{a} + T^l \hat{a}'\right) e^{-\mathrm{i}\omega t}, \tag{5.128}$$

$$\hat{b}^r_{\text{out}}(t) = \sqrt{\Delta\nu} \left(T^r \hat{a} + R^r \hat{a}'\right) e^{-\mathrm{i}\omega t}, \quad \Delta\nu = \frac{\Delta\omega}{2\pi}, \tag{5.129}$$

we can specify the positive frequency part of the left output electric field $(z < -L)$

$$\begin{aligned} \hat{\mathbf{E}}^{l(+)}_{\text{out}}(x,y,z<-L,t) &= \mathrm{i}\sqrt{\frac{\hbar\omega}{2\varepsilon_0 V}} \varkappa(x,y) \left(R^l \hat{a} + T^l \hat{a}'\right) e^{-\mathrm{i}\omega(t + z/c_0)} \mathbf{e}_y \\ &= v(x,y) \hat{b}^l_{\text{out}}\left(t + \frac{z}{c_0}\right) \mathbf{e}_y. \end{aligned} \tag{5.130}$$

In the same way, we find the output field entering the cavity on the right-hand side $(z > 0)$

$$\hat{\mathbf{E}}^{r(+)}_{\text{out}}(x,y,z>0,t) = v(x,y) \hat{b}^r_{\text{out}}\left(t - \frac{z}{c_0}\right) \mathbf{e}_y. \tag{5.131}$$

The input quantized radiation fields are defined by

$$\hat{\mathbf{E}}_{\text{in}}^{l(+)}(x,y,z<-L,t)=v(x,y)\hat{b}_{\text{in}}^{l}\left(t-\frac{z}{c_0}\right)\mathbf{e}_y, \tag{5.132}$$

$$\hat{\mathbf{E}}_{\text{in}}^{r(+)}(x,y,z>0,t)=v(x,y)\hat{b}_{\text{in}}^{r}\left(t+\frac{z}{c_0}\right)\mathbf{e}_y, \tag{5.133}$$

with **input operators**

$$\hat{b}_{\text{in}}^{l}(t)=\sqrt{\Delta\nu}\,\hat{a}e^{-\mathrm{i}\omega t}=\sqrt{\Delta\nu}\,\hat{a}(t), \tag{5.134}$$

$$\hat{b}_{\text{in}}^{r}(t)=\sqrt{\Delta\nu}\,\hat{a}'e^{-\mathrm{i}\omega t}=\sqrt{\Delta\nu}\,\hat{a}'(t),\quad \Delta\nu=\frac{\Delta\omega}{2\pi}, \tag{5.135}$$

and free evolution operators $\hat{a}(t)=\hat{a}e^{-\mathrm{i}\omega t}$ and $\hat{a}'(t)=\hat{a}'e^{-\mathrm{i}\omega t}$.

MULTIMODE EMISSION OF A FABRY-PÉROT CAVITY Clearly, the consideration of a single-mode inside a Fabry-Pérot cavity can be extended to many modes. This generalization gives rise to a total electric field of type (5.120) with input and output part on the left ($z<-L$),

$$\hat{\mathbf{E}}_{\text{in}}^{l(+)}(\mathbf{r},t)=\sum_{\{k_i>0\}}v_i(x,y)\hat{b}_{i,\text{in}}^{l}\left(t-\frac{z}{c_0}\right)\mathbf{e}_y, \tag{5.136}$$

$$\hat{\mathbf{E}}_{\text{out}}^{l(+)}(\mathbf{r},t)=\sum_{\{k_i>0\}}v_i(x,y)\hat{b}_{i,\text{out}}^{l}\left(t+\frac{z}{c_0}\right)\mathbf{e}_y, \tag{5.137}$$

as well as input and output on the right $(z>0)$

$$\hat{\mathbf{E}}_{\text{in}}^{r(+)}(\mathbf{r},t)=\sum_{\{k_i>0\}}v_i(x,y)\hat{b}_{i,\text{in}}^{r}(t+\frac{z}{c_0})\mathbf{e}_y, \tag{5.138}$$

$$\hat{\mathbf{E}}_{\text{out}}^{r(+)}(\mathbf{r},t)=\sum_{\{k_i>0\}}v_i(x,y)\hat{b}_{i,\text{out}}^{r}\left(t-\frac{z}{c_0}\right)\mathbf{e}_y, \tag{5.139}$$

with corresponding input- and output operators

$$\hat{b}_{i,\text{in}}^{l}(t)=\sqrt{\Delta\nu_i}\,\hat{a}_i e^{-\mathrm{i}\omega_i t}, \tag{5.140}$$

$$\hat{b}_{i,\text{in}}^{r}(t)=\sqrt{\Delta\nu_i}\,\hat{a}_i' e^{-\mathrm{i}\omega_i t}, \tag{5.141}$$

$$\hat{b}_{i,\text{out}}^{l}(t)=\sqrt{\Delta\nu_i}\left(R_i^l\hat{a}_i+T_i^l\hat{a}_i'\right)e^{-\mathrm{i}\omega_i t}, \tag{5.142}$$

$$\hat{b}_{i,\text{out}}^{r}(t)=\sqrt{\Delta\nu_i}\,(T_i^r\hat{a}_i+R_i^r\hat{a}_i')\,e^{-\mathrm{i}\omega_i t}. \tag{5.143}$$

The mode function of mode i is specified by

$$v_i(x,y)=\mathrm{i}\sqrt{\frac{\hbar\omega_i\pi}{\varepsilon_0 V\Delta\omega_i}}\varkappa(x,y) \tag{5.144}$$

and the quantized field amplitudes obey the usual bosonic commutation relations

$$[\hat{a}_i,\hat{a}_j]=\left[\hat{a}_i^\dagger,\hat{a}_j^\dagger\right]=\left[\hat{a}_i',\hat{a}_j'\right]=\left[\hat{a}_i'^\dagger,\hat{a}_j'^\dagger\right]=0, \tag{5.145}$$

$$\left[\hat{a}_i,\hat{a}_j'^\dagger\right]=\left[\hat{a}_i',\hat{a}_j^\dagger\right]=0, \tag{5.146}$$

$$\left[\hat{a}_i,\hat{a}_j^\dagger\right]=\left[\hat{a}_i',\hat{a}_j'^\dagger\right]=\delta_{ij}. \tag{5.147}$$

Having a closer look at the output quantized field amplitudes (5.142)-(5.143) and the definition of the input operators (5.140)-(5.141), it becomes quite obvious that the output is directly connected with the input. Assuming equally spaced frequency distances between adjacent modes, $\Delta\omega_i = \Delta\omega$, the left and right output amplitudes in terms of the inputs are given by

$$\boxed{\begin{aligned} \hat{b}^l_{i,\mathrm{out}}(t) &= R^l_i \hat{b}^l_{i,\mathrm{in}}(t) + \sqrt{\Delta\nu_\mathrm{F}} T^l_i \hat{a}'_i(t), \\ \hat{b}^r_{i,\mathrm{out}}(t) &= R^r_i \hat{b}^r_{i,\mathrm{in}}(t) + \sqrt{\Delta\nu_\mathrm{F}} T^r_i \hat{a}_i(t). \end{aligned}} \qquad \begin{aligned} (5.148) \\ (5.149) \end{aligned}$$

Obviously, the prefactor $\sqrt{\Delta\nu_\mathrm{F}}$ on the right-hand side of (5.148)-(5.149) is related with the free spectral range

$$\Delta\nu_\mathrm{F} = \frac{c_0}{2L} \equiv \frac{\Delta\omega}{2\pi} = \Delta\nu. \tag{5.150}$$

As a main result, we find an **input-output relation** of a simple empty cavity model by solving the boundary value problem.

5.2.3.2 Input-output relation by effective point interaction

The preceding section related the output field amplitudes with the input radiation field amplitudes via the concept of QED with corresponding boundary conditions at the two semi-transparent mirrors and introduced reflection as well as transmission amplitudes. In this section, we follow the ideas of *C. W. Gardiner* and *M. J. Collett* [50, 139, 144, 147] to formulate an alternative derivation of the relation between input and output fields of the virtual, two-sided cavity system depicted in figure 5.12, in which the boundary conditions are substituted by effective point interactions. Here, two external electric fields with corresponding system operators $\hat{b}^l_{iq}$ and $\hat{b}^r_{iq}$ are coupled to the radiation field inside the empty fictitious cavity with amplitudes $\hat{a}_i$. The Hamilton operator (5.48) reduces to

$$\hat{H} = \hat{H}_\mathrm{r} + \hat{H}_\mathrm{b} + \hat{H}_\mathrm{i} + \hat{H}_\mathrm{lr} \tag{5.151}$$

with the corresponding Hamiltonian of the internal radiation field $\hat{H}_\mathrm{r}$ (see equation (5.49)), the Hamiltonian of the left and right heat baths $\hat{H}_\mathrm{b}$ (see equation (5.52)) and their linear interaction between each other as well as their interaction with the intracavity radiation field, described by $\hat{H}_\mathrm{lr}$ and $\hat{H}_\mathrm{i}$ (cf. equation (5.53) and (5.54)), respectively. Again, we choose the Heisenberg picture and formulate equations of motion for the intracavity field amplitudes

$$\dot{\hat{a}}_i = -\frac{\mathrm{i}}{\hbar}\left[\hat{a}_i, \hat{H}\right] = -\mathrm{i}\omega_i\hat{a}_i - \sum_{q\in M_i} \boldsymbol{\kappa}^{*T}_{iq}\hat{\mathbf{b}}_{iq} \quad \text{with} \quad \hat{\mathbf{b}}_{iq} = \begin{pmatrix} \hat{b}^l_{iq} \\ \hat{b}^r_{iq} \end{pmatrix}, \quad \boldsymbol{\kappa}_{iq} = \begin{pmatrix} \kappa^l_{iq} \\ \kappa^r_{iq} \end{pmatrix}, \tag{5.152}$$

as well as for the reservoir field operators

$$\dot{\hat{\mathbf{b}}}_{iq} = -\mathrm{i}\Omega_{iq}\hat{\mathbf{b}}_{iq} + \boldsymbol{\kappa}_{iq}\hat{a}_i \quad \text{with} \quad \Omega_{iq} = \begin{pmatrix} \omega_q + \xi_{iq} & \mathrm{i}\eta_{iq} \\ -\mathrm{i}\eta^*_{iq} & \omega_q + \xi_{iq} \end{pmatrix} = (\omega_q + \xi_{iq})\mathbb{1} + \Phi_{iq}. \tag{5.153}$$

Formal integration of (5.153) in terms of the initial time $t_0 < t$ yields the dynamics of the heat bath mode amplitudes as a function of the internal radiation field operators $\hat{a}_i$,

$$\hat{\mathbf{b}}_{iq}(t) = e^{-\mathrm{i}\Omega_{iq}(t-t_0)}\hat{\mathbf{b}}_{iq}(t_0) + \int_{t_0}^{t} \mathrm{d}t'\, e^{-\mathrm{i}\Omega_{iq}(t-t')}\boldsymbol{\kappa}_{iq}\hat{a}_i(t'). \tag{5.154}$$

This solution can be directly inserted into the equation of motion of the internal radiation field amplitude (5.152), resulting into a differential equation of type

$$\dot{\hat{a}}_i(t) = -\mathrm{i}\omega_i\hat{a}_i(t) - \sum_{q\in M_i} \boldsymbol{\kappa}^{*T}_{iq} e^{-\mathrm{i}\Omega_{iq}(t-t_0)}\hat{\mathbf{b}}_{iq}(t_0) - \sum_{q\in M_i} \boldsymbol{\kappa}^{*T}_{iq} \int_{t_0}^{t} \mathrm{d}t'\, e^{-\mathrm{i}\Omega_{iq}(t-t')}\boldsymbol{\kappa}_{iq}\hat{a}_i(t'). \tag{5.155}$$

In the next step, we introduce the Langevin force operator $\hat{f}_i^\beta$ and the memory kernel K_i^β according to

$$\sum_{\beta\in\{l,r\}} \hat{f}_i^\beta(t) \equiv \sum_{q\in M_i} \boldsymbol{\kappa}_{iq}^{*T}\, e^{-\mathrm{i}\Omega_{iq}(t-t_0)} \hat{\mathbf{b}}_{iq}(t_0), \tag{5.156}$$

$$\sum_{\beta\in\{l,r\}} K_i^\beta(\tau) \equiv \sum_{q\in M_i} \boldsymbol{\kappa}_{iq}^{*T} e^{-\mathrm{i}\Omega_{iq}\tau} \boldsymbol{\kappa}_{iq}, \tag{5.157}$$

so that equation (5.155) simplifies to

$$\dot{\hat{a}}_i(t) = -\mathrm{i}\omega_i \hat{a}_i(t) - \sum_{\beta\in\{l,r\}} \int_{t_0}^{t} \mathrm{d}t'\, K_i^\beta(t-t')\hat{a}_i(t') - \sum_{\beta\in\{l,r\}} \hat{f}_i^\beta(t). \tag{5.158}$$

MARKOV APPROXIMATION In analogy to the derivation of the master equation (see appendix D) we utilize the sharpness of the memory kernel K_i^β at $t = t'$ for Markovian systems. Here, the convolution integral of $K_i^\beta(t-t')$ and an arbitrary system operator $\hat{c}(t)$ can be approximated by

$$\int_{t_0}^{t} \mathrm{d}t'\, K_i^\beta(t-t')\hat{c}(t') \approx \int_{t_0}^{t} \mathrm{d}t'\, K_i^\beta(t-t')\hat{c}(t) \overset{t\gg\tau_c}{\approx} \left(\frac{\gamma_i^\beta}{2} + \mathrm{i}\delta\omega\right)\hat{c}(t), \tag{5.159}$$

for times t much bigger than the correlation time τ_c of the reservoir fluctuations. γ defines a decay rate and is related with the coupling constant via $\gamma = 2\pi|\kappa|^2/\Delta\omega$. The line shift $\delta\omega$ will be neglected in the following. Please note, that in the Markov approximation, the coupling constants are only a function of frequency ω_i that is independent of frequency ω_q,

$$\kappa_{iq}^\beta \approx \kappa_i^\beta = |\kappa_i^\beta| e^{\mathrm{i}\phi_i^\beta}, \qquad \beta \in \{l,r\}. \tag{5.160}$$

Therefore the damping rates read

$$\gamma_i^\beta \equiv \frac{1}{\Delta\nu_i}|\kappa_i^\beta|^2, \qquad \beta \in \{l,r\}. \tag{5.161}$$

The temporal derivative of the mode field amplitude i is of Langevin type,

$$\dot{\hat{a}}_i = -\left(\mathrm{i}\omega_i + \frac{\gamma_i^l + \gamma_i^r}{2}\right)\hat{a}_i - \sum_{\beta\in\{l,r\}} \hat{f}_i^\beta, \tag{5.162}$$

including both a damping as well as a randomizing term. Therefore, $\hat{f}_i^\beta$ corresponds to a Langevin operator, describing fluctuations of $\hat{a}_i$ around its average.

We *define* an **input operator** in terms of the initial time $t_0 < t$,

$$\hat{b}_{i,\mathrm{in}}^\beta(t) \equiv \sqrt{\Delta\nu_i} \sum_{q\in M_i^\beta} e^{-\mathrm{i}\omega_q(t-t_0)} \hat{b}_{iq}^\beta(t_0), \qquad \beta \in \{l,r\}. \tag{5.163}$$

In the Markov approximation, also the coupling constants η_{iq} are flat around a certain central frequency ω_i so that we can make the replacement $\eta_{iq} \simeq \eta_i = |\eta_i| e^{\mathrm{i}\varphi_i}$ and the Langevin force is related to the input field amplitude by

$$\sum_{\beta\in\{l,r\}} \hat{f}_i^\beta(t) \simeq -\frac{\boldsymbol{\kappa}_i^{*T}}{\sqrt{\Delta\nu_i}} S_i(t-t_0)\, \hat{\mathbf{b}}_{i,\mathrm{in}}(t),\ S_i(\tau) = \begin{pmatrix} T_i(\tau) & R_i^r(\tau) \\ R_i^l(\tau) & T_i(\tau) \end{pmatrix},\ \hat{\mathbf{b}}_{i,\mathrm{in}} = \begin{pmatrix} \hat{b}_{i,\mathrm{in}}^l \\ \hat{b}_{i,\mathrm{in}}^r \end{pmatrix}. \tag{5.164}$$

Again, we identify the matrix elements of $S_i(\tau)$ as reflection and transmission amplitudes defined by[10]

$$T_i(\tau) = e^{-\mathrm{i}\xi_i(t)} \cos(|\eta_i|\tau), \tag{5.165}$$

$$R_i^r(\tau) = e^{-\mathrm{i}(\xi_i(t)-\varphi_i)} \sin(|\eta_i|\tau), \tag{5.166}$$

$$R_i^l(\tau) = -e^{-\mathrm{i}(\xi_i(t)+\varphi_i)} \sin(|\eta_i|\tau). \tag{5.167}$$

This result can be utilized to formulate the equation of motion for the field amplitude $\hat{a}_i$ in terms of the input operator according to

$$\boxed{\frac{\mathrm{d}}{\mathrm{d}t}\hat{a}_i(t) = -\left(\mathrm{i}\omega_i + \frac{\gamma_i^l + \gamma_i^r}{2}\right)\hat{a}_i(t) - \hat{b}_{i,\mathrm{in}}^L(t) - \hat{b}_{i,\mathrm{in}}^R(t)}. \tag{5.168}$$

Here, we introduced the abbreviations

$$\hat{b}_{i,\mathrm{in}}^L(t) \equiv X_i^l(t-t_0)\hat{b}_{i,\mathrm{in}}^l(t), \tag{5.169}$$

$$\hat{b}_{i,\mathrm{in}}^R(t) \equiv X_i^r(t-t_0)\hat{b}_{i,\mathrm{in}}^r(t) \tag{5.170}$$

with

$$X_i^\beta(\tau) = \mathscr{D}_i^{\beta *} T_i(\tau) + \mathscr{D}_i^{\alpha *} R_i^\beta(\tau) \quad \text{and} \quad \mathscr{D}_i^\beta = \sqrt{\gamma_i^\beta}\, e^{\mathrm{i}\phi_i^\beta}, \quad \alpha,\beta \in \{l,r\}, \quad \alpha \neq \beta. \tag{5.171}$$

The first term in (5.168) describes the free evolution and considers damping effects resulting from the left and right mirrors of the virtual cavity. Please note, that this damping term is Markovian as it is only a function of the system operator evaluated at time t and not at earlier times. The last two terms, which are proportional to the input field operators $\hat{b}_{i,\mathrm{in}}^{l/r}$ can be interpreted as noise contributions provided that the state of the total system at initial time t_0 factorizes and the state of the noise input is incoherent [50]. Thus, equation (5.168) represents a quantum stochastic differential equation (QSDE) for the quantized intracavity field amplitude $\hat{a}_i$ also known as *quantum Langevin equation* named after Langevin who invented a heuristic formulation of Brownian motion in classical physics [148], which became a standard method for describing stochastic processes.

In analogy to (5.154) the solution of the Heisenberg equation of the bath modes in terms of the final time $t_f > t$ is

$$\hat{\mathbf{b}}_{iq}(t) = e^{-\mathrm{i}\Omega_{iq}(t-t_f)}\hat{\mathbf{b}}_{iq}(t_f) - \int_t^{t_f} \mathrm{d}t'\, e^{-\mathrm{i}\Omega_{iq}(t-t')}\boldsymbol{\kappa}_{iq}\hat{a}_i(t'). \tag{5.172}$$

Applying the same calculations as before, we can specify the equation of motion for the internal radiation field amplitude

$$\boxed{\hat{a}_i(t) = -\left(\mathrm{i}\omega_i - \frac{\gamma_i^l + \gamma_i^r}{2}\right)\hat{a}_i(t) - \hat{b}_{i,\mathrm{out}}^L(t) - \hat{b}_{i,\mathrm{out}}^R(t)}, \tag{5.173}$$

with

$$\hat{b}_{i,\mathrm{out}}^L(t) = X_i^l(t-t_f)\hat{b}_{i,\mathrm{out}}^l(t), \tag{5.174}$$

$$\hat{b}_{i,\mathrm{out}}^R(t) = X_i^r(t-t_f)\hat{b}_{i,\mathrm{out}}^r(t) \tag{5.175}$$

---

[10] Here, the matrix $S_i(\tau)$ and its coefficients are equal to (5.66)-(5.67) except for a phase $e^{-\mathrm{i}\xi_i(\tau)}$.

as a function of the **output operators** depending on final time $t_f > t$, which are *defined* by

$$\hat{b}^{\beta}_{i,\text{out}}(t) \equiv \sqrt{\Delta\nu_i}\sum_{q\in M_i^{\beta}} e^{-\mathrm{i}\omega_q(t-t_f)}\hat{b}^{\beta}_{iq}(t_f), \qquad \beta\in\{l,r\}. \tag{5.176}$$

It must be pointed out that both, input and output operator (see equation (5.163) and (5.176)) have a dimension of $\mathrm{s}^{-1/2}$ in contrast to the dimensionless field amplitudes $\hat{b}^{\beta}_{iq}$ resulting in commutation relations

$$\boxed{\begin{aligned} \left[\hat{b}^{\alpha}_{i,\text{in}}(t), \hat{b}^{\beta\dagger}_{j,\text{in}}(t')\right] &= \delta_{\alpha\beta}\delta_{ij}\delta(t-t'), \\ \left[\hat{b}^{\alpha}_{i,\text{out}}(t), \hat{b}^{\beta\dagger}_{j,\text{out}}(t')\right] &= \delta_{\alpha\beta}\delta_{ij}\delta(t-t'), \quad \alpha\beta\in\{l,r\} \end{aligned}} \qquad \begin{aligned} &(5.177) \\ &(5.178) \end{aligned}$$

of unit s^{-1}. Please note, that the commutator of the input as well as the output amplitudes are delta functions resulting in a temporal delta correlation or rather a flat spectrum when transforming into the frequency regime. Thus equations (5.177)-(5.178) reflects the quantum white noise character of the input and output.

INPUT-OUTPUT RELATION A relation between the input and output field amplitudes is obtained by equating the right-hand side of equation (5.154) and the right-hand side of (5.172) which yields

$$e^{-\mathrm{i}\Omega_{iq}(t-t_f)}\hat{\mathbf{b}}_{iq}(t_f) = e^{-\mathrm{i}\Omega_{iq}(t-t_0)}\hat{\mathbf{b}}_{iq}(t_0) + \int_{t_0}^{t_f}\mathrm{d}t'\, e^{-\mathrm{i}\Omega_{iq}(t-t')}\boldsymbol{\kappa}_{iq}\hat{a}_i(t'). \tag{5.179}$$

We multiply both sides of (5.179) with $\sqrt{\Delta\nu_i}$ and sum over all q modes. Under consideration of the Markov approximation ($\eta_{iq}\simeq\eta_i$, $\kappa_{iq}\simeq\kappa_i$) and the definition of the input and output operators (5.163) and (5.176), we get

$$e^{-\mathrm{i}\Phi_i(t-t_f)}\hat{\mathbf{b}}_{i,\text{out}}(t) \simeq e^{-\mathrm{i}\Phi_i(t-t_0)}\hat{\mathbf{b}}_{i,\text{in}}(t) + \sqrt{\Delta\nu_i}\int_{t_0}^{t_f}\mathrm{d}t' \sum_{q\in M_i} e^{-\mathrm{i}\Omega_{iq}(t-t')}\boldsymbol{\kappa}_i\hat{a}_i(t'). \tag{5.180}$$

In the continuum limit, the summation term in the integrand corresponds to a delta distribution[11]. Due to the locality of the interaction at the output facets of the virtual cavity, we can expand the remote past and the remote future time, t_0 and t_f, to $\pm\infty$. Multiplying both sides of (5.180) with $e^{\mathrm{i}\Phi_i(t-t_f)}$, we find an input-output relation for the virtual cavity system

$$\boxed{\hat{\mathbf{b}}_{i,\text{out}}(t) = S_i\hat{\mathbf{b}}_{i,\text{in}}(t) + \boldsymbol{\Gamma}_i(t_f-t)\hat{a}_i(t)} \tag{5.181}$$

with

$$S_i \equiv \lim_{\substack{t_f-t_0\to\infty \\ \eta_i\to 0 \\ \eta_i(t_f-t_0)=\text{const.}}} S_i(t_f-t_0) = \begin{pmatrix} T_i & R_i^r \\ R_i^l & T_i \end{pmatrix}, \quad \boldsymbol{\Gamma}_i(\tau) = S_i(\tau)\begin{pmatrix} \mathscr{D}_i^l \\ \mathscr{D}_i^r \end{pmatrix}, \quad \hat{\mathbf{b}}_{i,\text{out}} = \begin{pmatrix} \hat{b}^r_{i,\text{out}} \\ \hat{b}^l_{i,\text{out}} \end{pmatrix}. \tag{5.182}$$

Again, we introduced the useful channel notation in agreement to figure 5.12. Here, the elements of the resulting S-matrix correspond to constant transmission and reflection amplitudes,

$$T_i \equiv T_i(t_f-t_0), \qquad R_i^{\beta} = R_i^{\beta}(t_f-t_0), \tag{5.183}$$

respectively, which are a direct result of the coupling mechanism between the left and right external fields at the single semi-transparent mirrors in analogy to the beam splitter system discussed in a previous section. Obviously, the output field is described by the input field plus the interaction with the internal radiation field in agreement to the previous section. Equation (5.181) represents a boundary condition which relates the output field modes to the internal cavity modes.

---

[11] We utilized the integral representation of a delta function $\delta(t) = \int_{-\infty}^{\infty}\frac{\mathrm{d}\omega}{2\pi}e^{-\mathrm{i}\omega t}$.

SMALL TRANSMISSION AMPLITUDE In case of a small transmission amplitude, that is $|T_i| \ll 1$, equation (5.181) reduces to

$$\begin{pmatrix} \hat{b}^r_{i,\mathrm{out}}(t) \\ \hat{b}^l_{i,\mathrm{out}}(t) \end{pmatrix} = \begin{pmatrix} 0 & R^r_i \\ R^l_i & 0 \end{pmatrix} \begin{pmatrix} \hat{b}^l_{i,\mathrm{in}}(t) \\ \hat{b}^r_{i,\mathrm{in}}(t) \end{pmatrix} + \sqrt{\Delta\nu_\mathrm{F}} \begin{pmatrix} T^r_i(t) \\ T^l_i(t) \end{pmatrix} \hat{a}_i(t), \tag{5.184}$$

with

$$T^\beta_i(t) = \frac{\mathscr{D}^\beta_i R^\beta_i(t_f - t) + \mathscr{D}^\alpha_i T_i(t_f - t)}{\sqrt{\Delta\nu_\mathrm{F}}}, \quad \alpha,\beta \in \{l,r\}, \quad \alpha \neq \beta. \tag{5.185}$$

Obviously, a comparison of equation (5.184) with (5.148)-(5.149) identifies a new transmission amplitude according to (5.185). The **input-output relation** for small transmission amplitude reads

$$\boxed{\hat{b}^\beta_{i,\mathrm{out}}(t) = R^\beta_i \hat{b}^\beta_{i,\mathrm{in}}(t) + \sqrt{\Delta\nu_\mathrm{F}} T^\beta_i(t) \hat{a}_i(t)}, \quad \beta \in \{l,r\}, \tag{5.186}$$

in fully agreement with the solutions (5.148)-(5.149) (see also references [149, 150]) except for a time-dependency of the transmission $T^\beta_i(t)$. In the following discussion of light emitting QDSLDs we will follow this assumption of a small transmission amplitude $|T_i| \ll 1$ resulting into an output amplitude described by (5.186).

ELECTROMAGNETIC FIELDS OF THE VIRTUAL CAVITY With these information in mind, we can determine electric fields located on the left- and right-hand side of the cavity,

$$\hat{\mathbf{E}}^r(x,y,z>0,t) = \hat{\mathbf{E}}^r_\mathrm{in}\left(x,y,t+\frac{z}{c_0}\right) + \hat{\mathbf{E}}^r_\mathrm{out}\left(x,y,t-\frac{z}{c_0}\right) \tag{5.187}$$

$$\hat{\mathbf{E}}^l(x,y,z<-L,t) = \hat{\mathbf{E}}^l_\mathrm{in}\left(x,y,t-\frac{z}{c_0}\right) + \hat{\mathbf{E}}^l_\mathrm{out}\left(x,y,t+\frac{z}{c_0}\right), \tag{5.188}$$

with positive frequency part of the input and the output ($\beta \in \{l,r\}$)

$$\hat{\mathbf{E}}^{\beta(+)}_{\mathrm{in(out)}}(x,y,t) \simeq \sum_{\{k_i>0\}} \tilde{v}_i(x,y) \hat{b}^\beta_{i,\mathrm{in(out)}}(t) \mathbf{e}_y, \tag{5.189}$$

and mode function $\tilde{v}_i(x,y)$ defined in equation (5.144).

SPECIAL CASE: TOTAL REFLECTION The validity of the identification of the parameters R^β_i and T^β_i with reflection and transmission amplitudes can easily be tested when studying the stationary electric field on the right-hand side of the cavity depicted in figure 5.15 by assuming a perfectly reflecting right mirror.

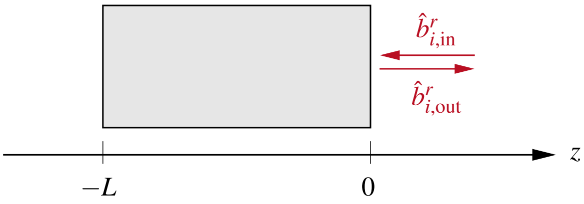

Figure 5.15: Sketch of the virtual cavity for the special case of total reflection on the right.

Here, the total electric field $\hat{\mathbf{E}}^r(x,y,z=0,t)$ vanishes, which defines a boundary condition. The field is not allowed to interact with the internal radiation so that the coupling constant and the transmission amplitudes are zero, $T^r_i = 0$, for all modes i. From this it follows

$$\hat{b}^r_{i,\mathrm{out}}(t) = R^r_i \hat{b}^r_{i,\mathrm{in}}(t) \quad \text{with} \quad R^r_i = -1, \quad \forall i. \tag{5.190}$$

Obviously, this is satisfied for a phase $|\eta_i|(t_f - t_0) = \pi/2$ and the output corresponds to the input shifted by π. The result (5.190) is in full agreement with the physical prediction.

It must be pointed out, that in reference [144] the reflection amplitude developed in equation (5.186) is equal to one, $R_i^\beta = 1$, for all field modes i so that no phase jump at the single mirror is observable, which is in direct contradictory to the solution of the congruent boundary value problem.

Indeed, one can state that the input-output relation derived in this section, in which the boundary conditions are replaced by effective interactions, is based on the concepts of *C. W. Gardiner* and *M. J. Collett* [144]. However, the derived relation (5.186) between the output and the input fields considers the existing boundary conditions at the single semi-transparent mirrors leading to the occurrence of reflection and transmission coefficients which again enforces a phase shift by π for total reflection. Thus, this input-output relation represents a generalization of [144]. Clearly, Gardiner's input-output formalism is an elegant and simple way to directly determine the far field output with the knowledge of the input field and the dynamics of the intra-cavity system. In addition, the approach is also applicable to nonlinear systems and allows to study cascaded systems [140] in which the output field of a system is simultaneously the input of an other one, a great benefit not only in the context of this thesis, but also for other fields of research like quantum optical networks [151–153].

Up to now, we have studied single subsystems, the beam splitter configuration and the virtual cavity, forming the empty diode model described at the beginning of this section. In the following we bring these separated systems together in order to determine the output emission of empty superluminescent diodes.

5.2.4 *Emission of the empty waveguide*

With the detailed information about the beam splitter and cavity sub-system in mind we can study the total emission of our empty superluminescent diode system. The physical problem under consideration is depicted in figure 5.16 once again.

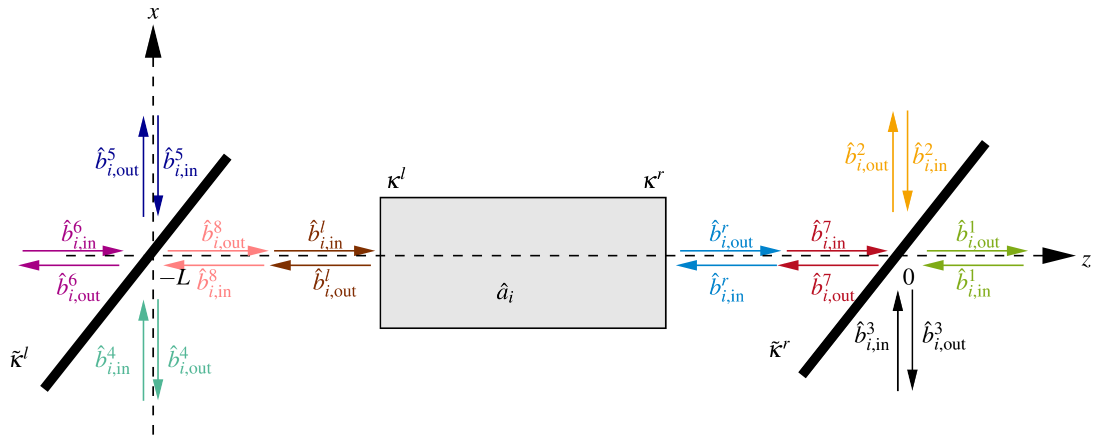

Figure 5.16: Sketch of the empty superluminescent diode system including the concept of channels in analogy to scattering theory.

As already mentioned, it corresponds to a cascaded system in which two output channels of the beam splitter are simultaneously the virtual cavity input fields (see equation (5.46)) and figure 5.16. Under consideration of (5.46) as well as the result of the cavity input-output formalism (5.186) and the beam splitter output channels described by (5.93)-(5.96), we can determine the input field operators of the radiation fields $\hat{\mathbf{E}}^7$ and $\hat{\mathbf{E}}^8$ in terms of the beam splitter's reflection and transmission amplitudes as well as the interaction with the intra-cavity modes according to

$$\begin{aligned}
\hat{b}^7_{i,\mathrm{in}}(t) &= \hat{b}^r_{i,\mathrm{out}}(t) = R^r_i \hat{b}^r_{i,\mathrm{in}}(t) + \sqrt{\Delta\nu_\mathrm{F}} T^r_i(t)\hat{a}_i(t) = R^r_i \hat{b}^7_{i,\mathrm{out}}(t) + \sqrt{\Delta\nu_\mathrm{F}} T^r_i(t)\hat{a}_i(t) \\
&= R^r_i \mathscr{T}_{i,r} \hat{b}^1_{i,\mathrm{in}}(t) + R^r_i \mathscr{R}^r_i \hat{b}^2_{i,\mathrm{in}}(t) + \sqrt{\Delta\nu_\mathrm{F}} T^r_i(t)\hat{a}_i(t), \\
\hat{b}^8_{i,\mathrm{in}}(t) &= \hat{b}^l_{i,\mathrm{out}}(t) = R^l_i \hat{b}^l_{i,\mathrm{in}}(t) + \sqrt{\Delta\nu_\mathrm{F}} T^l_i(t)\hat{a}_i(t) = R^l_i \hat{b}^8_{i,\mathrm{out}}(t) + \sqrt{\Delta\nu_\mathrm{F}} T^l_i(t)\hat{a}_i(t) \\
&= R^l_i \mathscr{R}^l_i \hat{b}^4_{i,\mathrm{in}}(t) + R^l_i \mathscr{T}^{\,l}_i \hat{b}^6_{i,\mathrm{in}}(t) + \sqrt{\Delta\nu_\mathrm{F}} T^l_i(t)\hat{a}_i(t).
\end{aligned} \tag{5.191}$$

Please note, the output field amplitudes $\hat{b}^\alpha_{i,\mathrm{out}}$ with $\alpha = 1,2,4,6$ depend explicitly on $\hat{b}^7_{i,\mathrm{in}}$ and $\hat{b}^8_{i,\mathrm{in}}$. Therefore, we can specify these operators in terms of the input channel amplitudes via

$$\begin{aligned}
\hat{b}^1_{i,\mathrm{out}}(t) &= R^r_i \mathscr{T}^{\,r2}_i \hat{b}^1_{i,\mathrm{in}}(t) + R^r_i \mathscr{R}^r_i \mathscr{T}^{\,r}_i \hat{b}^2_{i,\mathrm{in}}(t) + \mathscr{R}^r_i \hat{b}^3_{i,\mathrm{in}}(t) + \mathscr{T}^{\,r}_i \sqrt{\Delta\nu_\mathrm{F}} T^r_i(t)\hat{a}_i(t), \\
\hat{b}^2_{i,\mathrm{out}}(t) &= -R^r_i \mathscr{T}^{\,r}_i \mathscr{R}^{r*}_i \hat{b}^1_{i,\mathrm{in}}(t) - R^r_i \left|\mathscr{R}^r_i\right|^2 \hat{b}^2_{i,\mathrm{in}}(t) + \mathscr{T}^{\,r}_i \hat{b}^3_{i,\mathrm{in}}(t) - \mathscr{R}^{r*}_i \sqrt{\Delta\nu_\mathrm{F}} T^r_i(t)\hat{a}_i(t), \\
\hat{b}^4_{i,\mathrm{out}}(t) &= -R^l_i \left|\mathscr{R}^l_i\right|^2 \hat{b}^4_{i,\mathrm{in}}(t) + \mathscr{T}^{\,l}_i \hat{b}^5_{i,\mathrm{in}}(t) - R^l_i \mathscr{T}^{\,l}_i \mathscr{R}^{l*}_i \hat{b}^6_{i,\mathrm{in}}(t) - \mathscr{R}^{l*}_i \sqrt{\Delta\nu_\mathrm{F}} T^l_i(t)\hat{a}_i(t), \\
\hat{b}^6_{i,\mathrm{out}}(t) &= R^l_i \mathscr{R}^l_i \mathscr{T}^{\,l}_i \hat{b}^4_{i,\mathrm{in}}(t) + \mathscr{R}^l_i \hat{b}^5_{i,\mathrm{in}}(t) + R^l_i \mathscr{T}^{\,l2}_i \hat{b}^6_{i,\mathrm{in}}(t) + \mathscr{T}^{\,l}_i \sqrt{\Delta\nu_\mathrm{F}} T^l_i(t)\hat{a}_i(t).
\end{aligned} \tag{5.192}$$

Obviously, the system's degree of freedom have been reduced by a factor of 2. Accordingly, we find an input-output relation for the total empty superluminescent diode system with tilted end facets described by the matrix equation of type

$$\boxed{\hat{\mathbf{b}}_{i,\mathrm{out}}(t) = \mathbb{S}_i \hat{\mathbf{b}}_{i,\mathrm{in}}(t) + \mathbf{A}_i(t)\hat{a}_i(t).} \tag{5.193}$$

It states that the output fields are related with the input fields by the matrix

$$\mathbb{S}_i = \begin{pmatrix}
R^r_i \mathscr{T}^{\,r2}_i & R^r_i \mathscr{T}^{\,r}_i \mathscr{R}^r_i & \mathscr{R}^r_i & 0 & 0 & 0 \\
-R^r_i \mathscr{R}^{r*}_i \mathscr{T}^{\,r}_i & -R^r_i |\mathscr{R}^r_i|^2 & \mathscr{T}^{\,r}_i & 0 & 0 & 0 \\
-\mathscr{R}^{r*}_i & \mathscr{T}^{\,r}_i & 0 & 0 & 0 & 0 \\
0 & 0 & 0 & -R^l_i |\mathscr{R}^l_i|^2 & \mathscr{T}^{\,l}_i & -R^l_i \mathscr{R}^{l*}_i \mathscr{T}^{\,l}_i \\
0 & 0 & 0 & \mathscr{T}^{\,l}_i & 0 & -\mathscr{R}^{l*}_i \\
0 & 0 & 0 & R^l_i \mathscr{T}^{\,l}_i \mathscr{R}^l_i & \mathscr{R}^l_i & R^l_i \mathscr{T}^{\,l}_i \\
\mathscr{T}^{\,r}_i & \mathscr{R}^r_i & 0 & 0 & 0 & 0 \\
0 & 0 & 0 & \mathscr{R}^l_i & 0 & \mathscr{T}^{\,l}_i
\end{pmatrix}, \tag{5.194}$$

which depends on reflection and transmission amplitudes of the single sub-systems; beams splitter $(\mathscr{R}^r_i, \mathscr{T}^{\,r}_i, \mathscr{R}^l_i, \mathscr{T}^{\,l}_i)$ and virtual cavity $(R^r_i, T^r_i, R^l_i, T^l_i)$. The second term in equation (5.193) results from the interaction of the input field with the intracavity modes specified by

$$\hat{\mathbf{A}}_i(t) = \sqrt{\Delta\nu_\mathrm{F}} \begin{pmatrix} \mathscr{T}^{\,r}_i T^r_i(t) & -\mathscr{R}^{r*}_i T^r_i(t) & 0 & -\mathscr{R}^{l*}_i T^l_i(t) & 0 & \mathscr{T}^{\,l}_i T^l_i(t) & 0 & 0 \end{pmatrix}^T. \tag{5.195}$$

Clearly, the dynamics of the internal field modes $\hat{a}_i$ of an empty superluminescent diode is described by the quantum Langevin equation (5.168) with external channel noise inputs

$$\hat{b}^L_{i,\mathrm{in}}(t) \equiv X^l_i(t-t_0)\hat{b}^l_{i,\mathrm{in}}(t) = X^l_i(t-t_0)\hat{b}^8_{i,\mathrm{out}}(t) = X^l_i(t-t_0)(\mathscr{R}^l_i \hat{b}^4_{i,\mathrm{in}}(t) + \mathscr{T}^{\,l}_i \hat{b}^6_{i,\mathrm{in}}(t)), \tag{5.196}$$

$$\hat{b}^R_{i,\mathrm{in}}(t) \equiv X^r_i(t-t_0)\hat{b}^r_{i,\mathrm{in}}(t) = X^r_i(t-t_0)\hat{b}^7_{i,\mathrm{out}}(t) = X^r_i(t-t_0)(\mathscr{T}^{\,r}_i \hat{b}^1_{i,\mathrm{in}}(t) + \mathscr{R}^r_i \hat{b}^2_{i,\mathrm{in}}(t)). \tag{5.197}$$

ELECTROMAGNETIC CHANNEL FIELDS In analogy to appendix E, we can determine the single electromagnetic channel fields entering and simultaneously leaving the QDSLD at the output facets. As an example, we consider the positive frequency part of channel 1 located on the right-hand side of the QDSLD (cf. figure 5.16)

$$\hat{\mathbf{E}}^{1(+)}(x,y,z,t) = \hat{\mathbf{E}}^{1(+)}_{\text{in}}\left(x,y,t+\frac{z}{c_0}\right) + \hat{\mathbf{E}}^{1(+)}_{\text{out}}\left(x,y,t-\frac{z}{c_0}\right), \quad (z>0). \tag{5.198}$$

Due to the assumption of the centering of channel frequencies around the intra-cavity frequencies (cf. approximation (5.81)), the in- and output parts of the electric field read

$$\hat{\mathbf{E}}^{1(+)}_{\text{in(out)}}(x,y,t) = \hat{E}^{1(+)}_{\text{in(out)}}(x,y,t)\,\mathbf{e}_y \simeq \sum_{\{k_i>0\}} \tilde{v}^1_i(\mathbf{r})\hat{b}^1_{i,\text{in(out)}}(t)\mathbf{e}_y, \tag{5.199}$$

with the output operator characterized by equation (5.193), mode function

$$\tilde{v}^{\alpha}_i(\mathbf{r}) = \mathrm{i}\sqrt{\frac{\hbar\omega_i\pi}{\varepsilon_0 V\Delta\omega_i}} \times \begin{cases} \mu(x,y), & \alpha = 1,6 \\ \mu(y,z), & \alpha = 2,3,4,5, \end{cases} \tag{5.200}$$

and wave number $|k_q| = \omega_q/c_0$.

Analogously, we can calculate all the other external channel fields [12]

$$\hat{\mathbf{E}}^{2(+)}(x,y,z,t) = \hat{\mathbf{E}}^{2(+)}_{\text{in}}\left(y,z,t+\frac{x}{c_0}\right) + \hat{\mathbf{E}}^{2(+)}_{\text{out}}\left(y,z,t-\frac{x}{c_0}\right), \quad (x>0), \tag{5.201}$$

$$\hat{\mathbf{E}}^{3(+)}(x,y,z,t) = \hat{\mathbf{E}}^{3(+)}_{\text{in}}\left(y,z,t-\frac{x}{c_0}\right) + \hat{\mathbf{E}}^{3(+)}_{\text{out}}\left(y,z,t+\frac{x}{c_0}\right), \quad (x<0), \tag{5.202}$$

$$\hat{\mathbf{E}}^{4(+)}(x,y,z,t) = \hat{\mathbf{E}}^{4(+)}_{\text{in}}\left(y,z,t-\frac{x}{c_0}\right) + \hat{\mathbf{E}}^{4(+)}_{\text{out}}\left(y,z,t+\frac{x}{c_0}\right), \quad (x<0), \tag{5.203}$$

$$\hat{\mathbf{E}}^{5(+)}(x,y,z,t) = \hat{\mathbf{E}}^{5(+)}_{\text{in}}\left(y,z,t+\frac{x}{c_0}\right) + \hat{\mathbf{E}}^{5(+)}_{\text{out}}\left(y,z,t-\frac{x}{c_0}\right), \quad (x>0), \tag{5.204}$$

$$\hat{\mathbf{E}}^{6(+)}(x,y,z,t) = \hat{\mathbf{E}}^{6(+)}_{\text{in}}\left(x,y,t-\frac{z+L}{c_0}\right) + \hat{\mathbf{E}}^{6(+)}_{\text{out}}\left(x,y,t+\frac{z+L}{c_0}\right), \quad (z<0), \tag{5.205}$$

with corresponding output operators derived from equation (5.193).

In analogy to reference [144], we introduce an abbreviation for the output field on the right-hand side of the right beam splitter parallel to the z-direction,

$$\boxed{\hat{b}^1_{i,\text{out}}(t) = \hat{b}_{i,\text{in}}(t) + \sqrt{\Delta\nu_{\text{F}}}\,\mathscr{T}^{\,r}_i T^r_i(t)\hat{a}_i(t)} \tag{5.206}$$

with input operator,

$$\hat{b}_{i,\text{in}} = R^r_i \mathscr{T}^{\,r2}_i \hat{b}^1_{i,\text{in}} + R^r_i \mathscr{T}^{\,r}_i \mathscr{R}^r_i \hat{b}^2_{i,\text{in}} + \mathscr{R}^r_i \hat{b}^3_{i,\text{in}}, \tag{5.207}$$

in terms of channel fields $\alpha = 1-3$. Equation (5.206) looks quite similar to the solution of a single-sided optical one-dimensional cavity (cf. reference [144]), modified by the presence of the beam splitter system enclosing the cavity.

---

[12] For the electric field of channel 6 we had to apply a specific renormalization.

OUTPUT SPECTRUM OF EMPTY SLDS The output spectrum recorded by a single-photon counting detector with cross-section area A corresponds to the expectation value of the system's output operators in frequency space according to (2.94). The components of the optical power spectrum matrix $S_{\text{out}}(z,\omega)$, that is the optical power per frequency,

$$\begin{aligned} S_{\text{out}}(z,\omega)_{\alpha\beta} &= \mathscr{C} \int_A \mathrm{d}x\, \mathrm{d}y\, \langle \hat{\underline{E}}^{\alpha(-)}_{\text{out}}(\mathbf{r},\omega) \hat{\underline{E}}^{\beta(+)}_{\text{out}}(\mathbf{r},\omega) \rangle \\ &= \sum_{\{k_i,k_j>0\}} \Upsilon_i \Upsilon_j \langle \hat{\underline{b}}^{\alpha\dagger}_{i,\text{out}}(\omega) \hat{\underline{b}}^{\beta}_{j,\text{out}}(\omega) \rangle, \quad \Upsilon_i = \sqrt{\frac{2\hbar\pi c_0 \omega_i}{\Delta\omega_i L}}, \end{aligned} \tag{5.208}$$

depends on the components of $\hat{\underline{\mathbf{b}}}_{i,\text{out}}(\omega)$ which again can be calculated by taking the Fourier transform of the system's operator equation (5.193)

$$\hat{\underline{\mathbf{b}}}_{i,\text{out}}(\omega) = \mathbb{S}_i \hat{\underline{\mathbf{b}}}_{i,\text{in}}(\omega) + \frac{1}{2\pi} \int_{-\infty}^{\infty} \mathrm{d}t \mathbf{A}_i(t) \hat{a}_i(t) e^{\mathrm{i}\omega t}. \tag{5.209}$$

We assume that the time-dependent transmission amplitudes $T_i^{l/r}(t)$ arising in $\mathbf{A}_i(t)$ (cf. equation (5.195)) evolve slowly compared to the system's amplitude so it can be considered as a constant in good approximation. Thus, we can set

$$T_i^{\beta}(t) \simeq T_i^{\beta} = \frac{\mathscr{D}_i^{\beta} R_i^{\beta} + \mathscr{D}_i^{\alpha} T_i}{\sqrt{\Delta\nu_{\text{F}}}}, \quad \alpha,\beta \in \{l,r\}, \quad \alpha \neq \beta \tag{5.210}$$

and the reflection and transmission amplitudes, R_i^{β} and T_i, agree with the S-matrix elements (5.183). Within this approximation, equation (5.209) reduces to

$$\hat{\underline{\mathbf{b}}}_{i,\text{out}}(\omega) = \mathbb{S}_i \hat{\underline{\mathbf{b}}}_{i,\text{in}}(\omega) + \mathbf{A}_i \hat{\underline{a}}_i(\omega). \tag{5.211}$$

The internal field amplitudes in frequency space $\hat{\underline{a}}_i(\omega)$ in terms of the input system amplitudes can be calculated by Fourier transforming the quantum Langevin equation (5.168),

$$\hat{\underline{a}}_i(\omega) = \frac{\hat{\underline{b}}^{L}_{i,\text{in}}(\omega) + \hat{\underline{b}}^{R}_{i,\text{in}}(\omega)}{\mathrm{i}(\omega - \omega_i) - \frac{\gamma_i^l + \gamma_i^r}{2}} \tag{5.212}$$

with noise input amplitudes in frequency space

$$\hat{\underline{b}}^{L}_{i,\text{in}}(\omega) = (\mathscr{D}_i^{l*} T_i + \mathscr{D}_i^{r*} R_i^l)(\mathscr{T}_i^l \hat{\underline{b}}^{6}_{i,\text{in}}(\omega) + \mathscr{R}_i^l \hat{\underline{b}}^{4}_{i,\text{in}}(\omega)), \tag{5.213}$$

$$\hat{\underline{b}}^{R}_{i,\text{in}}(\omega) = (\mathscr{D}_i^{l*} R_i^r + \mathscr{D}_i^{r*} T_i)(\mathscr{T}_i^r \hat{\underline{b}}^{1}_{i,\text{in}}(\omega) + \mathscr{R}_i^r \hat{\underline{b}}^{2}_{i,\text{in}}(\omega)). \tag{5.214}$$

Finally inserting $\hat{\underline{a}}_i(\omega)$ into the external field modes in frequency space, we find

$$\hat{\underline{\mathbf{b}}}_{i,\text{out}}(\omega) = \mathscr{M}_i(\omega)\, \hat{\underline{\mathbf{b}}}_{i,\text{in}}(\omega), \tag{5.215}$$

with

$$\mathscr{M}_i = \begin{pmatrix} \Gamma_i^r R_i^r \mathscr{T}_i^{r2} & \Gamma_i^r R_i^r \mathscr{T}_i^r \mathscr{R}_i^r & \mathscr{R}_i^r & \lambda_i^r R_i^l \mathscr{T}_i^r \mathscr{R}_i^l & 0 & \lambda_i^r R_i^l \mathscr{T}_i^r \mathscr{T}_i^l \\ -\Gamma_i^r R_i^r \mathscr{R}_i^{r*} \mathscr{T}_i^r & -\Gamma_i^r R_i^r |\mathscr{R}_i^r|^2 & \mathscr{T}_i^r & -\lambda_i^r R_i^l \mathscr{R}_i^{r*} \mathscr{R}_i^l & 0 & -\lambda_i^r R_i^l \mathscr{R}_i^{r*} \mathscr{T}_i^l \\ -\mathscr{R}_i^{r*} & \mathscr{T}_i^r & 0 & 0 & 0 & 0 \\ -\lambda_i^l R_i^r \mathscr{R}_i^{l*} \mathscr{T}_i^r & -\lambda_i^l R_i^r \mathscr{R}_i^{l*} \mathscr{R}_i^r & 0 & -\Gamma_i^l R_i^l |\mathscr{R}_i^l|^2 & \mathscr{T}_i^l & -\Gamma_i^l R_i^l \mathscr{T}_i^l \mathscr{R}_i^{l*} \\ 0 & 0 & 0 & \mathscr{T}_i^l & 0 & -\mathscr{R}_i^{l*} \\ \lambda_i^l R_i^r \mathscr{T}_i^l \mathscr{T}_i^r & \lambda_i^l R_i^r \mathscr{T}_i^l \mathscr{R}_i^r & 0 & \Gamma_i^l R_i^l \mathscr{T}_i^l \mathscr{R}_i^l & \mathscr{R}_i^l & \Gamma_i^l R_i^l \mathscr{T}_i^{l2} \\ \mathscr{T}_i^r & \mathscr{R}_i^r & 0 & 0 & 0 & 0 \\ 0 & 0 & 0 & \mathscr{R}_i^l & 0 & \mathscr{T}_i^l \end{pmatrix}$$

and

$$\lambda_i^{\beta} = \frac{\mathscr{D}_i^{\alpha}\mathscr{D}_i^{\beta *}}{\varepsilon_i}, \quad \Gamma_i^{\beta} = 1 + \frac{\gamma_i^{\alpha}}{\varepsilon_i}, \quad \varepsilon_i = \mathrm{i}(\omega - \omega_i) - \frac{\gamma_i^r + \gamma_i^l}{2}, \quad \alpha,\beta \in \{l,r\}, \quad \alpha \neq \beta.$$

Thus, the output vector operator $\underline{\hat{\mathbf{b}}}_{i,\mathrm{out}}$ depends linearly on the input vector operator $\underline{\hat{\mathbf{b}}}_{i,\mathrm{in}}$, revealing that the power spectrum depends significantly on the choice of the input field. It is precisely a convolution of the input field with the response function of the beam splitters. The next subsections deal with the white noise and phase-randomized Gaussian noise input.

5.2.4.1 Response to white noise input

Quantum white noise is characterized by its spectral density independent of frequency,

$$S(\omega) = \bar{S}. \tag{5.216}$$

As in the case of white light, all frequencies appear equally. Clearly, the choice of quantum white noise as an input, having infinite energy densities, is an idealization and therefore not observable in real physical systems. It is rather the thermal state which describes the truly physical nature of the input resulting into a Planck distribution for the mean thermal occupation number.

According to the Wiener-Khintchine theorem, the first-order autocorrelation function is specified by the Fourier transform of the spectral density, resulting into a delta-function, meaning that white noise fluctuations are uncorrelated in case of different time events. In summary, for white noise input with the number of quanta $\bar{N}$, the following correlations hold

$$\langle \hat{b}_{\mathrm{in}}^{\dagger}(t)\hat{b}_{\mathrm{in}}(t')\rangle = \bar{N}\delta(t-t'), \tag{5.217}$$

$$\langle \hat{b}_{\mathrm{in}}(t)\hat{b}_{\mathrm{in}}^{\dagger}(t')\rangle = (\bar{N}+1)\delta(t-t'). \tag{5.218}$$

Therefore, $\hat{b}_{\mathrm{in}}$ is Markovian. Please note, $\bar{N}$ is constant compared to thermal noise, in which the photon number is described by a Planck distribution, $\bar{N}(\omega) = n_T(\omega)$ (cf. equation (2.76)).

In this section, we study the simple case of white noise input entering the empty cavity system from both sides. The concept of white noise discussed above can be directly applied to our complex input-output cavity setup. Denoting $\bar{N}_{\alpha}$ as the mean occupation number of channel α, the frequency correlation of the input mode i is given by

$$\langle \underline{\hat{b}}_{i,\mathrm{in}}^{\alpha\dagger}(\omega)\underline{\hat{b}}_{j,\mathrm{in}}^{\beta}(\omega')\rangle = (S_{ij,\mathrm{in}})_{\alpha\beta}\delta(\omega-\omega'), \quad (S_{ij,\mathrm{in}})_{\alpha\beta} = \bar{N}_{\alpha}\delta_{\alpha\beta}\delta_{ij}, \quad \alpha,\beta = 1,\ldots,6, \tag{5.219}$$

with input spectral density matrix element $(S_{ij,\mathrm{in}})_{\alpha\beta}$ [139]. Here, we claimed that different channel modes are uncorrelated. In addition, we neglected correlations between different modes of the same channel.

A single-photon counting detector of finite cross-section area is assumed to be located on the right-hand side and far away from of the empty SLD perpendicular to the z-direction. Consequently, only the output of channel 1 is recorded and contributes to the spectral density, because output fields propagate perpendicular to the z direction as well as the field on the left-hand side, are not striking the detector, i.e. $\hat{\mathbf{E}}_{\mathrm{out}} = \hat{\mathbf{E}}_{\mathrm{out}}^{1}$. The output of channel 1 is exactly specified by the first element of the spectrum matrix $S_{\mathrm{out}}(\omega)$.

In case of white noise input and equal damping rates, $\gamma^l = \gamma^r = \gamma$, we find

$$\begin{aligned} S(\omega) \equiv (S_{\mathrm{out}}(\omega))_{11} =& \pi\gamma \sum_{\{k_i\}} \Upsilon_i^2 |R_i^r|^2 \mathscr{T}_i^{r2} \times \Big[(\bar{N}_1 \mathscr{T}_i^{r2} + \bar{N}_2 |\mathscr{R}_i^r|^2)\big(\frac{1}{\pi\gamma} - \mathscr{L}(\omega-\omega_i)\big) \\ & + \bar{N}_3 \frac{|\mathscr{R}_i^r|^2}{\pi\gamma \mathscr{T}_i^{r2} |R_i^r|^2} + (\bar{N}_4 |\mathscr{R}_i^l|^2 + \bar{N}_6 \mathscr{T}_i^{l2}) \mathscr{L}(\omega-\omega_i) \Big] \end{aligned} \tag{5.220}$$

with the Lorentzian function

$$\mathscr{L}(\omega)=\frac{1}{\pi}\frac{\gamma}{\gamma^2+\omega^2}. \tag{5.221}$$

For $\bar{N}_1=\bar{N}_2=\bar{N}_3=\bar{N}_4=0$ and $\bar{N}_6=\bar{N}$, the output spectrum,

$$S(\omega)=p\sum_{\{k_i\}}\frac{\omega_i}{\Delta\omega_i}|R_i^r|^2\mathscr{T}_i^{l2}\mathscr{T}_i^{r2}\,\mathscr{L}(\omega-\omega_i),\quad p=\frac{2\pi^2\hbar c_0\gamma\bar{N}}{L}, \tag{5.222}$$

is a sum of Lorentzians with maximum value at $\omega=\omega_i$ and a full width at half maximum of $\sqrt{2}\gamma$.

Making the continuum transition we find a continuous power spectrum,

$$S(\omega)=e\int\limits_{\omega_{-N/2}}^{\omega_{N/2-1}}\mathrm{d}\tilde{\omega}\;\tilde{\omega}|R^r(\tilde{\omega})|^2\mathscr{T}^{l2}(\tilde{\omega})\mathscr{T}^{r2}(\tilde{\omega})\,\mathscr{L}(\omega-\tilde{\omega}),\quad e=\frac{p}{\Delta\omega^2}, \tag{5.223}$$

with $\Delta\omega=(\omega_{N/2-1}-\omega_{-N/2})/(N-1)$, given by a convolution of a Lorentzian curve and three transfer functions (spectra) weighted by frequency $\tilde{\omega}$. Here, we supposed equal frequency separation between adjacent modes, i.e. $\Delta\omega_i=\Delta\omega$. Please note, that these transfer functions vary slowly as a function of angular frequency $\tilde{\omega}$ as a result of the Markovian system's dynamics.

LIMITING CASE $\gamma\ll 1$ Consider the power spectral density (5.223) having a sharp Lorentzian with γ much smaller than any other relevant system frequency. In this case we can write

$$\lim_{\gamma\ll 1}\mathscr{L}(\omega)=\frac{1}{\pi}\lim_{\gamma\ll 1}\frac{\gamma}{\gamma^2+\omega^2}=\frac{1}{2\mathrm{i}\pi}\lim_{\gamma\ll 1}\left[\frac{1}{\omega-\mathrm{i}\gamma}-\frac{1}{\omega+\mathrm{i}\gamma}\right]. \tag{5.224}$$

The single terms in the brackets are evaluable using the Sokhotski–Plemelj formula [154]

$$\lim_{\gamma\to 0}\frac{1}{\omega\pm\mathrm{i}\gamma}=\mathscr{P}\left(\frac{1}{\omega}\right)\mp\mathrm{i}\pi\delta(\omega), \tag{5.225}$$

which results into the power spectral density

$$S(\omega)=e\int\limits_{\omega_{-N/2}}^{\omega_{N/2-1}}\mathrm{d}\tilde{\omega}\;\tilde{\omega}|R^r(\tilde{\omega})|^2\mathscr{T}^{l2}(\tilde{\omega})\mathscr{T}^{r2}(\tilde{\omega})\delta(\omega-\tilde{\omega}). \tag{5.226}$$

For a natural line width γ much smaller than the frequency bandwidth b, we can extend the integration limits to $\pm\infty$ leading to a constant optical power spectrum,

$$S(\omega)\approx e\omega|R^r(\omega)|^2\mathscr{T}^{l2}(\omega)\mathscr{T}^{r2}(\omega), \tag{5.227}$$

of unit $\mathrm{W}\cdot\mathrm{s}$. Obviously, for a narrow line width γ, the output spectrum of an empty QDSLD for white noise as an input depends on the pointwise multiplication of the three single spectra $|R^r(\omega)|^2$, $\mathscr{T}^{l2}(\omega)$ and $\mathscr{T}^{r2}(\omega)$. However, as already mentioned, these spectra vary slowly as a function of frequency.

We consider again the convolution integral (5.226) and eliminate the explicit frequency dependency in the integrand by setting $\tilde{\omega}$ approximately equal to the mean value, $\tilde{\omega}\simeq\bar{\omega}$. Therefore, in case of constant reflection and transmission amplitudes, the output spectrum is independent of frequency suggesting that the output is again quantum white noise.

5.2.4.2 Response to phase-randomized Gaussian noise input

Obviously, the choice of noise input influences the shape of the optical power spectrum significantly in case of an empty SLD. According to the investigation of light emitted by QDSLDs in chapter 4, it is interesting to study phase-randomized Gaussian noise input with a density operator defined in equation (4.6). Here, the mean photon number $\bar{N}$ in (5.219) becomes a function of frequency ω,

$$\bar{N}(\omega) = C\left[p^s(\omega) + p^t(\omega)\right], \qquad C = \frac{L}{\hbar\omega c_0}, \tag{5.228}$$

depending on the distributions $p^s(\omega)$ and $p^t(\omega)$ introduced in equation (4.14). Please note, in case of near-infrared photons, $p^t(\omega)$ is negligible, as already shown in chapter 4. Motivated by the measured optical power spectrum, we assume again a Gaussian distribution for $p^s(\omega)$ equivalent to equation (4.41) in section 4.5.1. Regarding the Markovian character of the system under study, reflection and transmission amplitudes are slowly varying in terms of frequency $\tilde{\omega}$ and we can extract these functions out of the integral according to the mean value theorem. The integration limits are extended to $\pm\infty$ in analogy to the studied case of white noise input. Finally, we get a simple expression for the power spectrum

$$S(\omega) \simeq \frac{2\pi^2\gamma}{(\Delta\omega)^2}|R^r(\omega)|^2\mathscr{T}^{l2}(\omega)\mathscr{T}^{r2}(\omega)\int_{-\infty}^{\infty}\mathrm{d}\tilde{\omega}\; p^s(\tilde{\omega})\mathscr{L}(\omega-\tilde{\omega}). \tag{5.229}$$

Equation (5.229) corresponds to a convolution of a Lorentzian and a Gaussian curve. Accordingly, the power spectrum of an empty SLD with PRAG input noise exhibits a Voigt profile multiplied with the flat spectra $\mathscr{T}^{l2}(\omega)$, $\mathscr{T}^{r2}(\omega)$ and $|R^r(\omega)|^2$. Please note, that these spectral densities have upper bounds due to their definition in (5.96) and (5.183).

5.3 INTRAWAVEGUIDE QUANTUM DOT SUPERLUMINESCENT DIODE SYSTEM

The last two sections dealt with a quantum mechanical description of the components forming the special QDSLD system: the gain medium composed of M QDs and the semiconductor waveguide with tilted end facets. The model of the total diode system was already introduced at the beginning of this chapter. Now we have reached a point at which we are able to determine the full intrawaveguide dynamics, relevant to obtain knowledge about crucial physical processes like gain, absorption, saturation etc., which again affect the spectral density and the photon statistics of the QDSLD. In addition, we will observe amplified spontaneous emission as a natural consequence of a microscopic description of this semiconductor device.

In order to describe the total QDSLD intrawaveguide system, we follow the concepts introduced by *C. W. Gardiner* and *M. J. Collett* in 1985 [144] to deal with open quantum systems as motivated in the section before. The resulting input-output formalism allows to determine the output electric field, necessary to calculate first- and second-order temporal autocorrelation functions of the radiation field recorded by detectors far away from the small system under study. Pursuant to their definition (see section 2.3.1 and 2.3.2), two-time averages have to be calculated. It turns out, that the determination of these correlations in terms of quantum Langevin equations, describing the dynamics of the dissipative and fluctuating system, becomes a quite gratuitous complex challenge. As a consequence, we introduce a further well established formulation of a stochastic differential equation (SDE) having some more mathematical advantages which allows to calculate first- and second-order correlations in a very simple and elegant way. This formalism is referred to the Japanese mathematician *K. Itô*, who invented a classical formulation of stochastic processes. Another, more physical, alternative classical description was developed by the Russian physicist *R. Stratonovich*. For someone who is not familiar with both formalisms, appendix F summarizes the main characteristics and differences of Itô's and Stratonovich's SDEs applied to quantum mechanics. As a main result we show in this appendix that the Itô form of a quantum stochastic differential equation (QSDE) is equivalent to the Stratonovich one which again corresponds to the quantum Langevin equation. Thus, knowing the quantum Langevin equation we can directly deduce the corresponding Itô QSDE.

The Itô differential of the ith ASE field mode in terms of the input noise operators reads[13]

$$\mathrm{d}\hat{a}_i(t) = -\left[\mathrm{i}\Delta_i + \frac{1}{2}(\gamma_i^l + \gamma_i^r)\right]\hat{a}_i(t)\,\mathrm{d}t + \sum_{j=1}^{M} g_i^{j^*}\hat{\sigma}_{21}^j(t)\,\mathrm{d}t - \mathrm{d}\hat{B}_i^L(t) - \mathrm{d}\hat{B}_i^R(t). \tag{5.230}$$

The first term in equation (5.230) describes the free evolution of the mode i with frequency Δ_i and includes the external damping rates γ_i^l, γ_i^r resulting from the left and right input noise fields leading to damping effects of the system. The second term includes the coupling constant between mode i and quantum dot j defined in equation (5.17) as well as the lowering operator $\hat{\sigma}_{21}^j$. Therefore, this contribution describes the interaction of ASE field mode i with all M QDs. The last two terms consider noise fluctuations described by the noise differentials (cf. equations (5.196)-(5.197))

$$\mathrm{d}\hat{B}_i^L(t) = X_i^l(t-t_0)(\mathscr{T}_i^l\mathrm{d}\hat{B}_i^6(t) + \mathscr{R}_i^l\mathrm{d}\hat{B}_i^4(t)), \tag{5.231}$$

$$\mathrm{d}\hat{B}_i^R(t) = X_i^r(t-t_0)(\mathscr{T}_i^r\mathrm{d}\hat{B}_i^1(t) + \mathscr{R}_i^r\mathrm{d}\hat{B}_i^2(t)), \tag{5.232}$$

depending on the Itô increments of the external channels $\alpha \in \{1,...,6\}$ labeled by $\mathrm{d}\hat{B}_i^\alpha$. They have the dimension of the square root of reciprocal time and obey the commutation relation and Itô rules (cf. equation (5.71) and appendix F),

$$\left[\mathrm{d}\hat{B}_i^\alpha(t), \mathrm{d}\hat{B}_j^{\beta\dagger}(t')\right] = \delta_{\alpha\beta}\delta_{ij}\delta(t-t')\mathrm{d}t\mathrm{d}t', \quad \alpha,\beta \in \{1,...,6\}, \tag{5.233}$$

$$\mathrm{d}\hat{B}_i^\beta(t)\mathrm{d}\hat{B}_i^{\beta\dagger}(t) = (\bar{N}_i^\beta + 1)\mathrm{d}t, \tag{5.234}$$

$$\mathrm{d}\hat{B}_i^{\beta\dagger}(t)\mathrm{d}\hat{B}_i^\beta(t) = \bar{N}_i^\beta\mathrm{d}t, \tag{5.235}$$

with and mean occupation numbers $\bar{N}_i^\beta$. Clearly, the rescaled noise operators introduced in (5.231)-(5.232) have to satisfy the commutation relation and Itô rules

$$\left[\mathrm{d}\hat{B}_i^\alpha(t), \mathrm{d}\hat{B}_j^{\beta\dagger}(t')\right] = \vartheta_i^\alpha(t)\delta(t-t')\delta_{ij}\delta_{\alpha\beta}\,\mathrm{d}t\mathrm{d}t', \quad \alpha,\beta \in \{L,R\}, \tag{5.236}$$

$$\mathrm{d}\hat{B}_i^\beta(t)\mathrm{d}\hat{B}_i^{\beta\dagger}(t) = (\bar{N}_i^\beta(t) + 1)\mathrm{d}t, \tag{5.237}$$

$$\mathrm{d}\hat{B}_i^{\beta\dagger}(t)\mathrm{d}\hat{B}_i^\beta(t) = \bar{N}_i^\beta(t)\mathrm{d}t, \tag{5.238}$$

which obviously shows slight deviations compared to (5.233)-(5.235). Here, we introduced the abbreviations

$$\vartheta_i^L(t) = \gamma_i^l|T_i(t-t_0)|^2|\mathscr{T}_i^l|^2 + \gamma_i^r|R_i^l(t-t_0)|^2|\mathscr{R}_i^l|^2, \tag{5.239}$$

$$\vartheta_i^R(t) = \gamma_i^l|R_i^r(t-t_0)|^2|\mathscr{T}_i^r|^2 + \gamma_i^r|T_i(t-t_0)|^2|\mathscr{R}_i^r|^2 \tag{5.240}$$

and

$$\bar{N}_i^L(t) = X_i^l(t-t_0)\bar{N}_i^l, \quad \bar{N}_i^R(t) = X_i^r(t-t_0)\bar{N}_i^r \tag{5.241}$$

---

[13] In contrast to appendix F, we omit the notation (I) labeling the Itô formulation of a QSDE.

with mean occupation numbers

$$\bar{N}_i^l = |\mathscr{T}_i^l|^2 \bar{N}_i^6 + |\mathscr{R}_i^l|^2 \bar{N}_i^4, \tag{5.242}$$

$$\bar{N}_i^r = |\mathscr{T}_i^r|^2 \bar{N}_i^1 + |\mathscr{R}_i^r|^2 \bar{N}_i^2. \tag{5.243}$$

Thus, $\mathrm{d}B_i^\beta$, $\beta \in \{L, R\}$ should not be confused with the Ito increments in the sense of quantum white noise (5.233)-(5.235).

Please note that the input fields of channel 3 and 5 never enter the waveguide. Therefore, the corresponding damping rates γ_i^3 and γ_i^5, which are proportional to the coupling strength between reservoir and ASE field, are equal to zero.
In the same way, we can derive QSDEs for all atomic coherences and populations of each quantum dot depending on pumping rate $R \equiv R^j = \bar{N}_{20}^j \gamma_{20}^j$, acting equally strong on each individual nanostructure (cf. section 5.1 and figure 5.3), as well as on the Itô increments $\mathrm{d}\hat{B}_m^j / \mathscr{D}_m^j$, where m represents the dot transitions $m \in \{(21), (20), (10) \,|\, (ij) : |i\rangle \to |j\rangle\}$. They are given by:

Populations

$$\mathrm{d}\hat{\sigma}_{00}^j = -(\Gamma_{00}^j + R)\hat{\sigma}_{00}^j \,\mathrm{d}t + \gamma_{10}^j \bar{N}_{10}^j \hat{\sigma}_{11}^j \,\mathrm{d}t + R\hat{\sigma}_{22}^j \,\mathrm{d}t - \big(\hat{\sigma}_{10}^{j\dagger} \,\mathrm{d}\hat{B}_{10}^j + \hat{\sigma}_{20}^{j\dagger} \mathrm{d}\hat{B}_{20}^j + \mathrm{h.c.}\big) \tag{5.244a}$$

$$\begin{aligned}\mathrm{d}\hat{\sigma}_{11}^j = &- \Gamma_{11}^j \hat{\sigma}_{11}^j \,\mathrm{d}t - \sum_{\{k_i\}} \big(g_i^{j*} \hat{a}_i^\dagger \hat{\sigma}_{21}^j \,\mathrm{d}t + \mathrm{h.c.}\big) + \gamma_{10}^j (\bar{N}_{10}^j + 1)\hat{\sigma}_{00}^j \,\mathrm{d}t \\ &+ \gamma_{21}^j \bar{N}_{21}^j \hat{\sigma}_{22}^j \,\mathrm{d}t - \big(\hat{\sigma}_{21}^{j\dagger} \mathrm{d}\hat{B}_{21}^j - \hat{\sigma}_{10}^{j\dagger} \mathrm{d}\hat{B}_{10}^j + \mathrm{h.c.}\big)\end{aligned} \tag{5.244b}$$

$$\begin{aligned}\mathrm{d}\hat{\sigma}_{22} = &- (\Gamma_{22}^j + R)\hat{\sigma}_{22}^j \,\mathrm{d}t + \sum_{\{k_i\}} \big(g_i^{j*} \hat{a}_i^\dagger \hat{\sigma}_{21}^j \,\mathrm{d}t + \mathrm{h.c.}\big) + \gamma_{21}^j (\bar{N}_{21}^j + 1)\hat{\sigma}_{11}^j \,\mathrm{d}t \\ &+ (R + \gamma_{20}^j)\hat{\sigma}_{00}^j \,\mathrm{d}t + \big(\hat{\sigma}_{21}^{j\dagger} \mathrm{d}\hat{B}_{21}^j + \hat{\sigma}_{20}^{j\dagger} \mathrm{d}\hat{B}_{20}^j + \mathrm{h.c.}\big)\end{aligned} \tag{5.244c}$$

Coherences

$$\begin{aligned}\mathrm{d}\hat{\sigma}_{21}^j = &- \Big(\mathrm{i}\delta\omega_{12}^j + \frac{1}{2}(\Gamma_{21}^j + R)\Big)\hat{\sigma}_{21}^j \,\mathrm{d}t - \sum_{\{k_i\}} g_i^j (\hat{\sigma}_{22}^j - \hat{\sigma}_{11}^j)\hat{a}_i \,\mathrm{d}t \\ &- (\hat{\sigma}_{22}^j - \hat{\sigma}_{11}^j) \,\mathrm{d}\hat{B}_{21}^j + \mathrm{d}\hat{B}_{10}^{j\dagger} \hat{\sigma}_{20}^j + \hat{\sigma}_{10}^{j\dagger} \,\mathrm{d}\hat{B}_{20}^j\end{aligned} \tag{5.245a}$$

$$\begin{aligned}\mathrm{d}\hat{\sigma}_{20}^j = &- \Big(\frac{\Gamma_{20}^j}{2} + R\Big)\hat{\sigma}_{20}^j \,\mathrm{d}t + \sum_{\{k_i\}} g_i^j \hat{\sigma}_{10}^j \hat{a}_i \,\mathrm{d}t \\ &+ \hat{\sigma}_{10}^j \,\mathrm{d}\hat{B}_{21}^j - (\hat{\sigma}_{22}^j - \hat{\sigma}_{00}^j) \,\mathrm{d}\hat{B}_{20}^j - \hat{\sigma}_{21}^j \,\mathrm{d}\hat{B}_{10}^j\end{aligned} \tag{5.245b}$$

$$\begin{aligned}\mathrm{d}\hat{\sigma}_{10}^j = &\Big(\mathrm{i}\delta\omega_{12}^j - \frac{1}{2}(\Gamma_{10}^j + R)\Big)\hat{\sigma}_{10}^j \,\mathrm{d}t - \sum_{\{k_i\}} g_i^{j*} \hat{a}_i^\dagger \hat{\sigma}_{20}^j \,\mathrm{d}t \\ &- \mathrm{d}\hat{B}_{21}^{j\dagger} \hat{\sigma}_{20}^j - \hat{\sigma}_{21}^{j\dagger} \,\mathrm{d}\hat{B}_{20}^j - (\hat{\sigma}_{11}^j - \hat{\sigma}_{00}^j) \,\mathrm{d}\hat{B}_{10}^j\end{aligned} \tag{5.245c}$$

Decay and excitation rates

$$\Gamma_{00}^{j} = \gamma_{10}^{j}(\bar{N}_{10}^{j}+1) + \gamma_{20}^{j} \tag{5.246a}$$

$$\Gamma_{11}^{j} = \gamma_{21}^{j}(\bar{N}_{21}^{j}+1) + \gamma_{10}^{j}\bar{N}_{10}^{j} \tag{5.246b}$$

$$\Gamma_{22}^{j} = \gamma_{21}^{j}\bar{N}_{21}^{j} \tag{5.246c}$$

$$\Gamma_{21}^{j} = \gamma_{21}^{j}(2\bar{N}_{21}^{j}+1) + \gamma_{10}^{j}\bar{N}_{10}^{j} \tag{5.246d}$$

$$\Gamma_{20}^{j} = \gamma_{21}^{j}\bar{N}_{21}^{j} + \gamma_{20}^{j} + \gamma_{10}^{j}\big(\bar{N}_{10}^{j}+1\big) \tag{5.246e}$$

$$\Gamma_{10}^{j} = +\gamma_{21}^{j}\big(\bar{N}_{21}^{j}+1\big) + \gamma_{20}^{j} + \gamma_{10}^{j}\big(2\bar{N}_{10}^{j}+1\big) \tag{5.246f}$$

5.3.1 On the nature of the QDSLD quantum state

Up to now, we are left with a set of coupled nonlinear Itô quantum stochastic differential equations for all multiple radiation ASE modes as well as all populations and coherences for each quantum dot system. This system of differential equations can be studied numerically in more detail. However, at this point of the thesis, it is reasonable to incorporate experimental observations of the quantum state of the QDSLD system in order to limit the following considerations to a more specific physical problem by making some assumptions and approximations motivated by the observed characteristics of the amplified spontaneous emission.

Due to the experimental measurements of the spectrum of highly incoherent broadband radiation fields (see figure 3.3), we assume a vanishing expectation value, i.e. no coherent amplitude of the i^{th} ASE mode,

$$\langle \hat{a}_i \rangle = 0. \tag{5.247}$$

Furthermore, we assume that there are no correlations between different ASE field modes at the same space-time event, so that the average value

$$\langle \hat{a}_i^{\dagger}\hat{a}_j \rangle = n_i \delta_{ij} \tag{5.248}$$

is given by the photon number n_i of mode i. We disregard correlations between the different external channel radiation field modes as well as interactions between these external modes with the intrawaveguide quantum dot bath modes. The occupation numbers as well as the decay rates of the left- and right-hand side of the waveguide are assumed to be equal for all ASE field modes, i.e. $\bar{N}_i^{\beta} = \bar{N}^{\beta}$ with $(\beta \in \{L,R\})$ and $\gamma_i^{\beta} = \gamma^{\beta}$ with $\beta \in \{l,r\}$.

DECORRELATION APPROXIMATION Since the influence of a single quantum dot on the i^{th} mode of the multimode ASE radiation field is small, higher-order corrections are negligible by decorrelating field and atomic operator [155], e.g.

$$\langle \hat{a}_i^{\dagger}\big(\hat{\sigma}_{22}^{j} - \hat{\sigma}_{11}^{j}\big)\hat{a}_j \rangle \approx \langle \hat{a}_i^{\dagger}\hat{a}_j \rangle \langle \hat{\sigma}_{22}^{j} - \hat{\sigma}_{11}^{j} \rangle \quad \text{(decorrelation approximation).} \tag{5.249}$$

This separation into a product of second-order quantum dot and field variables is of course an approximation, but nevertheless more realistic compared to a mean-field theory [156].

In addition, correlations between different QDs are negligible, so that in good approximation

$$\langle \hat{\sigma}_{21}^{j\dagger}\hat{\sigma}_{21}^{j'} \rangle = \langle \hat{\sigma}_{11}^{j} \rangle \delta_{jj'} \tag{5.250}$$

holds.

ADIABATIC ELIMINATION We adiabatically eliminate coherences as dynamical variables in the averaged QSDEs by replacing $\langle\hat{\sigma}_{21}^{j\dagger}\hat{a}_i\rangle$ by its stationary solution $\langle\hat{\sigma}_{21}^{j\dagger}\hat{a}_i\rangle_s$. In doing so, we apply the Ito product rule according to

$$\mathrm{d}\langle\hat{\sigma}_{21}^{j\dagger}\hat{a}_i\rangle = \langle(\mathrm{d}\hat{\sigma}_{21}^{j\dagger})\hat{a}_i\rangle + \langle\hat{\sigma}_{21}^{j\dagger}\mathrm{d}\hat{a}_i\rangle + \langle(\mathrm{d}\hat{\sigma}_{21}^{j\dagger})(\mathrm{d}\hat{a}_i)\rangle. \tag{5.251}$$

Under consideration of equations (5.230) and (5.245a) as well as the mentioned decorrelation approximation, we end up in an equation of motion

$$\frac{\mathrm{d}\langle\hat{\sigma}_{21}^{j\dagger}\hat{a}_i\rangle}{\mathrm{d}t} = -\Big(\mathrm{i}\Delta_i^j + \frac{\Gamma^j}{2}\Big)\langle\hat{\sigma}_{21}^{j\dagger}\hat{a}_i\rangle + g_i^{j*}\Big(n_i(\langle\hat{\sigma}_{11}^j\rangle - \langle\hat{\sigma}_{22}^j\rangle) + \langle\hat{\sigma}_{11}^j\rangle\Big), \tag{5.252}$$

with

$$\Gamma^j \equiv R + \gamma^l + \gamma^r + \Gamma_{21}^j, \tag{5.253}$$

where Γ_{21}^j is defined in equation (5.246d) and detuning $\Delta_i^j = \Delta_i - \delta\omega_{12}^j = \omega_i - \omega_{12}^j$, which again results into a stationary solution of type

$$\langle\hat{\sigma}_{21}^{j\dagger}\hat{a}_i\rangle_s = \frac{g_i^{j*}\Big(n_i(\langle\hat{\sigma}_{11}^j\rangle - \langle\hat{\sigma}_{22}^j\rangle) + \langle\hat{\sigma}_{11}^j\rangle\Big)}{\mathrm{i}\Delta_i^j + \frac{1}{2}\Gamma^j} \approx \langle\hat{\sigma}_{21}^{j\dagger}\hat{a}_i\rangle \qquad \text{(adiabatic elimination)}. \tag{5.254}$$

This approximation states, that the evolution of $\langle\hat{\sigma}_{21}^{j\dagger}\hat{a}_i\rangle$ is *slaved* to that of the photon number n_i [157, 158]. Please note, that adiabatic elimination of the artificial atom coherences is appropriate in case of good cavities. In general QDSLDs, having inhomogeneous gain medium and tilted end facets, operate far away from the good-cavity regime. However, experimental results of the second-order degree of coherence in terms of temperature highlight a considerable increase in coherence, generally not expected in bad cavities. Therefore, as a first step we assume that the concept of atomic adiabatic elimination is applicable.

5.3.2 Rate equations

A measured power spectrum reflects the behavior of the optical power as a function of angular frequency. The power itself is directly related to the stationary photon number (see equation (2.94)). Its dynamics is determined again by the rate equations of the system, whose derivation is straightforward within the Itô formalism. Here, we only have to investigate the average value of the QSDE of creation and annihilation operator products from the ASE field mode according to (5.248) as well as the populations of the j^{th} quantum dot, utilizing the properties of the Itô increments (see appendix F). Applying all mentioned assumptions and approximations introduced in section 5.3.1 as well as regarding the fact that the Itô increments commute with the system operators at the same time, we find the **rate equations of the QDSLD system**

$$\boxed{\begin{aligned}
\dot{n}_i &= \sum_{j=1}^{M} \gamma G_i^j\big(n_i w^j + \sigma_{11}^j\big) - (\gamma^l + \gamma^r)n_i + \bar{N}^L + \bar{N}^R, \\
\dot{\sigma}_{22}^j &= \sum_{\{k_i\}} \gamma G_i^j\big(n_i w^j + \sigma_{11}^j\big) - (\Gamma_{22}^j + R)\sigma_{22}^j + \gamma_{21}^j\big(\bar{N}_{21}^j + 1\big)\sigma_{11}^j + \big(R + \gamma_{20}^j\big)\sigma_{00}^j, \\
\dot{\sigma}_{11}^j &= -\sum_{\{k_i\}} \gamma G_i^j\big(n_i w^j + \sigma_{11}^j\big) - \Gamma_{11}^j\sigma_{11}^j + \gamma_{10}^j\big(\bar{N}_{10}^j + 1\big)\sigma_{00}^j + \gamma_{21}^j\bar{N}_{21}^j\sigma_{22}^j, \\
\dot{\sigma}_{00}^j &= -(\Gamma_{00}^j + R)\sigma_{00}^j + \gamma_{10}^j\bar{N}_{10}^j\sigma_{11}^j + R\sigma_{22}^j,
\end{aligned}}
\qquad
\begin{aligned}
&(5.255) \\
&(5.256) \\
&(5.257) \\
&(5.258)
\end{aligned}$$

with the inversion $w^j = \langle \hat{w}^j \rangle = \sigma_{11}^j - \sigma_{22}^j$ and the population of the i^{th} level of the j^{th} quantum dot $\langle \hat{\sigma}_{ii}^j \rangle = \sigma_{ii}^j$, which sum over all populations remains one, that is $\sum_{i=0}^2 \sigma_{ii} = 1$. The coupling strength parameter, which we call *cooperativity strength*,

$$G_i^j \equiv \frac{1}{\gamma} \frac{|g_i^j|^2 \Gamma^j}{\Delta_i^{j2} + (\Gamma^j/2)^2}, \quad \Gamma^j \equiv R + \gamma^l + \gamma^r + \Gamma_{21}^j, \tag{5.259}$$

assesses the relative importance of the coherent atomic field coupling strength g_i^j to the incoherent processes represented by pump rates R, external damping rates γ^l, γ^r and atomic decay rates Γ_{21}^j. Referred to equation (5.259), this parameter is always positive and equal to or less than the so called *cooperativity parameter* $G_{i,c}^j$, that is

$$G_i^j \leq G_{i,c}^j \quad \text{with} \quad G_{i,c}^j \equiv \frac{4|g_i^j|^2}{\gamma \tilde{\gamma}^j}, \quad \tilde{\gamma}^j = \min(\gamma^l + \gamma^r, \Gamma_{21}^j), \tag{5.260}$$

which classifies the coupling strength between the j^{th} single QDs to the i^{th} ASE field mode according to [159]

$$G_{i,c}^j \begin{cases} < 1 & \text{weak interaction} \\ > 1 & \text{strong interaction} \end{cases}. \tag{5.261}$$

Later we will see that the frequency distribution of G_i^j determines effectively the shape of the stationary photon number. Figure 5.17 (left) shows G_i^j as a function of scaled detunings Δ_i^j/γ for varying pumping rates $R = 0.1\gamma$ (red), $R = 0.5\gamma$ (blue), $R = \gamma$ (yellow), $R = 5\gamma$ (green) and $R = 10\gamma$ (purple). Figure 5.17 (right) depicts G_i^j as a function of the incoherent pumping rate R/γ for different detuning $\Delta_i^j = 0$ (red), $\Delta_i^j = 0.5\gamma$ (blue), $\Delta_i^j = \gamma$ (yellow), $\Delta_i^j = 5\gamma$ (green), $\Delta_i^j = 10\gamma$ (purple). In both pictures we have chosen a quantum dot decay rate of $\gamma_{21}^j = 0.1\gamma$.

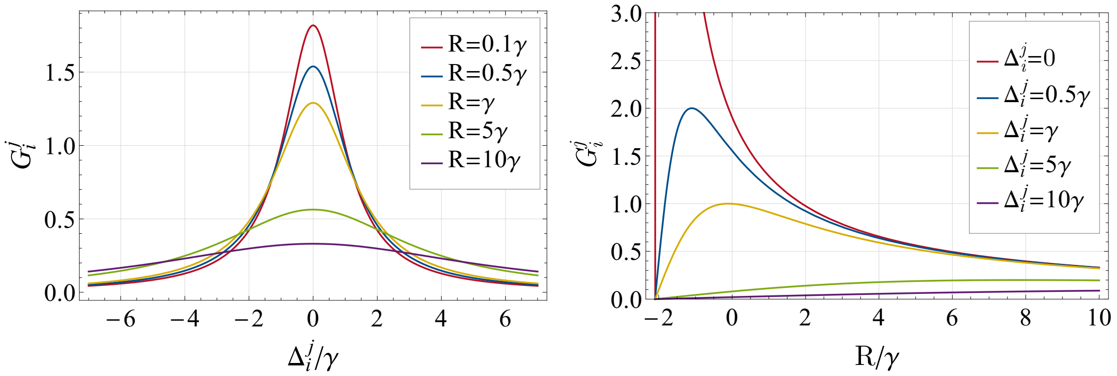

Figure 5.17: (left): Cooperativity strength G_i^j of mode i and quantum dot j as a function of scaled detuning Δ_i^j/γ for decay rate $\gamma_{21}^j = 0.1\gamma$, coupling constant $g_i^j = \gamma$ and pump rates $R = 0.1\gamma$ (red), $R = 0.5\gamma$ (blue), $R = \gamma$ (yellow), $R = 5\gamma$ (green) and $R = 10\gamma$ (purple).
(right): G_i^j of mode i and quantum dot j as a function of scaled pumping rate R/γ with decay rate $\gamma_{21}^j = 0.1\gamma$, coupling constant $g_i^j = \gamma$ as well as detunings $\Delta_i^j = 0$ (red), $\Delta_i^j = 0.5\gamma$ (blue), $\Delta_i^j = \gamma$ (yellow), $\Delta_i^j = 5\gamma$ (green) and $\Delta_i^j = 10\gamma$ (purple).

Please note that the coupling constant g_i^j is generally a function of detuning Δ_i^j. However in figure 5.17 we assumed a slowly varying, approximately frequency independent coupling strength of $g^j(\Delta_i^j) = g_i^j = \gamma$. Figure 5.17 (left) shows Lorentzian shaped cooperativity strengths G_i^j with a maximum value at resonance, $\Delta_i^j = 0$, corresponding to the cooperativity parameter. For increasing pumping rates R the distributions spread, that is the amplitude becomes smaller whereas the width of G_i^j increases. In case of varying pumping rates (cf. figure 5.17 (right)), this cooperativity strength first increases until it reaches its maximum value. Then, a decreasing tendency for increasing pumping rates with asymptote at $G_i^j = 0$ is observable. For decreasing detuning the maximum value of G_i^j decreases and is shifted to the left, simultaneously. It must be pointed out, that negative values of R are not physically meaningful. Therefore, only G_i^j with $R > 0$ have to be considered.

Obviously, the coupled nonlinear rate equation system (5.255)-(5.258) can be solved numerically. However, we are interested in two limiting cases: a single ASE mode and a real multimode radiation field interacting with identical QDs. Thereby, we assume vanishing thermal occupation numbers $\bar{N}_{10} = 0$ and $\bar{N}_{21} = 0$, vanishing damping rate $\gamma_{20} = 0$, vacuum input fields, i.e. $\bar{N}^R = \bar{N}^L = 0$, as well as equal external damping rates $\gamma^l = \gamma^r \equiv \gamma$. The limiting case of a single-mode field is analytically solvable, whereas the multimode case can be calculated in an analytic way within an approximation. The following two subsections will deal with these special cases.

5.3.2.1 Single-mode ASE field and identical quantum dots

A single-mode radiation field inside a QDSLD of equal QDs is didactically of great interest as it offers the observation of the amplified spontaneous emission in a very simple, analytic way. First, we discuss the model of a quasi-three-level laser system in order to define a laser threshold. Later, we will see that this parameter is relevant to classify the ASE transition in a QDSLD. Then, we study the QDSLD rate equations in absence of spontaneous emission. In order to model broadband light of QDSLDs based on ASE, the investigation of a quasi-three-level laser system and a QDSLD in absence of spontaneous emission sounds contradictory at a first glance. However, we will see that the mentioned resulting parameters, laser threshold or rather a critical pumping rate, are relevant to analyze the amplified spontaneous emission of a single-mode QDSLD composed of M identical QDs.

QUASI-THREE-LEVEL LASER THRESHOLD To define a threshold condition for the diode under study, which is relevant for further interpretation of the amplified spontaneous emission in the semiconductor device, we neglect spontaneous emission processes occurring in the rate equation of the intrawaveguide system (5.255)-(5.258). Furthermore, we assume that the highest level $|0\rangle$ is pumped constantly, so that the time derivative of the upper level approximately vanishes, $\dot{\sigma}_{00} \approx 0$, and the population of the highest level evolves much faster than σ_{11}, σ_{22} or n. The pumping rate R is assumed to be significantly smaller than the decay rate γ_{10}, $R < \gamma_{10}$, in a way that all charge carriers which are incoherently pumped to the energy level $|0\rangle$ relax immediately to the first excited state $|1\rangle$. If this is the case, we talk about a **quasi-three-level laser** system according to *H. Haken* [11]. The rate equations (5.255)-(5.258) reduce to [14]

$$\dot{n} = M\gamma G n w - 2\gamma n, \tag{5.262}$$

$$\dot{\sigma}_{22} = \gamma G n w - R\sigma_{22} + \gamma_{21}\sigma_{11} + R\sigma_{00} \tag{5.263}$$

$$\dot{\sigma}_{11} = -\gamma G n w - \gamma_{21}\sigma_{11} + \gamma_{10}\sigma_{00}, \tag{5.264}$$

$$\dot{\sigma}_{00} = -(\gamma_{10} + R)\sigma_{00} + R\sigma_{22}, \tag{5.265}$$

---

[14] In case of a single-mode QDSLD composed of identical QDs, the index i in (5.255)-(5.258), which enumerates the different radiating modes as well as the sum over all individual QDs, collapse.

with $\sigma_{00}+\sigma_{11}+\sigma_{22}=1$ and the cooperativity strength

$$G=\frac{1}{\gamma}\frac{|g|^2\Gamma}{\Delta^2+(\Gamma/2)^2},\quad \Gamma=R+2\gamma+\gamma_{21}. \tag{5.266}$$

Equation (5.265) and the additional requirement of an approximately constant highest level population, $\dot{\sigma}_{00}\approx 0$, result in a population, $\sigma_{00}\approx R\sigma_{22}/(\gamma_{10}+R)$, which can be directly inserted into equations (5.263)-(5.264). From this follows a differential equation for the inversion,

$$\dot{w}=\dot{\sigma}_{11}-\dot{\sigma}_{22}=(w_{21}-w_{12})\sigma-(w_{12}+w_{21})w-2\gamma Gnw, \tag{5.267}$$

with $\sigma=\sigma_{11}+\sigma_{22}$, $w_{12}=\gamma_{21}$ and $w_{21}=\gamma_{10}R/(\gamma_{10}+R)$, which is in full agreement with reference [11]. We further follow the concepts of *H. Haken* and consider only the system far away from laser operation, so that the last term in equation (5.267) vanishes. The stationary inversion in absence of the laser process defines the *unsaturated inversion* w_0,

$$\dot{w}\approx(w_{21}-w_{12})\sigma-(w_{12}+w_{21})w_0=0\quad\rightarrow\quad w_0=\frac{w_{21}-w_{12}}{w_{21}+w_{12}}\sigma. \tag{5.268}$$

The stationary solution w^s of the general differential equation (5.267) including laser operation in terms of the new variable w_0 reads

$$w^s=\frac{w_0}{1+\frac{2\gamma Gn}{w_{21}+w_{12}}}. \tag{5.269}$$

For an increasing photon number n, the stationary inversion w^s becomes smaller compared to the unsaturated inversion w_0 which considers only relaxation and pumping processes, that is a saturation of inversion sets in. Inserting equation (5.269) into the photon number equation of motion (5.262) offers a nonlinear differential equation

$$\dot{n}=2\gamma n\left(\frac{MGw_0}{2+\frac{4\gamma Gn}{w_{21}+w_{12}}}-1\right), \tag{5.270}$$

which has two fixed points at $n_1^*=0$ and $n_2^*=(w_{21}+w_{12})(MGw_0-2)/(4\gamma G)$. The first solution n_1^* for the stationary photon number is the trivial one in which no laser operation sets in. The second fixed point n_2^* is the physical interesting case. Here, a laser process is observable provided that $n_2^*>0$. Otherwise, we would have negative photon numbers which is physically forbidden. $n_2^*=0$ represents a bifurcation point, which defines a *laser threshold* at a critical inversion

$$w_c=\frac{2}{MG}. \tag{5.271}$$

Applying linear stability analysis of nonlinear, deterministic, dynamic systems [158], we can analyze the stability of the fixed points n_1^* and n_2^* by considering the value of the derivative of $f(n)=\dot{n}$ in terms of n, $f'(n)=\mathrm{d}f(n)/\mathrm{d}n$, evaluated at the corresponding fixed points. If $f'(n^*)$ is positive, then n^* is unstable, whereas for negative $f'(n^*)$ the fixed point is stable,

$$f'(n_1^*)=\gamma MGw_0\left(1-\frac{w_c}{w_0}\right)\begin{cases}<0 & w_c<w_0\ \Rightarrow\ n_1^*\text{ is stable fixed point}\\ >0 & w_c>w_0\ \Rightarrow\ n_1^*\text{ is unstable fixed point}\end{cases}, \tag{5.272}$$

$$f'(n_2^*)=2\gamma\left(\frac{w_c}{w_0}-1\right)\begin{cases}<0 & w_c>w_0\ \Rightarrow\ n_2^*\text{ is stable fixed point}\\ >0 & w_c<w_0\ \Rightarrow\ n_2^*\text{ is unstable fixed point}\end{cases}. \tag{5.273}$$

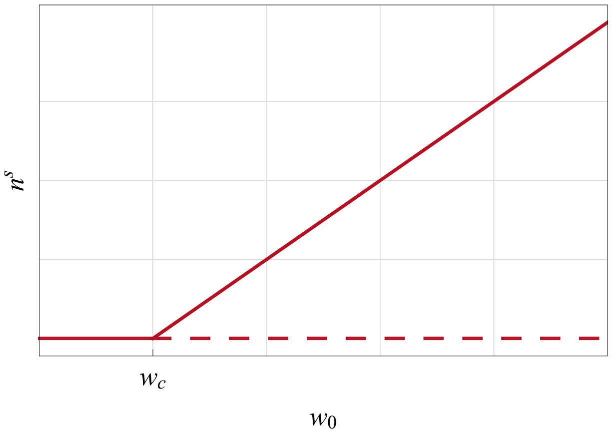

Figure 5.18: Sketch of the stationary photon number n^s as a function of unsaturated inversion w_0 showing a transcritical bifurcation with bifurcation point at critical inversion $w_0 = w_c$.

As $n_1^* = 0$ exists for all inversion values w_0, but changes its stability properties at the critical point $w_0 = w_c$, it corresponds to a **transcritical bifurcation** as depicted in figure 5.18. The solid line represents the stable path, whereas the dashed line symbolizes the unstable one. Thus, the (stable) stationary photon number is given by

$$n^s = \begin{cases} 0 & \text{for} \quad w_0 \leq w_c \\ \frac{(MGw_0-2)(w_{21}+w_{12})}{4\gamma G} = \frac{M}{4\gamma}(w_0 - w_c)(w_{21} + w_{12}) & \text{for} \quad w_0 > w_c \end{cases}. \tag{5.274}$$

Obviously, the laser threshold tends to lower unsaturated inversion values for an increasing number of QDs.

CRITICAL PUMPING RATE WITHOUT SPONTANEOUS EMISSION Before considering the amplified spontaneous emission of the QDSLD, we will study the special case of **absent spontaneous emission** [10, 11, 160], which is not applicable for the description of the diode radiation but defines a critical pumping rate at which stimulated emission processes dominate. The set of coupled equations of motion is given by equation (5.262)-(5.265). We find a stationary photon number,

$$n^s = \frac{R\gamma_{10} - \gamma_{21}(R + \gamma_{10}) - w_c(\gamma_{10}\gamma_{21} + R\gamma_{10} + 2R\gamma_{21})}{w_c(2G\gamma\gamma_{10} + 3G\gamma R)} \geq 0, \qquad n^s(R_c) = 0 \tag{5.275}$$

which defines a critical pumping rate R_c leading to a bifurcation with bifurcation point at $R = R_c$. Clearly, there exists an analytic solution of R_c. However, the exact expression of this pumping rate turns out to be uninspiring.

AMPLIFIED SPONTANEOUS EMISSION OF THE QDSLD In case of a single-mode radiation field ($N = 1$) with frequency ω acting on each transition $|1\rangle \leftrightarrow |2\rangle$ of M identical QDs with transition frequency ω_{12}, the equation of motion for the photon number and the atomic populations including spontaneous emission processes read,

$$\dot{n} = M\gamma G(nw + \sigma_{11}) - 2\gamma n, \tag{5.276}$$

$$\dot{\sigma}_{22} = \gamma G(nw + \sigma_{11}) - R\sigma_{22} + \gamma_{21}\sigma_{11} + R\sigma_{00}, \tag{5.277}$$

$$\dot{\sigma}_{11} = -\gamma G(nw + \sigma_{11}) - \gamma_{21}\sigma_{11} + \gamma_{10}\sigma_{00}, \tag{5.278}$$

$$\dot{\sigma}_{00} = -(\gamma_{10} + R)\sigma_{00} + R\sigma_{22}. \tag{5.279}$$

Here, the sum of all populations is equal to one, $\sigma_{00} + \sigma_{11} + \sigma_{22} = 1$. The stationary solution of the coupled nonlinear equation system can be obtained analytically. We find the stationary quantum dot populations

$$\sigma_{00}^{s} = \frac{R\gamma G n^{s} + R(\gamma G + \gamma_{21})}{\alpha n^{s} + \beta}, \tag{5.280}$$

$$\sigma_{11}^{s} = \frac{\gamma G n^{s}(R + \gamma_{10}) + R\gamma_{10}}{\alpha n^{s} + \beta}, \tag{5.281}$$

$$\sigma_{22}^{s} = \frac{(R + \gamma_{10})(\gamma G(n^{s} + 1) + \gamma_{21})}{\alpha n^{s} + \beta}, \tag{5.282}$$

with $\alpha = \gamma G(3R + 2\gamma_{10})$ and $\beta = \gamma G(2R + \gamma_{10}) + \gamma_{10}\gamma_{21} + R(\gamma_{10} + 2\gamma_{21})$ in terms of the stationary photon number given by

$$n^{s} = a\left(1 + \sqrt{1 + \frac{b}{a^{2}}}\right), \tag{5.283}$$

with

$$a = \frac{-\gamma_{21}(\gamma_{10} + R) + \gamma_{10}R - w_c((\gamma G + \gamma_{21})(\gamma_{10} + 2R) + \gamma_{10}R)}{2w_c\gamma G(3R + 2\gamma_{10})}, \quad b = \frac{\gamma_{10}R}{w_c\gamma G(3R + 2\gamma_{10})}.$$

This photon number depends on the internal damping rates γ_{10}, γ_{21} of the QDs, the incoherent pumping rate R, the laser threshold w_c and the cooperativity strength G. Due to the condition of positive photon numbers as well as equation (5.283) it is clear, that the parameter a has to be a positive number, $a > 0$.

Figure 5.19 shows the stationary photon number n^{s} as a function of the scaled incoherent pumping rate R/γ for a single-mode radiation field interacting with $M = 1000$ identical QDs. The internal damping rates are chosen to be $\gamma_{21} = 0.1\gamma$, $\gamma_{10} = \gamma$, the coupling constant is $g = \gamma$ and the detuning is given by $\Delta = 0$. Here, only pumping rates smaller than the external damping cavity rate are considered, $R < \gamma$, motivated by experimental measurements and theoretical parameter studies in terms of strong coupling cavity QED [161–163]. The red curve reflects the analytical solution given by equation (5.283). The green, dashed line represents the stationary photon number when neglecting spontaneous emission processes (cf. equation (5.275)), showing a bifurcation with critical point at a pumping rate $R_c = 0.111\gamma$. The blue, dotted curve shows the photon number of the single-mode field interacting with quasi-three-level QDs described by equation (5.274). A comparison between the red and green curve points out, that the threshold of the red line is smeared out and the typical amplified spontaneous emission behavior is visible in agreement with experimental observations [107, 116, 164]. The blue line offers the same laser threshold at pumping rate R_c and shows increasing deviations from the red and green line with increasing pumping rate R.

Regarding the exact, stationary photon number as a function of pumping rate for increasing detuning Δ, the laser threshold $R_{c,k}$ ($k = 1,2,3,4$) tends to higher values of R. Figure 5.20 reflects this behavior for fix coupling constant $g = \gamma$, number of QDs $M = 1000$ and decay rates $\gamma_{21} = 0.1\gamma$ and $\gamma_{10} = \gamma$. Here, the detuning is chosen to be $\Delta = 0$ (red; critical pumping rate $R_{c,1} = 0.111\ \gamma$), $\Delta = 10\gamma$ (green; critical pumping rate $R_{c,2} = 0.138\gamma$), $\Delta = 15\gamma$ (blue; critical pumping rate $R_{c,3} = 0.181\gamma$) and $\Delta = 20\gamma$ (orange; critical pumping rate $R_{c,4} = 0.271\gamma$). Obviously, for decreasing detuning, the slope of the stationary photon number as a function of pumping rate R increases until saturation occurs.

A similar characteristic can be observed when studying the stationary photon number versus pumping rate for a decreasing coupling constant and a fix detuning, as depicted in figure 5.21

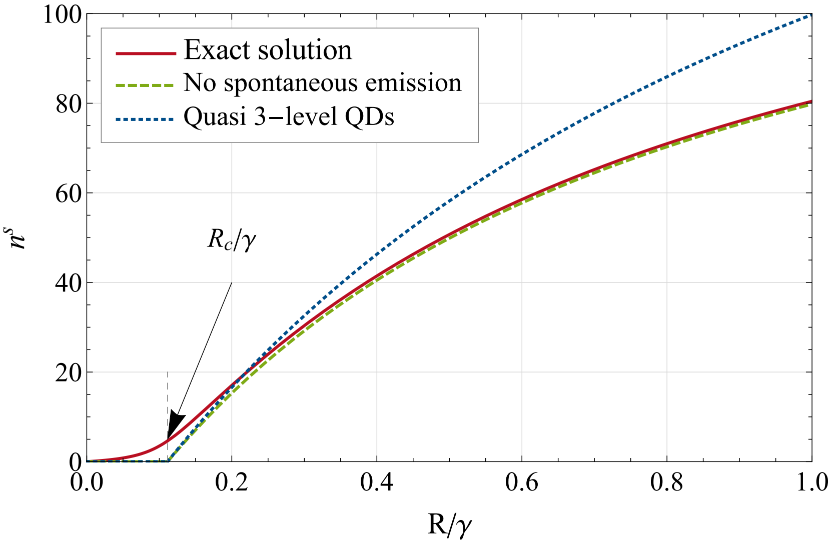

Figure 5.19: Stationary single-mode ($N=1$) photon number n^s versus incoherent pumping rate R scaled with external damping rate γ. The single-mode radiation field is assumed to interact with $M=1000$ identical QDs. The red curve reflects the analytical solution (5.283), the green, dashed line shows the photon number for the case of negligible spontaneous emission (cf. equation (5.275)). The blue, dotted line exhibits the standard laser equations for the photon number corresponding to the case of a quasi-three-level laser system (cf. equation (5.274)) [11]. Here, the internal damping rates are chosen to be $\gamma_{10}=\gamma$, $\gamma_{21}=0.1\gamma$, the coupling constant is $g=\gamma$ and we assume a vanishing detuning, i.e. $\Delta=0$. The critical pumping rate reaches a value of $R_c=0.111\gamma$.

with parameters $\gamma_{21}=0.1\gamma$, $\gamma_{10}=\gamma$, $\Delta=0$ and $M=1000$. The coupling constants are $g=0.06\gamma$ (green; critical pumping rate $R_{c,1}=0.262\gamma$), $g=0.1\gamma$ (blue; critical pumping rate $R_{c,2}=0.145\gamma$) and $g=\gamma$ (red; critical pumping rate $R_{c,3}=0.111\gamma$). For a decreasing coupling constant g, the laser threshold tends to higher values of R. In the strong coupling regime, where $g\gg\gamma$, the photon number for varying pumping rates follows the same behavior as in the case of $g=\gamma$ corresponding to the red, dashed curve in figure 5.21. Thus, within this microscopic model, the photon number exhibits a "cut off" at $g=\gamma$.

5.3.2.2 Multimode ASE field

An analytical solution for the photon number of a multimode radiation field coupling to a huge set of QDs is unfeasible. However, in case of identical dots, we can find an approximate expression for the stationary photon number in terms of the external current. First, we consider the rate equations of identical QDs coupled to a multimode radiation field,

$$\dot{n}_i = M\gamma G_i(n_i w+\sigma_{11})-2\gamma n_i, \tag{5.284}$$

$$\dot{\sigma}_{22} = \sum_{\{k_i\}}\gamma G_i(n_i w+\sigma_{11})-R\sigma_{22}+\gamma_{21}\sigma_{11}+R\sigma_{00}, \tag{5.285}$$

$$\dot{\sigma}_{11} = -\sum_{\{k_i\}}\gamma G_i(n_i w+\sigma_{11})-\gamma_{21}\sigma_{11}+\gamma_{10}\sigma_{00}, \tag{5.286}$$

$$\dot{\sigma}_{00} = -(\gamma_{10}+R)\sigma_{00}+R\sigma_{22}. \tag{5.287}$$

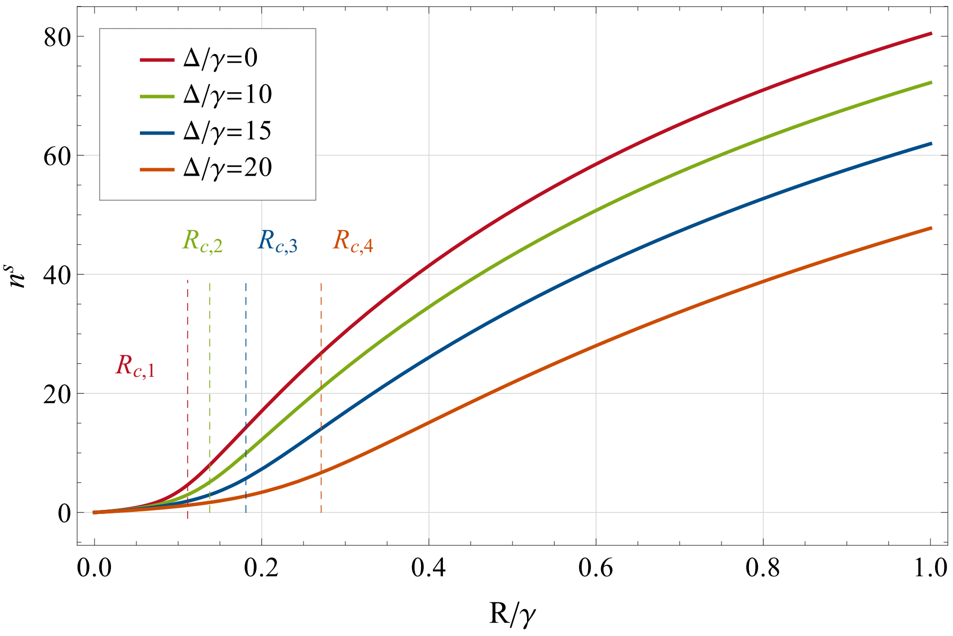

Figure 5.20: Stationary single-mode ($N = 1$) photon number n^s versus scaled pumping rate R/γ with fix coupling constant $g = \gamma$, number of QDs $M = 1000$, decay rates $\gamma_{21} = 0.1\gamma$, $\gamma_{10} = \gamma$ and detuning $\Delta = 0$ (red; critical pumping rate $R_{c,1} = 0.111\gamma$), $\Delta = 10\gamma$ (green; critical pumping rate $R_{c,2} = 0.138\gamma$), $\Delta = 15\gamma$ (blue; critical pumping rate $R_{c,3} = 0.181\gamma$) and $\Delta = 20\gamma$ (orange; critical pumping rate $R_{c,4} = 0.271\gamma$) with corresponding critical pumping rates R_c.

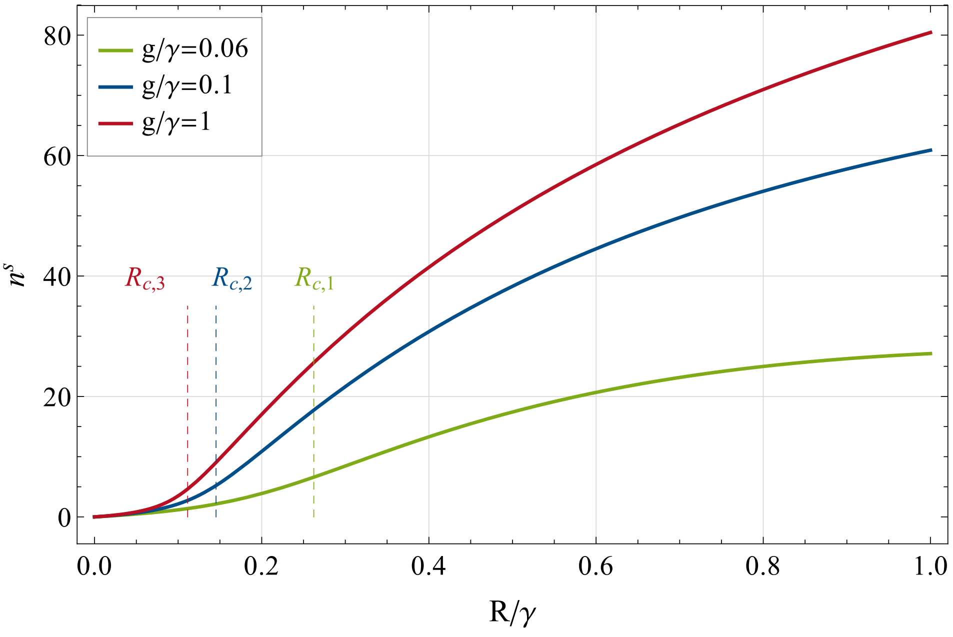

Figure 5.21: Stationary single-mode ($N = 1$) photon number n^s versus scaled pumping rate R/γ for vanishing detuning, i.e. $\Delta = 0$, parameters $M = 1000$, $\gamma_{21} = 0.1\gamma$, $\gamma_{10} = \gamma$ and varying coupling constant $g = 0.06\gamma$ (green; critical pumping rate $R_{c,1} = 0.262\gamma$), $g = 0.1\gamma$ (blue; critical pumping rate $R_{c,2} = 0.145\gamma$) and $g = \gamma$ (red; critical pumping rate $R_{c,3} = 0.111\gamma$).

The photon number n is given by the sum of the N mode photon numbers n_i,

$$n = \sum_{\{k_i\}} n_i. \tag{5.288}$$

In detailed balance [165], the stationary total photon number is determined by its zero temporal derivatives formed by each mode, $\dot{n} = 0 \leftrightarrow \dot{n}_i = 0$. In order to solve the multimode problem under consideration, we introduce an order parameter,

$$\varphi \equiv \gamma \sum_{\{k_i\}} G_i n_i^s, \tag{5.289}$$

corresponding to the stationary number of photons for the diode system $n^s = \sum_{\{k_i\}} n_i^s$, weighted with the cooperativity strength G_i. According to equation (5.284), the i^{th} mode photon number n_i^s itself,

$$n_i^s(\varphi) = \frac{\sigma_{11}^s(\varphi)}{w_i^c - w^s(\varphi)}, \quad w_i^c = \frac{2}{MG_i}, \tag{5.290}$$

is a function of the order parameter φ with the stationary excited state and the inversion,

$$\sigma_{11}^s(\varphi) = \frac{\varphi(\gamma_{10}+R)+\gamma_{10}R}{\alpha\varphi+\beta}, \quad w^s(\varphi) = \frac{\gamma_{10}R-(\gamma\bar{G}+\gamma_{21})(\gamma_{10}+R)}{\alpha\varphi+\beta}. \tag{5.291}$$

They depend significantly on the incoherent pumping rate R due to the definitions

$$\bar{G} = \sum_{\{k_i\}} G_i, \quad \alpha = 3R+2\gamma_{10}, \quad \beta = (\gamma\bar{G}+\gamma_{21})(\gamma_{10}+2R)+\gamma_{10}R, \tag{5.292}$$

where $\bar{G}$ is the sum over all N cooperativity strengths, G_i. By inserting equation (5.290) into equation (5.289), we find a closed relation for the order parameter,

$$\varphi = \sum_{\{k_i\}} \frac{\gamma G_i \sigma_{11}^s(\varphi)}{w_i^c - w^s(\varphi)} = \frac{\sigma_{11}^s(\varphi)}{w^s(\varphi)}\left[-\gamma\bar{G} + \sum_{\{k_i\}} \frac{\gamma G_i w_i^c}{w_i^c - w^s(\varphi)}\right]. \tag{5.293}$$

The solution of φ and therefore the stationary photon number can be calculated numerically. However, as a good approximation we can replace w_i^c in the enumerator of the second term in the brackets of equation (5.293) by the constant minimum laser threshold $w_{\text{min}}^c = 2/(MG_{\text{max}})$ (cf. equation (5.271)) with $G_{\text{max}} \equiv G(g_i = 2/3 \cdot g_{\text{max}}, R)$ which is inverse proportional to the square of the absolute maximum value of the coupling constant g_{max}. Equation (5.293) reduces to the analytic expression

$$\begin{aligned}\varphi \simeq -\gamma\bar{G}\frac{\sigma_{11}^s(\varphi)}{w^s(\varphi)} + w_{\text{min}}^c\frac{\varphi}{w^s(\varphi)} = \frac{\gamma_{10}R-\gamma_{21}(\gamma_{10}+R)-w_{\text{min}}^c\beta}{2w_{\text{min}}^c\alpha} \\ +\sqrt{\left(\frac{\gamma_{10}R-\gamma_{21}(\gamma_{10}+R)-w_{\text{min}}^c\beta}{2w_{\text{min}}^c\alpha}\right)^2 + \frac{\gamma\bar{G}\gamma_{10}R}{w_{\text{min}}^c\alpha}}.\end{aligned} \tag{5.294}$$

Thus, knowing all experimentally available parameters, we can specify the intrawaveguide photon number (cf. equation (5.290)) of a light emitting QDSLD from microscopic considerations within our approximation. It is not surprising that in case of equal cooperativity strength, $G_i = G$, the analytic solution is exact.

SMALL COOPERATIVITY STRENGTH: $w_i^c \gg |w^s(\varphi)|$ Consider again the exact expression of the stationary photon number of mode i (see equation (5.290)) in terms of the order parameter

$$n_i^s(\varphi) = \frac{\sigma_{11}^s(\varphi)}{w_i^c - w^s(\varphi)} = \frac{\sigma_{11}^s(\varphi)}{w_i^c\left(1 - \frac{w^s(\varphi)}{w_i^c}\right)}. \tag{5.295}$$

In case of $w_i^c \gg |w^s(\varphi)|$, that is the cooperativity strength is very small with $G_i \ll 2/(M|w^s(\varphi)|)$, the right-hand side of equation (5.295) corresponds to a geometric series as

$$n_i^s(\varphi) = \frac{\sigma_{11}^s(\varphi)}{w_i^c} \sum_{k=0}^{\infty} \left(\frac{w^s(\varphi)}{w_i^c}\right)^k = \frac{\sigma_{11}^s(\varphi)}{w^s(\varphi)} \sum_{k=1}^{\infty} \left(\frac{M w^s(\varphi)}{2}\right)^k G_i^k = \sum_{k=1}^{\infty} c_k(\varphi) G_i^k. \tag{5.296}$$

In the first-order perturbation theory in G_i, all stationary quantum dot populations are independent of φ, which in turn implies a coefficient c_k independent of φ. Thus, the stationary photon number of mode i reads

$$n_i^s(\varphi) \approx \sum_{k=1}^{\infty} c_k G_i^k. \tag{5.297}$$

Within the regime of a small cooperativity strength, the stationary photon number of the ASE field modes inside the diode system is specified by a polynomial in G_i and multiple c_k. This solution is not quite obvious. Concerning the set of coupled nonlinear differential equations (5.284)-(5.287), one would expect a much more complex system behavior. In summary, small cooperativity strengths result in stationary photon numbers in terms of angular frequency whose distributions are dominated by the shape of G_i.

INHOMOGENEOUS COUPLING Motivated by the experimental Gaussian power spectrum, we study the stationary photon number n^s as a function of the scaled incoherent pumping rate R/γ for the special case of a radiation field composed of $N = 10$ modes interacting with $M = 1000$ identical QDs for a Gaussian shaped coupling constant with

$$g(\Delta_i) = \gamma \exp\left(-\frac{(\Delta_i - \bar{\Delta})^2}{2\sigma^2}\right). \tag{5.298}$$

This photon number is plotted in figure 5.22 for a Gaussian coupling amplitude γ, expectation value $\bar{\Delta} = 0$ and width $\sigma = \gamma$. The damping rates and detuning are given by $\gamma_{21} = 0.1\gamma$, $\gamma_{10} = \gamma$ and $\Delta_i = \gamma i$. The red line shows the numerical solution and the blue line is the approximated photon number (cf. equation (5.290)) depending on the order parameter φ given by equation (5.294). The green line represents the stationary number of photons n^s for negligible spontaneous emission in the sense of reference [10] with a critical pumping rate, $R_c = 0.112\gamma$. Obviously, the approximate photon number agrees well with the exact solution for smaller values of R. For $R > 0.4\gamma$, the deviation between the approximated and the exact solution increases in contrast to the case of absent spontaneous emission processes (green line) approximating the exact solution. Furthermore, depending on the values of the Gaussian distributed coupling constants g_i of the multimode radiation field, the deviation between the multimode and single-mode photon number (black line) as a function of the pumping rate R is more or less significant. Here, the photon number of the single-mode radiation field for increasing $R\gamma > 0.4\gamma$ becomes lager than in the approximate multimode case. All four cases show saturation for sufficiently large pumping rate.

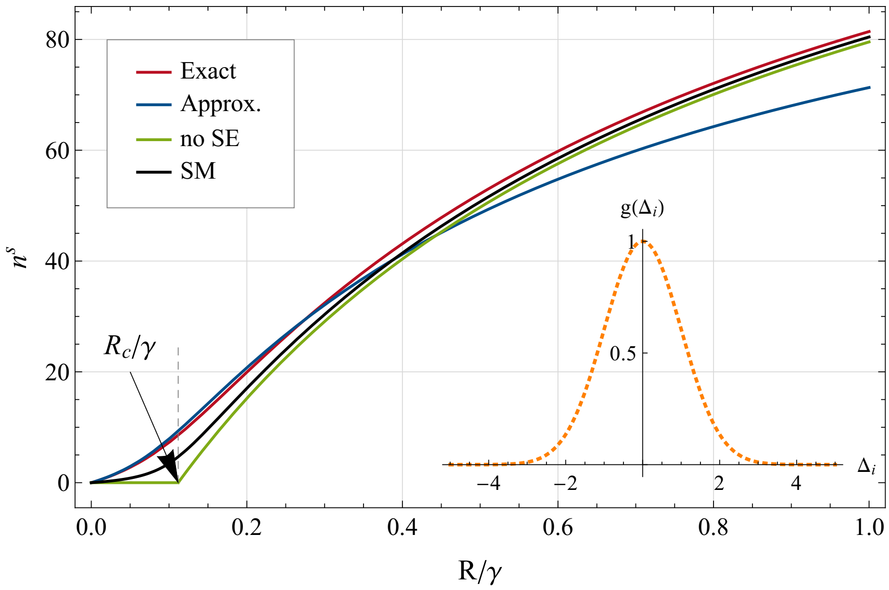

Figure 5.22: Photon number n^s versus incoherent pumping rate R scaled with external damping rate γ for a multimode radiation field composed of $N = 10$ modes, interacting with $M = 1000$ identical QDs for Gaussian shaped coupling constant g_i (see equation (5.298)) with amplitude γ, expectation value $\bar{\Delta} = 0$ and width $\sigma = \gamma$. We choose the following parameter values: $\gamma_{21} = 0.1\gamma$, $\gamma_{10} = \gamma$, $\Delta_i = \gamma i$. The red line is the exact, numerically calculated photon number, the blue line shows the approximated number of photons, the green line is the solution for the case of negligible spontaneous emission (SE) processes and finally the black curve shows the single-mode (SM) photon number already depicted in figure 5.19. The critical pumping rate is $R_c = 0.112\gamma$.

APPROXIMATE STATIONARY PHOTON NUMBER Figure 5.23 shows the approximate intrawaveguide photon number of a radiation field with $N = 30$ modes as a function of scaled detuning Δ_i/γ with Gaussian distributed coupling constants, described by equation (5.298), having a mean value of $\bar{\Delta} = 3\gamma$ and a standard deviation of $\sigma = 6\gamma$. The external damping rates are again $\gamma_{21} = 0.1\gamma$ and $\gamma_{10} = \gamma$. The pumping rate was chosen to be $R = 0.1\gamma$ (orange), $R = 0.3\gamma$ (blue), $R = 0.5\gamma$ (red), $R = 0.7\gamma$ (green) and $R = \gamma$ (purple). The gain medium consists of $M = 10^4$ QDs. For increasing pumping rates R, the number of photons increases. In addition, for high pumping rates the distribution of n^s approaches a Gaussian. Figure 5.24 illustrates this statement by representing the approximate stationary photon number (red) for a pumping rate of $R = 0.5\gamma$ as a function of detuning Δ_i/γ already shown in figure 5.23 and a Gaussian fit (blue),

$$n_{\text{fit}} = n_{\max} e^{-\frac{(\Delta-\mu)^2}{2\sigma^2}}, \tag{5.299}$$

with fit parameters $\sigma = 4.43\gamma$, $n_{\max} = 739.42$ and $\mu = 15\gamma$, substantiating the Gaussian nature of the photon number. However, $n^s(\Delta_i)$ exhibits a small deviation from the fitted Gaussian distribution. Especially in the maximum range, the intrawaveguide photon number becomes flatter than the Gaussian fit. Obviously, a Gaussian shaped coupling constant gives rise to a Gaussian-like stationary photon number, which again brings us to the important predication that the photon number is determined by the shape of the cooperativity strength G_i. Once more, this statement becomes apparent by a direct comparison of the quantum model photon number with the experimentally measured optical power spectrum.

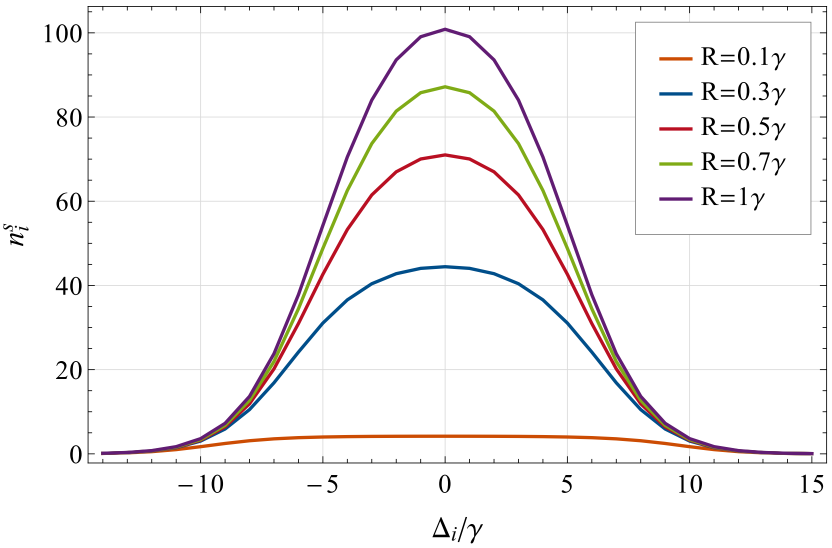

Figure 5.23: Approximate stationary multimode photon number n_i^s of the radiation field with $N = 30$ modes versus scaled detuning Δ_i/γ for pumping rates $R = 0.1\gamma$ (orange), $R = 0.3\gamma$ (blue), $R = 0.5\gamma$ (red), $R = 0.7\gamma$ (green) and $R = \gamma$ (purple). Here, the coupling constants g_i are Gaussian distributed (see equation (5.298)) with mean value $\bar{\Delta}_i = 3\gamma$ and standard deviation $\sigma = 6\gamma$. The damping rates are chosen to be $\gamma_{10} = \gamma$, $\gamma_{21} = 0.1\gamma$ and the gain medium consists of $M = 10^4$ QDs.

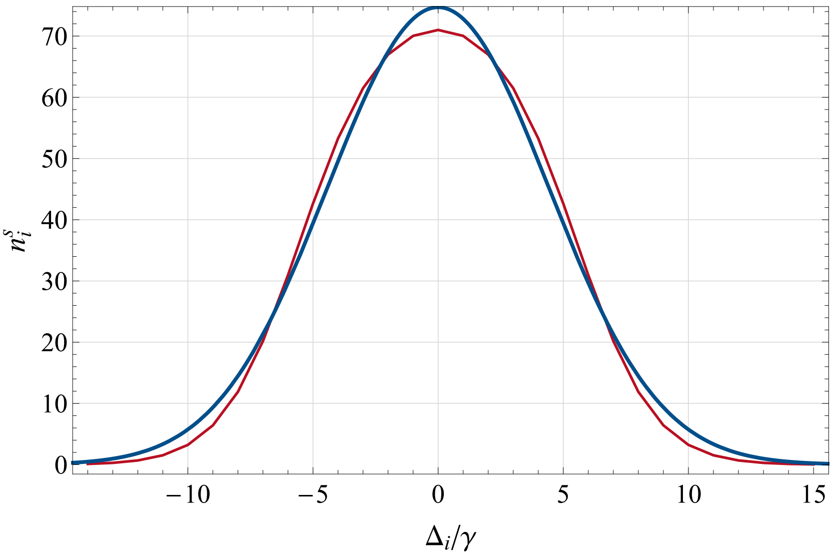

Figure 5.24: Approximate stationary multimode photon number n_i^s (red) of the radiation field with $N = 30$ modes versus scaled detuning Δ_i/γ for Gaussian distributed coupling constants g_i (see equation (5.298)) with mean value $\bar{\Delta}_i = 3\gamma$ and standard deviation $\sigma = 6\gamma$. The damping rates are chosen to be $\gamma_{10} = \gamma$, $\gamma_{21} = 0.1\gamma$ and the gain medium consists of $M = 10^4$ QDs incoherently pumped with rate $R = 0.5\gamma$. The blue line shows a Gaussian fit (see equation (5.299)) with fit parameters $\sigma = 4.43\gamma$, $n_{\max} = 739.42$ and $\mu = 15\gamma$.

Clearly, the multimode stationary photon number determined by the set of coupled differential equations (5.284)-(5.287) can also be solved numerically, leading to a similar behavior when considering the distribution in terms of frequency. This solution is presented in the next section when studying the emission spectrum of light emitting QDSLDs.

In summary, we presented a microscopic theory of QDSLDs which considers the specific gain medium, formed by an inhomogeneous ensemble of QDs, as well as the special geometry of the end facets. The former is modeled by M distinguishable three-level systems, incoherently pumped with rate R and interacting with a multimode radiation field, which couples to the outside by two beam splitters enclosing the active medium. The resulting rate equations of the system were studied in detail for the special cases of a single-mode as well as a truly multimode radiation field interacting with equal QDs inside the waveguide. The stationary photon number as a function of pumping rate exhibited the typical ASE transition. Furthermore, assuming a Gaussian cooperativity strength, the spectrum also showed a Gaussian-like distribution for varying angular frequency, suggesting that the shape of this cooperativity strength dictates the shape of the power spectral density. To proof this statement or rather our microscopic theory itself, the next section deals with the theoretically predicted power spectrum measured by a single-photon detector which allows a direct comparison with experimentally available data.

6

SPECTRUM OF QUANTUM DOT SUPERLUMINESCENT DIODES

In the previous chapter we presented a microscopic theory of ASE of QDSLDs with particular emphasis on the waveguide geometry and the gain medium. Motivated by the occurrence of hybrid coherent light as a pure optical phenomenon, our physical ansatz was based on quantum optical considerations. We had found QSDEs as well as rate equations which describe the dynamics of each system operator of the many-body system and their corresponding average dynamics, respectively. It turns out that the stationary solution of the photon number in terms of the incoherent pumping rate portraits ASE correctly. Simultaneously, assuming a Gaussian coupling, a Gaussian-like photon number distribution for varying frequency is observable. This suggests a big advantage to model first-order correlations of hybrid coherent light due to the THz broadband Gaussian shape of the optical power spectra measured in the lab. However, the properties of the stationary photon number studied in section 5.3.2 corresponds to the intrawaveguide number of photons. This quantity is physically not measurable and is particularly not equivalent to the number of photons recorded by a detector. The following chapter deals with this problem by studying the first-order temporal autocorrelation function or rather the power spectral density outside the QDSLD system. In order to proof the validity of our theory for describing hybrid coherent light, we compare the theoretical results with the experimental one.

6.1 THEORY OF THE OPTICAL POWER SPECTRUM EMITTED BY QDSLDS

The detection process for measuring the optical power spectrum is sketched in figure 6.1.

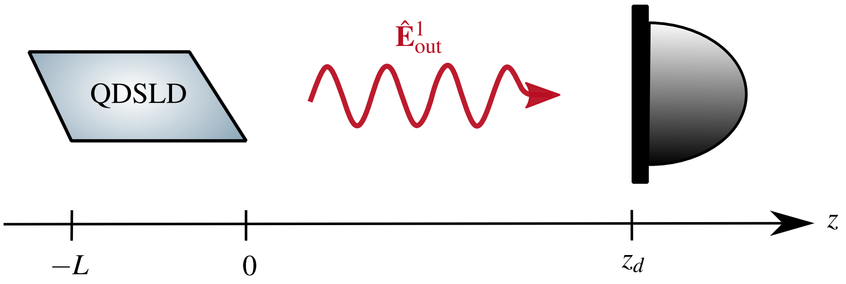

Figure 6.1: Sketch of the detection process to measure the optical power spectrum. The QDSLD system of length L is located on the left-hand side and emits an electromagnetic field $\hat{\mathbf{E}}^1_{\text{out}}$ which is recorded by a spectrum analyzer at position $z = z_d$.

Here, the QDSLD of length L emits an electromagnetic field which is measured by a spectrum analyzer delivering the optical power spectrum. In chapter 5, we already investigated in detail the spectral density of an empty diode without a gain medium. Therefore, we take on the main ideas and proceedings made in the previous sections and apply them to the case of a truly incoherent QDSLD amplified by many quantum dots. According to the orientation of the output facets shown in figure 5.11, channel 1 enters the diode system on the right hand side at $z = 0$. The electric output field $\hat{\mathbf{E}}^1_{\text{out}}$ is assumed to be guided in a single-mode fiber yielding to an radiation field propagating along the z-direction in the sense of equation (5.199). It strikes the detector at position $z = z_d$.

Clearly, for calculating the temporal correlation function of the emitted QDSLD light, we need the entire information about the dynamics of the single ASE modes as well as the populations and coherences of the single QDs described by the QSDEs (5.230) and (5.244a)-(5.245c), respectively. According to the Wiener-Khintchine theorem (cf. equation (2.95) and (2.97)), the output spectrum corresponds to the Fourier transform of the temporal first-order autocorrelation function

$$G^{(1)}(\tau) = \lim_{t\to\infty} \int_{A_d} \mathrm{d}x\,\mathrm{d}y\; \langle \hat{E}^{1(-)}_{\text{out}}(x,y,t - z_d/c_0) \hat{E}^{1(+)}_{\text{out}}(x,y,t - z_d/c_0 + \tau)\rangle. \tag{6.1}$$

The output radiation field $\hat{\mathbf{E}}^1_{\text{out}}$ is specified in equation (5.199) with mode function defined in (5.200). Regarding the expression of electric field (5.199), the first-order correlation function (6.1) is only a function of time difference τ [4, 49, 122] and the integrand is proportional to the two-time correlation $\langle \hat{b}^\dagger_{i,\text{out}}(t) \hat{b}_{j,\text{out}}(t')\rangle$ with $t < t' = t + \tau$.

Relying on the concept of the input-output formalism introduced in the previous chapter, the output is related with the input and the internal field modes according to equation (5.206) or in terms of Itô increments,

$$\mathrm{d}\hat{B}^1_{i,\text{out}}(t) = \mathrm{d}\hat{B}_i(t) + \sqrt{\Delta\nu_F}\, \mathscr{T}^r_i T^r_i(t) \hat{a}_i(t)\, \mathrm{d}t, \tag{6.2}$$

respectively, in which the input (cf. equation (5.207)),

$$\mathrm{d}\hat{B}_i(t) = R^r_i \mathscr{T}^{r2}_i \mathrm{d}\hat{B}^1_i(t) + R^r_i \mathscr{T}^r_i \mathscr{R}^r_i \mathrm{d}\hat{B}^2_i(t) + \mathscr{R}^r_i \mathrm{d}\hat{B}^3_i(t), \tag{6.3}$$

is given by a sum of the single input channels $\alpha = 1, 2, 3$.

Thus, the two-time output average at time events t, t' with $t < t' = t + \tau$ reads

$$\begin{aligned} \langle \mathrm{d}\hat{B}^\dagger_{i,\text{out}}(t) \mathrm{d}\hat{B}_{j,\text{out}}(t')\rangle =& \langle \mathrm{d}\hat{B}^\dagger_i(t) \mathrm{d}\hat{B}_j(t')\rangle + \Delta\nu_{\text{F}} \mathscr{T}^r_i \mathscr{T}^r_j T^{r*}_i(t) T^r_j(t') \langle \hat{a}^\dagger_i(t) \hat{a}_j(t')\rangle \mathrm{d}t\, \mathrm{d}t' \\ &+ \sqrt{\Delta\nu_{\text{F}}} \mathscr{T}^r_i T^{r*}_i(t) \langle \hat{a}^\dagger_i(t) \mathrm{d}\hat{B}_j(t')\rangle \mathrm{d}t \\ &+ \sqrt{\Delta\nu_{\text{F}}} \mathscr{T}^r_j T^r_j(t') \langle \mathrm{d}\hat{B}^\dagger_i(t) \hat{a}_j(t')\rangle \mathrm{d}t'. \end{aligned} \tag{6.4}$$

It corresponds to the sum of two-time correlations of the input and the internal field operators as well as correlations between the input and the intrawaveguide field amplitudes. Obviously, equation (6.4) depends significantly on the choice of the input. For example, input noise describable by thermal states possesses an explicit temperature dependency. However, we suppose that the choice of the input is not relevant for observing hybrid coherent light. For simplicity we choose vacuum as an input. Therefore, the output field is directly related to the first-order autocorrelation function of the ASE field modes at different time events t, t', according to

$$\langle \mathrm{d}\hat{B}^\dagger_{i,\text{out}}(t) \mathrm{d}\hat{B}_{j,\text{out}}(t')\rangle = \Delta\nu_{\text{F}} \mathscr{T}^r_i \mathscr{T}^r_j T^{r*}_i(t) T^r_j(t') \langle \hat{a}^\dagger_i(t) \hat{a}_j(t')\rangle \mathrm{d}t\, \mathrm{d}t', \quad t' > t. \tag{6.5}$$

To evaluate the second-order moment of the intrawaveguide field modes on the right-hand side of equation (6.5), we utilize the Itô QSDE (5.230) in terms of t'. Multiplying from the left with the creation operator $\hat{a}^\dagger_i(t)$ and taking the ensemble average results in

$$\begin{aligned} \mathrm{d}\langle \hat{a}^\dagger_i(t) \hat{a}_m(t')\rangle_{t'} =& - \left[\mathrm{i}\Delta_m + \frac{1}{2}(\gamma^l_m + \gamma^r_m)\right] \langle \hat{a}^\dagger_i(t) \hat{a}_m(t')\rangle \mathrm{d}t' + \sum_{j=1}^{M} g^{j*}_m \langle \hat{a}^\dagger_i(t) \hat{\sigma}^j_{21}(t')\rangle \mathrm{d}t' \\ &- \langle \hat{a}^\dagger_i(t) \mathrm{d}\hat{B}^L_m(t')\rangle - \langle \hat{a}^\dagger_i(t) \mathrm{d}\hat{B}^R_m(t')\rangle, \end{aligned} \tag{6.6}$$

with the input noise operators (5.231)-(5.232). Due to causality (cf. equation (F.3)) the last two terms in equation (6.6), describing correlations between the internal field amplitude at time t and the input noise increments at future time $t' > t$, are equal to zero and the second-order moment of the internal field amplitudes reduces to

$$\mathrm{d}\langle \hat{a}_i^\dagger(t)\hat{a}_m(t')\rangle_{t'} = -\left[\mathrm{i}\Delta_m + \frac{1}{2}(\gamma_m^l + \gamma_m^r)\right]\langle \hat{a}_i^\dagger(t)\hat{a}_m(t')\rangle \mathrm{d}t' + \sum_{j=1}^{M} g_m^{j*}\langle \hat{a}_i^\dagger(t)\hat{\sigma}_{21}^j(t')\rangle \mathrm{d}t'. \tag{6.7}$$

We can express the two-time correlation of the intrawaveguide amplitude and the ASE transition operator of the j^{th} quantum dot (last term in equation (6.7)) in terms of the average of the internal radiation amplitudes at different time events by applying the decorrelation approximation and the adiabatic elimination in analogy to section 5.3.1. Within these approximations the last term in equation (6.7) reads

$$\langle \hat{a}_i^\dagger(t)\hat{\sigma}_{21}^j(t')\rangle \approx \sum_{\{k_r\}} \frac{g_r^j w^j(t')}{(\Gamma_{21}^j + R)/2 + \mathrm{i}\delta\omega_{12}^j}\langle \hat{a}_i^\dagger(t)\hat{a}_r(t')\rangle. \tag{6.8}$$

This approximate solution can be directly inserted into equation (6.7) and the QSDE of the two-time internal field modes is given by

$$\begin{aligned}\mathrm{d}\langle \hat{a}_i^\dagger(t)\hat{a}_m(t')\rangle_{t'} = &-\left[\mathrm{i}\Delta_m + \frac{\gamma_m^l + \gamma_m^r}{2} - \sum_{j=1}^{M}\frac{|g_m^j|^2 w^j(t')}{(\Gamma_{21}^j + R)/2 + \mathrm{i}\delta\omega_{12}^j}\right]\langle \hat{a}_i^\dagger(t)\hat{a}_m(t')\rangle \mathrm{d}t' \\ &+ \sum_{j=1}^{M}\sum_{\substack{\{k_r\}\\ r\neq m}} \frac{g_r^j g_m^{j*} w^j(t')}{(\Gamma_{21}^j + R)/2 + \mathrm{i}\delta\omega_{12}^j}\langle \hat{a}_i^\dagger(t)\hat{a}_r(t')\rangle \mathrm{d}t'.\end{aligned} \tag{6.9}$$

Regarding the coupling matrix elements, we claim that off-diagonal elements are small compared to the diagonal one. Accordingly, we neglect the last term in equation (6.9) in first-order perturbation theory. Furthermore, we consider the last term in the brackets, which is proportional to the time-dependent inversion $w^j(t') = w^j(t+\tau)$. For $t \to \infty$ this inversion tends to a constant value, i.e. $\lim_{t\to\infty}\langle \hat{w}^j(t+\tau)\rangle = w^{js} = \text{const.}$. As we are interested in the stationary power spectrum of a QDSLD, we replace the time-dependent inversion in equation (6.9) by its stationary value w^{js} in good approximation. Equation (6.9) reduces to the expression

$$\mathrm{d}\langle \hat{a}_i^\dagger(t)\hat{a}_m(t')\rangle_{t'} \approx -\left(\mathrm{i}\chi_i + \eta_i\right)\langle \hat{a}_i^\dagger(t)\hat{a}_m(t')\rangle \mathrm{d}t', \tag{6.10}$$

with the following abbreviations

$$\chi_i = \Delta_i + \sum_{j=1}^{M}\frac{|g_i^j|^2 w^{js}\delta\omega_{12}^j}{((\Gamma_{21}^j + R)/2)^2 + \delta\omega_{12}^{j2}} = \Delta_i + \mathscr{O}(\delta\omega_{12}^j) \approx \Delta_i, \tag{6.11}$$

$$\begin{aligned}\eta_i &= \frac{\gamma_i^l + \gamma_i^r}{2} - \sum_{j=1}^{M}\frac{|g_i^j|^2 w^{js}(\Gamma_{21}^j + R)}{(\Gamma_{21}^j + R)^2/2 + 2\delta\omega_{12}^{j2}} = \frac{\gamma_i^l + \gamma_i^r}{2} - 2\sum_{j=1}^{M}\frac{|g_i^j|^2 w^{js}}{\Gamma_{21}^j + R} + \mathscr{O}(\delta\omega_{12}^j) \\ &\approx \frac{\gamma_i^l + \gamma_i^r - \xi_i}{2}, \quad \xi_i = 4\sum_{j=1}^{M}\frac{|g_i^j|^2 w^{js}}{\Gamma_{21}^j + R}.\end{aligned} \tag{6.12}$$

In the last step of equations (6.11) and (6.12) we assumed a small frequency discrepancy $\delta\omega_{12}^j$ of the j^{th} quantum dot from the mean value $\bar{\omega}_{12}$ so that all terms of the order $\mathscr{O}(\delta\omega_{12}^j)$ are negligible. A central assumption of broadband ASE was presented in section 5.3.1, in which we required vanishing correlations between different field modes at equal time with $\langle \hat{a}_i^\dagger(t)\hat{a}_m(t)\rangle = n_i(t)\delta_{im}$

(cf. equation (5.248)). In this context we can formally integrate equation (6.10) so that the intrawaveguide field correlation function is determined by

$$\langle \hat{a}_i^\dagger(t)\hat{a}_m(t')\rangle = n_i(t)e^{-(\mathrm{i}\chi_i+\eta_i)(t'-t)}\delta_{im}, \quad t' > t. \tag{6.13}$$

Finally, the correlation function of the output increments $\mathrm{d}\hat{B}_{i,\mathrm{out}}$ (see equation (6.5)) at different time events t, t' reads

$$\langle \mathrm{d}\hat{B}_{i,\mathrm{out}}^\dagger(t)\mathrm{d}\hat{B}_{j,\mathrm{out}}(t')\rangle = \Delta\nu_{\mathrm{F}}\mathscr{T}_i^{r2}T_i^{r*}(t)T_i^r(t')n_i(t)e^{-(\mathrm{i}\chi_i+\eta_i)(t'-t)}\delta_{ij}\ \mathrm{d}t\ \mathrm{d}t'. \tag{6.14}$$

Please note, that equation (6.14) corresponds to a two-time correlation function of the Itô increments. In order to determine the optical power spectral density measured by the detector, we have to calculate the second-order moment of the Heisenberg system operator $\hat{b}_{\mathrm{out}}$ at different time events. However, this transition is quite obvious when considering the definition of a quantum Wiener process (see equation (F.8)), where the Langevin-type temporal correlation can be directly determined from the corresponding Itô equation (6.14) according to [139]

$$\langle \mathrm{d}\hat{B}_{i,\mathrm{out}}^\dagger(t)\mathrm{d}\hat{B}_{j,\mathrm{out}}(t')\rangle = \langle \hat{b}_{i,\mathrm{out}}^\dagger(t)\hat{b}_{j,\mathrm{out}}(t')\rangle \mathrm{d}t\,\mathrm{d}t' \tag{6.15}$$

$$\Rightarrow \quad \langle \hat{b}_{i,\mathrm{out}}^\dagger(t)\hat{b}_{j,\mathrm{out}}(t')\rangle = \Delta\nu_{\mathrm{F}}\mathscr{T}_i^{r2}T_i^{r*}(t)T_i^r(t')n_i(t)e^{-(\mathrm{i}\chi_i+\eta_i)(t'-t)}\delta_{ij}. \tag{6.16}$$

We assume a slowly varying transmission amplitude $T_i^\beta(t)$ compared to the system's amplitudes, so that $T_i^\beta(t)$ can be replaced by a constant T_i^β that is

$$T_i^\beta(t) \simeq T_i^\beta. \tag{6.17}$$

Finally back-transformation to the original Heisenberg picture yields the discrete stationary optical power spectrum

$$\begin{aligned} S(\omega) &= \frac{\mathscr{C}}{\pi}\mathrm{Re}\int_0^\infty \mathrm{d}\tau\, G^{(1)}(\tau)e^{i\omega\tau} = \sum_{\{k_i,k_j>0\}} \Upsilon_i\Upsilon_j \mathrm{Re}\int_0^\infty \mathrm{d}\tau e^{\mathrm{i}\omega\tau}\langle \hat{b}_{i,\mathrm{out}}^\dagger(t)\hat{b}_{j,\mathrm{out}}(t+\tau)\rangle_{t\to\infty} \\ &= \sum_{\{k_i>0\}} \frac{P_i\eta_i n_i^s}{\eta_i^2+(\omega-\omega_i)^2}, \qquad \Upsilon_i = \sqrt{\frac{2\hbar c_0\omega_i}{\Delta\omega_i L}}, \quad P_i = \frac{2\hbar\omega_i\Delta\nu_{\mathrm{F}}c_0\mathscr{T}_i^{r2}|T_i^r|^2}{\Delta\omega_i L} \end{aligned} \tag{6.18}$$

with optical power P_i. Again, we consider equal external decay rates and transmission amplitudes for all modes, that is $\gamma_i^\beta = \gamma^\beta$, $\mathscr{T}_i^\beta = \mathscr{T}^\beta$ and $T_i^\beta = T^\beta$ with $\beta \in \{l, r\}$. Furthermore, we demand that the angular frequency appearing in the enumerator of equation (6.18) differs only slightly from a mean value $\bar{\omega}$ so that we can set $\omega_i \approx \bar{\omega}$ in good approximation. We suppose equal frequency separation between adjacent modes, i.e. $\Delta\omega_i = \Delta\omega = (\omega_{N/2-1} - \omega_{-N/2})/(N-1)$. Within these approximations we find an optical spectrum,

$$S(\omega) \approx P\sum_{\{k_i>0\}} \mathscr{L}_{\Gamma_i}(\omega-\omega_i)\ n^s(\omega_i), \qquad P = \frac{2\hbar\bar{\omega}\Delta\nu_{\mathrm{F}}c_0\mathscr{T}^{r2}|T^r|^2}{\Delta\omega L}, \tag{6.19}$$

given by a convolution of a Lorentzian curve,

$$\mathscr{L}_\Gamma(\omega) = \frac{1}{\pi}\frac{\Gamma}{(\Gamma/2)^2+\omega^2}, \quad \Gamma = \gamma^l + \gamma^r - \xi,$$

with the stationary intrawaveguide photon number $n^s(\omega_i)$, which in turn was studied in detail in section 5.3. In the continuous limit, the sum in equation (6.19) is replaced by an integral, resulting into a continuous power spectrum of type[1]

$$\boxed{S(\omega) \approx \frac{P}{\Delta\omega} \int_{-\infty}^{\infty} \mathrm{d}\omega' \, \mathscr{L}_{\Gamma}(\omega - \omega') \, n^s(\omega')} \, . \tag{6.20}$$

This closed expression of the power spectral density corresponds to a convolution of a Lorentzian curve with the stationary internal number of photons. It permits a direct comparison with the experimentally available power spectrum, which is examined in the following section.

6.2 COMPARISON WITH A MEASURED POWER SPECTRUM

In theory, the spectral density is directly related to the internal stationary photon number of the QDSLD under study. This result is of great relevance and allows a direct comparison with the experimental data. In this section we will demonstrate that the experimentally measured optical power spectrum is basically reflected by the intrawaveguide photon number described in detail in chapter 5.

Figure 6.2 shows again the experimental power spectrum $S(\omega)$ (black) (cf. figure 3.3) together with a Gaussian interpolation (green line),

$$S_{\text{fit}}(\omega) = \frac{S_0}{\sqrt{2\pi}\sigma} e^{-\frac{(\omega-\bar{\omega})^2}{2\sigma^2}}, \qquad \int_{-\infty}^{\infty} \mathrm{d}\omega \, S_{\text{fit}} = S_0, \tag{6.21}$$

and the numerical solution of the stationary internal photon number $n^s = \sum_{\{k_i\}} n_i^s$ (red, dashed line) resulting from the rate equations (5.284)-(5.287) under the assumption of $M = 10^4$ identical quantum dots. In addition, we use a Gaussian profile for the cooperativity strength[2],

$$G(\omega) = G_0 e^{-\frac{(\omega-\bar{\omega})^2}{2\sigma^2}} \, . \tag{6.22}$$

Other parameters which are included in this multimode theory are assumed to be well-known and given by $R = 0.5\gamma$, $\gamma_{10} = \gamma$, $\gamma_{21} = 0.1\gamma$ and $\gamma^l = \gamma^r = \gamma$. Please note, that the fit parameters of both, the Gaussian fit as well as the multimode stationary photon number, are effected by the choice of this set of parameters, more precisely on the pumping rate R, the number of QDs M and the damping rates γ_{10}, γ_{21}, γ^l and γ^r.

FITTING THE OPTICAL POWER SPECTRUM The available experimental data provided by *S. Blumenstein* were uncalibrated, that is information about the absolute values of the optical power at different frequencies are lost. Only the spectral shape or rather the relative change in the optical spectrum is available. Therefore, the main challenge is to fit the shape of $S(\omega)$ without knowing the absolute values.

To be specific, we consider the change in the optical power spectrum of two adjacent frequencies [166], $\Delta S(\omega_i)$, which is related to the differences of the logarithm. To demonstrate this, we set

$$S(\omega_{i+1}) = S(\omega_i) + \Delta S(\omega_i) \tag{6.23}$$

---

[1] Here, the integration limits were extended to ±∞ which is valid regarding the frequency band $[\omega_{-N/2}, \omega_{N/2-1}]$ in which $n^s(\omega) = 0$ for $\omega > \omega_{N/2-1}$ and $\omega < \omega_{-N/2}$.

[2] Please note, that the dimension of the amplitude S_0 of the power spectral density fit and the cooperativity strength G_0 are different. However, as the experimental data are not calibrated we choose arbitrary units.

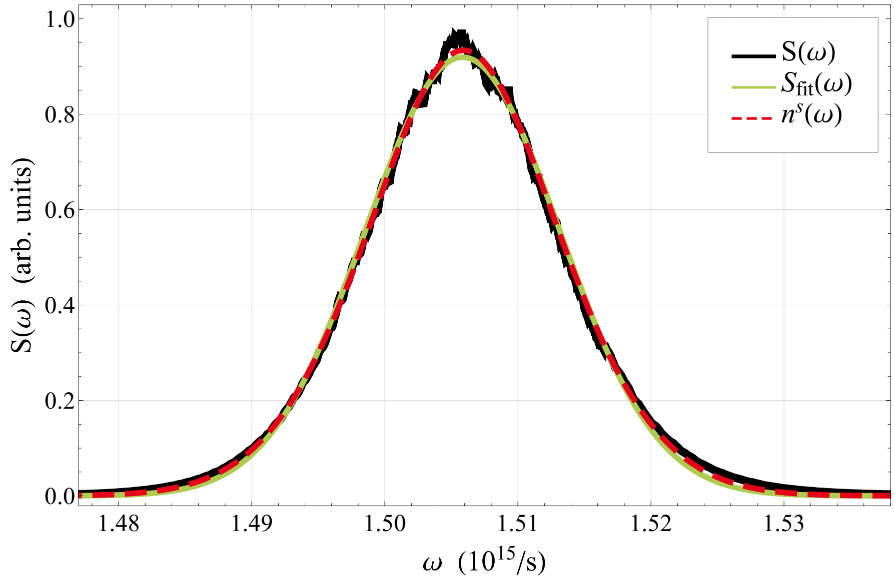

Figure 6.2: Experimental power spectrum $S(\omega)$ (black), Gaussian fit $S_{\text{fit}}(\omega)$ (green) analogous to figure 3.3 and stationary intrawaveguide photon number $n^s(\omega)$ (red, dashed) for $M = 10^4$ identical QDs, pumping rate $R = 0.5\gamma$, decay rates $\gamma_{10} = \gamma$, $\gamma_{21} = 0.1\gamma$, $\gamma^l = \gamma^r = \gamma$ and Gaussian cooperativity strength $G(\omega)$ (cf. equation (6.22)) with fit parameters listed in table 6.1.

with slight deviation $\Delta S(\omega_i)$. For $\Delta S(\omega_i) \ll S(\omega_i)$ the logarithmic difference is written as

$$\log(S(\omega_{i+1})) - \log(S(\omega_i)) = \log\left(\frac{S(\omega_{i+1})}{S(\omega_i)}\right) = \log\left(1 + \frac{\Delta S(\omega_i)}{S(\omega_i)}\right) \approx \frac{\Delta S(\omega_i)}{S(\omega_i)}. \tag{6.24}$$

It describes the percentage or relative change of $S(\omega)$ at two adjacent frequencies. Thus, the change in the optical power spectrum,

$$\Delta S(\omega_i) = S(\omega_i)\left[\log(S(\omega_{i+1})) - \log(S(\omega_i))\right], \tag{6.25}$$

is proportional to the difference of the logarithm of the optical power spectrum at frequency ω_{i+1} and ω_i.

Practically, the numerical solution of $n^s(\omega)$ is investigated by solving the rate equations (5.284)-(5.287) and using Newton's method [167]. Then we calculate the difference of the relative changes of the stationary photon number and the experimental values. Weighting this expression with the experimental data itself defines a useful error measure

$$F(n^s, S) = \sum_i \left[S(\omega_{i+1})\left(\log\left(\frac{n^s(\omega_{i+1})}{n^s(\omega_i)}\right) - \log\left(\frac{S(\omega_{i+1})}{S(\omega_i)}\right)\right)\right]^2, \tag{6.26}$$

with the two distributions $n^s(\omega)$ and $S(\omega)$ as an input. $F(n^s, S)$ is minimized by applying again Newton's method. The corresponding fit parameters as well as the sum of the square of the residuals weighted by the total number of modes N of both the Gaussian fit and the stationary photon number of the diode model are listed in table 6.1.

At first sight, both, the Gaussian fit as well as the numerical solution of the internal photon number depicted in figure 6.2, fit the data in an excellent way revealing a THz broadband power spectrum. Thus, the optical power spectrum of a QDSLD is primarily determined by the internal stationary photon number itself, which is a basic insight. The Gaussian behavior of $n^s(\omega)$ suggests that the shape of the optical power spectrum is mainly specified by the intrawaveguide

	$\bar{\omega}$ $(10^{15}/s)$	σ $(10^{12}/s)$	S_0, G_0 (arb. units)	$\sum_{\{k_i\}} r_i^2/N$
Gaussian fit $S_{\text{fit}}(\omega)$	1.506	7.286	$S_0 = 0.017$	$1.137 \cdot 10^{-4}$
QDSLD model $G(\omega)$	1.506	7.962	$G_0 = 2.467 \cdot 10^{-4}$	$0.526 \cdot 10^{-4}$

Table 6.1: Fit parameters of the Gaussian fit and the photon number of the QDSLD model with cooperativity strength $G(\omega)$ (see equation (6.22)) corresponding to the power spectrum depicted in figure 3.3 and figure 6.2 as well as the normalized sum of the squared residuals, r_i.

photon number itself. However, this shape of the number of photons originates from the choice of the cooperativity strength $G(\omega)$.

This perfect Gaussian behavior of the optical power spectrum is substantiated by plotting $\Delta S(\omega_i)$ [166]. Figure 6.3 shows $\Delta S(\omega_i)$ as a function of frequency ω_i resulting from the experimental data (black line) and the Gaussian fit (green line). The red, dashed line corresponds to the change of the modeled multimode stationary photon number $n^s(\omega_i)$. The antisymmetric behavior is observable for the theoretical model of the intrawaveguide photon number as well as for the optimal fitted Gaussian. Comparison between the red and green line exhibits very good agreement.

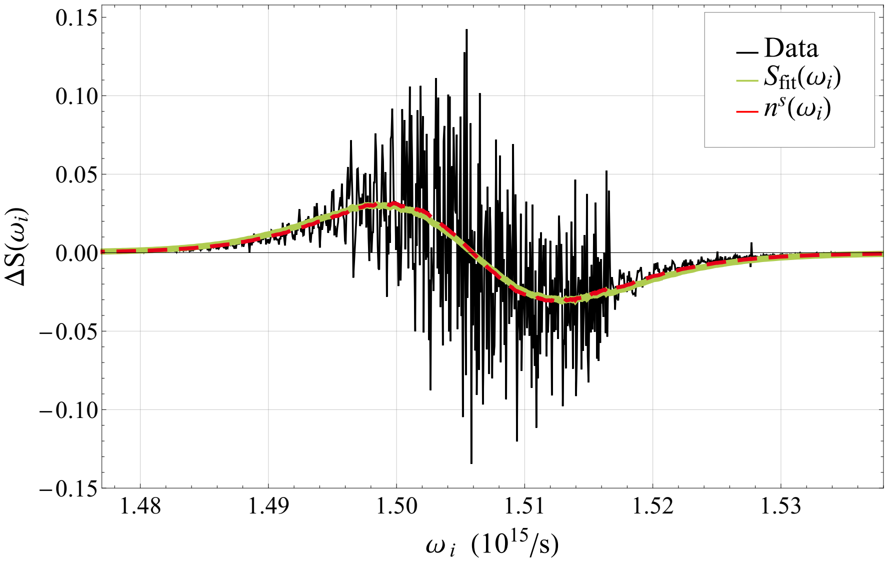

Figure 6.3: Change of the power spectrum (see figure 6.2) weighted with the experimental data $S(\omega_i)$ as a function of frequency ω_i.

In summary, the internal stationary photon number is significantly responsible for the shape of the power spectrum. On the other hand, the distribution of the intrawaveguide photon number is related to the cooperativity strength, $G(\omega)$, which we assumed to be of Gaussian shape described by equation (6.22). In order to study their connection, we consider again the numerical solution of the intrawaveguide photon number and the corresponding cooperativity strength for different pumping rates R.

Figure 6.4 shows the internal photon number (red dashed line) with associated cooperativity strength $\tilde{S}_0 G(\omega)$ (blue line) weighted with $\tilde{S}_0 = \max(n^s(\omega))/G_0$ as a function of angular frequency ω. Again, the gain medium is formed by $M = 10^4$ identical quantum dots with decay rates $\gamma_{21} = 0.1\gamma$ and $\gamma_{10} = \gamma$. The external damping rates are given by $\gamma^l = \gamma^r = \gamma$. In case

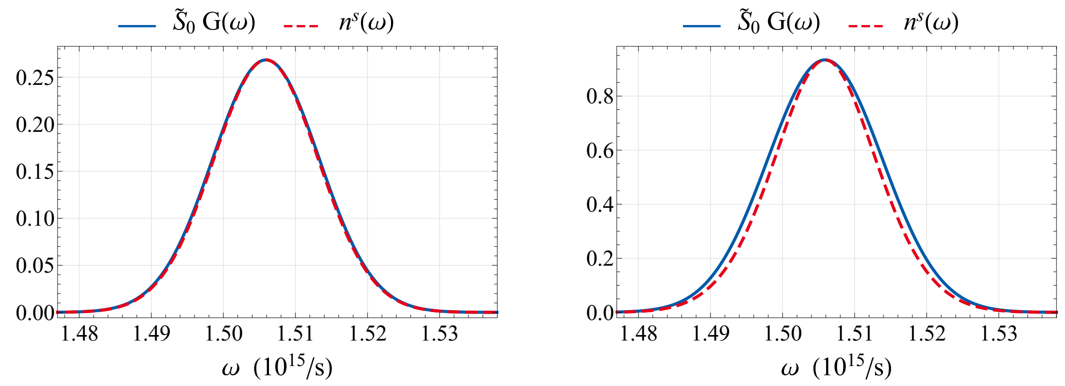

(a) $R = 0.2\gamma$ (b) $R = 0.5\gamma$

Figure 6.4: Numerical solution of the internal photon number (red dashed line) with associated cooperativity strength $\tilde{S}_0 G(\omega)$ (blue line) weighted with $\tilde{S}_0 = \max(n^s(\omega))/G_0$ as a function of angular frequency with parameters $M = 10^4$, $\gamma_{21} = 0.1\gamma$, $\gamma_{10} = \gamma$ and $\gamma^l = \gamma^r = \gamma$ and pumping rate (a) $R = 0.2\gamma$ and (b) $R = 0.5\gamma$.

of a small pumping rate $R = 0.2\gamma$ (see figure 6.4(a)) the photon number and the cooperativity strength agree very well. For an increasing pumping rate $R = 0.5\gamma$ depicted in figure 6.4(b), $n^s(\omega)$ becomes more narrow-band compared to the Gaussian interpolation. Simultaneously, the number of photons at the central frequency of both, Gaussian fit and multimode photon number, increases by a factor of 4 compared to figure 6.4(a). This behavior can be traced back to an increasing number of stimulated emission processes when operating sufficiently above the laser threshold with a critical pumping rate of $R_c = 0.111\gamma$. Figure 6.5 shows the deviation of the numerically calculated photon numbers form the Gaussian shaped cooperativity strength by plotting $n^s(\omega)$ as a function of $G(\omega)$ (red line). The green and blue line correspond to a linear ($x = 1$) and quadratic ($x = 2$) fit, respectively, with

$$n^s(\omega) = \sum_{k=0}^{x} c_k G^k(\omega). \tag{6.27}$$

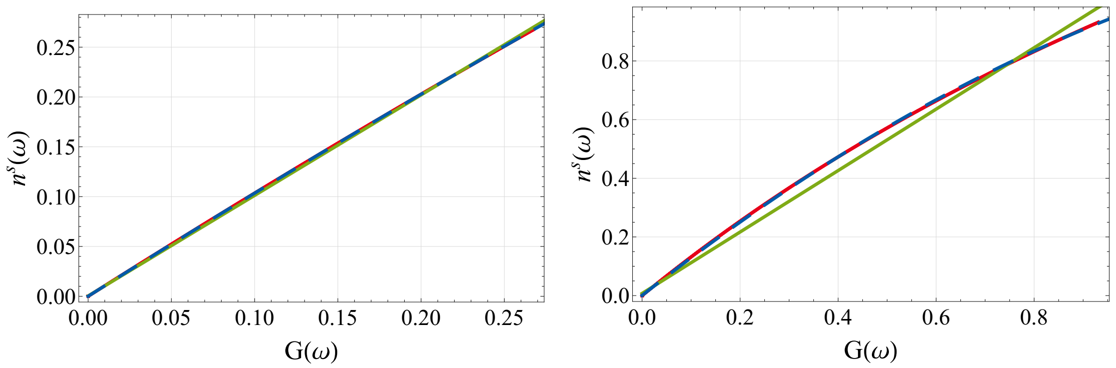

(a) $R = 0.2\gamma$ (b) $R = 0.5\gamma$

Figure 6.5: Stationary intrawaveguide photon number $n^s(\omega)$ as a function of cooperativity strength $G(\omega)$ given by equation (6.22) for $M = 10^4$ identical quantum dots, decay rates $\gamma_{10} = 0.1\gamma$, $\gamma_{10} = \gamma$, $\gamma^l = \gamma^r = \gamma$ and pumping rate (a) $R = 0.2\gamma$ and (b) $R = 0.5\gamma$. The red line is the numerical solution, the green and blue line show a linear and quadratic fit, respectively.

The fit parameters are listed in table 6.2.

$n^s = \sum_{k=0}^{2} c_k G^k$	c_0	c_1	c_2
$R = 0.2\gamma$	3.243×10^{-4}	1.009	–
$R = 0.5\gamma$	7.30×10^{-3}	1.047	–
$R = 0.2\gamma$	3.458×10^{-6}	1.056	-0.208
$R = 0.5\gamma$	4.468×10^{-4}	1.320	-0.348

Table 6.2: Linear and quadratic fit parameters of the polynomial photon number (see equation (6.27)) belonging to the green ($x = 1$) and blue ($x = 2$) line in figures 6.5(a)-(b).

Whereas, figure 6.5(a) shows a linear slope, figure 6.5(b) offers a quadratic behavior. Obviously, $n^s(\omega)$ behaves like a polynomial in the cooperativity strength. This corresponds exactly to the solution which we have found by studying the stationary intrawaveguide photon number for the special case of a small G_i (cf. equation (5.297)). Figure 6.5 illustrates that this polynomial is describable by equation (6.27) with $x = 2$ in good approximation. The internal stationary photon number exhibits a simple dynamics, directly related to the cooperativity strength. This study brings us to the perception that $G(\omega)$ and therefore the intrawaveguide dynamics determines the spectral density, entirely. Thus, knowing all experimental parameters, we are able to reconstruct each measured optical power spectrum of a QDSLD from microscopic considerations.

In summary, we showed that our quantum theory of light emitting quantum dot superluminescent diodes allows to determine the electromagnetic output field striking the detector. First-order temporal correlations were studied which are directly related to the optical power spectrum. It turns out, that the stationary photon number fits the experimental data very well. Its shape again depends significantly on the distribution of the cooperativity strength. This remarkable agreement between our theory and experiment allows the hypothesis that we are able to replicate each QDSLD spectra on the one hand. On the other hand, knowing the experimental data, we can specify unknown, relevant parameters like coupling strength between quantum dot and ASE field and so on.

The broadband behavior of the optical power spectrum is reflected by our theory correctly, which is one of the main ingredients for an accurate description of hybrid coherent light. Please remember, the hybrid coherent light phenomenon highlights its astonishing unusual character in terms of the temporal central second-order degree of coherence within a finite temperature regime showing a laser-like value of $g^{(2)}(0) = 1.33$ which is in contrast to its first-order highly incoherent character. The following chapter deals with the challenge of finding an explanation of the occurrence of this reduced central second-order degree of coherence by taking into account a broadband spectra, simultaneously.

7

PHOTON STATISTICS OF QUANTUM DOT SUPERLUMINESCENT DIODES

Photon statistics is a study about the statistical properties of radiation, which classifies light sources in terms of their coherence properties and provides evidence to the quantum nature of the considered radiation. The photon statistics is related to the second-order correlation function as indicated in chapter 2. In general, this correlation is measured by standard HBT experiments. As already mentioned, for the THz broad emission of QDSLDs with a coherence length of some femtoseconds, this measurement technique is not available due to the finite temporal resolution of commercial detectors. The invention of the two-photon detector by *F. Boitier et al.* [29] circumvents this problem and delivers a competitive feasibility for measuring broadband radiation. In particular, it allows for the analysis of the photon statistical properties of hybrid coherent light, which exhibits a reduction of $g^{(2)}(0)$ at an external temperature T = 190 K (see section 3.2).

To find an explanation of this unusual characteristic, this chapter is dedicated to the determination of the second-order correlation function of QDSLDs resulting from the microscopic field theory studied in section 5. Within this context we analyze the central second-order degree of coherence. The chapter ends with a discussion of the photon statistics of a single-mode QDSLD with identical QDs.

7.1 TEMPORAL SECOND-ORDER CORRELATION OF QDSLDS

In this section we formally calculate the temporal second-order correlation function of light emitted by a QDSLD, which is described by our microscopic theory presented in chapter 5. A two-photon detector of finite cross-section area A_d is assumed to be located at the right-hand side of the semiconductor device with distance z_d in analogy to the previous chapter where we studied the power spectrum (see figure 6.1). The electric field emitted by the QDSLD on the right-hand side parallel to the z-direction is assumed to be guided into a single-mode fiber till it enters the detector.

The positive frequency part of the electric field, which is measured by the two-photon detector at $z = z_d \gg 0$, is given by (cf. equation (5.199))

$$\hat{\mathbf{E}}^{(+)}_{\text{out}}(\mathbf{r},t) = \hat{E}^{(+)}_{\text{out}}(\mathbf{r},t)\mathbf{e}_y \equiv \hat{\mathbf{E}}^{1(+)}_{\text{out}}(x,y,t-\frac{z_d}{c_0}) \simeq \sum_{\{k_i>0\}} \tilde{v}_i(x,y)\hat{b}^{1}_{i,\text{out}}(t-\frac{z_d}{c_0})\mathbf{e}_y, \tag{7.1}$$

with the mode functions (cf. equation (5.200))

$$\tilde{v}_i(x,y) = \mathrm{i}\sqrt{\frac{\hbar\pi\omega_i}{\varepsilon_0 V\Delta\omega_i}}\,\mu(x,y). \tag{7.2}$$

As discussed in section 2.3.2 the temporal second-order correlation function $G^{(2)}(\mathbf{r},t;\mathbf{r},t')$ and the second-order degree of coherence $g^{(2)}(\mathbf{r},t;\mathbf{r},t')$ of the output radiation field with $t<t'$ correspond to the fourth-order moments

$$G^{(2)}(\mathbf{r},t;\mathbf{r},t') = \langle \hat{E}^{(-)}_{\text{out}}(\mathbf{r},t)\hat{E}^{(-)}_{\text{out}}(\mathbf{r},t')\hat{E}^{(+)}_{\text{out}}(\mathbf{r},t')\hat{E}^{(+)}_{\text{out}}(\mathbf{r},t)\rangle, \tag{7.3}$$

$$g^{(2)}(\mathbf{r},t;\mathbf{r},t') = \frac{\langle \hat{E}^{(-)}_{\text{out}}(\mathbf{r},t)\hat{E}^{(-)}_{\text{out}}(\mathbf{r},t')\hat{E}^{(+)}_{\text{out}}(\mathbf{r},t')\hat{E}^{(+)}_{\text{out}}(\mathbf{r},t)\rangle}{\langle \hat{E}^{(-)}_{\text{out}}(\mathbf{r},t)\hat{E}^{(+)}_{\text{out}}(\mathbf{r},t)\rangle\langle \hat{E}^{(-)}_{\text{out}}(\mathbf{r},t')\hat{E}^{(+)}_{\text{out}}(\mathbf{r},t')\rangle}. \tag{7.4}$$

To find an explicit expression of these physical quantities we utilize the input-output formalism in equation (5.206). In the following, we choose vacuum as an input in analogy to the previous chapter. It turns out, that the two-time correlation of the output operators only depends on the correlation of the intrawaveguide field amplitudes as

$$\langle \hat{b}^{1\dagger}_{i,\text{out}}(t)\hat{b}^{1\dagger}_{k,\text{out}}(t')\hat{b}^{1}_{m,\text{out}}(t')\hat{b}^{1}_{n,\text{out}}(t)\rangle = \Xi_{ikmn}(t,t')\langle \hat{a}^\dagger_i(t)\hat{a}^\dagger_k(t')\hat{a}_m(t')\hat{a}_n(t)\rangle \tag{7.5}$$

with

$$\Xi_{ikmn}(t,t') \equiv (\Delta\nu_{\text{F}})^2 \mathscr{T}^{r*}_i \mathscr{T}^{r*}_k \mathscr{T}^{r}_m \mathscr{T}^{r}_n T^{r*}_i(t) T^{r*}_k(t') T^{r}_m(t') T^{r}_n(t). \tag{7.6}$$

The dynamics of the intrawaveguide field operators is described by the stochastic differential equation (5.230). Inserting the solution (7.5) into the definition (7.3) and integrating over the total cross-section of the detector A_d finally results into an expression of the **temporal second-order correlation function**

$$G^{(2)}(t;t') = \sum_{\{k_i,k_k,k_m,k_n>0\}} \mathrm{w}_{ikmn}(t,t')\langle \hat{a}^\dagger_i(t)\hat{a}^\dagger_k(t')\hat{a}_m(t')\hat{a}_n(t)\rangle, \tag{7.7}$$

in which

$$\mathrm{w}_{ikmn}(t,t') = \left(\frac{\hbar\pi}{\varepsilon_0 L}\right)^2 \sqrt{\frac{\omega_i\omega_k\omega_m\omega_n}{\Delta\omega_i\Delta\omega_k\Delta\omega_m\Delta\omega_n}}\,\Xi_{ikmn}(t,t'). \tag{7.8}$$

Only stationary situations will be considered. Thus, the physical quantity of interest

$$G^{(2)}(\tau) = \lim_{t\to\infty} G^{(2)}(t;t'=t+\tau) \tag{7.9}$$

is only a function of time delay $\tau = t'-t>0$. In analogy to the previous section we assume that the time-dependent transmission amplitude $T^r_i(t)$ evolves slowly compared to the system's amplitudes, which results into an approximately constant transmission contribution so that,

$$\Xi_{ikmn}(t,t+\tau) \simeq \Xi^s_{ikmn} = (\Delta\nu_{\text{F}})^2 \mathscr{T}^{r*}_i \mathscr{T}^{r*}_k \mathscr{T}^{r}_m \mathscr{T}^{r}_n T^{r*}_i T^{r*}_k T^{r}_m T^{r}_n = \text{const.}, \tag{7.10}$$

$$\mathrm{w}_{ikmn}(t,t+\tau) \simeq \mathrm{w}^s_{ikmn} = \text{const.}. \tag{7.11}$$

Thus, knowing the two-time, fourth-order moment of the internal field operators we can specify the second-order correlation explicitly.

7.2 CENTRAL SECOND-ORDER DEGREE OF COHERENCE

In this section, we study the central second-order degree of coherence of a QDSLD with the help of our microscopic model. The theoretical result could provide an explanation of the experimental observation of the $g^{(2)}(0)$ reduction at a special temperature, which again grants more insight into the quantum nature of light emitting diodes. Simultaneously, an explanation of the observed coherence properties of broadband QDSLDs could enable the establishment of novel light sources possessing a wide range of applications for both commercial and fundamental purposes. It should be noted that the general measure of the second-order degree of coherence $g^{(2)}(\tau)$ as a function of time delay τ, is also determinable (see appendix H). However, with regard to the hybrid coherent light effect, we are focused on the analysis of the central second-order correlation function.

To specify this physical quantity of interest, we set up an Itô QSDE for the average of the intrawaveguide field operators $\langle \hat{a}_i^\dagger \hat{a}_k^\dagger \hat{a}_m \hat{a}_n \rangle$. This differential equation can be determined by the help of the QSDE of a single field amplitude given in equation (5.230) together with the Itô product rule (F.20) or directly from the definition of an Itô QSDE (see equation (F.16)). In the following we assume vacuum as an input, identical external decay rates for each mode i, $\gamma_i^l = \gamma^l$ and $\gamma_i^r = \gamma^r$, as well as uncorrelated input modes of different reservoirs, $\langle \mathrm{d}\hat{B}^{L(\dagger)} \mathrm{d}\hat{B}^{R(\dagger)} \rangle = 0$. Due to quantum causality and the fact that the increments commute with and are statistically independent of the system operators at the same time [50], the stochastic differential equation reads

$$\begin{aligned}\frac{\mathrm{d}}{\mathrm{d}t}\langle \hat{a}_i^\dagger \hat{a}_k^\dagger \hat{a}_m \hat{a}_n \rangle = &- \alpha_{ikmn} \langle \hat{a}_i^\dagger \hat{a}_k^\dagger \hat{a}_m \hat{a}_n \rangle + \sum_{j=1}^{M} \Big(g_i^j \langle \hat{\sigma}_{21}^{j\dagger} \hat{a}_k^\dagger \hat{a}_m \hat{a}_n \rangle + g_k^j \langle \hat{a}_i^\dagger \hat{\sigma}_{21}^{j\dagger} \hat{a}_m \hat{a}_n \rangle \\ &+ g_m^{j^*} \langle \hat{a}_i^\dagger \hat{a}_k^\dagger \hat{\sigma}_{21}^j \hat{a}_n \rangle + g_n^{j^*} \langle \hat{a}_i^\dagger \hat{a}_k^\dagger \hat{a}_m \hat{\sigma}_{21}^j \rangle \Big),\end{aligned} \tag{7.12}$$

with

$$\alpha_{ikmn} = \mathrm{i}(\Delta_m + \Delta_n - \Delta_i - \Delta_k) + 2(\gamma^l + \gamma^r). \tag{7.13}$$

We are left with the determination of correlations between quantum dot transitions and multimode radiation field amplitudes of type $\langle \hat{\sigma}_{21}^{j\dagger} \hat{a}_k^\dagger \hat{a}_m \hat{a}_n \rangle$. First, we consider the second correlation term on the right hand side of equation (7.12). With the help of the QSDE (5.230), equation (5.245a) and the Itô rule (F.20) we get

$$\begin{aligned}\frac{\mathrm{d}}{\mathrm{d}t}\langle \hat{\sigma}_{21}^{j\dagger} \hat{a}_k^\dagger \hat{a}_m \hat{a}_n \rangle = &- \vartheta_{kmn}^j \langle \hat{\sigma}_{21}^{j\dagger} \hat{a}_k^\dagger \hat{a}_m \hat{a}_n \rangle + \sum_{\{k_r\}} g_r^{j*} \langle \hat{w}^j \hat{a}_r^\dagger \hat{a}_k^\dagger \hat{a}_m \hat{a}_n \rangle \\ &+ \sum_{j'=1}^{M} \Big(g_k^{j'} \langle \hat{\sigma}_{21}^{j\dagger} \hat{\sigma}_{21}^{j'\dagger} \hat{a}_m \hat{a}_n \rangle + g_m^{j'*} \langle \hat{\sigma}_{21}^{j\dagger} \hat{a}_k^\dagger \hat{\sigma}_{21}^{j'} \hat{a}_n \rangle + g_n^{j'*} \langle \hat{\sigma}_{21}^{j\dagger} \hat{a}_k^\dagger \hat{a}_m \hat{\sigma}_{21}^{j'} \rangle \Big),\end{aligned} \tag{7.14}$$

with

$$\vartheta_{kmn}^j = -\mathrm{i}(\delta\omega_{12}^j + \Delta_k - \Delta_m - \Delta_n) + \frac{1}{2}(\Gamma_{21}^j + R) + \frac{3}{2}(\gamma^l + \gamma^r). \tag{7.15}$$

Approximations that were already introduced in connection with the rate equations (cf. section 5.3.1) allow to simplify this first-order differential equation. We apply the decorrelation approximation and neglect correlations between different QDs, so that $\langle \hat{\sigma}_{21}^{j\dagger} \hat{\sigma}_{21}^{j'} \rangle = \sigma_{11}^j \delta_{jj'}$ holds (cf. equation (5.250)). Furthermore, we neglect squeezing effects, that is $\langle \hat{a}_i \hat{a}_j \rangle = \langle \hat{a}_i^\dagger \hat{a}_j^\dagger \rangle = 0$ as well as counter-propagating contributions like $\langle \hat{\sigma}_{21}^{j\dagger} \hat{a}_k^\dagger \rangle = \langle \hat{\sigma}_{21}^j \hat{a}_k \rangle = 0$. The single correlation terms in equation (7.14) factorize to

$$\langle \hat{w}^j \hat{a}_s^\dagger \hat{a}_k^\dagger \hat{a}_m \hat{a}_n \rangle \approx w^j \langle \hat{a}_s^\dagger \hat{a}_k^\dagger \hat{a}_m \hat{a}_n \rangle, \tag{7.16}$$

$$\langle \hat{\sigma}_{21}^{j\dagger} \hat{\sigma}_{21}^{j'\dagger} \hat{a}_m \hat{a}_n \rangle \approx \langle \hat{\sigma}_{21}^{j\dagger} \hat{a}_m \rangle \langle \hat{\sigma}_{21}^{j'\dagger} \hat{a}_n \rangle + \langle \hat{\sigma}_{21}^{j\dagger} \hat{a}_n \rangle \langle \hat{\sigma}_{21}^{j'\dagger} \hat{a}_m \rangle, \tag{7.17}$$

$$\langle \hat{\sigma}_{21}^{j\dagger} \hat{a}_k^\dagger \hat{\sigma}_{21}^{j'} \hat{a}_n \rangle \approx \sigma_{11}^j n_k \delta_{jj'} \delta_{kn} + \langle \hat{\sigma}_{21}^{j\dagger} \hat{a}_n \rangle \langle \hat{a}_k^\dagger \hat{\sigma}_{21}^{j'} \rangle. \tag{7.18}$$

According to section 5.3.1 we adiabatically eliminate correlations of the quantum dot transition and the radiation field by setting the right-hand side of equation (7.14) equal to zero,

$\frac{\mathrm{d}}{\mathrm{d}t}\langle\hat{\sigma}_{21}^{j^\dagger}\hat{a}_k^\dagger\hat{a}_m\hat{a}_n\rangle \approx 0$ and finally replacing the correlation by its stationary value. We obtain an expression for the expectation value

$$
\begin{aligned}
\langle\hat{\sigma}_{21}^{j\dagger}\hat{a}_k^\dagger\hat{a}_m\hat{a}_n\rangle \approx \frac{1}{\vartheta_{kmn}^j}\Big\{ & \sum_{\{k_r>0\}} g_r^{j*} w^j \langle\hat{a}_r^\dagger\hat{a}_k^\dagger\hat{a}_m\hat{a}_n\rangle + (g_m^{j*}\delta_{kn} + g_n^{j*}\delta_{km}) n_k \sigma_{11}^j \\
& + g_k^j g_m^{j*} g_n^{j*} \Big[\frac{2(n_m w^j + \sigma_{11}^j)(n_n w^j + \sigma_{11}^j)}{(\mathrm{i}\Delta_m^j + \Gamma^j/2)(\mathrm{i}\Delta_n^j + \Gamma^j/2)} \\
& + \frac{n_k w^j + \sigma_{11}^j}{-\mathrm{i}\Delta_k^j + \Gamma^j/2}\Big(\frac{n_n w^j + \sigma_{11}^j}{\mathrm{i}\Delta_n^j + \Gamma^j/2} + \frac{n_m w^j + \sigma_{11}^j}{\mathrm{i}\Delta_m^j + \Gamma^j/2}\Big)\Big]\Big\}
\end{aligned} \tag{7.19}
$$

in terms of $\langle\hat{a}_i^\dagger\hat{a}_k^\dagger\hat{a}_m\hat{a}_n\rangle$ and lower-order moments. All other correlations arising in equation (7.14) can be investigated in the same way. The differential equation of the fourth-order moment for the radiation field amplitudes $\langle\hat{a}_i^\dagger\hat{a}_k^\dagger\hat{a}_m\hat{a}_n\rangle$ is listed in appendix G. However, we only consider terms which are at most quadratic in the coupling constant which provides the major contribution for weak coupling strengths. Accordingly, we neglect terms of the order of $|g|^4$. Furthermore, we claim that off-diagonal elements of type $g_i^j g_j^{j*}$ with $i \neq j$ are small compared to the diagonal ones. As a main result we find that the first-order differential equation of the internal expectation value $\langle\hat{a}_i^\dagger\hat{a}_k^\dagger\hat{a}_m\hat{a}_n\rangle$ is determined by

$$
\begin{aligned}
\frac{\mathrm{d}}{\mathrm{d}t}\langle\hat{a}_i^\dagger\hat{a}_k^\dagger\hat{a}_m\hat{a}_n\rangle \approx & \left[-\alpha_{ikmn} + \alpha_{ikmn}^{(2)}\right]\langle\hat{a}_i^\dagger\hat{a}_k^\dagger\hat{a}_m\hat{a}_n\rangle \\
& + \sum_{j=1}^M g_i^j \left(\frac{g_m^{j*}}{\vartheta_{kmk}^j} + \frac{g_n^{j*}}{\vartheta_{kkn}^j}\right)\sigma_{11}^j n_k + \sum_{j=1}^M g_k^j \left(\frac{g_m^{j*}}{\vartheta_{imi}^j} + \frac{g_n^{j*}}{\vartheta_{iin}^j}\right)\sigma_{11}^j n_i \\
& + \sum_{j=1}^M g_m^{j*} \left(\frac{g_k^j}{\vartheta_{nkn}^{j*}} + \frac{g_i^j}{\vartheta_{nni}^{j*}}\right)\sigma_{11}^j n_n + \sum_{j=1}^M g_n^{j*} \left(\frac{g_k^j}{\vartheta_{mkm}^{j*}} + \frac{g_i^j}{\vartheta_{mmi}^{j*}}\right)\sigma_{11}^j n_m,
\end{aligned} \tag{7.20}
$$

with second-order energy shift

$$
\alpha_{ikmn}^{(2)} = \sum_{j=1}^M \left(\frac{|g_i^j|^2}{\vartheta_{kmn}^j} + \frac{|g_k^j|^2}{\vartheta_{imn}^j} + \frac{|g_m^j|^2}{\vartheta_{nki}^{j*}} + \frac{|g_n^j|^2}{\vartheta_{mki}^{j*}}\right) w^j. \tag{7.21}
$$

The resulting stationary solution of the fourth-order moment of the internal field amplitudes reads

$$
\langle\hat{a}_i^\dagger\hat{a}_k^\dagger\hat{a}_m\hat{a}_n\rangle_s = \frac{\sum_{j=1}^M \beta_{ikmn}^j}{\alpha_{ikmn} - \alpha_{ikmn}^{(2)s}}, \quad \alpha_{ikmn}^{(2)s} = \sum_{j=1}^M \left(\frac{|g_i^j|^2}{\vartheta_{kmn}^j} + \frac{|g_k^j|^2}{\vartheta_{imn}^j} + \frac{|g_m^j|^2}{\vartheta_{nki}^{j*}} + \frac{|g_n^j|^2}{\vartheta_{mki}^{j*}}\right) w^{js} \tag{7.22}
$$

with

$$
\begin{aligned}
\beta_{ikmn}^j = & g_i^j \left(\frac{g_m^{j*}}{\vartheta_{kmk}^j} + \frac{g_n^{j*}}{\vartheta_{kkn}^j}\right)\sigma_{11}^{js} n_k^s + g_k^j \left(\frac{g_m^{j*}}{\vartheta_{imi}^j} + \frac{g_n^{j*}}{\vartheta_{iin}^j}\right)\sigma_{11}^{js} n_i^s \\
& + g_m^{j*} \left(\frac{g_k^j}{\vartheta_{nkn}^{j*}} + \frac{g_i^j}{\vartheta_{nni}^{j*}}\right)\sigma_{11}^{js} n_n^s + g_n^{j*} \left(\frac{g_k^j}{\vartheta_{mkm}^{j*}} + \frac{g_i^j}{\vartheta_{mmi}^{j*}}\right)\sigma_{11}^{js} n_m^s.
\end{aligned} \tag{7.23}
$$

Here, the labeling s emphasized the corresponding stationary solution of the considered physical measure. Therefore, the temporal second-order correlation function and the temporal second-order degree of coherence of a QDSLD with zero time delay are given by

$$
G^{(2)}(0) = \sum_{\{k_i,k_k,k_m,k_n>0\}} \mathrm{w}_{ikmn}^s \langle\hat{a}_i^\dagger\hat{a}_k^\dagger\hat{a}_m\hat{a}_n\rangle_s, \tag{7.24}
$$

$$\boxed{g^{(2)}(0)=\frac{\sum_{\{k_i,k_k,k_m,k_n>0\}}\mathrm{w}^s_{ikmn}\langle\hat{a}_i^\dagger\hat{a}_k^\dagger\hat{a}_m\hat{a}_n\rangle_s}{\sum_{\{k_i,k_k>0\}}\mathrm{w}^s_{ikik}n_i^s n_k^s}}, \tag{7.25}$$

with the average $\langle\hat{a}_i^\dagger\hat{a}_k^\dagger\hat{a}_m\hat{a}_n\rangle_s$ specified in equation (7.22). This temporal central second-order degree of coherence depends on the stationary photon number n^s which was already analyzed in detail in section 5.3.2.

SPECIAL CASE: THERMAL LIGHT SOURCE In order to check the general multimode result of the central second-order degree of coherence (cf. equation (7.25)), we consider the case of a QDSLD acting as a thermal light source. Here, we already know that $g^{(2)}(0)=2$ (see section 2.3.4). This expected bunching effect has to be reflected by our theory. According to the generalized Wick theorem (see appendix A), the fourth-order thermal average is

$$\begin{aligned}\langle\hat{a}_i^\dagger\hat{a}_k^\dagger\hat{a}_m\hat{a}_n\rangle_s&=\langle\hat{a}_i^\dagger\hat{a}_k^\dagger\rangle_s\langle\hat{a}_m\hat{a}_n\rangle_s+\langle\hat{a}_i^\dagger\hat{a}_m\rangle_s\langle\hat{a}_k^\dagger\hat{a}_n\rangle_s+\langle\hat{a}_i^\dagger\hat{a}_n\rangle_s\langle\hat{a}_k^\dagger\hat{a}_m\rangle_s\\&=n_i^s n_k^s\left(\delta_{im}\delta_{kn}+\delta_{in}\delta_{km}\right).\end{aligned} \tag{7.26}$$

Inserting equation (7.26) into equation (7.25) yields the predicted solution

$$g^{(2)}(0)=2. \tag{7.27}$$

However, a realistic light-emitting QDSLD exhibits a reduced $g^{(2)}(0)$-value within a certain temperature regime measured by the central experiment [1]. We suppose that this phenomenon is also included in our model solution (7.25). Thus, equation (7.25) together with the calculated power spectral density (6.20) are the main ingredients for describing and interpreting the phenomenon of hybrid coherent light from a theoretical point of view which in turn represents the essence of the entire thesis. In this context, we have a closer look at the temporal second-order degree of coherence (7.25) and study in the following the simple case of a single-mode QDSLD composed of M identical quantum dots.

7.2.1 Single-mode QDSLD with identical quantum dots

The single-mode electric field emitted by the semiconductor device,

$$\hat{\mathbf{E}}^{(+)}(\mathbf{r},t)=\tilde{v}(x,y)\hat{b}^1_{\text{out}}(t-z/c_0)\mathbf{e}_y, \tag{7.28}$$

is proportional to the quantized field amplitude $\hat{b}^1_{\text{out}}(t)$, which again is related with the input and the internal field operator via the input-output formalism (cf. equation (5.206))

$$\hat{b}^1_{\text{out}}(t)=\hat{b}_{\text{in}}(t)+\sqrt{\Delta\nu_{\text{F}}}\mathscr{T}^r T^r(t)\hat{a}(t). \tag{7.29}$$

The stationary fourth-order moment of the internal radiation field (cf. equation (7.22)) reduces to the simple, analytic expression

$$\langle\hat{a}^\dagger\hat{a}^\dagger\hat{a}\hat{a}\rangle_s=\frac{4M|g|^2\sigma^s_{11}n^s\,\mathrm{Re}\big(\frac{1}{\vartheta}\big)}{\gamma^l+\gamma^r-2M|g|^2w^s\,\mathrm{Re}\big(\frac{1}{\vartheta}\big)},\quad\vartheta=\mathrm{i}\Delta+\frac{1}{2}(\gamma_{21}+R)+\frac{3}{2}(\gamma^l+\gamma^r). \tag{7.30}$$

This expectation value depends explicitly on the internal stationary number of photons n^s, the inversion $w^s=\sigma^s_{11}-\sigma^s_{22}$ and the quantum dot population σ^s_{11} calculated in (5.281)-(5.283). For vacuum input, the central second-order degree of coherence is

$$g^{(2)}(0)=\frac{\langle\hat{a}^\dagger\hat{a}^\dagger\hat{a}\hat{a}\rangle_s}{(\langle\hat{a}^\dagger\hat{a}\rangle_s)^2}=\frac{\langle\hat{a}^\dagger\hat{a}^\dagger\hat{a}\hat{a}\rangle_s}{n^{s2}}=\frac{4M|g|^2\sigma^s_{11}\,\mathrm{Re}\big(\frac{1}{\vartheta}\big)}{n^s\left(\gamma^l+\gamma^r-2M|g|^2w^s\,\mathrm{Re}\big(\frac{1}{\vartheta}\big)\right)}. \tag{7.31}$$

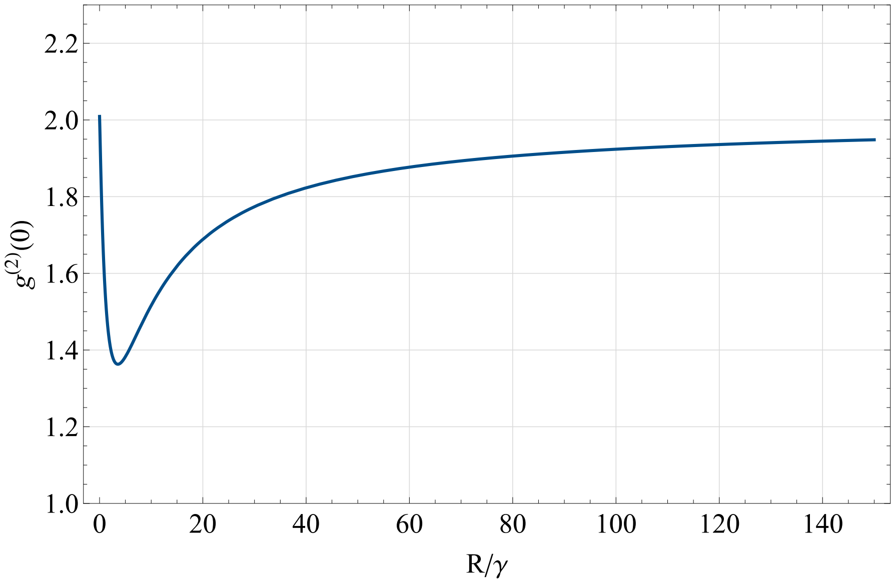

Figure 7.1: Central second-order degree of coherence $g^{(2)}(0)$ as a function of the scaled pumping rate R/γ for a single-mode QDSLD composed of $M = 10^4$ identical quantum dots with coupling constant $g = 0.01\gamma$ ($M|g|^2 = \gamma^2$), detuning $\Delta = 1.8\gamma$ and line widths $\gamma^l = \gamma^r = \gamma_{10} = \gamma$, $\gamma_{21} = 0.1\gamma$.

Figure 7.1 shows $g^{(2)}(0)$ as a function of pumping rate R/γ in the weak coupling regime with chosen parameters $g = 0.01\gamma$, $\gamma^l = \gamma^r = \gamma_{10} = \gamma$, $\gamma_{21} = 0.1\gamma$, $M = 10^4$, $\Delta = 1.8\gamma$ and cooperativity parameter $G_c = 0.004 < 1$ (cf. equation (5.260)). Obviously, an increasing pumping rate highlights a reduction of the central second-order degree of coherence from $g^{(2)}(0) = 2$ for $R \to 0$ to $g^{(2)}(0) = 1.36$ at $R = 3.55\gamma$. For $R > 3.55\gamma$ the measure $g^{(2)}(0)$ increases and approaches a maximum value of $\lim_{R\to\infty} g^{(2)}(0) = 2$.

Figure 7.2 illustrates $g^{(2)}(0)$ as a function of scaled detuning Δ/γ_{10} for $M = 150$ identical quantum dots with coupling constant $g = 7.8\gamma$, pumping rate $R = 1200\gamma$ as well as line widths $\gamma^l = \gamma^r = \gamma$, $\gamma_{21} = 139\gamma$ and $\gamma_{10} = 250\gamma$. Due to the definition of equation (5.260), we are dealing with a strong coupling system of large cooperativity parameter $G_c = 121.68 > 1$. A reduction of the second-order degree of coherence from 2 to 1.33 around zero detuning $\Delta = 0$ is clearly observable for the chosen set of parameters. This behavior reminds us of the experimentally observed $g^{(2)}(0)$ behavior of hybrid coherent light as a function of temperature. Also here, a reduction from $g^{(2)}(0) = 2$ to $g^{(2)}(0) = 1.33$ was observed in the lab within the temperature regime of about 190 K. The red dots are the corresponding experimental data extracted from reference [1] (cf. also figure 3.6).

TEMPERATURE-DEPENDENT DETUNING This quite obvious equivalent qualitative behavior of $g^{(2)}(0)$ with regard to temperature and detuning is comprehensible regarding the general semiconductor characteristic of a temperature dependent energy band gab [168]. Clearly, all quantum dot decay rates and of course detunings as well as coupling constants are also functions of temperature T. Based on this knowledge about the T dependency of the energy band gap in semiconductors, a standard method in the lab for observing $g^{(2)}(0)$ as a function of detuning Δ is based on a temperature tuning [169–171]. *A. Kiraz et al.* [172] showed that the T dependency primarily effects the detuning rather than any line widths of the quantum dot system. Therefore, from a theoretical point of view, changing of temperature is treated as being synonymous to changing the detuning. All further parameters are assumed to be independent of T. Taking into account this equivalence between T and Δ, highlights quite clearly a remarkable agreement

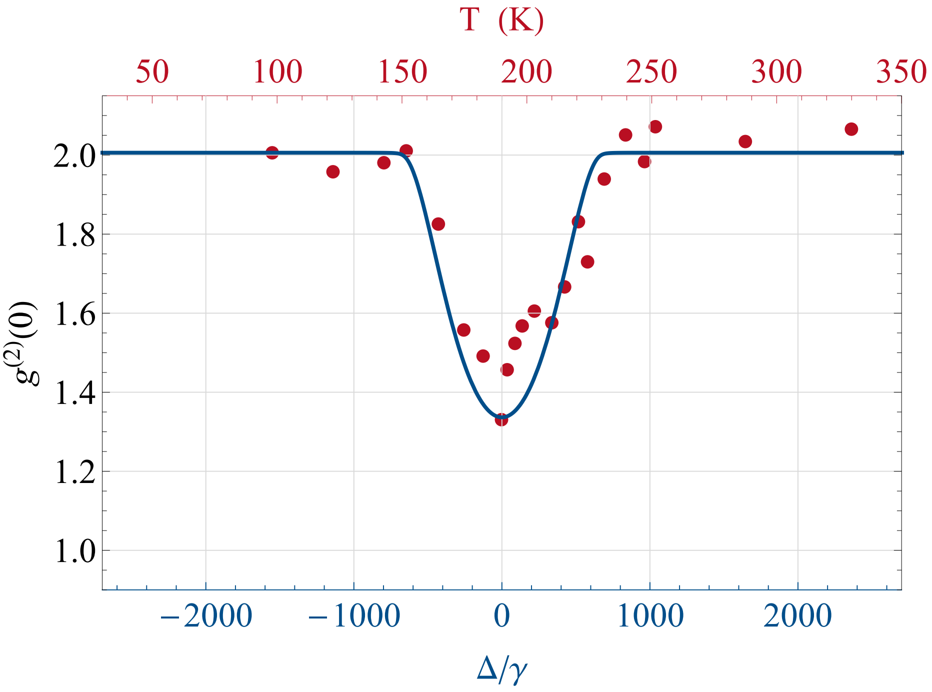

Figure 7.2: (Blue): Central second-order degree of coherence $g^{(2)}(0)$ as a function of the scaled detuning Δ/γ for a single-mode QDSLD composed of $M = 150$ identical quantum dots with coupling constant $g = 7.8\gamma$ ($M|g|^2 = 9126\gamma^2$), pumping rate $R = 1200\gamma$ and line widths $\gamma^l = \gamma^r = \gamma$, $\gamma_{21} = 139\gamma$ and $\gamma_{10} = 250\gamma$. (Red): Experimental data [1] of central second-oder degree of coherence $g^{(2)}(0)$ versus temperature T (cf. figure 3.6).

between the experimental observation [1] and our quantum theory of QDSLDs (see figure 7.2). It also implies that the physical effect provoking the occurrence of hybrid coherent light is included within our microscopic model.

Please note, that we considered here a single-mode emitting QDSLD system. The fact that here a reduced second-order degree of coherence is observable reveals that the physical effect of noise suppression at a particular temperature regime is also included in the limiting single-mode case. Nevertheless, a reduction of $g^{(2)}(0)$ is also theoretically predicted for the full multimode theory. Thus, the hybrid coherent light phenomenon of being incoherent in first- and simultaneously coherent in second-order of correlation is presumably not a purely collective mode effect. Naturally, the broadband spectral density of hybrid coherent light as visualized in figure 6.2 originates from the multimode character of the amplified spontaneous emission.

7.2.2 Physical explanation of the occurrence of hybrid coherent light

Our quantum theory reflects the key measurements of hybrid coherent light: a broadband optical power spectrum (see figure 6.2) as well as a reduction of the central second-order degree of coherence (see figure 7.2). Our modeling ansatz presented in chapter 5 is based on quantum optical considerations. Semiconductor effects like the formation of excitons, polaritons etc. are disregarded within our field theory. This essential fact suggests that hybrid coherent light is essentially a purely optical effect, which again permits the speculation that these novel states of light are also reproducible in other optical devices. It is even conceivable that gas lasers operated in the regime of the amplified spontaneous emission exhibit a reduced $g^{(2)}(0)$-value, that is noise suppression. A direct measurement of hybrid coherent light with other, suitable light sources would prove our hypothesis.

Obviously, a reduction of $g^{(2)}(0)$ is observable for small coupling strengths and large incoherent pumping rates. Due to this strong pumping mechanism, the system at resonance gets 'stiff'. This effect is also observable in non-linear systems (cf. Van der Pol oscillator model [173]). The system passes into saturation leading to a reduction of intensity fluctuations, which again is noticeable in a reduced central second-order degree of coherence. Such a noise reduction corresponds to classical squeezing [174]. Simultaneously, the power spectrum, determined by the first-order temporal autocorrelation function, remains broadband.

Clearly, this single-mode discussion of $g^{(2)}(0)$ should be extended to the more realistic and more exciting case of a truly multimode QDSLD for which a suppression of noise fluctuation is also predicted.

In this section, we analyzed the central second-order degree of coherence of a light emitting QDSLD. As a result of our microscopic theory, we found a general expression of $g^{(2)}(0)$ in terms of the stationary photon number, excited state population and inversion. For the special case of a single-mode QDSLD composed of identical quantum dots and a particular set of parameters a reduction of $g^{(2)}(0)$ as a function of detuning appeared. A direct comparison with the experimental data highlighted a very good agreement, quantitatively. This fact illustrates that hybrid coherent light is describable in the context of our quantum theory which again allows an interpretation of the observed noise suppression of broadband QDSLDs at a particular temperature. It turns out that the hybrid coherent light phenomenon is attributable to a saturation effect.

8

CONCLUSION AND OUTLOOK

Motivated by the unusual behavior at a special temperature regime observed in the experiment [1], we investigated the emission and photon statistical properties of light emitting quantum dot superluminescent diodes (QDSLDs). At about $T = 190$ K the field-correlation $g^{(1)}(\tau)$ remained highly incoherent with a spectral width of several THz, whereas the second-order correlation $g^{(2)}(\tau)$ reduced from 2 to 1.33. Thus, so-called hybrid coherent light is simultaneously incoherent in first- and coherent in second-order correlation function.

To find an explanation of the occurrence of these novel states of light, we studied the amplified spontaneous emission of the QDSLD [122]. We postulated a quantum state, a multimode phase-randomized Gaussian (PRAG) state, which corresponds to a superposition of Gaussian states with shifted complex amplitudes and randomized phases. This multimode quantum state reflected the incoherent character of the broadband semiconductor device and revealed correct intensity correlations. We determined temporal correlations analytically in terms of first- and second-order, $g^{(1)}(\tau)$ and $g^{(2)}(\tau)$. A comparison with a feedback [121] and a mixed light experiment, conducted by the Semiconductor Optics group of W. Elsäßer at TU Darmstadt highlighted an overall good match. As a main result, we found that the second-order correlation depends on the number of modes of the multimode amplified spontaneous emission field. Furthermore, mixing light from a QDSLD with light emitted by a single-mode laser revealed tunable photon statistics ranging from Poissonian to Gaussian distributions.

In the second part of the thesis, a microscopic theory of the amplified spontaneous emission of broadband QDLSDs was formulated. This model of the diode considered the gain medium to be composed of many distinguishable quantum dots, each one described by a three-level system. They are embedded in a strong absorptive bulk material, which defines a waveguide. In this context, the dissipative dynamics as well as gain and absorption of a single quantum dot at room temperature was analyzed. The waveguide itself was represented by a cavity. The waveguide's output facets of typical QDSLDs are tilted and anti-reflection coated to guarantee the suppression of longitudinal modes. This special geometry of the device was modeled by beam splitters enclosing the active medium, which couples the internal field to the environment at the same time. This three-component model of beam splitter - cavity - beam splitter was treated as a cascaded system [139] in which the input of one system is simultaneously the output of the other one. The broadband radiation inside the waveguide itself was described by a multimode quantized electric field. We established quantum stochastic differential equations for the field amplitudes and quantum dot operators as well as rate equations for the spectral densities and quantum dot populations. We studied in detail the amplified spontaneous emission of a single-mode as well as a multimode QDSLD in terms of the external pumping rate and frequency for the special case of identical quantum dots. We applied the input-output formalism [144] under consideration of boundary conditions to specify the output radiation field and the optical power spectrum recorded by a single-photon detector. We found that this spectral density is a convolution of the internal stationary photon number with a Lorentzian. A comparison with experimental data highlighted good agreement. Therefore, our microscopic theory allows to reproduce measured

QDSLD spectra. Also knowing the experimental data, we can specify relevant parameters which are in general unavailable for these broadband semiconductor devices.

Based on our quantum theory of the QDSLD, we calculated the central second-order degree of coherence $g^{(2)}(0)$. We found an explicit expression of this measure, which depends on the internal spectra and the stationary quantum dot populations. Also in this context, we studied the limiting case of a single-mode QDSLD with identical quantum dots. For a special set of parameters we observed a reduction of $g^{(2)}(0)$ from 2 to 1.33 when the detuning has been varied. Notice that changing the detuning is equivalent to changing the temperature [172]. This quantitative agreement with experimental observations allowed an interpretation of the hybrid coherent light phenomenon from a theoretical perspective. The occurrence of these novel states of light can be traced back to a saturation effect resulting in noise suppression. Therefore, by the help of our microscopic theory, we found an explanation for the observation of hybrid coherent light of broadband emitting QDSLDs.

The presented microscopic description of the amplified spontaneous emission of QDSLDs is based on pure quantum optical considerations. The semiconductor properties of the device were disregarded within our theory. Considering these characteristics makes our theory more realistic. Additionally, it could provide a precise connection between the detuning and the temperature. Knowing this fundamental relation of these physical quantities allows to predict theoretically the critical temperature at which hybrid coherent light is observable for an arbitrary QDSLD.

Up to now, we only observed a reduction of the second-order degree of coherence for the special case of a single-mode QDSLD composed of identical QDs. For the multimode QDSLD emission we expect the same behavior. However, $g^{(2)}(0)$ and of course $g^{(2)}(\tau)$ as a function of detuning for a broadband, multimode QDSLD described by our quantum theory has not been studied yet. Naturally, this more realistic case should be necessarily analyzed in the context of hybrid coherent light.

Our general quantum optical ansatz, which reflects a reduction of the $g^{(2)}(0)$-value in terms of temperature is extensible or even directly applicable to further commercial devices. It is even conceivable, that such a noise suppression is also observable in multimode gas lasers operated in the regime of the amplified spontaneous emission. This would encourage our hypothesis of hybrid coherent light as a purely optical phenomenon and provides new insights into the quantum nature of light emitting semiconductor devices.

Clearly, higher-order correlations are theoretically available and could be studied in detail within the context of our quantum theory.

Especially for ghost imaging in which broadband, highly incoherent light sources are essential, QDSLDs are a good choice [105]. In this context, beside the investigation of the temporal properties of QDSLDs, the spatial correlations are also of interest which are predictable with our quantum theory of light emitting QDSLDs.

A

WICK THEOREM FOR BOSONIC GAUSSIAN STATES

The estimation of equal-time higher-order moments can become quite challenging. However, for Gaussian states, there exists a useful mathematical rule which allows to overcome a direct evaluation of these expectation values, known as *generalized Wick theorem* [175]. It states that multiple operator averages factorize into a sum of (two-point) pairwise averages, which in turn are more easy to handle. In particular, with regard to this thesis, we restrict our study to bosonic operators.

Consider a set of operators $\hat{X}_1, \hat{X}_2, ..., \hat{X}_{2n}$ corresponding to either bosonic annihilation, $\hat{a}_i$, or creation operators, $\hat{a}_i^\dagger$, of a set of harmonic oscillators with Hamilton operator

$$\hat{H} = \sum_i \hbar\omega_i \hat{a}_i^\dagger \hat{a}_i\,. \tag{A.1}$$

In thermal equilibrium the density operator of the system is given by

$$\hat{\rho}_t = \frac{e^{-\beta\hat{H}}}{Z}, \tag{A.2}$$

with partition function $Z = \mathrm{Tr}\{\exp(-\beta\hat{H})\}$ and $\beta = 1/(k_\mathrm{B}T)$. The generalized Wick theorem for equal-time multi-operator Gaussian averages with characteristic properties,

$$\langle\hat{a}_i\rangle = \langle\hat{a}_i^\dagger\rangle = \langle\hat{a}_i\hat{a}_j\rangle = \langle\hat{a}_i^\dagger\hat{a}_j^\dagger\rangle = 0, \tag{A.3}$$

$$\langle\hat{a}_i^\dagger\hat{a}_j\rangle = n_i\delta_{ij}, \quad \langle\hat{a}_i\hat{a}_j^\dagger\rangle = (1+n_i)\delta_{ij}, \tag{A.4}$$

reads [176]

$$\langle\hat{X}_1\hat{X}_2...\hat{X}_{2n}\rangle = \langle\hat{X}_1\hat{X}_2\rangle\langle\hat{X}_3\hat{X}_4...\hat{X}_{2n}\rangle + \langle\hat{X}_1\hat{X}_3\rangle\langle\hat{X}_2\hat{X}_4...\hat{X}_{2n}\rangle + ... + \langle\hat{X}_1\hat{X}_{2n}\rangle\langle\hat{X}_2\hat{X}_3...\hat{X}_{2n-1}\rangle. \tag{A.5}$$

B

TEMPORAL CORRELATIONS OF PRAG & MIXED LIGHT STATES

In this appendix we represent detailed calculations of first-, second- and fourth-order moments, first- and second-order temporal autocorrelation functions and the optical power spectrum of the multimode phase-randomized Gaussian (PRAG) state. Finally, we study temporal first- and second-order correlations of the mixed light state, introduced in chapter 4.

B.1 PRAG STATES

B.1.1 First- and second-order moments

A multimode PRAG state is defined by the integral (cf. equation (4.6))

$$\hat{\rho}_s = \frac{1}{(2\pi)^N}\int_0^{2\pi} \mathrm{d}\phi^N \hat{D}(\gamma)\hat{\rho}_t\hat{D}^\dagger(\gamma), \quad \hat{D}(\gamma) = e^{\sum_{i=1}^N(\gamma_i\hat{a}_i^\dagger - \gamma_i^*\hat{a}_i)}, \quad \gamma_i = |\gamma_i|e^{\mathrm{i}\phi_i}. \tag{B.1}$$

Here, $\hat{D}(\gamma)$ is the multimode displacement operator acting on the thermal state,

$$\hat{\rho}_t = \frac{e^{-\beta\hat{H}}}{\mathrm{Tr}\{e^{-\beta\hat{H}}\}}, \quad \hat{H} = \sum_{i=1}^N \hbar\omega_i\hat{a}_i^\dagger\hat{a}_i\,. \tag{B.2}$$

Applying the harmonic oscillator algebra [124],

$$\hat{D}^\dagger(\gamma)\hat{a}_j\hat{D}(\gamma) = \hat{a}_j + \gamma_j, \tag{B.3}$$

the quantum mechanical average of the operator $\hat{a}_i$ is given by

$$\begin{aligned}\langle\hat{a}_i\rangle = \mathrm{Tr}\{\hat{a}_i\hat{\rho}_s\} &= \int_0^{2\pi}\frac{\mathrm{d}\phi^N}{(2\pi)^N}\mathrm{Tr}\{\hat{a}_i\hat{D}(\gamma)\hat{\rho}_t\hat{D}^\dagger(\gamma)\} = \int_0^{2\pi}\frac{\mathrm{d}\phi^N}{(2\pi)^N}\mathrm{Tr}\{\hat{D}^\dagger(\gamma)\hat{a}_i\hat{D}(\gamma)\hat{\rho}_t\}\\ &= \int_0^{2\pi}\frac{\mathrm{d}\phi^N}{(2\pi)^N}\mathrm{Tr}\{(\hat{a}_i+\gamma_i)\hat{\rho}_t\} = \langle\hat{a}_i\rangle_t + \frac{|\gamma_i|}{(2\pi)^N}\int_0^{2\pi}\mathrm{d}\phi^N e^{\mathrm{i}\phi_i} = 0.\end{aligned} \tag{B.4}$$

Here, we utilized the cyclical permutability of the operators within the trace and a vanishing first-order moment of the thermal state

$$\langle\hat{a}_i\rangle_t = 0 \tag{B.5}$$

with new notation $\langle...\rangle_t = \mathrm{Tr}\{...\hat{\rho}_t\}$.

In the same way, we can calculate the second moment under consideration of the unitarity of the displacement operator

$$\begin{aligned}\langle\hat{a}_i^\dagger\hat{a}_j\rangle = \mathrm{Tr}\{\hat{a}_i^\dagger\hat{a}_j\hat{\rho}_s\} &= \int_0^{2\pi}\frac{\mathrm{d}\phi^N}{(2\pi)^N}\mathrm{Tr}\{\hat{a}_i^\dagger\hat{a}_j\hat{D}(\gamma)\hat{\rho}_t\hat{D}^\dagger(\gamma)\}\\ &= \int_0^{2\pi}\frac{\mathrm{d}\phi^N}{(2\pi)^N}\mathrm{Tr}\{\hat{D}^\dagger(\gamma)\hat{a}_i^\dagger\hat{D}(\gamma)\hat{D}^\dagger(\gamma)\hat{a}_j\hat{D}(\gamma)\hat{\rho}_t\}.\end{aligned} \tag{B.6}$$

Again, we use the harmonic oscillator algebra in equation (B.3) and consider a zero first moment of a thermal state. Additionally, we have to keep in mind that the second-order moment of a thermal state defines a mean thermal occupation number with $\langle \hat{a}_i^\dagger \hat{a}_j \rangle_t = n_T(\omega_i)\delta_{ij}$.
Thus, we find that the second moment of the PRAG state,

$$\begin{aligned}\langle \hat{a}_i^\dagger \hat{a}_j \rangle &= \int_0^{2\pi} \frac{\mathrm{d}\phi^N}{(2\pi)^N} \mathrm{Tr}\{(\hat{a}_i^\dagger + \gamma_i^*)(\hat{a}_j + \gamma_j)\hat{\rho}_t\} \\ &= \int_0^{2\pi} \frac{\mathrm{d}\phi^N}{(2\pi)^N} (\langle \hat{a}_i^\dagger \hat{a}_j \rangle_t + \gamma_j \langle \hat{a}_i^\dagger \rangle_t + \gamma_i^* \langle \hat{a}_j \rangle_t + \gamma_i^* \gamma_j) \\ &\overset{(B.5)}{=} \int_0^{2\pi} \frac{\mathrm{d}\phi^N}{(2\pi)^N} (n_T(\omega_i)\delta_{ij} + |\gamma_i||\gamma_j| e^{\mathrm{i}(\phi_j - \phi_i)}) \\ &= n_S(\omega_i)\delta_{ij} \quad \text{with} \quad n_S(\omega_i) = n_T(\omega_i) + n_C(\omega_i),\end{aligned} \tag{B.7}$$

corresponds to the sum of the occupation number $n_T(\omega_i)$ and the distribution $n_C(\omega_i) = |\gamma_i|^2$ of mode i.

B.1.2 First-order correlation and power spectrum

The first-order temporal autocorrelation function with time delay τ is given by the electric field average

$$\begin{aligned}G^{(1)}(\tau) &= \int \mathrm{d}x\mathrm{d}y \langle \hat{E}^{(-)}(\mathbf{r},t)\hat{E}^{(+)}(\mathbf{r},t+\tau)\rangle = \int \mathrm{d}x\mathrm{d}y \sum_{i,j=1}^{N} u_i^*(\mathbf{r})u_j(\mathbf{r})\langle \hat{a}_i^\dagger(t)\hat{a}_j(t+\tau)\rangle \\ &= \sum_{i,j=1}^{N} \frac{\hbar\sqrt{\omega_i\omega_j}}{2\varepsilon_0 L} e^{\mathrm{i}(k_j-k_i)z} e^{-\mathrm{i}(\omega_j-\omega_i)t} e^{-\mathrm{i}\omega_j\tau} \langle \hat{a}_i^\dagger \hat{a}_j \rangle.\end{aligned} \tag{B.8}$$

In the last step we considered the definition of the mode function (4.2) as well as the normalization condition (4.4). Under consideration of the solution of the second moment derived in the previous section (cf. equation (B.7)), we get

$$G^{(1)}(\tau) = \sum_{i=1}^{N} \frac{\hbar\omega_i}{2\varepsilon_0 L} e^{-\mathrm{i}\omega_i\tau} n_S(\omega_i) = \frac{1}{\mathscr{C}} \sum_{i=1}^{N} p_i^s e^{-\mathrm{i}\omega_i\tau}, \qquad p_i^s = p_i^c + p_i^t, \tag{B.9}$$

with $\mathscr{C}$ and optical power p_i^c, p_i^t defined in (2.59) and (4.14), respectively.

The spatially averaged temporal first-order degree of coherence is approximately given by the ratio of the first-order temporal correlation and the equal-space-time first-order correlation

$$g^{(1)}(\tau) \simeq \frac{G^{(1)}(\tau)}{G^{(1)}(0)} = \frac{1}{P}\sum_{i=1}^{N} p_i^s e^{-\mathrm{i}\omega_i\tau}, \qquad P = \sum_i p_i^s = \sum_i p_i^c + p_i^t, \tag{B.10}$$

with total optical power P.

The power spectrum can be easily calculated by Fourier transforming the first-order temporal autocorrelation function (B.8) according to

$$S(\omega) = \frac{\mathscr{C}}{2\pi} \mathrm{Re} \int_{-\infty}^{\infty} \mathrm{d}\tau e^{\mathrm{i}\omega\tau} G^{(1)}(\tau) = \sum_{i=1}^{N} \frac{1}{2\pi} \int_{-\infty}^{\infty} \mathrm{d}\tau\, e^{\mathrm{i}(\omega-\omega_i)\tau} p_i^s = \sum_{i=1}^{N} p_i^s \delta(\omega - \omega_i). \tag{B.11}$$

In the last step we utilized the integral representation of the delta function

$$\delta(\omega) = \frac{1}{2\pi} \int_{-\infty}^{\infty} \mathrm{d}t\, e^{\mathrm{i}\omega t}. \tag{B.12}$$

With the help of the Euler-Maclaurin formula (see appendix C), we can approximate the sum over all modes of the discrete spectrum by an integral,

$$S(\omega) = \sum_{i=1}^{N} p_i^s \delta(\omega - \omega_i) \simeq \frac{1}{\Delta\omega} \int_{\omega_1}^{\omega_N} \mathrm{d}\tilde{\omega}\, p^s(\tilde{\omega}) \delta(\omega - \tilde{\omega}), \quad p^s(\omega) = p^c(\omega) + p^t(\omega). \tag{B.13}$$

Here,

$$\Delta\omega = \frac{\omega_N - \omega_1}{N - 1} \tag{B.14}$$

describes the equal frequency separation between adjacent modes. An expansion of the lower and upper integration limits $[\omega_1, \omega_N]$ to $(-\infty, \infty)$ yields the optical power spectrum of light described by a multimode PRAG state,

$$S(\omega) \simeq \frac{1}{\Delta\omega} \int_{-\infty}^{\infty} \mathrm{d}\tilde{\omega}\; p^s(\tilde{\omega}) \delta(\omega - \tilde{\omega}) = \frac{p^s(\omega)}{\Delta\omega} = \frac{1}{\Delta\omega}(p^c(\omega) + p^t(\omega)), \tag{B.15}$$

which depends only on the contribution of the optical power $p^c(\omega) \propto n_C(\omega)$ and $p^t(\omega) \propto n_T(\omega)$.

B.1.3 Second-order correlation

The temporal second-order correlation function,

$$\begin{aligned} G^{(2)}(\tau) &= \int\!\!\int \mathrm{d}x\,\mathrm{d}y\, \langle \hat{E}^{(-)}(\mathbf{r},t) \hat{E}^{(-)}(\mathbf{r},t+\tau) \hat{E}^{(+)}(\mathbf{r},t+\tau) \hat{E}^{(+)}(\mathbf{r},t) \rangle \\ &= \sum_{ijlm=1}^{N} \frac{\hbar^2 \sqrt{\omega_i \omega_j \omega_l \omega_m}}{4\varepsilon_0^2 L^2} e^{\mathrm{i}(k_l + k_m - k_i - k_j)z} e^{-\mathrm{i}(\omega_l + \omega_m - \omega_i - \omega_j)t} e^{-\mathrm{i}(\omega_l - \omega_j)\tau} \langle \hat{a}_i^\dagger \hat{a}_j^\dagger \hat{a}_l \hat{a}_m \rangle, \end{aligned} \tag{B.16}$$

is proportional to the fourth-order moment $\langle \hat{a}_i^\dagger \hat{a}_j^\dagger \hat{a}_l \hat{a}_m \rangle$. In analogy to the previous subsection, we utilize the permutation rule of the trace as well as the properties of the harmonic oscillator Lie algebra (B.3). We find that the average is given by

$$\begin{aligned} \langle \hat{a}_i^\dagger \hat{a}_j^\dagger \hat{a}_l \hat{a}_m \rangle = \mathrm{Tr}\{\hat{a}_i^\dagger \hat{a}_j^\dagger \hat{a}_l \hat{a}_m \hat{\rho}_s\} &= \int_0^{2\pi} \frac{\mathrm{d}\phi^N}{(2\pi)^N} \mathrm{Tr}\{\hat{a}_i^\dagger \hat{a}_j^\dagger \hat{a}_l \hat{a}_m \hat{D}(\gamma) \hat{\rho}_t \hat{D}^\dagger(\gamma)\} \\ &= \int_0^{2\pi} \frac{\mathrm{d}\phi^N}{(2\pi)^N} \mathrm{Tr}\{\hat{D}^\dagger(\gamma) \hat{a}_i^\dagger \hat{D}(\gamma) \hat{D}^\dagger(\gamma) \hat{a}_j^\dagger \hat{D}(\gamma) \hat{D}^\dagger(\gamma) \hat{a}_l \hat{D}(\gamma) \hat{D}^\dagger(\gamma) \hat{a}_m \hat{D}(\gamma) \hat{\rho}_t\} \\ &= \int_0^{2\pi} \frac{\mathrm{d}\phi^N}{(2\pi)^N} \mathrm{Tr}\{(\hat{a}_i^\dagger + \gamma_i^*)(\hat{a}_j^\dagger + \gamma_j^*)(\hat{a}_l + \gamma_l)(\hat{a}_m + \gamma_m) \hat{\rho}_t\} \\ &\overset{(B.5)}{=} \int_0^{2\pi} \frac{\mathrm{d}\phi^N}{(2\pi)^N} (\langle \hat{a}_i^\dagger \hat{a}_j^\dagger \hat{a}_l \hat{a}_m \rangle_t + \gamma_l \gamma_m \langle \hat{a}_i^\dagger \hat{a}_j^\dagger \rangle_t + \gamma_i^* \gamma_j^* \langle \hat{a}_l \hat{a}_m \rangle_t + \gamma_j^* \gamma_m \langle \hat{a}_i^\dagger \hat{a}_l \rangle_t \\ &\qquad + \gamma_j^* \gamma_l \langle \hat{a}_i^\dagger \hat{a}_m \rangle_t + \gamma_i^* \gamma_m \langle \hat{a}_j^\dagger \hat{a}_l \rangle_t + \gamma_i^* \gamma_l \langle \hat{a}_j^\dagger \hat{a}_m \rangle_t + \gamma_i^* \gamma_j^* \gamma_l \gamma_m). \end{aligned} \tag{B.17}$$

In the last step, we utilized vanishing expectation values for an odd amount of operators, which is a consequence of the generalized Wick theorem (see appendix A). Additionally, we apply this theorem to the fourth-order average of the field operators which results into a sum of products of second-order moments according to

$$\langle \hat{a}_i^\dagger \hat{a}_j^\dagger \hat{a}_l \hat{a}_m \rangle_t = \langle \hat{a}_i^\dagger \hat{a}_j^\dagger \rangle_t \langle \hat{a}_l \hat{a}_m \rangle_t + \langle \hat{a}_i^\dagger \hat{a}_l \rangle_t \langle \hat{a}_j^\dagger \hat{a}_m \rangle_t + \langle \hat{a}_i^\dagger \hat{a}_m \rangle_t \langle \hat{a}_j^\dagger \hat{a}_l \rangle_t. \tag{B.18}$$

Using the thermal characteristics of a second-order moment $\langle \hat{a}_i \hat{a}_j \rangle_t = \langle \hat{a}_i^\dagger \hat{a}_j^\dagger \rangle_t = 0$ as well as $\langle \hat{a}_i^\dagger \hat{a}_j \rangle_t = n_T(\omega_i)\delta_{ij}$ we end up in a simple expression for the PRAG state fourth-order moment,

$$\begin{aligned}\langle \hat{a}_i^\dagger \hat{a}_j^\dagger \hat{a}_l \hat{a}_m \rangle =& n_T(\omega_i) n_T(\omega_j)(\delta_{il}\delta_{jm} + \delta_{im}\delta_{jl}) + n_T(\omega_i)\delta_{il} \int \frac{\mathrm{d}\phi^N}{(2\pi)^N} |\gamma_j||\gamma_m| e^{\mathrm{i}(\phi_m - \phi_j)} \\ & + n_T(\omega_i)\delta_{im} \int \frac{\mathrm{d}\phi^N}{(2\pi)^N} |\gamma_j||\gamma_l| e^{\mathrm{i}(\phi_l - \phi_j)} \\ & + n_T(\omega_j)\delta_{jl} \int \frac{\mathrm{d}\phi^N}{(2\pi)^N} |\gamma_i||\gamma_m| e^{\mathrm{i}(\phi_m - \phi_i)} \\ & + n_T(\omega_j)\delta_{jm} \int \frac{\mathrm{d}\phi^N}{(2\pi)^N} |\gamma_i||\gamma_l| e^{\mathrm{i}(\phi_l - \phi_i)} \\ & + \int \frac{\mathrm{d}\phi^N}{(2\pi)^N} |\gamma_i||\gamma_j||\gamma_l||\gamma_m| e^{\mathrm{i}(\phi_l + \phi_m - \phi_i - \phi_j)}.\end{aligned} \tag{B.19}$$

Inserting this solution into the second-order temporal correlation function (B.16) results in

$$\begin{aligned}G^{(2)}(\tau) =& \sum_{ij=1}^{N} \frac{\hbar^2 \omega_i \omega_j}{4\varepsilon_0^2 L^2} \Big[\big(n_T(\omega_i) n_T(\omega_j) + n_T(\omega_i)|\gamma_j|^2 + n_T(\omega_j)|\gamma_i|^2 + |\gamma_i|^2 |\gamma_j|^2 \big) \\ & \cdot \big(1 + e^{-\mathrm{i}(\omega_i - \omega_j)\tau}\big) - |\gamma_i|^4 \delta_{ij} \Big] \\ =& \Big| \sum_{i=1}^{N} \frac{\hbar\omega_i}{2\varepsilon_0 L} n_S(\omega_i) \Big|^2 + \Big| \sum_{i=1}^{N} \frac{\hbar\omega_i}{2\varepsilon_0 L} n_S(\omega_i) e^{-\mathrm{i}\omega_i \tau} \Big|^2 - \sum_{i=1}^{N} \Big(\frac{\hbar\omega_i}{2\varepsilon_0 L} n_C(\omega_i) \Big)^2.\end{aligned} \tag{B.20}$$

Finally, the normalized second-order temporal correlation function reads

$$\begin{aligned}g^{(2)}(\tau) \simeq& \frac{G^{(2)}(\tau)}{G^{(2)}(0)} \\ =& \frac{\Big| \sum_{i=1}^{N} \frac{\hbar\omega_i}{2\varepsilon_0 L} n_S(\omega_i) \Big|^2 + \Big| \sum_{i=1}^{N} \frac{\hbar\omega_i}{2\varepsilon_0 L} n_S(\omega_i) e^{-\mathrm{i}\omega_i \tau} \Big|^2 - \sum_{i=1}^{N} \Big(\frac{\hbar\omega_i}{2\varepsilon_0 L} n_C(\omega_i) \Big)^2}{\Big| \sum_{i=1}^{N} \frac{\hbar\omega_i}{2\varepsilon_0 L} n_S(\omega_i) \Big|^2} \\ =& 1 + \frac{\Big| \sum_{i=1}^{N} p_i^s e^{-\mathrm{i}\omega_i \tau} \Big|^2}{P^2} - \frac{\sum_{i=1}^{N} p_i^{c2}}{P^2} = 1 + |g^{(1)}(\tau)|^2 - \frac{\sum_{i=1}^{N} p_i^{c2}}{P^2}.\end{aligned} \tag{B.21}$$

B.2 MIXED LIGHT STATES

Consider a superposition of light emitted by an incoherent radiation with density operator (4.6) and a laser, described by a coherent state with displacement operator $\hat{D}(\alpha)$ obeying the harmonic oscillator algebra

$$\hat{D}^{\dagger}(\alpha)\hat{a}_j\hat{D}(\alpha) = \hat{a}_j + \alpha_j. \tag{B.22}$$

Clearly, from (B.3) and (B.22) it follows the harmonic algebra of this mixed light

$$\begin{aligned}\hat{D}^{\dagger}(\gamma+\alpha)\hat{a}_j\hat{D}(\gamma+\alpha) &= \hat{a}_j + \alpha_j + \gamma_j = \hat{D}^{\dagger}(\alpha)\hat{a}_j\hat{D}(\alpha) + \gamma_j \\ &= \hat{D}^{\dagger}(\gamma)\hat{D}^{\dagger}(\alpha)\hat{a}_j\hat{D}(\alpha)\hat{D}(\gamma).\end{aligned} \tag{B.23}$$

Therefore, the mixed light density operator considered in section 4.5 is determined by a product of displacement operators according to

$$\hat{\rho}_m = \frac{1}{(2\pi)^N}\int_0^{2\pi} \mathrm{d}\phi^N \hat{D}(\alpha)\hat{D}(\gamma)\hat{\rho}_t\hat{D}^{\dagger}(\gamma)\hat{D}^{\dagger}(\alpha) = \hat{D}(\alpha)\hat{\rho}_s\hat{D}^{\dagger}(\alpha). \tag{B.24}$$

B.2.1 First-order correlation and power spectrum

Some experimentally available measures like intensities or first-order correlations are related to the first-order moment

$$\begin{aligned}\langle\hat{a}_i^{\dagger}\hat{a}_j\rangle &= \mathrm{Tr}\{\hat{a}_i^{\dagger}\hat{a}_j\hat{\rho}_m\} = \frac{1}{(2\pi)^N}\int_0^{2\pi}\mathrm{d}\phi^N\ \mathrm{Tr}\{\hat{a}_i^{\dagger}\hat{a}_j\hat{D}(\alpha_k)\hat{D}(\gamma)\hat{\rho}_t\hat{D}^{\dagger}(\gamma)\hat{D}^{\dagger}(\alpha_k)\} \\ &= \int_0^{2\pi}\frac{\mathrm{d}\phi^N}{(2\pi)^N}\ \mathrm{Tr}\{\hat{D}^{\dagger}(\gamma)\hat{D}^{\dagger}(\alpha_k)\hat{a}_i^{\dagger}\hat{D}(\alpha_k)\hat{D}(\gamma)\hat{D}^{\dagger}(\gamma)\hat{D}^{\dagger}(\alpha_k)\hat{a}_j\hat{D}(\alpha_k)\hat{D}(\gamma)\hat{\rho}_t\} \\ &\overset{(B.23)}{=} \int_0^{2\pi}\frac{\mathrm{d}\phi^N}{(2\pi)^N}\ \mathrm{Tr}\{(\hat{a}_i^{*} + \gamma_i^{*} + \alpha_i^{*}\delta_{ik})(\hat{a}_j + \gamma_j + \alpha_j\delta_{jk})\hat{\rho}_t\} \\ &\overset{(B.5)}{=} \int_0^{2\pi}\frac{\mathrm{d}\phi^N}{(2\pi)^N}\ (\langle\hat{a}_i\hat{a}_j\rangle_t + \gamma_i^{*}\gamma_j + \gamma_i^{*}\alpha_j\delta_{jk} + \alpha_i^{*}\gamma_j\delta_{ik} + |\alpha_i|^2\delta_{ik}\delta_{jk}) \\ &= n_S(\omega_i)\delta_{ij} + |\alpha_i|^2\delta_{ik}\delta_{jk}.\end{aligned} \tag{B.25}$$

Obviously, this ensemble average is given by the sum of a thermal, incoherent and coherent contribution, $n_T(\omega)$, $n_C(\omega)$, and $|\alpha|^2$. Thus, the first-order autocorrelation function of the mixed-light state is determined by

$$\begin{aligned}G^{(1)}(\tau) &= \sum_{i=1}^{N}\frac{\hbar\omega_i}{2\varepsilon_0 L}(n_S(\omega_i)\delta_{ij} + |\alpha_i|^2\delta_{ik}\delta_{jk})e^{-\mathrm{i}\omega_i\tau} \\ &= \frac{1}{\mathscr{C}}\sum_{i=1}^{N}p_i^m e^{-\mathrm{i}\omega_i\tau}, \quad p_i^m = p_i^t + p_i^c + p_i^l = p_i^s + p_i^l\end{aligned} \tag{B.26}$$

with laser power p_i^l defined in (4.33). The temporal first-order degree of coherence in terms of the total optical power P^m (see equation (4.32)) reads

$$g^{(1)}(\tau) \simeq \frac{G^{(1)}(\tau)}{G^{(1)}(0)} = \frac{\mathscr{C}}{P^m}G^{(1)}(\tau) = \frac{1}{P^m}\sum_{i=1}^{N}p_i^m e^{-\mathrm{i}\omega_i\tau}. \tag{B.27}$$

The optical power spectrum of the mixed light is specified by the Fourier transform of the first-order correlation (B.26),

$$\begin{aligned} S(\omega) &= \frac{\mathscr{C}}{2\pi}\int_{-\infty}^{\infty} \mathrm{d}\tau\, e^{\mathrm{i}\omega\tau} G^{(1)}(\tau) = \sum_{i=1}^{N} p_i^m \frac{1}{2\pi}\int_{-\infty}^{\infty} \mathrm{d}\tau\, e^{\mathrm{i}(\omega-\omega_i)\tau} = \sum_{i=1}^{N} p_i^m \delta(\omega-\omega_i) \\ &= P^l \delta(\omega-\omega_k) + \sum_{i=1}^{N} p_i^s \delta(\omega-\omega_i). \end{aligned} \tag{B.28}$$

Here, P^l is the total laser power defined in (4.33). In analogy to section B.1.2 we determine the continuous power spectrum by replacing the sum in (B.28) by an integral,

$$S(\omega) = P^l \delta(\omega-\omega_k) + \frac{p^s(\omega)}{\Delta\omega}, \tag{B.29}$$

with equally spaced integration intervals $\Delta\omega$.

B.2.2 *Second-order correlation*

The second-order moment of the mixed light state described by equation (B.24) can be determined in the same way as in case of the first-order moment. We find

$$\begin{aligned} \langle \hat{a}_i^\dagger \hat{a}_j^\dagger \hat{a}_l \hat{a}_m \rangle =& n_T(\omega_i) n_T(\omega_j)(\delta_{il}\delta_{jm} + \delta_{im}\delta_{jl}) + n_C(\omega_j) n_T(\omega_i)(\delta_{jm}\delta_{il} + \delta_{jl}\delta_{im}) \\ &+ n_C(\omega_i) n_T(\omega_j)(\delta_{im}\delta_{jl} + \delta_{il}\delta_{jm}) + |\alpha_k|^2 n_T(\omega_i)(\delta_{jk}\delta_{lk}\delta_{im} + \delta_{il}\delta_{jk}\delta_{mk}) \\ &+ |\alpha_k|^2 n_T(\omega_j)(\delta_{ik}\delta_{mk}\delta_{jl} + \delta_{ik}\delta_{lk}\delta_{jm}) + |\alpha_k|^2 n_C(\omega_j)(\delta_{ik}\delta_{lk}\delta_{jm} + \delta_{ik}\delta_{mk}\delta_{jl}) \\ &+ |\alpha_k|^2 n_C(\omega_i)(\delta_{jk}\delta_{mk}\delta_{il} + \delta_{jk}\delta_{lk}\delta_{im}) + |\alpha_k|^4 \delta_{ik}\delta_{jk}\delta_{lk}\delta_{mk} \\ &+ \int_0^{2\pi} \frac{\mathrm{d}\phi^N}{(2\pi)^N} |\gamma_i||\gamma_j||\gamma_l||\gamma_m| e^{\mathrm{i}(\phi_l+\phi_m-\phi_i-\phi_j)}. \end{aligned} \tag{B.30}$$

As a result, the temporal second-order degree of coherence is determined by

$$\begin{aligned} G^{(2)}(\tau) = |G^{(1)}(0)|^2 + \frac{\hbar}{2\varepsilon_0 L}\Big[& |\sum_{i=1}^{N} \omega_i n_T(\omega_i) e^{-\mathrm{i}\omega_i\tau}|^2 + |\sum_{i=1}^{N} \omega_i n_C(\omega_i) e^{-\mathrm{i}\omega_i\tau}|^2 \\ & + 2\sum_{i,j=1}^{N} \omega_i\omega_j n_C(\omega_j) n_T(\omega_i) \cos(\Delta_{ij}\tau) \\ & + 2\omega_k|\alpha_k|^2 \sum_{i=1}^{N} \omega_i n_S(\omega_i) \cos(\Delta_{ik}\tau) \\ & - \sum_{i=1}^{N} (\omega_i n_C(\omega_i))^2 \Big]. \end{aligned} \tag{B.31}$$

Finally, we end up in a simple expression for the temporal second-order degree of coherence in terms of the optical powers of the thermal and incoherent contributions as well as the optical power of the laser,

$$g^{(2)}(\tau) \simeq \frac{G^{(2)}(\tau)}{|G^{(1)}(0)|^2} = 1 + |g^{(1)}(\tau)|^2 - \frac{P^{l2} + \sum_{i=1}^{N} p_i^{c2}}{P^{m2}}, \tag{B.32}$$

with

$$\begin{aligned} |g^{(1)}(\tau)|^2 = \frac{1}{P^{m2}}\Big[& P^{l2} + |\sum_{i=1}^{N} p_i^c e^{-i\omega_i\tau}|^2 + |\sum_{i=1}^{N} p_i^t e^{-i\omega_i\tau}|^2 \\ & + 2\sum_{i,j=1}^{N} p_j^c p_i^t \cos(\Delta_{ij}\tau) + 2P^l \sum_{i=1}^{N} p_i^s \cos(\Delta_{ik}\tau) \Big]. \end{aligned} \tag{B.33}$$

C

EULER-MACLAURIN SERIES

The Euler-Maclaurin formula approaches an arbitrary sum by its integral plus higher-order corrections according to

$$\begin{aligned}\sum_{i=1}^{N} f(a+(i-1)\Delta) =& \frac{1}{\Delta}\int_a^b \mathrm{d}t\, f(t) + \frac{f(a)+f(b)}{2} \\ &+ \sum_{m=1}^{M-1} \frac{\Delta^{2m-1} B_{2m}}{(2m)!}\left(f^{(2m-1)}(b) - f^{(2m-1)}(a)\right) + R_M.\end{aligned} \tag{C.1}$$

In case of negligible residual R_M, we find a series approximation of the order of M in terms of Bernoulli numbers B_k as well as higher derivatives $f^{(k)}$. Here, $\Delta \equiv (b-a)/(N-1)$ corresponds to the width of $N-1$ equal spaced integration intervals [177, 178].

D

DAMPING IN THE SCHRÖDINGER PICTURE

This appendix deals with the derivation of an equation of motion for the reduced system's density operator known as master equation, an important tool for describing dissipative quantum systems [32, 41, 42, 155, 179].

Figure 4.1 sketches the physical problem under study. The analysis of this problem, namely the mathematical description of the interaction of a single driven quantum dot (small system) with the large enclosing semiconductor medium (large reservoir), is the aim of this section.

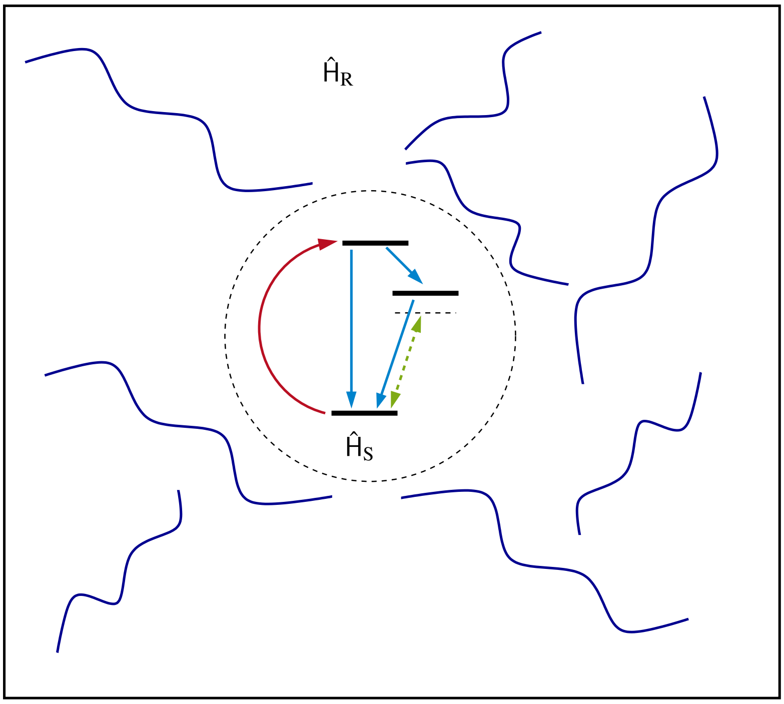

Figure 4.1: Sketch of the small quantum dot system $\hat{\mathsf{H}}_\mathrm{S}$ coupling to a reservoir $\hat{\mathsf{H}}_\mathrm{R}$.

The equation of motion in the Schrödinger picture, which characterizes the temporal dynamics of the system, is the fundamental Liouville-von-Neumann equation,

$$i\hbar \frac{\mathrm{d}}{\mathrm{d}t}\hat{\rho}(t) = \left[\hat{\mathsf{H}}, \hat{\rho}(t)\right]. \tag{D.1}$$

It corresponds to an equation of motion for the density operator $\hat{\rho}$. For simplicity, we consider the Hamiltonian of the total, dissipative system in dipole and rotating wave approximation

$$\hat{\mathsf{H}} = \hat{\mathsf{H}}_\mathrm{S} + \hat{\mathsf{H}}_\mathrm{R} + \hat{\mathsf{H}}_\mathrm{I}. \tag{D.2}$$

Here, the first term on the right hand side is the system Hamilton operator $\hat{\mathsf{H}}_\mathrm{S}$. We will see that the exact knowledge of the expression for $\hat{\mathsf{H}}_\mathrm{S}$ is irrelevant for the derivation of the master equation.

Merely, it is required that the Hamiltonian is describable by excitation and deexcitation operators, $\hat{S}^\dagger$ and $\hat{S}$, defined by

$$\mathscr{L}_s\hat{S} = -\frac{\mathrm{i}}{\hbar}\left[\hat{\mathsf{H}}_\mathrm{S}, \hat{S}\right] = \mathrm{i}\bar{\omega}\hat{S}. \tag{D.3}$$

Equation (D.3) states, that $\hat{S}$ and $\hat{S}^\dagger$ are eigen-operators of the Liouvillian $\mathscr{L}_s$, freely propagating with eigenfrequency $\bar{\omega}$ in the absence of any interaction for example with the environment. Certainly, this operator class can be generalized by considering a whole set of excitation and deexcitation operators enumerated by an index i, $\{\hat{S}_i^\dagger, \hat{S}_i\}$.

We assume a one-dimensional reservoir with Hamilton operator

$$\hat{\mathsf{H}}_\mathrm{R} = \int_0^\infty \mathrm{d}\omega\, \hbar\omega \hat{b}^\dagger(\omega)\hat{b}(\omega), \tag{D.4}$$

with annihilation and creation reservoir operators, $\hat{b}(\omega)$ and $\hat{b}^\dagger(\omega)$, satisfying the commutation relation

$$\left[\hat{b}(\omega), \hat{b}^\dagger(\omega')\right] = \delta(\omega - \omega'). \tag{D.5}$$

Please note that in contrast to the assumption of a discrete set of harmonic oscillators in equation (5.11) we choose a continuum of harmonic oscillators of frequency ω for the derivation of the master equation. Thus, these operators have a dimension of $\mathrm{s}^{-1/2}$.

The Hamiltonian describing the interaction of the subsystem (S) with the reservoir (R) within the rotating wave and dipole approximation,

$$\hat{\mathsf{H}}_\mathrm{I} = \hbar \int_0^\infty \mathrm{d}\omega \left[\mathscr{W}(\omega)\hat{S}^\dagger\hat{b}(\omega) + \mathrm{h.c.}\right], \tag{D.6}$$

depends on the coupling strength, $\mathscr{W}(\omega)$, between the small system and the reservoir.

In order to eliminate irrelevant eigendynamics of the system and the reservoir, a transformation into a convenient interaction picture is useful. Here, the interaction state $|\psi(t)\rangle_\mathrm{I}$ is related with the state vector in the Schrödinger picture $|\psi(t)\rangle_\mathrm{S}$ by the transformation operator $\hat{U}$

$$|\psi(t)\rangle_\mathrm{I} = \hat{U}^\dagger(t)\,|\psi(t)\rangle_\mathrm{S}, \qquad \hat{U}(t) = e^{-\frac{\mathrm{i}}{\hbar}(\hat{\mathsf{H}}_\mathrm{S}+\hat{\mathsf{H}}_\mathrm{R})t}. \tag{D.7}$$

The total interaction Hamiltonian in terms of the detuning $\Delta = \omega - \bar{\omega}$ reads

$$\hat{H}_\mathrm{I}(t) = \hat{U}^\dagger(t)\hat{\mathsf{H}}_\mathrm{I}\hat{U}(t) = \hbar\int_{-\bar{\omega}}^\infty \mathrm{d}\Delta\left[W(\Delta)\hat{S}^\dagger\hat{b}(\Delta) + \mathrm{h.c.}\right] \approx \mathrm{i}\hbar\left[\hat{S}^\dagger\hat{F}(t) - \hat{F}^\dagger(t)\hat{S}\right], \tag{D.8}$$

$$\hat{F}(t) \equiv -\mathrm{i}\int_{-\infty}^\infty \mathrm{d}\Delta\, W(\Delta)\hat{b}(\Delta)e^{-\mathrm{i}\Delta t}. \tag{D.9}$$

In the last step of equation (D.8), we extended the lower integration limit $-\bar{\omega}$ to $-\infty$, which is a good approximation as for optical systems, the eigenfrequency $\bar{\omega}$ is much larger than any detuning, Rabi-frequency or other relevant system frequencies. The explicit time dependent operator $\hat{F}(t)$ is called *Langevin force*. Note, that its integrand is proportional to the annihilation operator $\hat{b}(\Delta)$ of the bath. Thus, the Liouville equation in the interaction picture is

$$\mathrm{i}\hbar\frac{\mathrm{d}}{\mathrm{d}t}\hat{\tilde{\rho}}(t) = \left[\hat{H}_\mathrm{I}(t), \hat{\tilde{\rho}}(t)\right], \tag{D.10}$$

with total interaction picture density operator $\hat{\tilde{\rho}}$ and Hamiltonian (D.8).

We are primarily interested in the dynamics of the system and not in the total temporal evolution of system and reservoir. The state of the subsystem is described by the reduced density matrix,

$\hat{\rho}_{\mathrm{S}}$, defined by the partial trace over all reservoir degrees of freedom of the Hilbert space $\mathcal{H}_{\mathrm{R}}$, $\hat{\rho}_{\mathrm{S}}(t) = \mathrm{Tr}_{\mathrm{R}}\{\hat{\rho}(t)\}$. At the initial time $t = 0$, the system $\hat{\rho}_{\mathrm{S}}$ and the reservoir $\hat{\rho}_{\mathrm{R}}$ are assumed to be decorrelated. Thus, the state factorizes, $\hat{\rho}(0) = \hat{\rho}_{\mathrm{S}}(0) \otimes \hat{\rho}_{\mathrm{R}}(0)$. Taking the partial trace over the reservoir degrees of freedom of equation (D.10) the resulting Liouville equation for the system density operator is

$$\mathrm{i}\hbar \frac{\mathrm{d}}{\mathrm{d}t} \hat{\hat{\rho}}_{\mathrm{S}}(t) = \mathrm{Tr}_{\mathrm{R}}\Big\{ \big[\hat{H}_{\mathrm{I}}(t), \hat{\hat{\rho}}(t)\big] \Big\}. \tag{D.11}$$

This differential equation, depending on the density operator $\hat{\hat{\rho}}_{\mathrm{S}}$ as well as $\hat{\hat{\rho}}_{\mathrm{R}}$, is not closed and can therefore not be solved directly. In order to evaluate the trace on the right hand side of equation (D.11), the evolution of $\hat{\hat{\rho}}_{\mathrm{R}}$ under the influence of the coupling has to be determined.

Assuming a weak coupling between the system and the reservoir, the total density operator can be evolved perturbatively by iterating the formal solution of its equation of motion (D.10) with $t \geq t'$,

$$\hat{\hat{\rho}}(t) = \hat{\hat{\rho}}(0) - \frac{\mathrm{i}}{\hbar} \int_0^t \mathrm{d}t' \; \big[\hat{H}_{\mathrm{I}}(t'), \hat{\hat{\rho}}(t')\big]. \tag{D.12}$$

Due to the weak interaction, we can stop after the second iteration process. Subsequently, resubstitution solution (D.12) into the equation of motion for the reduced density operator (D.11) yields

$$\frac{\mathrm{d}}{\mathrm{d}t}\hat{\hat{\rho}}_{\mathrm{S}}(t) = -\frac{\mathrm{i}}{\hbar}\mathrm{Tr}_{\mathrm{R}}\Big\{ \big[\hat{H}_{\mathrm{I}}(t), \hat{\hat{\rho}}(0)\big] \Big\} - \frac{1}{\hbar^2} \int_0^t \mathrm{d}t' \; \mathrm{Tr}_{\mathrm{R}}\Big\{ \big[\hat{H}_{\mathrm{I}}(t), \big[\hat{H}_{\mathrm{I}}(t'), \hat{\hat{\rho}}(t')\big]\big] \Big\}, \tag{D.13}$$

in which the first term on the right hand side is proportional to the mean value of the Langevin force operator, $\langle \hat{F}(t) \rangle$, and therefore equal to zero.

For finding a closed first-order differential equation for the subsystem, we rewrite the total density operator according to

$$\hat{\rho}(t) = \hat{\rho}_{\mathrm{S}}(t) \otimes \hat{\rho}_{\mathrm{R}} + \underbrace{(\hat{\rho}(t) - \hat{\rho}_{\mathrm{S}}(t) \otimes \hat{\rho}_{\mathrm{R}})}_{=\delta\hat{\rho}(t)} = \hat{\rho}_{\mathrm{S}}(t) \otimes \hat{\rho}_{\mathrm{R}} + \delta\hat{\rho}(t). \tag{D.14}$$

As we consider subsystems that are much smaller than the surrounding reservoir, their interaction among each other do not really affect the dynamics of the large environment. For a reservoir being in thermodynamic equilibrium, $\delta\hat{\rho}(t) \ll \hat{\rho}_{\mathrm{S}}(t) \otimes \hat{\rho}_{\mathrm{R}}$ holds and the total density operator in decorrelation approximation reads

$$\hat{\rho}(t) = \hat{\rho}_{\mathrm{S}}(t) \otimes \hat{\rho}_{\mathrm{R}} \quad \text{(decorrelation approximation)}, \tag{D.15}$$

leading to a closed differential equation when inserting this ansatz into equation (D.13),

$$\begin{aligned} \frac{\mathrm{d}}{\mathrm{d}t}\hat{\hat{\rho}}_{\mathrm{S}}(t) = \int_0^t \mathrm{d}t' \Big[&(\hat{S}\hat{\hat{\rho}}_{\mathrm{S}}(t')\hat{S}^\dagger - \hat{S}^\dagger\hat{S}\hat{\hat{\rho}}_{\mathrm{S}}(t'))\langle \hat{F}(t)\hat{F}^\dagger(t') \rangle \\ &+ (\hat{S}\hat{\hat{\rho}}_{\mathrm{S}}(t')\hat{S}^\dagger - \hat{\hat{\rho}}_{\mathrm{S}}(t')\hat{S}^\dagger\hat{S})\langle \hat{F}(t')\hat{F}^\dagger(t) \rangle \\ &+ (\hat{S}^\dagger\hat{\hat{\rho}}_{\mathrm{S}}(t')\hat{S} - \hat{S}\hat{S}^\dagger\hat{\hat{\rho}}_{\mathrm{S}}(t'))\langle \hat{F}^\dagger(t)\hat{F}(t') \rangle \\ &+ (\hat{S}^\dagger\hat{\hat{\rho}}_{\mathrm{S}}(t')\hat{S} - \hat{\hat{\rho}}_{\mathrm{S}}(t')\hat{S}\hat{S}^\dagger)\langle \hat{F}^\dagger(t')\hat{F}(t) \rangle \Big]. \end{aligned} \tag{D.16}$$

Here, terms proportional to $\langle \hat{F}(t)\hat{F}(t') \rangle$ or $\langle \hat{F}^\dagger(t)\hat{F}^\dagger(t') \rangle$ vanished in equation (D.16) due to the assumption of a non-squeezed reservoir.

To evaluate the force averages in equation (D.16), further assumptions regarding the reservoir state have to be formulated. The choice of a canonical ensemble in thermodynamic equilibrium with density operator

$$\hat{\rho}_{\mathrm{R}}(t) = \frac{1}{Z} e^{-\beta \hat{H}_{\mathrm{R}}}, \quad Z = \mathrm{Tr}\{e^{-\beta \hat{H}_{\mathrm{R}}}\}, \quad \beta = \frac{1}{k_{\mathrm{B}} T}, \tag{D.17}$$

is convenient. The Hamiltonian in the exponent, $\hat{H}_{\mathrm{R}} = \int_0^\infty \mathrm{d}\Delta \hbar \Delta \hat{b}^\dagger(\Delta)\hat{b}(\Delta)$, corresponds to equation (D.4) transformed in the considered interaction picture. Such a canonical reservoir has no mean-field component, no correlation between the modes and of course no squeezing, but a non-vanishing lowest-order moment proportional to the mean-thermal occupation number (cf. equation (2.76))

$$\bar{N}(\Delta) = (e^{\beta\hbar(\bar{\omega}+\Delta)} - 1)^{-1}, \tag{D.18}$$

that is

$$\langle \hat{b}(\Delta) \rangle = \langle \hat{b}(\Delta)\hat{b}(\Delta') \rangle = \langle \hat{b}^\dagger(\Delta)\hat{b}^\dagger(\Delta') \rangle = 0, \tag{D.19}$$

$$\langle \hat{b}^\dagger(\Delta)\hat{b}(\Delta') \rangle = \bar{N}(\Delta)\delta(\Delta - \Delta'), \quad \langle \hat{b}(\Delta)\hat{b}^\dagger(\Delta') \rangle = (\bar{N}(\Delta) + 1)\delta(\Delta - \Delta'). \tag{D.20}$$

Therefore, the Langevin force averages occurring in equation (D.16) are given by

$$\langle \hat{F}(t)\hat{F}^\dagger(t') \rangle = \int_{-\infty}^{\infty} \mathrm{d}\Delta \, |W(\Delta)|^2 e^{-\mathrm{i}\Delta(t-t')} (\bar{N}(\Delta) + 1), \tag{D.21}$$

$$\langle \hat{F}^\dagger(t)\hat{F}(t') \rangle = \int_{-\infty}^{\infty} \mathrm{d}\Delta \, |W(\Delta)|^2 e^{-\mathrm{i}\Delta(t-t')} \bar{N}(\Delta). \tag{D.22}$$

Inserting these correlations into the equation of motion for the system density operator (cf. equation (D.16)) results into an integro-differential equation, which still remains difficult to solve without further simplifications regarding the time integration.

The *Markov approximation* enables a conversion to a relatively simple expression. In order to explain the main idea behind this important approximation, we introduce the complex memory kernel,

$$K(t - t') \equiv \int_{-\infty}^{\infty} \mathrm{d}\Delta \, |W(\Delta)|^2 e^{-\mathrm{i}\Delta(t-t')} = \left[\hat{F}(t), \hat{F}^\dagger(t')\right], \tag{D.23}$$

equivalent to the Fourier transform of the square of the absolute value of the coupling constant $W(\Delta)$. Because $W(\Delta)$ is a slowly varying function of detuning Δ, the memory kernel $K(\tau)$ is sharply peaked at $\tau = 0$ and vanishes rapidly for times t larger than the correlation time τ_c of the reservoir fluctuations. In contrast, the system density operator $\hat{\bar{\rho}}_{\mathrm{S}}$ varies slowly for times $|t - t'| < \tau_c$, so that the replacement $\hat{\bar{\rho}}_{\mathrm{S}}(t') \approx \hat{\bar{\rho}}_{\mathrm{S}}(t)$ is justified within the Markov approximation. Therefore we can write for the integral

$$\int_0^t \mathrm{d}t' \, K(t - t')\hat{\bar{\rho}}_{\mathrm{S}}(t') \approx \int_0^t \mathrm{d}t' \, K(t - t')\hat{\bar{\rho}}_{\mathrm{S}}(t) = \gamma(t)\hat{\bar{\rho}}_{\mathrm{S}}(t), \quad \gamma(t) = \int_0^t \mathrm{d}\tau \, K(\tau), \tag{D.24}$$

with rate γ reaching its complex limiting value very quickly, so that the upper integration limit can be extended to infinity in good approximation. Applying methods of complex analysis, it can be shown, that the integral [155]

$$\gamma_\infty = \lim_{t \gg \tau_c} \gamma(t) = \int_0^\infty \mathrm{d}\tau \, K(\tau) = \Gamma + \mathrm{i}\delta\omega, \tag{D.25}$$

is the sum of a damping rate $\Gamma = \pi |W(\bar{\omega})|^2$ and an energy shift $\delta\omega$. Applying the Markov approximation to the integro-differential equation (D.16) and subsequently back transforming into the initial Schrödinger picture results in a birth-death process [180], the *master equation* in *Lindblad form* [132]

$$\boxed{\frac{\mathrm{d}}{\mathrm{d}t}\hat{\rho}_{\mathrm{S}}(t) = (\mathfrak{L}_{\mathrm{S}} + \mathfrak{L}_{\mathrm{R}})\hat{\rho}_{\mathrm{S}}(t)}. \tag{D.26}$$

Here, the system Liouville operator,

$$\mathfrak{L}_{\mathrm{S}}\,\hat{\rho}_{\mathrm{S}}(t) = -\frac{\mathrm{i}}{\hbar}\left[\hat{\mathsf{H}}_{\mathrm{S}}, \hat{\rho}_{\mathrm{S}}\right], \tag{D.27}$$

describes the unperturbed system. The damping Liouville operator,

$$\begin{aligned}\mathfrak{L}_{\mathrm{R}}\,\hat{\rho}_{\mathrm{S}}(t) = \Gamma(\underbrace{\bar{N}(0)}_{\text{stim. emission}} + \underbrace{1}_{\text{spon. emission}})&(2\hat{S}\hat{\rho}_{\mathrm{S}}(t)\hat{S}^{\dagger} - \hat{S}^{\dagger}\hat{S}\hat{\rho}_{\mathrm{S}}(t) - \hat{\rho}_{\mathrm{S}}(t)\hat{S}^{\dagger}\hat{S})\\ + \underbrace{\Gamma\bar{N}(0)}_{\text{stim. absoption}}&(2\hat{S}^{\dagger}\hat{\rho}_{\mathrm{S}}(t)\hat{S} - \hat{S}\hat{S}^{\dagger}\hat{\rho}_{\mathrm{S}}(t) - \hat{\rho}_{\mathrm{S}}(t)\hat{S}\hat{S}^{\dagger})\\ - \mathrm{i}\left[\delta\omega\hat{S}^{\dagger}\hat{S} + \delta\omega_{\mathrm{th}}\left[\hat{S}^{\dagger}, \hat{S}\right], \hat{\rho}_{\mathrm{S}}(t)\right]&,\end{aligned} \tag{D.28}$$

considers the coupling between the environment and the system, leading to dissipation captured by relaxation rate Γ, energy shift $\delta\omega$ as well as thermal energy shift $\delta\omega_{\mathrm{th}}$. These energy shifts are defined by the principle part integrals

$$\delta\omega = -\mathscr{P}\int \mathrm{d}\Delta\,|W(\Delta)|^2/\Delta, \tag{D.29}$$

$$\delta\omega_{\mathrm{th}} = -\mathscr{P}\int \mathrm{d}\Delta\,|W(\Delta)|^2\bar{N}(\Delta)/\Delta. \tag{D.30}$$

The latter depends on the thermal occupation number $\bar{N}(\Delta)$. The first term in the damping Liouvillian (D.28) characterizes stimulated and spontaneous emission whereas the second one specifies stimulated absorption processes.

For a set of system operators $\{\hat{S}_i, \hat{S}_i^{\dagger}\}$ equation (D.26) can be generalized by just summing over all system operators with corresponding damping rates Γ_i and occupation numbers $\bar{N}_i$. Choosing an appropriate renormalization of the energy shifts, the master equation for the reduced density operator with several system operator components reads

$$\boxed{\begin{aligned}\frac{\mathrm{d}}{\mathrm{d}t}\hat{\rho}_{\mathrm{S}}(t) = \underbrace{-\frac{\mathrm{i}}{\hbar}\left[\hat{\mathsf{H}}_{\mathrm{S}}, \hat{\rho}_{\mathrm{S}}\right]}_{\mathfrak{L}_{\mathrm{S}}\hat{\rho}_{\mathrm{S}}(t)} &+ \sum_i \Gamma_i(\bar{N}_i + 1)(2\hat{S}_i\,\hat{\rho}_{\mathrm{S}}(t)\hat{S}_i^{\dagger} - \hat{S}_i^{\dagger}\hat{S}_i\,\hat{\rho}_{\mathrm{S}}(t) - \hat{\rho}_{\mathrm{S}}(t)\hat{S}_i^{\dagger}\hat{S}_i\,)\\ &+ \sum_i \Gamma_i\bar{N}_i(2\hat{S}_i^{\dagger}\hat{\rho}_{\mathrm{S}}(t)\hat{S}_i\, - \hat{S}_i\,\hat{S}_i^{\dagger}\hat{\rho}_{\mathrm{S}}(t) - \hat{\rho}_{\mathrm{S}}(t)\hat{S}_i\,\hat{S}_i^{\dagger}).\end{aligned} \quad (\text{D.31})}$$

E

NOISE INPUT AND OUTPUT

The total electromagnetic field located at an arbitrary output port of the QDSLD is relevant in order to describe the diode model. This physical problem is depicted in figure 5.1 and will be examined in detail in this appendix. The following content is adapted from [50].

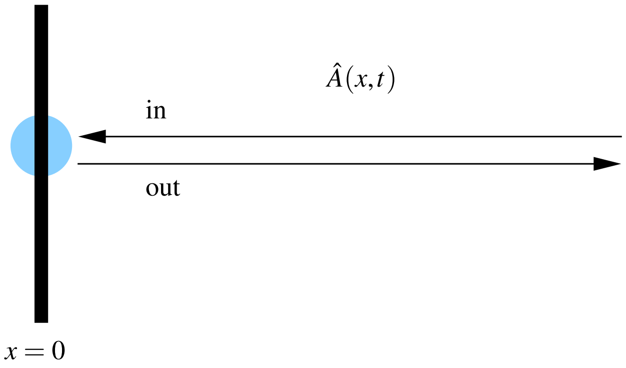

Figure 5.1: Input and output of a one-dimensional radiation field $\hat{A}(x,t)$ interacting with a system at position $x=0$.

The blue circle visualizes a system, described by the Lagrangian $\hat{L}_{\mathrm{sys}}(\hat{\mathbf{Z}})$, which depends on the vector $\hat{\mathbf{Z}}$ composed of a finite number of system operators. This system interacts with a heat bath modeled by a one-dimensional electromagnetic field $\hat{A}(x,t)=\hat{A}^{\dagger}(x,t)$. The full Lagrangian in terms of the dynamical variables $\hat{A}$ and $\dot{\hat{A}}$ can be written as

$$\hat{L}(\hat{A}(t),\dot{\hat{A}}(t))=\hat{L}_{\mathrm{sys}}(\mathbf{Z})+\int_0^{\infty}\mathrm{d}x\,\mathscr{L}(\hat{A}(x,t),\dot{\hat{A}}(x,t)) \tag{E.1}$$

with Lagrangian density

$$\hat{\mathscr{L}}(\hat{A}(x,t),\dot{\hat{A}}(x,t))=\frac{1}{2}\left[\dot{\hat{A}}^2(x,t)-c^2(\partial_x\hat{A}(x,t))^2\right]+\hat{X}\kappa(x)\dot{\hat{A}}(x,t). \tag{E.2}$$

Here, $\hat{X}=\hat{X}^{\dagger}$ is a particular operator which interacts with $\hat{A}(x,t)$, c is the speed of light and $\kappa(x)\in\mathbb{R}$ determines the interaction domain. The canonical momentum is given by the sum of the electromagnetic field and the product of the interaction and the system operator $\hat{X}$,

$$\hat{\pi}(x,t)=\frac{\partial\hat{\mathscr{L}}(x,t)}{\partial\dot{\hat{A}}(x,t)}=\dot{\hat{A}}(x,t)+\hat{X}\kappa(x). \tag{E.3}$$

Therefore, the Hamiltonian of the total system is specified by

$$\begin{aligned}\hat{H}&=\hat{H}_{\mathrm{sys}}(\hat{\mathbf{Z}})+\int_0^{\infty}\mathrm{d}x\,\left(\hat{\pi}(x,t)\dot{\hat{A}}(x,t)-\hat{\mathscr{L}}(x,t)\right)\\&=\hat{H}_{\mathrm{sys}}(\hat{\mathbf{Z}})+\frac{1}{2}\int_0^{\infty}\mathrm{d}x\,\left[(\hat{\pi}(x,t)-\hat{X}\kappa(x))^2+c^2(\partial_x\hat{A}(x,t))^2\right],\end{aligned} \tag{E.4}$$

with system Hamiltonian $\hat{H}_{\text{sys}}$ corresponding to the system Lagrangian $\hat{L}_{\text{sys}}$. Introducing Fourier transform variables,

$$\hat{A}(x,t) = \sqrt{\frac{2}{\pi c}} \int_0^\infty \mathrm{d}\omega \; \hat{q}(\omega,t) \cos(\omega x/c), \tag{E.5}$$

$$\hat{\pi}(x,t) = \sqrt{\frac{2}{\pi c}} \int_0^\infty \mathrm{d}\omega \; \hat{p}(\omega,t) \cos(\omega x/c), \tag{E.6}$$

$$\kappa(x) = \sqrt{\frac{2}{\pi c}} \int_0^\infty \mathrm{d}\omega \; \tilde{\kappa}(\omega) \cos(\omega x/c), \tag{E.7}$$

equation (E.4) can be written as

$$\hat{H} - \hat{H}_{\text{sys}}(\hat{\mathbf{Z}}) = \frac{1}{2} \int_0^\infty \mathrm{d}\omega \; \left[(\hat{p}(\omega,t) - \tilde{\kappa}(\omega)\hat{X})^2 + \omega^2 \hat{q}(\omega,t)^2 \right]. \tag{E.8}$$

The new variables satisfy the commutation relation

$$[\hat{q}(\omega,t), \hat{p}(\omega',t)] = \mathrm{i}\hbar\delta(\omega - \omega'). \tag{E.9}$$

As a solution of the Lagrange equation,

$$\frac{\mathrm{d}}{\mathrm{d}t} \frac{\partial \hat{\mathscr{L}}}{\partial \dot{\hat{q}}} - \frac{\partial \hat{\mathscr{L}}}{\partial \hat{q}} = 0, \tag{E.10}$$

we obtain an equation of motion for the heat bath operator $\hat{A}(x,t)$,

$$\ddot{\hat{A}}(x,t) - c^2 \partial_x^2 \hat{A}(x,t) = -\kappa(x)\dot{\hat{X}}, \tag{E.11}$$

corresponding to a wave equation in the presence of a source. To solve this differential equation, destruction and creation operators are defined,

$$\hat{a}(\omega,t) = \frac{\omega\hat{q}(\omega,t) + \mathrm{i}\hat{p}(\omega,t)}{\sqrt{2\hbar\omega}}, \quad \hat{a}^\dagger(\omega,t) = \frac{\omega\hat{q}(\omega,t) - \mathrm{i}\hat{p}(\omega,t)}{\sqrt{2\hbar\omega}}, \tag{E.12}$$

in terms of continuous canonical operators,

$$\hat{p}(\omega,t) = \mathrm{i}\sqrt{\frac{\hbar\omega}{2}} (\hat{a}^\dagger(\omega,t) - \hat{a}(\omega,t)), \quad \hat{q} = \sqrt{\frac{\hbar}{2\omega}} (\hat{a}(\omega,t) + \hat{a}^\dagger(\omega,t)). \tag{E.13}$$

We differentiate the annihilation operator (cf. equation (E.12)) with respect to time t and consider the Heisenberg equation of motion for the radiation field operators,

$$\dot{\hat{q}}(\omega,t) = \hat{p}(\omega,t) - \kappa(\omega)\hat{X}, \tag{E.14}$$

$$\dot{\hat{p}}(\omega,t) = -\omega^2 \hat{q}(\omega,t). \tag{E.15}$$

Inserting equations (E.14)-(E.15) into the temporal derivatives of the annihilation operator results in

$$\dot{\hat{a}}(\omega,t) = \frac{\omega\dot{\hat{q}}(\omega,t) + \mathrm{i}\dot{\hat{p}}(\omega,t)}{\sqrt{2\hbar\omega}} = -\mathrm{i}\omega\hat{a}(\omega,t) - \kappa(\omega)\sqrt{\frac{\omega}{2\hbar}}\hat{X}. \tag{E.16}$$

This differential equation is solvable by formal integration in terms of initial, $t_0 < t$, and analogous of final time, $t_f > t > t_0$,

$$\hat{a}(\omega,t) = \hat{a}(\omega,t_0)e^{-\mathrm{i}\omega(t-t_0)} - \kappa(\omega)\sqrt{\frac{\omega}{2\hbar}} \int_{t_0}^t \mathrm{d}t' \; e^{-\mathrm{i}\omega(t-t')}\hat{X}(t'). \tag{E.17}$$

The first term on the right-hand side describes the free oscillating behavior of the radiation field and the second term characterizes the interaction with the system. Next, we introduce the definition of input and output field operators,

$$\hat{A}_{\text{in}}(t) \equiv \frac{1}{2}\int_0^\infty \mathrm{d}\omega \sqrt{\frac{\hbar}{\pi\omega c}} \left[\hat{a}(\omega,t_0)e^{-\mathrm{i}\omega(t-t_0)} + \hat{a}^\dagger(\omega,t_0)e^{\mathrm{i}\omega(t-t_0)}\right], \tag{E.18}$$

$$\hat{A}_{\text{out}}(t) \equiv \frac{1}{2}\int_0^\infty \mathrm{d}\omega \sqrt{\frac{\hbar}{\pi\omega c}} \left[\hat{a}(\omega,t_f)e^{-\mathrm{i}\omega(t-t_f)} + \hat{a}^\dagger(\omega,t_f)e^{\mathrm{i}\omega(t-t_f)}\right]. \tag{E.19}$$

Obviously, the input operator is a function of the initial time t_0 whereas the output operator depends on the final time t_f. By rewriting $\hat{q}(\omega,t)$ in equation (E.5) with respect to the annihilation and creation operator (cf. equation (E.13)) and subsequently applying equation (E.17) as well as its Hermitian conjugate, the canonical operator in terms of the input field operator reads [1]

$$\begin{aligned}
\hat{A}(x,t) &= \sqrt{\frac{\hbar}{\pi c}}\int_0^\infty \mathrm{d}\omega\, \frac{\hat{a}(\omega,t)+\hat{a}^\dagger(\omega,t)}{\sqrt{\omega}} \cos\left(\frac{\omega x}{c}\right) \\
&= \hat{A}_{\text{in}}\left(t+\frac{x}{c}\right) + \hat{A}_{\text{in}}\left(t-\frac{x}{c}\right) - \int_{t_0}^{t} \mathrm{d}t'\hat{X}(t')\sqrt{\frac{2}{\pi c}}\int_0^\infty \mathrm{d}\omega\tilde{\kappa}(\omega)\cos(\omega(t-t'))\cos\left(\frac{\omega x}{c}\right) \\
&= \hat{A}_{\text{in}}\left(t+\frac{x}{c}\right) + \hat{A}_{\text{in}}\left(t-\frac{x}{c}\right) - \frac{1}{2}\int_{t_0}^{t} \mathrm{d}t'\hat{X}(t')\sqrt{\frac{2}{\pi c}}\int_0^\infty \mathrm{d}\omega\tilde{\kappa}(\omega)\cos\left(\frac{\omega x}{c} - \omega(t-t')\right) \\
&\quad - \frac{1}{2}\int_{t_0}^{t} \mathrm{d}t'\hat{X}(t')\sqrt{\frac{2}{\pi c}}\int_0^\infty \mathrm{d}\omega\tilde{\kappa}(\omega)\cos\left(\frac{\omega x}{c} + \omega(t-t')\right) \\
&= \hat{A}_{\text{in}}\left(t+\frac{x}{c}\right) + \hat{A}_{\text{in}}\left(t-\frac{x}{c}\right) - \frac{1}{2}\int_{t_0}^{t} \mathrm{d}t'\hat{X}(t')\left[\kappa(x-c(t-t')) + \kappa(x+c(t-t'))\right] \\
&\quad - \frac{1}{2}\int_{t_0}^{t} \mathrm{d}t'\hat{X}(t')\kappa(x+c(t-t')).
\end{aligned} \tag{E.20}$$

In the last step, we used the definition of the Fourier transform of the coupling constant (see equation (E.7)). Suitable substitution with $c\tau = x - c(t-t')$ in the upper first and $c\tau = x + c(t-t')$ in the second integral of (E.20) yields

$$\begin{aligned}
\hat{A}(x,t) &= \hat{A}_{\text{in}}\left(t+\frac{x}{c}\right) + \hat{A}_{\text{in}}\left(t-\frac{x}{c}\right) - \frac{1}{2}\int_{\frac{x}{c}-(t-t_0)}^{\frac{x}{c}} \mathrm{d}\tau\ \kappa(c\tau)\hat{X}\left(t + \left(\tau - \frac{x}{c}\right)\right) \\
&\quad - \frac{1}{2}\int_{\frac{x}{c}}^{\frac{x}{c}+(t-t_0)} \mathrm{d}\tau\ \kappa(c\tau)\hat{X}\left(t - \left(\tau - \frac{x}{c}\right)\right) \\
&= \hat{A}_{\text{in}}\left(t+\frac{x}{c}\right) + \hat{A}_{\text{in}}\left(t-\frac{x}{c}\right) - \frac{1}{2}\int_{\frac{x}{c}-(t-t_0)}^{\frac{x}{c}+(t-t_0)} \mathrm{d}\tau\ \kappa(c\tau)\hat{X}\left(t - |\tau - \frac{x}{c}|\right).
\end{aligned} \tag{E.21}$$

In the same way, we can find an expression in terms of the output field,

$$\hat{A}(x,t) = \hat{A}_{\text{in}}\left(t+\frac{x}{c}\right) + \hat{A}_{\text{in}}\left(t-\frac{x}{c}\right) - \frac{1}{2}\int_{\frac{x}{c}-(t-t_0)}^{\frac{x}{c}+(t-t_0)} \mathrm{d}\tau\ \kappa(c\tau)\hat{X}\left(t - |\tau - \frac{x}{c}|\right) \tag{E.22}$$

$$= \hat{A}_{\text{out}}\left(t+\frac{x}{c}\right) + \hat{A}_{\text{out}}\left(t-\frac{x}{c}\right) - \frac{1}{2}\int_{\frac{x}{c}+(t-t_f)}^{\frac{x}{c}-(t-t_f)} \mathrm{d}\tau\ \kappa(c\tau)\hat{X}\left(t + |\tau - \frac{x}{c}|\right). \tag{E.23}$$

For x lying outside the interaction regime, $\tau < x/c$ for $\kappa(c\tau) \neq 0$, the argument of $\hat{X}$ in the integrand can be replaced by $|\tau - x/c| = x/c - \tau$. Additionally, we can set t_0 and t_f equal

---

[1] A similar expression of $\hat{A}(x,t)$ in terms of the output operator can be found by using the solution of the annihilation operator as a function of future time t_f, following the same calculation as in case of initial time t_0.

to ±∞, provided that t_0 is in the remote past and t_f is in the remote future so that equation (E.22) and (E.23) are simplified to

$$\begin{aligned} \hat{A}(x,t) &= \hat{A}_{\text{in}}\left(t+\frac{x}{c}\right) + \hat{A}_{\text{in}}\left(t-\frac{x}{c}\right) - \frac{1}{2}\int_{-\infty}^{\infty} \mathrm{d}\tau\, \kappa(c\tau)\hat{X}\left(t-\frac{x}{c}+\tau\right) && \text{(E.24)} \\ &= \hat{A}_{\text{out}}\left(t+\frac{x}{c}\right) + \hat{A}_{\text{out}}\left(t-\frac{x}{c}\right) - \frac{1}{2}\int_{-\infty}^{\infty} \mathrm{d}\tau\, \kappa(c\tau)\hat{X}\left(t+\frac{x}{c}-\tau\right). && \text{(E.25)} \end{aligned}$$

Obviously, the canonical operator $\hat{A}(x,t)$ is given by the input and the output field operators at retarded and advanced time, $t-x/c$ and $t+x/c$, plus a convolution integral with an integrand depending on κ and the system operator $\hat{X}$. Equating the right-hand sides of (E.24) and (E.25) and sorting it according to the two arguments $t-x/c$ and $t+x/c$, we find a relation between the input and output operator with respect to advanced time,

$$\hat{A}_{\text{out}}\left(t+\frac{x}{c}\right) = \hat{A}_{\text{in}}\left(t+\frac{x}{c}\right) - \frac{1}{2}\int_{-\infty}^{\infty} \mathrm{d}\tau\, \kappa(c\tau)\hat{X}\left(t+\frac{x}{c}-\tau\right). \qquad \text{(E.26)}$$

The solution is valid for a finite time t even if x are lying outside the interaction regime. Thus, we can make the replacement $t+x/c \to t$ and equation (E.26) simplifies to

$$\hat{A}_{\text{out}}(t) = \hat{A}_{\text{in}}(t) - \frac{1}{2}\int_{-\infty}^{\infty} \mathrm{d}\tau\, \kappa(c\tau)\hat{X}(t-\tau). \qquad \text{(E.27)}$$

This result implies, that the output field is the sum of the incoming field and a radiating field described by the integral expression, which depends explicitly on the system operator and is therefore specified by the equation of motion of $\hat{X}$. Thus, in case of x lying outside the interaction regime, that is outside the range of $\kappa(x)$, equation (E.24) can be written as

$$\boxed{\hat{A}(x,t) = \hat{A}_{\text{in}}\left(t+\frac{x}{c}\right) + \hat{A}_{\text{out}}\left(t-\frac{x}{c}\right)}. \qquad \text{(E.28)}$$

The total field $\hat{A}(x,t)$ is given by the sum of the incoming field $\hat{A}_{\text{in}}(t+x/c)$ at advanced time $t+x/c$ and the outgoing field $\hat{A}_{\text{out}}(t-x/c)$ at retarded time $t-x/c$.

POINTWISE LOCALIZED INTERACTION Consider the case of a negligibly small system localized at position $x=0$ which interacts with the electromagnetic field $\hat{A}(x,t)$ within a small ε-region (such a system could be e.g. an atom). The pointwise localized coupling can be described by a delta distribution

$$\kappa(x) = 2\sqrt{\gamma c}\,\delta(x). \qquad \text{(E.29)}$$

Its Fourier transform corresponds to a constant, frequency-independent coupling strength

$$\tilde{\kappa}(\omega) = \sqrt{2\gamma/\pi}, \qquad \text{(E.30)}$$

Equation (E.30) is the Markov approximation, discussed in appendix D. Inserting equation (E.29) into the output relation (E.27) leads to the simple expression

$$\hat{A}_{\text{out}}(t) = \hat{A}_{\text{in}}(t) - \sqrt{\frac{\gamma}{c}}\hat{X}(t). \qquad \text{(E.31)}$$

The input field $\hat{A}_{\text{in}}(t)$ can be interpreted as noise input. The type of noise depends on the statistics of the field amplitudes $\hat{a}(\omega,t_0)$ and $\hat{a}^{\dagger}(\omega,t_0)$ (see equation (E.18)). Obviously, their dependency on the initial time t_0 reveals that the choice of the input field is arbitrary, that is, $\hat{A}_{\text{in}}$ is not affected by the system itself. In contrast, the output field described by equation (E.31) is specified by the input noise and the small system.

F

QUANTUM STOCHASTIC PROCESSES: ITÔ VS. STRATONOVICH

This appendix deals with the *quantum white noise* concept for quantum systems clearly formulated by *C. W. Gardiner* and *M. J. Collett* [144]. After its formulation we define quantum stochastic integral equations in terms of the quantum Wiener process corresponding to quantum white noise. In close analogy to classical considerations, one can define two different integrals named after their inventors *K. Itô* and *R. Stratonovich*, which again result into different quantum stochastic differential equations (QSDEs) directly related with the quantum Langevin equation. Additionally, we will study the relation between the Itô and Stratonovich QSDE and summarize the main differences between them. We will see that the Itô version has some more mathematical advantages compared to Stratonovich which in turn has more in common with physical considerations. A detailed analysis of classical stochastic processes as well as the quantum mechanical analog is written in reference [181] and [50, 144].

Consider an open, noisy system described by the system Hamilton operator $\hat{H}_s$ which linearly couples to a heat bath of harmonic oscillators $\hat{H}_r$ described by the interaction Hamiltonian $\hat{H}_i$, that is the total Hamiltonian is given by

$$\hat{H} = \hat{H}_s + \hat{H}_r + \hat{H}_i. \tag{F.1}$$

From the knowledge of this Hamiltonian, we can specify the quantum Langevin equation by formal integration (in terms of initial time) of the Heisenberg equations of motion for each system operator and assuming an approximately constant coupling between system and reservoir (Markov approximation). A detailed derivation of the quantum Langevin equation of an arbitrary system operator $\hat{a}$ with system Hamiltonian $\hat{H}_s$ in terms of the system operators $\hat{c}$, decay rates γ and noise terms $\hat{b}_{\text{in}}$ can be found in reference [50]. Here, we only will give the result

$$\dot{\hat{a}} = -\frac{\mathrm{i}}{\hbar}\left[\hat{a}, \hat{H}_s\right] - \left[\hat{a}, \hat{c}^\dagger\right]\left(\frac{\gamma}{2}\hat{c} + \sqrt{\gamma}\hat{b}_{\text{in}}\right) + \left(\frac{\gamma}{2}\hat{c}^\dagger + \sqrt{\gamma}\hat{b}_{\text{in}}^\dagger\right)\left[\hat{a}, \hat{c}\right]. \tag{F.2}$$

Please note, the noise operators depend explicitly on initial time $t_0 < t$ (see equation (5.163)). With the help of the input-output relation, the quantum Langevin equation can also be expressed in terms of the output operator $\hat{b}_{\text{out}}$ depending on the final time $t_f > t$ (see equation (5.176)). Due to causality, the system operator $\hat{a}(t)$ is independent of $\hat{b}_{\text{in}}(t')$ for $t' > t$. Vice versa, $\hat{a}(t)$ is independent of $\hat{b}_{\text{out}}(t')$ for $t' < t$, captured by the commutation relations

$$\left[\hat{a}(t), \hat{b}_{\text{in}}(t')\right] = -\Theta(t-t')\sqrt{\gamma}\left[\hat{a}(t), \hat{c}(t')\right], \tag{F.3}$$

$$\left[\hat{a}(t), \hat{b}_{\text{out}}(t')\right] = \Theta(t'-t)\sqrt{\gamma}\left[\hat{a}(t), \hat{c}(t')\right], \tag{F.4}$$

which depend on the Heaviside function

$$\Theta(t) = \begin{cases} 1, & t > 0 \\ \frac{1}{2}, & t = 0\,. \\ 0, & t < 0 \end{cases} \tag{F.5}$$

QUANTUM WIENER PROCESS The quantum state of the operator $\hat{b}_{\text{in}}$ determines the kind of noise input of a system with Hamiltonian $\hat{H}_s$. Quantum mechanically, there always exists quantum noise due to zero-point fluctuations of the external input field. Depending on the system under study, additional noises contributing to the total spectrum have to be considered. As already mentioned, the idealized white noise input will be studied in detail within this appendix. Compared to classical white noise theory, quantum white noise can be described by a density operator resulting in delta-correlated expectation values,

$$\langle \hat{b}^\dagger_{\text{in}}(t)\hat{b}_{\text{in}}(t')\rangle = \bar{N}\delta(t-t'), \tag{F.6}$$

$$\langle \hat{b}_{\text{in}}(t)\hat{b}^\dagger_{\text{in}}(t')\rangle = (\bar{N}+1)\delta(t-t'), \tag{F.7}$$

depending on the constant value $\bar{N}$. In analogy to classical stochastic methods one can define a *quantum Wiener process*[1] by the integral

$$\hat{B}(t,t_0) = \int_{t_0}^{t} \mathrm{d}t' \hat{b}_{\text{in}}(t'). \tag{F.8}$$

From this definition, we find the commutation relation and expectation values for the Wiener process

$$\left[\hat{B}(t,t_0), \hat{B}^\dagger(t,t_0)\right] = t - t_0, \tag{F.9}$$

$$\langle \hat{B}^\dagger(t,t_0)\hat{B}(t,t_0)\rangle = \bar{N}(t-t_0), \tag{F.10}$$

$$\langle \hat{B}(t,t_0)\hat{B}^\dagger(t,t_0)\rangle = (\bar{N}+1)(t-t_0). \tag{F.11}$$

Furthermore, the operators $\hat{B}(t,t_0)$ have to reveal a Gaussian distribution with density operator

$$\hat{\rho}(t,t_0) = (1-e^{-\beta})\exp\left(-\frac{\beta\hat{B}^\dagger(t,t_0)\hat{B}(t,t_0)}{t-t_0}\right) \tag{F.12}$$

and mean occupation number

$$\bar{N} = (e^{\beta}-1)^{-1}. \tag{F.13}$$

The basic principles are established for formulating quantum stochastic integrations in terms of Itô and Stratonovich which will be discussed in the next subsections.

F.1 ITÔ CALCULUS

Generally, for an arbitrary system operator $\hat{X}(t)$, the **quantum Itô integral** with time ordering $t_0 < t_1 < ... < t_n = t$ is defined by

$$(I) \int_{t_0}^{t} \hat{X}(t')\mathrm{d}\hat{B}(t') = \lim_{n\to\infty}\sum_{i=0}^{n} \hat{X}(t_i)\left[\hat{B}(t_{i+1},t_0) - \hat{B}(t_i,t_0)\right]. \tag{F.14}$$

For notational convenience we introduced the abbreviation (I) in order to distinguish between the Itô and the Stratonovich formulation of stochastic integrals. One can verify that the increments $\mathrm{d}\hat{B}(t)$, $\mathrm{d}\hat{B}^\dagger(t)$ commute with the system operator $\hat{X}(t)$,

$$(I) \int_{t_0}^{t} \hat{X}(t')\mathrm{d}\hat{B}(t') = (I) \int_{t_0}^{t} \mathrm{d}\hat{B}(t')\hat{X}(t'), \tag{F.15}$$

---

[1] Classically, a Wiener process is described by a Fokker Planck equation with constant diffusion and zero drift term.

as a result of equation (F.14) and quantum causality (F.3).

The **Itô quantum stochastic differential equation** (QSDE) of a system operator $\hat{a}(t)$ in terms of an arbitrary system operator $\hat{c}$ with system Hamiltonian $\hat{H}_s$ is defined by

$$\boxed{\begin{aligned}(I)\ \mathrm{d}\hat{a} = &-\frac{\mathrm{i}}{\hbar}\left[\hat{a}, \hat{H}_s\right]\mathrm{d}t + \frac{\gamma}{2}(\bar{N}+1)(2\hat{c}^\dagger\hat{a}\hat{c} - \hat{a}\hat{c}^\dagger\hat{c} - \hat{c}^\dagger\hat{c}\hat{a})\mathrm{d}t \\ &+ \frac{\gamma}{2}\bar{N}(2\hat{c}\hat{a}\hat{c}^\dagger - \hat{a}\hat{c}\hat{c}^\dagger - \hat{c}\hat{c}^\dagger\hat{a})\mathrm{d}t - \sqrt{\gamma}\left[\hat{a}, \hat{c}^\dagger\right]\mathrm{d}\hat{B}(t) + \sqrt{\gamma}\mathrm{d}\hat{B}^\dagger(t)\left[\hat{a}, \hat{c}\right]\end{aligned}} \tag{F.16}$$

with $\bar{N}$ described by equation (F.13).

The Itô increments satisfy the identities

$$(\mathrm{d}\hat{B}(t))^2 = (\mathrm{d}\hat{B}^\dagger(t))^2 = 0, \tag{F.17}$$

$$\mathrm{d}\hat{B}(t)\mathrm{d}\hat{B}^\dagger(t) = (\bar{N}+1)\mathrm{d}t, \tag{F.18}$$

$$\mathrm{d}\hat{B}^\dagger(t)\mathrm{d}\hat{B}(t) = \bar{N}\mathrm{d}t. \tag{F.19}$$

Furthermore, terms like $\mathrm{d}t\mathrm{d}\hat{B}$, $\mathrm{d}t\mathrm{d}\hat{B}^\dagger$, $\mathrm{d}t^2$ and higher orders are negligible, in direct analogy to classical considerations. By the help of these relations, one can derive the Itô rules of calculus

$$\mathrm{d}(\hat{a}\hat{b}) = \hat{a}\mathrm{d}\hat{b} + (\mathrm{d}\hat{a})\hat{b} + (\mathrm{d}\hat{a})(\mathrm{d}\hat{b}), \tag{F.20}$$

which obviously does not agree with the ordinary calculus.

F.2 STRATONOVICH CALCULUS

The **Stratonovich quantum stochastic integral** is defined by

$$(S)\ \int_{t_0}^{t}\hat{X}(t')\mathrm{d}\hat{B}(t') = \lim_{n\to\infty}\sum_{i=0}^{n}\frac{\hat{X}(t_i)+\hat{X}(t_{i+1})}{2}\left[\hat{B}(t_{i+1},t_0) - \hat{B}(t_i,t_0)\right], \tag{F.21}$$

where (S) labels the Stratonovich version of a stochastic integral for an arbitrary system operator $\hat{X}$. Please note, that this increment does not commute with $\hat{X}$, which can be directly verified by calculating the difference of the integrals under considerations of the causality condition (F.3)

$$(S)\ \int_{t_0}^{t}\hat{X}(t')\mathrm{d}\hat{B}(t') - (S)\ \int_{t_0}^{t}\mathrm{d}\hat{B}(t')\hat{X}(t') = \frac{\sqrt{\gamma}}{2}\int_{t_0}^{t}\mathrm{d}t'\left[\hat{X}(t'), \hat{c}(t')\right]. \tag{F.22}$$

F.2.1 Connection between Itô and Stratonovich stochastic integral

In order to formulate the Stratonovich version of a quantum stochastic differential equation, it is quite reasonable to study the connection between the integral definitions of Itô and Stratonovich. In doing so, we rewrite equation (F.21) in terms of the mean time $\bar{t}_i = (t_i + t_{i+1})/2$, leading to the integral equation

$$(S)\ \int_{t_0}^{t}\hat{X}(t')\mathrm{d}\hat{B}(t') = \lim_{n\to\infty}\left[\sum_{i=0}^{n}\hat{X}(\bar{t}_i)\big(\hat{B}(t_{i+1}) - \hat{B}(\bar{t}_i)\big) + \sum_{i=0}^{n}\hat{X}(\bar{t}_i)\big(\hat{B}(\bar{t}_i) - \hat{B}(t_i)\big)\right]. \tag{F.23}$$

In addition, we set

$$\hat{X}(\bar{t}_i) = \hat{X}(t_i) + \mathrm{d}\hat{X}(t_i), \tag{F.24}$$

where $\mathrm{d}\hat{X}(t_i)$ is specified by equation (F.16) and

$$\mathrm{d}t_i = \bar{t}_i - t_i, \tag{F.25}$$

$$\mathrm{d}\hat{B}(t_i) = \hat{B}(\bar{t}_i) - \hat{B}(t_i), \tag{F.26}$$

which will be valid to lowest order [144]. Thus, the Stratonovich stochastic integral (F.23) can be written as

$$\begin{aligned}(S)\int_{t_0}^{t} \hat{X}(t')\mathrm{d}\hat{B}(t') = \lim_{n\to\infty}\Bigg[&\sum_{i=0}^{n}\hat{X}(\bar{t}_i)\big(\hat{B}(t_{i+1})-\hat{B}(\bar{t}_i)\big)+\sum_{i=0}^{n}\hat{X}(t_i)\big(\hat{B}(\bar{t}_i)-\hat{B}(t_i)\big)\\ &-\sqrt{\gamma}\sum_{i=0}^{n}\left[\hat{X}(t_i),\hat{c}^\dagger(t_i)\right]\big(\hat{B}(\bar{t}_i)-\hat{B}(t_i)\big)\big(\hat{B}(\bar{t}_i)-\hat{B}(t_i)\big)\\ &+\sqrt{\gamma}\sum_{i=0}^{n}\left[\hat{X}(t_i),\hat{c}(t_i)\right]\big(\hat{B}^\dagger(\bar{t}_i)-\hat{B}^\dagger(t_i)\big)\big(\hat{B}(\bar{t}_i)-\hat{B}(t_i)\big)\Bigg].\end{aligned} \tag{F.27}$$

Considering the identities (F.17)-(F.19), one can express the Stratonovich integral in terms of the Itô integral (cf. equation (F.14)) via

$$(S)\int_{t_0}^{t}\hat{X}(t')\mathrm{d}\hat{B}(t') = (I)\int_{t_0}^{t}\hat{X}(t')\mathrm{d}\hat{B}(t') + \frac{1}{2}\sqrt{\gamma}\bar{N}\int_{t_0}^{t}\left[\hat{X}(t'),\hat{c}(t')\right]\mathrm{d}t'. \tag{F.28}$$

In the same way, we find

$$(S)\int_{t_0}^{t}\hat{X}(t')\mathrm{d}\hat{B}^\dagger(t') = (I)\int_{t_0}^{t}\hat{X}(t')\mathrm{d}\hat{B}^\dagger(t') - \frac{1}{2}\sqrt{\gamma}(\bar{N}+1)\int_{t_0}^{t}\left[\hat{X}(t'),\hat{c}^\dagger(t')\right]\mathrm{d}t', \tag{F.29}$$

$$(S)\int_{t_0}^{t}\mathrm{d}\hat{B}(t')\hat{X}(t') = (I)\int_{t_0}^{t}\hat{X}(t')\mathrm{d}\hat{B}(t') + \frac{1}{2}\sqrt{\gamma}(\bar{N}+1)\int_{t_0}^{t}\left[\hat{X}(t'),\hat{c}(t')\right]\mathrm{d}t', \tag{F.30}$$

$$(S)\int_{t_0}^{t}\mathrm{d}\hat{B}^\dagger(t')\hat{X}(t') = (I)\int_{t_0}^{t}\hat{X}(t')\mathrm{d}\hat{B}^\dagger(t') - \frac{1}{2}\sqrt{\gamma}\bar{N}\int_{t_0}^{t}\left[\hat{X}(t'),\hat{c}^\dagger(t')\right]\mathrm{d}t'. \tag{F.31}$$

With these connections between the integral representations of both, Stratonovich and Itô, we can specify the **Stratonovich** version of a **quantum stochastic differential equation**

$$\boxed{\begin{aligned}(S)\ \mathrm{d}\hat{a} = -\frac{\mathrm{i}}{\hbar}\left[\hat{a},\hat{H}_s\right]\mathrm{d}t - \frac{\gamma}{2}\left(\left[\hat{a},\hat{c}^\dagger\right]\hat{c}-\hat{c}^\dagger\left[\hat{a},\hat{c}\right]\right)\mathrm{d}t - \sqrt{\gamma}\left[\hat{a},\hat{c}^\dagger\right]\mathrm{d}\hat{B}(t)\\ +\sqrt{\gamma}\mathrm{d}\hat{B}^\dagger(t)\left[\hat{a},\hat{c}\right]\end{aligned}} \tag{F.32}$$

This can be proven by inserting the integral representation implicitly into equation (F.32), that is

$$\begin{aligned}(S)\int_{t_0}^{t}\mathrm{d}\hat{a} = -\frac{\mathrm{i}}{\hbar}(S)\int_{t_0}^{t}\left[\hat{a},\hat{H}_s\right]\mathrm{d}t - \frac{\gamma}{2}(S)\int_{t_0}^{t}\left(\left[\hat{a},\hat{c}^\dagger\right]\hat{c}-\hat{c}^\dagger\left[\hat{a},\hat{c}\right]\right)\mathrm{d}t\\ -\sqrt{\gamma}(S)\int_{t_0}^{t}\left[\hat{a},\hat{c}^\dagger\right]\mathrm{d}\hat{B}(t)+\sqrt{\gamma}(S)\int_{t_0}^{t}\mathrm{d}\hat{B}^\dagger(t)\left[\hat{a},\hat{c}\right].\end{aligned} \tag{F.33}$$

Using equation (F.28) and (F.31) in the second line of the Stratonovich equation (F.33) and evaluating the commutators, we find

$$\begin{aligned}(I)\ \mathrm{d}\hat{a} = -\frac{\mathrm{i}}{\hbar}\left[\hat{a},\hat{H}_s\right]\mathrm{d}t + \frac{\gamma}{2}(\bar{N}+1)(2\hat{c}^\dagger\hat{a}\hat{c}-\hat{a}\hat{c}^\dagger\hat{c}-\hat{c}^\dagger\hat{c}\hat{a})\mathrm{d}t\\ +\frac{\gamma}{2}\bar{N}(2\hat{c}\hat{a}\hat{c}^\dagger-\hat{a}\hat{c}\hat{c}^\dagger-\hat{c}\hat{c}^\dagger\hat{a})\mathrm{d}t - \sqrt{\gamma}\left[\hat{a},\hat{c}^\dagger\right]\mathrm{d}\hat{B}(t)+\sqrt{\gamma}\mathrm{d}\hat{B}^\dagger(t)\left[\hat{a},\hat{c}\right].\end{aligned} \tag{F.34}$$

The solution corresponds exactly to the Itô quantum stochastic differential equation (cf. equation (F.16)). Please note, that the Stratonovich QSDE (F.32) is again exactly the quantum Langevin equation form [148] and therefore justifies Itô's QSDE definition (F.16).

Furthermore, as a result of the Itô formalism, one can easily show that the Stratonovich version obeys the usual rules of calculus according to

$$(S)\ \mathrm{d}(\hat{a}\hat{b}) = (\mathrm{d}\hat{a})\hat{b} + \hat{a}\mathrm{d}\hat{b}. \tag{F.35}$$

F.3 FORMULATION OF ITÔ QSDES

Upon introducing Itô and Stratonovich QSDEs we are left with the technical problem of setting up an Itô QSDE from the knowledge of the total system described by the Hamiltonian (F.1). Former considerations of this section highlights the equivalent form of the Stratonovich equation and the quantum Langevin equation. Thus, from the knowledge of the quantum Langevin equation (F.2) we can directly specify the Stratonovich QSDE with increment $\mathrm{d}\hat{B} = \hat{b}_{\mathrm{in}}\mathrm{d}t$ yielding exactly equation (F.32). On the other hand, we are allowed to directly determine the Itô QSDE (F.16) from the knowledge of the Stratonovich form.

F.4 COMPARISON BETWEEN ITÔ AND STRATONOVICH

Table A1 summarizes relevant differences between the Itô and Stratonovich quantum stochastic differential equations. For further information, please have a look at [50].

Itô QSDE (F.16)	Stratonovich QSDE (F.32)
No natural physically motivated choice	Natural physical choice (equivalent to Langevin equation)
Increments commute with system operators	Increments do not commute with system operators
Special calculus	Ordinary calculus
No QSDE definition without knowledge about $\bar{N}$ and bath statistics	No integral equation definition without knowledge about QSDE
A quantum white noise theory	Also valid for non-white noise

Table A1: Comparison of Itô and Stratonovich QSDE [50].

G

DIFFERENTIAL EQUATION OF THE FOURTH-ORDER MOMENT OF THE QDSLD FIELD AMPLITUDES

In section 7.2 we analyzed the central second-order degree of coherence of light-emitting QDLSDs based on our microscopic theory introduced in chapter 5. In this context, we set up a differential equation for the internal field amplitudes $\langle \hat{a}_i^\dagger \hat{a}_k^\dagger \hat{a}_m \hat{a}_n \rangle$ (cf. equation (7.12)). This equation of motion itself depends on further fourth-order moments in terms of quantum dot coherences and field amplitudes. Their solutions are determined within the approximations listed in section 5.3.1. In general these approximations result in the factorization of averages (see equations (7.16)-(7.18)). The application of adiabatic elimination delivers the desired results, which can be inserted directly into the first-order differential equation (7.12). We find the general expression

$$
\begin{aligned}
\frac{\mathrm{d}}{\mathrm{d}t}\langle \hat{a}_i^\dagger \hat{a}_k^\dagger \hat{a}_m \hat{a}_n \rangle \approx & -\alpha_{ikmn}\langle \hat{a}_i^\dagger \hat{a}_k^\dagger \hat{a}_m \hat{a}_n \rangle + \sum_{j=1}^{M} g_i^j g_k^j g_m^{j*} g_n^{j*}\, \xi_{ikmn}^j \\
&+ \sum_{j=1}^{M} \sum_{\{k_s\}} w_j \Big[\frac{g_i^j g_s^{j*}}{\vartheta_{kmn}^j} \langle \hat{a}_s^\dagger \hat{a}_k^\dagger \hat{a}_m \hat{a}_n \rangle + \frac{g_k^j g_s^{j*}}{\vartheta_{imn}^j} \langle \hat{a}_i^\dagger \hat{a}_s^\dagger \hat{a}_m \hat{a}_n \rangle \\
&\qquad + \frac{g_m^{j*} g_s^j}{\vartheta_{nki}^{j*}} \langle \hat{a}_i^\dagger \hat{a}_k^\dagger \hat{a}_s \hat{a}_n \rangle + \frac{g_n^{j*} g_s^j}{\vartheta_{mki}^{j*}} \langle \hat{a}_i^\dagger \hat{a}_k^\dagger \hat{a}_m \hat{a}_s \rangle \Big] \\
&+ \sum_{j=1}^{M} \Big[\frac{g_i^j}{\vartheta_{kmn}^j} (g_m^{j*}\delta_{kn} + g_n^{j*}\delta_{km}) n_k + \frac{g_k^j}{\vartheta_{imn}^j} (g_m^{j*}\delta_{in} + g_n^{j*}\delta_{im}) n_i \\
&\qquad + \frac{g_m^{j*}}{\vartheta_{nki}^{j*}} (g_k^j \delta_{in} + g_i^j \delta_{kn}) n_n + \frac{g_n^{j*}}{\vartheta_{mki}^{j*}} (g_k^j \delta_{mi} + g_i^j \delta_{km}) n_m \Big] \sigma_{11}^j
\end{aligned}
\tag{G.1}
$$

with

$$
\begin{aligned}
\xi_{ikmn}^j = & 2\lambda_m^j \lambda_n^j \left(\frac{1}{\vartheta_{kmn}^j} + \frac{1}{\vartheta_{imn}^j} \right) + 2\lambda_k^{j*} \lambda_i^{j*} \left(\frac{1}{\vartheta_{nki}^{j*}} + \frac{1}{\vartheta_{mki}^{j*}} \right) + \lambda_k^{j*} \lambda_n^j \left(\frac{1}{\vartheta_{kmn}^j} + \frac{1}{\vartheta_{nki}^{j*}} \right) \\
&+ \lambda_k^{j*} \lambda_m^j \left(\frac{1}{\vartheta_{kmn}^j} + \frac{1}{\vartheta_{mki}^{j*}} \right) + \lambda_i^{j*} \lambda_n^j \left(\frac{1}{\vartheta_{imn}^j} + \frac{1}{\vartheta_{nki}^{j*}} \right) + \lambda_i^{j*} \lambda_m^j \left(\frac{1}{\vartheta_{imn}^j} + \frac{1}{\vartheta_{mki}^{j*}} \right)
\end{aligned}
\tag{G.2}
$$

and

$$
\lambda_i^j = \frac{n_i w^j + \sigma_{11}^j}{\Gamma^j/2 + \mathrm{i}\Delta_i^j}. \tag{G.3}
$$

H

SECOND-ORDER DEGREE OF COHERENCE OF QDSLDS

In this appendix we specify the temporal second-order degree of coherence $g^{(2)}(\tau)$ of our modeled QDSLD. In doing so, we first set up a fourth-order moment QSDE for the field operators with regard to time $t' > t$, $\langle \hat{a}_i^\dagger(t)\hat{a}_k^\dagger(t')\hat{a}_m(t')\hat{a}_n(t)\rangle_{t'}$, emphasized by the index t' at the bottom right of the quantum average bracket, $\langle ... \rangle_{t'}$. We apply the Itô derivation rule with respect to t' (see equation (F.20)) and find

$$\begin{aligned} \mathrm{d}\langle \hat{a}_i^\dagger(t)\hat{a}_k^\dagger(t')\hat{a}_m(t')\hat{a}_n(t)\rangle_{t'} =& \langle \hat{a}_i^\dagger(t)\mathrm{d}\hat{a}_k^\dagger(t')\hat{a}_m(t')\hat{a}_n(t)\rangle + \langle \hat{a}_i^\dagger(t)\hat{a}_k^\dagger(t')\mathrm{d}\hat{a}_m(t')\hat{a}_n(t)\rangle \\ &+ \langle \hat{a}_i^\dagger(t)(\mathrm{d}\hat{a}_k^\dagger(t'))(\mathrm{d}\hat{a}_m(t'))\hat{a}_n(t)\rangle. \end{aligned} \tag{H.1}$$

Considering quantum causality and the fact that the increments commute with and are statistically independent of the system operators at the same time [50], the first term on the right-hand side of equation (H.1) under the assumption of vacuum input reads

$$\begin{aligned} \langle \hat{a}_i^\dagger(t)\mathrm{d}\hat{a}_k^\dagger(t')\hat{a}_m(t')\hat{a}_n(t)\rangle =& \left[\mathrm{i}\Delta_k - \frac{\gamma^l + \gamma^r}{2}\right] \langle \hat{a}_i^\dagger(t)\hat{a}_k^\dagger(t')\hat{a}_m(t')\hat{a}_n(t)\rangle \mathrm{d}t' \\ &+ \sum_{j=1}^{M} g_k^j \langle \hat{a}_i^\dagger(t)\hat{\sigma}_{21}^{j\dagger}(t')\hat{a}_m(t')\hat{a}_n(t)\rangle \mathrm{d}t'. \end{aligned} \tag{H.2}$$

The second term in equation (H.1) is determined in the same way whereas the last term vanishes under consideration of absent correlations between left and right bath modes, $\langle \mathrm{d}\hat{B}^{L(\dagger)}\mathrm{d}\hat{B}^{R(\dagger)}\rangle = 0$, as well as vacuum input. Equation (H.1) can be written as

$$\begin{aligned} \mathrm{d}\langle \hat{a}_i^\dagger(t)\hat{a}_k^\dagger(t')\hat{a}_m(t')\hat{a}_n(t)\rangle_{t'} =& -\left[\mathrm{i}(\Delta_m - \Delta_k) + \gamma^l + \gamma^r\right] \langle \hat{a}_i^\dagger(t)\hat{a}_k^\dagger(t')\hat{a}_m(t')\hat{a}_n(t)\rangle \mathrm{d}t' \\ &+ \sum_{j=1}^{M} \Big[g_k^j \langle \hat{a}_i^\dagger(t)\hat{\sigma}_{21}^{j\dagger}(t')\hat{a}_m(t')\hat{a}_n(t)\rangle \\ &\quad + g_m^{j*} \langle \hat{a}_i^\dagger(t)\hat{a}_k^\dagger(t')\hat{\sigma}_{21}^{j}(t')\hat{a}_n(t)\rangle \Big] \mathrm{d}t'. \end{aligned} \tag{H.3}$$

This solution includes averages between quantum dot transitions and field operators. We consider the second correlation term in equation (H.3), which is described by the QSDE

$$\begin{aligned} \mathrm{d}\langle \hat{a}_i^\dagger(t)\hat{\sigma}_{21}^{j\dagger}(t')\hat{a}_m(t')\hat{a}_n(t)\rangle_{t'} =& -\left(\mathrm{i}\Delta_m^j + \frac{\Gamma^j}{2}\right) \langle \hat{a}_i^\dagger(t)\hat{\sigma}_{21}^{j\dagger}(t')\hat{a}_m(t')\hat{a}_n(t)\rangle \mathrm{d}t' \\ &+ \sum_{\{k_r\}} g_r^{j*} \langle \hat{a}_i^\dagger(t)\hat{w}^j(t')\hat{a}_r^\dagger(t')\hat{a}_m(t')\hat{a}_n(t)\rangle \mathrm{d}t' \\ &+ \sum_{j=1}^{M} g_m^{j*} \langle \hat{a}_i^\dagger(t)\hat{\sigma}_{11}^{j}(t')\hat{a}_n(t)\rangle \mathrm{d}t' \end{aligned} \tag{H.4}$$

with

$$\Delta_m^j = \Delta_m - \delta\omega_{12}^j, \qquad \Gamma^j = \Gamma_{21}^j + R + \gamma^l + \gamma^r. \tag{H.5}$$

We follow the assumptions made in section 5.3.1 and decorrelate quantum dot populations and internal waveguide modes by making the replacements,

$$\langle \hat{a}_i^\dagger(t)\hat{w}^j(t')\hat{a}_k^\dagger(t')\hat{a}_m(t')\hat{a}_n(t)\rangle \approx w^j(t')\langle \hat{a}_i^\dagger(t)\hat{a}_k^\dagger(t')\hat{a}_m(t')\hat{a}_n(t)\rangle, \tag{H.6}$$

$$\langle \hat{a}_i^\dagger(t)\hat{\sigma}_{21}^{j\dagger}(t')\hat{\sigma}_{21}^{j'}(t')\hat{a}_n(t)\rangle \approx \sigma_{11}^j(t')\langle \hat{a}_i^\dagger(t)\hat{a}_n(t)\rangle\delta_{jj'} + \langle \hat{a}_i^\dagger(t)\hat{\sigma}_{21}^{j'}(t')\rangle\langle \hat{\sigma}_{21}^{j\dagger}(t')\hat{a}_n(t)\rangle, \tag{H.7}$$

with $\langle \hat{a}_i^\dagger(t)\hat{\sigma}_{21}^{j'}(t')\rangle$ specified in equation (6.8). Finally, we adiabatically eliminate the average $\langle \hat{a}_i^\dagger(t)\hat{\sigma}_{21}^{j\dagger}(t')\hat{a}_m(t')\hat{a}_n(t)\rangle$. In the same way we can calculate the last correlation term on the right-hand side of equation (H.3). Again, we only consider coupling strength terms which are at most of the order of 2. Therefore, the Itô QSDE (H.3) reduces to

$$\begin{aligned}\frac{\mathrm{d}}{\mathrm{d}t'}\langle \hat{a}_i^\dagger(t)\hat{a}_k^\dagger(t')\hat{a}_m(t')\hat{a}_n(t)\rangle =& -\left[\mathrm{i}(\Delta_m-\Delta_k)+\gamma^l+\gamma^r\right]\langle \hat{a}_i^\dagger(t)\hat{a}_k^\dagger(t')\hat{a}_m(t')\hat{a}_n(t)\rangle\\ &+\sum_{j=1}^{M}\frac{\sum_{\{k_r\}} g_k^j g_r^{j*} w^j(t')\langle \hat{a}_i^\dagger(t)\hat{a}_r^\dagger(t')\hat{a}_m(t')\hat{a}_n(t)\rangle}{\Lambda_m^j}\\ &+\sum_{j=1}^{M}\frac{\sum_{\{k_r\}} g_m^{j*} g_r^j w^j(t')\langle \hat{a}_i^\dagger(t)\hat{a}_k^\dagger(t')\hat{a}_r(t')\hat{a}_n(t)\rangle}{\Lambda_k^{j*}}\\ &+\sum_{j=1}^{M} g_k^j g_m^{j*}\sigma_{11}^j(t')n_i(t)\delta_{in}\Big(\frac{1}{\Lambda_m^j}+\frac{1}{\Lambda_k^{j*}}\Big)\end{aligned} \tag{H.8}$$

with

$$\Lambda_i^j = \Gamma^j/2 + \mathrm{i}\Delta_i^j. \tag{H.9}$$

This equation can be separated into diagonal and off-diagonal elements in terms of the coupling strength. We assume that the off-diagonal ones weakly contribute compared to the diagonal elements in direct analogy to the assumption made in section 7. Thus, in first-order perturbation theory, we can neglect the off-diagonal terms. Furthermore, we replace the inversion $w^j(t')$ by its stationary solution w^{js}, $w^j(t') \approx w^{js}$, analog to the calculation of $g^{(2)}(0)$ in section 7.2. The equation of motion for the fourth-order moment reads

$$\lim_{t\to\infty}\frac{\mathrm{d}}{\mathrm{d}t'}\langle \hat{a}_i^\dagger(t)\hat{a}_k^\dagger(t')\hat{a}_m(t')\hat{a}_n(t)\rangle = -\alpha_{km}\langle \hat{a}_i^\dagger(t)\hat{a}_k^\dagger(t')\hat{a}_m(t')\hat{a}_n(t)\rangle + \beta_{ikm}\delta_{in} \tag{H.10}$$

with

$$\alpha_{km} = \mathrm{i}(\Delta_m-\Delta_k)+\gamma^l+\gamma^r-\sum_{j=1}^{M} w^{js}\left(\frac{|g_k^j|^2}{\Lambda_m^j}+\frac{|g_m^j|^2}{\Lambda_k^{j*}}\right), \tag{H.11}$$

$$\beta_{ikm} = \sum_{j=1}^{M} g_k^j g_m^{j*}\sigma_{11}^{js}n_i^s\frac{\mathrm{i}(\Delta_m-\Delta_k)+\Gamma^j}{\Lambda_m^j\Lambda_k^{j*}}. \tag{H.12}$$

This differential equation is solvable by the method of variation of constants with $\tau = t'-t > 0$, which leads to

$$\lim_{t\to\infty}\langle \hat{a}_i^\dagger(t)\hat{a}_k^\dagger(t+\tau)\hat{a}_m(t+\tau)\hat{a}_n(t)\rangle = \frac{\beta_{ikm}}{\alpha_{km}}\delta_{in} + e^{-\alpha_{km}\tau}\left(\langle \hat{a}_i^\dagger\hat{a}_k^\dagger\hat{a}_m\hat{a}_n\rangle_s - \frac{\beta_{ikm}}{\alpha_{km}}\delta_{in}\right). \tag{H.13}$$

The resulting temporal second-order correlation function is given by

$$g^{(2)}(\tau) \simeq \frac{G^{(2)}(\tau)}{|G^{(1)}(0)|^2} = \frac{\sum_{\{k_i,k_k,k_m,k_n>0\}}\mathrm{w}_{ikmn}^s\frac{\beta_{ikm}}{\alpha_{km}}\delta_{in}\left(1-e^{-\alpha_{km}|\tau|}\right)}{\sum_{\{k_i,k_k>0\}}\mathrm{w}_{ikik}^s n_i^s n_k^s} + g^{(2)}(0)e^{-\alpha_{km}|\tau|}, \tag{H.14}$$

with w_{ikmn} specified by equations (7.8) and (7.11). Obviously, $g^{(2)}(\tau)$ depends on the central second-order degree of coherence, calculated in section 7. Please note, that we utilized the symmetry relation $g^{(2)}(\tau) = g^{(2)}(-\tau)$ (cf. equation (2.114)). This analytical expression of $g^{(2)}(\tau)$ depends explicitly on the stationary photon number of each mode already studied in detail in section 5.3.2. It shows an exponential decay for increasing time delay.

H.1 SINGLE-MODE QDSLD

We consider the special case of a single-mode QDSLD composed of M identical QDs. Here, the temporal second-order degree of coherence (cf. equation (H.14)) reduces to

$$g^{(2)}(\tau) = \frac{\sigma_{11}^{s}}{n^{s}} \left[\frac{(\gamma^{l}+\gamma^{r})(\Delta^{2}+(\Gamma/2)^{2})}{M\Gamma|g|^{2}} - w^{s} \right]^{-1} \left(1-e^{-\alpha|\tau|}\right) + g^{(2)}(0)e^{-\alpha|\tau|}. \tag{H.15}$$

Figure 8.1 shows $g^{(2)}(\tau)$ with the same set of parameters as already chosen in figure 7.2 for the central second-order degree of coherence. The red line corresponds to the resonant case $\Delta = 0$. The blue line shows $g^{(2)}(\tau)$ for a detuning of $\Delta = 10^{3}\gamma$. Clearly, an exponential decay is observable, ranging from the maximum value of $g^{(2)}(\tau = 0, \Delta = 10^{3}\gamma) = 2$ (blue) and $g^{(2)}(\tau = 0, \Delta = 0) = 1.33$ (red) to one, $\lim_{\tau\to\infty} g^{(2)}(\tau) = 1$. The coherence time τ_c for the resonant case is much larger than the coherence time for $\Delta = 10^{3}\gamma$. Beside the reduced central second-order degree of coherence for zero detuning, $g^{(2)}(\tau = 0, \Delta = 0) = 1.33$, this increasing coherence time emphasizes the noise suppressed character of the QDSLD with the special set of parameters.

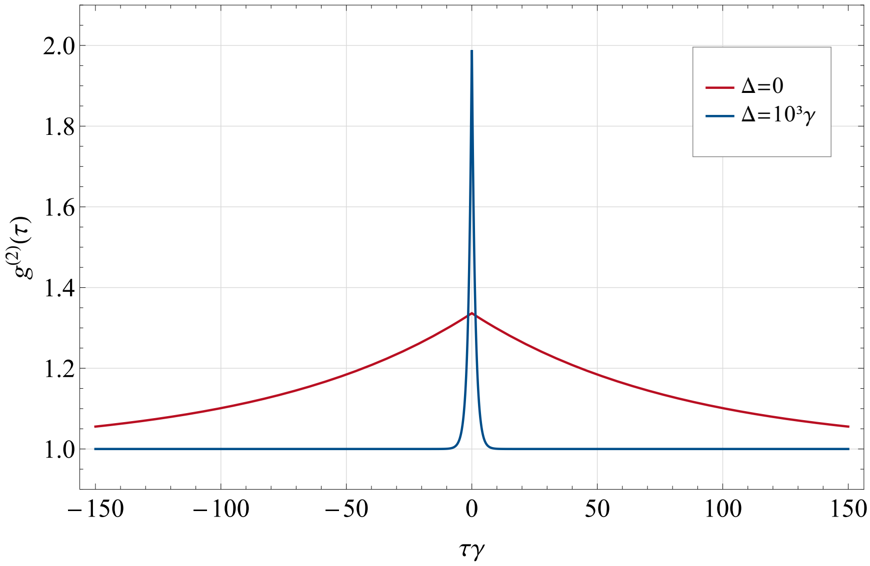

Figure 8.1: Second-order degree of coherence $g^{(2)}(\tau)$ as a function of scaled time delay $\tau\gamma$ of a single-mode QDSLD with $M = 150$ identical quantum dots, coupling constant $g = 7.8\gamma$ and detuning $\Delta = 0$ (red) and $\Delta = 10^{3}\gamma$ (blue). The decay and pumping rates are $\gamma^{l} = \gamma^{r} = \gamma$, $\gamma_{21} = 139\gamma$, $\gamma_{10} = 250\gamma$ and $R = 1200\gamma$.

BIBLIOGRAPHY

[1] M. Blazek and W. Elsäßer, "Coherent and thermal light: Tunable hybrid states with second-order coherence without first-order coherence," *Phys. Rev. A*, vol. 84, p. 063840, 2011.

[2] T. H. Maiman, "Stimulated optical radiation in ruby," *Nature*, vol. 187, pp. 493–494, 1960.

[3] R. J. Glauber, "Photon correlations," *Phys. Rev. Lett.*, vol. 10, pp. 84–86, 1963.

[4] R. J. Glauber, "The quantum theory of optical coherence," *Phys. Rev.*, vol. 130, pp. 2529–2539, 1963.

[5] R. J. Glauber, "Coherent and incoherent states of the radiation field," *Phys. Rev.*, vol. 131, pp. 2766–2788, 1963.

[6] R. J. Glauber, *The quantum theory of optical coherence*. Wiley-VCH Verlag GmbH & Co. KGaA, 2007.

[7] R. J. Glauber, "One hundred years of light quanta," *Nobel Lecture*, 2005.

[8] M. Lax, "Quantum noise. X. density-matrix treatment of field and population-difference fluctuations," *Phys. Rev.*, vol. 157, pp. 213–231, 1967.

[9] M. Lax and W. H. Louisell, "Quantum noise. XII. Density-operator treatment of field and population fluctuations," *Phys. Rev.*, vol. 185, pp. 568–591, 1969.

[10] H. Haken, *Laser theory*. Springer-Verlag, 1984.

[11] H. Haken, *Light: Laser light dynamics*. No. Bd. 2, North-Holland Publishing Company, 1985.

[12] R. Graham and H. Haken, "Quantum theory of light propagation in a fluctuating laser-active medium," *Zeitschrift für Physik A Hadrons and Nuclei*, vol. 213, no. 5, pp. 420–450, 1968.

[13] M. O. Scully and W. E. Lamb, "Quantum theory of an optical maser. I. General theory," *Phys. Rev.*, vol. 159, pp. 208–226, 1967.

[14] M. Sargent, M. Scully, and W. Lamb, *Laser physics*. Addison-Wesley Pub. Co., 1976.

[15] R. Hanbury Brown and R. Q. Twiss, "Correlation between photons in two coherent beams of light," *Nature*, vol. 177, pp. 27–29, 1956.

[16] H. J. Carmichael and D. F. Walls, "Proposal for the measurement of the resonant Stark effect by photon correlation techniques," *J. Phys. B: Atom. Molec. Phys.*, vol. 9, no. 4, p. L43, 1976.

[17] H. J. Kimble, M. Dagenais, and L. Mandel, "Photon antibunching in resonance fluorescence," *Phys. Rev. Lett.*, vol. 39, pp. 691–695, 1977.

[18] P. Michler, A. Imamoglu, M. D. Mason, P. J. Carson, G. F. Strouse, and S. K. Buratto, "Quantum correlation among photons from a single quantum dot at room temperature," *Nature*, vol. 406, pp. 968–970, 2000.

[19] T. H. Stievater, X. Li, D. G. Steel, D. Gammon, D. S. Katzer, D. Park, C. Piermarocchi, and L. J. Sham, "Rabi oscillations of excitons in single quantum dots," *Phys. Rev. Lett.*, vol. 87, p. 133603, 2001.

[20] A. Wallraff, D. I. Schuster, A. Blais, L. Frunzio, R. S. Huang, J. Majer, S. Kumar, S. M. Girvin, and R. J. Schoelkopf, "Strong coupling of a single photon to a superconducting qubit using circuit quantum electrodynamics," *Nature*, vol. 431, pp. 162–167, 2004.

[21] T. Basché, W. E. Moerner, M. Orrit, and H. Talon, "Photon antibunching in the fluorescence of a single dye molecule trapped in a solid," *Phys. Rev. Lett.*, vol. 69, pp. 1516–1519, 1992.

[22] R. Brouri, A. Beveratos, J.-P. Poizat, and P. Grangier, "Photon antibunching in the fluorescence of individual color centers in diamond," *Opt. Lett.*, vol. 25, no. 17, pp. 1294–1296, 2000.

[23] M. A. Nielsen and I. L. Chuang, *Quantum computation and quantum information: 10th anniversary edition.* Cambridge University Press, 2010.

[24] M. C. Amann and J. Boeck, "High-efficiency superluminescent diodes for optical-fibre transmission," *Electronics Letters*, vol. 15, no. 2, pp. 41–42, 1979.

[25] K. Böhm, R. Ulrich, P. Russer, and E. Weidel, "Low-noise fiber-optic rotation sensing," *Opt. Lett.*, vol. 6, no. 2, pp. 64–66, 1981.

[26] X. Li, Q. Sun, J. Wo, M. Zhang, and D. Liu, "Hybrid TDM/WDM-based fiber-opticptic sensor network for perimeter intrusion detection," *Journal of Lightwave Technology*, vol. 30, no. 8, pp. 1113–1120, 2012.

[27] R. Slavík and J. Homola, "Ultrahigh resolution long range surface plasmon-based sensor," *Sensors and Actuators B: Chemical*, vol. 123, no. 1, pp. 10 – 12, 2007.

[28] D. Huang, E. A. Swanson, C. P. Lin, J. S. Schuman, W. G. Stinson, W. Chang, M. R. Hee, T. Flotte, K. Gregory, C. A. Puliafito, and J. G. Fujimoto, "Optical coherence tomography," *Science*, vol. 254, no. 5035, pp. 1178–1181, 1991.

[29] F. Boitier, A. Godard, E. Rosencher, and C. Fabre, "Measuring photon bunching at ultrashort timescale by two-photon absorption in semiconductors," *Nature Physics*, vol. 5, pp. 267–270, 2009.

[30] F. Boitier, *Absorption à deux photons et effets de correlation quantique dans les semiconducteurs*. PhD thesis, Office Nat. d'études et de Recherchers Aérospat., Châtillon Cedex, 2011.

[31] R. J. Glauber and M. Lewenstein, "Quantum optics of dielectric media," *Phys. Rev. A*, vol. 43, pp. 467–491, 1991.

[32] W. Vogel and D. G. Welsch, *Quantum optics*. Wiley, 2006.

[33] M. Wubs, L. G. Suttorp, and A. Lagendijk, "Multipole interaction between atoms and their photonic environment," *Phys. Rev. A*, vol. 68, p. 013822, 2003.

[34] O. Heaviside, *Electrical Papers*. No. Bd. 1 in AMS Chelsea Publishing Series, American Mathematical Society, 2003.

[35] J. C. Maxwell, "A dynamical theory of the elektromagnetic field," *Philos. Trans. Roy. Soc. London*, vol. 155, pp. 459–512, 1865.

[36] J. D. Jackson, *Classical electrodynamics*. Wiley, 2012.

[37] C. C. Tannoudji, J. D. Roc, and G. Grynberg, *Photons and atoms: Introduction to quantum electrodynamics*. New York: Wiley, 1989.

[38] R. Loudon, *The quantum theory of light*. OUP Oxford, 2000.

[39] W. H. Louisell, *Quantum statistical properties of radiation*. John Wiley & Sons Canada, Limited, 1973.

[40] R. Loudon, *The quantum theory of light*. Oxford university press, 1978.

[41] D. F. Walls and G. J. Milburn, *Quantum optics*. Springer Berlin Heidelberg, 2012.

[42] M. O. Scully and M. S. Zubairy, *Quantum optics*. Cambridge University Press, 1997.

[43] J. Garrison and R. Chiao, *Quantum optics*. OUP Oxford, 2008.

[44] E. Schrödinger, "Der stetige Übergang von der Mikro- zur Makromechanik," *Naturwissenschaften*, vol. 14, pp. 664–666, 1926.

[45] H. Weyl, *The theory of groups and quantum mechanics*. Dover books on advanced mathematics, Dover Publications, 1950.

[46] R. M. Wilcox, "Exponential operators and parameter differentiation in quantum physics," *J. Math. Phys.*, vol. 8, no. 4, pp. 962–982, 1967.

[47] E. Wigner, "On the quantum correction for thermodynamic equilibrium," *Phys. Rev.*, vol. 40, pp. 749–759, 1932.

[48] W. P. Schleich, *Quantum optics in phase space*. Berlin: Wiley-VCH Verlag GmbH & Co, 2001.

[49] L. Mandel and E. Wolf, *Optical coherence and quantum optics*. Cambridge University Press, 1995.

[50] C. Gardiner and P. Zoller, *Quantum noise*. Springer, 2000.

[51] C. C. Tannoudji, J. D. Roc, and G. Grynberg, *Atom - photon interactions: Basic process and appilcations*. WILEY-VCH Verlag GmbH & Co, 2008.

[52] R. J. Glauber, "The quantum theory of optical coherence," *Phys. Rev.*, vol. 130, pp. 2529–2539, 1963.

[53] M. D. Srinivas and E. B. Davies, "Photon counting probabilities in quantum optics," *Optica Acta: International Journal of Optics*, vol. 28, no. 7, pp. 981–996, 1981.

[54] P. Lambropoulos and D. Petrosyan, *Fundamentals of quantum optics and quantum information*. Springer Berlin Heidelberg, 2007.

[55] N. Wiener, "Generalized harmonic analysis," *Acta Math.*, vol. 55, pp. 117–258, 1930.

[56] A. Khintchine, “Korrelationstheorie der stationären stochastischen Prozesse,” *Mathematische Annalen*, vol. 109, pp. 604–615, 1934.

[57] I. Hertel and C. Schulz, *Atoms, molecules and optical physics 2: Molecules and photons - Spectroscopy and collisions*. Springer Berlin Heidelberg, 2014.

[58] L. Mandel and E. Wolf, “The measures of bandwidth and coherence time in optics,” *Proceedings of the Physical Society*, vol. 80, no. 4, p. 894, 1962.

[59] L. Mandel, “Fluctuations of photon beam: The distribution of the photo-electrons,” *Proc. Phys. Soc.*, vol. 74, pp. 233–243, 1959.

[60] F. Friedrich, “Hybrid coherent light: Modeling quantum-dot superluminescent diodes,” Master’s thesis, Technische Universität Darmstadt, 2013.

[61] F. Jahnke, *Quantum optics with semiconductor nanostructures*. Elsevier, 2012.

[62] L. Gao-xiang and P. Jin-sheng, *Introduction to modern quantum optics*. World Scientific Publishing Company, 1998.

[63] H. J. Kimble and L. Mandel, “Theory of resonance fluorescence,” *Phys. Rev. A*, vol. 13, pp. 2123–2144, 1976.

[64] H. Paul, “Photon antibunching,” *Rev. Mod. Phys.*, vol. 54, pp. 1061–1102, 1982.

[65] J. R. Klauder, M. R. Strayer, and D. Feng, *Coherent states: Past, present and future - Proceedings of the international symposium*. World Scientific Publishing Company, 1994.

[66] Z. Yuan, B. E. Kardynal, R. M. Stevenson, A. J. Shields, C. J. Lobo, K. Cooper, N. S. Beattie, D. A. Ritchie, and M. Pepper, “Electrically driven single-photon source,” *Science*, vol. 295, no. 5552, pp. 102–105, 2002.

[67] K. J. McNeil and D. F. Walls, “Possibility of observing enhanced photon bunching from two photon emission,” *Physics Letters A*, vol. 51, no. 4, pp. 233 – 234, 1975.

[68] N. B. Grosse, T. Symul, M. Stobińska, T. C. Ralph, and P. K. Lam, “Measuring photon antibunching from continuous variable sideband squeezing,” *Phys. Rev. Lett.*, vol. 98, p. 153603, 2007.

[69] F. Boitier, A. Godard, N. Dubreuil, P. Delaye, C. Fabre, and R. Rosencher, “Photon extrabunching in ultrabright twin beams measured by two-photon counting in a semiconductor,” *Nat. Comm.*, vol. 2, 2011.

[70] P. Hong, J. Liu, and G. Zhang, “Two-photon superbunching of thermal light via multiple two-photon path interference,” *Phys. Rev. A*, vol. 86, p. 013807, 2012.

[71] A. Gatti, E. Brambilla, M. Bache, and L. A. Lugiato, “Ghost imaging with thermal light: Comparing entanglement and classical correlation,” *Phys. Rev. Lett.*, vol. 93, p. 093602, 2004.

[72] D. V. Strekalov, A. V. Sergienko, D. N. Klyshko, and Y. H. Shih, “Observation of two-photon “ghost” interference and diffraction,” *Phys. Rev. Lett.*, vol. 74, pp. 3600–3603, 1995.

[73] S. Hartmann, A. Molitor, and W. Elsäßer, "Ultrabroadband ghost imaging exploiting optoelectronic amplified spontaneous emission and two-photon detection," *Opt. Lett.*, vol. 40, no. 24, pp. 5770–5773, 2015.

[74] M. Blazek, *Thermisch und kohärent: Erzeugung neuartiger Lichtzustände mittels Quantenpunkt-Superlumineszenzdioden*. PhD thesis, Technische Universität Darmstadt, 2011.

[75] S. Blumenstein, *Classical ghost imaging with opto-electronic light sources: novel and highly incoherent concepts*. PhD thesis, Technische Universität Darmstadt, 2017.

[76] T. Lee, C. A. J. Burrus, and B. I. Miller, "A stripe-geometry double-heterostructure amplified-spontaneous-emission (superluminescent) diode," *IEEE J. Quantum Electron.*, vol. QE-9, pp. 820–828, 1973.

[77] C. K. Hitzenberger, M. Danner, W. Drexler, and A. F. Fercher, "Measurement of the spatial coherence of superluminescent diodes," *J. Mod. Opt.*, vol. 46, no. 12, pp. 1763–1774, 1999.

[78] Z. Y. Zhang, R. A. Hogg, X. Q. Lv, and Z. G. Wang, "Self-assembled quantum-dot superluminescent light-emitting diodes," *Adv. Opt. Photon.*, vol. 2, no. 2, pp. 201–228, 2010.

[79] B. E. A. Saleh and M. C. Teich, *Fundamentals of photonics*. Wiley, 2007.

[80] P. Michler, *Quantum qots for quantum information technologies*. Springer, 2017.

[81] U. Woggon, *Optical properties of semiconductor quantum dots*. Springer, 1997.

[82] J. Cibert, P. M. Petroff, G. J. Dolan, S. J. Pearton, A. C. Gossard, and J. H. English, "Optically detected carrier confinement to one and zero dimension in GaAs quantum well wires and boxes," *Applied Physics Letters*, vol. 49, no. 19, pp. 1275–1277, 1986.

[83] O. Stier, M. Grundmann, and D. Bimberg, "Electronic and optical properties of strained quantum dots modeled by 8-band $\mathrm{k} \cdot \mathrm{p}$ theory," *Phys. Rev. B*, vol. 59, pp. 5688–5701, 1999.

[84] W. E. Buhro and V. L. Colvin, "Semiconductor nanocrystals: Shape matters," *Nat Mater*, vol. 2, pp. 138–139, 2003.

[85] Y. Arakawa and H. Sakaki, "Multidimensional quantum well laser and temperature dependence of its threshold current," *Applied Physics Letters*, vol. 40, no. 11, pp. 939–941, 1982.

[86] M. Grundmann, *Nano-optoelectronics*. Berlin: Springer, 2002.

[87] J. Lee, D. Son, T. K. Ahn, H. Shin, I. Y. Kim, S. Hwang, M. J. Ko, S. Sul, H. Han, and N. Park, "Quantum-dot-sensitized solar cell with unprecedentedly high photocurrent," *Scientific Reports*, vol. 3, no. 1050, 2013.

[88] S. J. Rosenthal, J. C. Chang, O. Kovtun, J. R. McBride, and I. D. Tomlinson, "Biocompatible quantum dots for biological applications," *Chemistry & Biology*, vol. 18, no. 1, pp. 10 – 24, 2011.

[89] J. C. Blakesley, P. See, A. J. Shields, B. E. Kardynał, P. Atkinson, I. Farrer, and D. A. Ritchie, "Efficient single photon detection by quantum dot resonant tunneling diodes," *Phys. Rev. Lett.*, vol. 94, p. 067401, 2005.

[90] M. Bayer, P. Hawrylak, K. Hinzer, S. Fafard, M. Korkusinski, Z. R. Wasilewski, O. Stern, and A. Forchel, “Coupling and entangling of quantum states in quantum dot molecules,” *Science*, vol. 291, no. 5503, pp. 451–453, 2001.

[91] M. Veldhorst, J. C. C. Hwang, C. H. Yang, A. W. Leenstra, B. de Ronde, J. P. Dehollain, J. T. Muhonen, F. E. Hudson, K. M. Itoh, A. Morello, and A. S. Dzurak, “An addressable quantum dot qubit with fault-tolerant control-fidelity,” *Nature Nanotechnology*, vol. 9, p. 981–985, 2014.

[92] I. N. Stranski and L. Krastanow, “Zur Theorie der orientierten Ausscheidung von Ionenkristallen aufeinander,” *Monatshefte für Chemie und verwandte Teile anderer Wissenschaften*, vol. 71, no. 1, pp. 351–364, 1937.

[93] M. Grundmann, J. Christen, N. N. Ledentsov, J. Böhrer, D. Bimberg, S. S. Ruvimov, ‡, P. Werner, U. Richter, U. Gösele, J. Heydenreich, V. M. Ustinov, A. Y. Egorov, A. E. Zhukov, P. S. Kop’ev, and Z. I. Alferov, “Ultranarrow luminescence lines from single quantum dots,” *Phys. Rev. Lett.*, vol. 74, pp. 4043–4046, 1995.

[94] A. L. Efros, D. J. Lockwood, and L. Tsybeskov, *Semiconductor nanocrystals: From basic principles to applications*. Nanostructure Science and Technology, Springer US, 2013.

[95] L. A. Banyai and S. W. Koch, *Semiconductor quantum dots*. World Scientific Publishing Company, 1993.

[96] Z. Y. Zhang, X. Q. Meng, P. Jin, C. M. Li, S. C. Qu, B. Xu, X. L. Ye, and Z. G. Wang, “A novel application to quantum dot materials to the active region of superluminescent diodes,” *Journal of Crystal Growth*, vol. 243, no. 1, pp. 25 – 29, 2002.

[97] A. F. Fercher, “Optical coherence tomography,” *Journal of Biomedical Optics*, vol. 1, no. 2, pp. 157–173, 1996.

[98] V. R. Shidlovski and J. Wei, “Superluminescent diodes for optical coherence tomography,” *Proc. SPIE*, vol. 4648, pp. 139–147, 2002.

[99] C. Velez, L. Occhi, and M. B. Raschle, “Superluminescent LEDs enter the mainstream,” *Phot. Spectra*, vol. 39, 2005.

[100] P. D. L. Judson, K. M. Groom, D. T. D. Childs, M. Hopkinson, N. Krstajic, and R. A. Hogg, “Maximising performance of optical coherence tomography systems using a multi-section chirped quantum dot superluminescent diode,” *Microelectron. J.*, vol. 40, no. 3, pp. 588 – 591, 2009. Workshop of Recent Advances on Low Dimensional Structures and Devices (WRA-LDSD).

[101] P. Urquhart, O. G. Lopez, G. Boyen, and A. Bruckmann, “Optical amplifiers for telecommunications,” *Int. Signal Processing*, pp. 1–6, 2007.

[102] O. Çelikel and S. E. San, “Design details and characterization of all digital closed-loop interferometric fiber optic gyroscope with superluminescent light emitting diode,” *Optical Review*, vol. 16, no. 1, pp. 35–43, 2009.

[103] T. B. Pittman, Y. H. Shih, D. V. Strekalov, and A. V. Sergienko, “Optical imaging by means of two-photon quantum entanglement,” *Phys. Rev. A*, vol. 52, pp. R3429–R3432, 1995.

[104] S. Kuhn, S. Hartmann, and W. Elsäßer, “Photon-statistics-based classical ghost imaging with one single detector,” *Opt. Lett.*, vol. 41, no. 12, pp. 2863–2866, 2016.

[105] S. Hartmann and W. Elsäßer, "A novel semiconductor-based, fully incoherent amplified spontaneous emission light source for ghost imaging," *Sci. Rep.*, vol. 7, p. 41866, 2017.

[106] M. Blazek, S. Hartmann, A. Molitor, and W. Elsäßer, "Unifying intensity noise and second-order coherence properties of amplified spontaneous emission sources," *Opt. Lett.*, vol. 36, no. 17, pp. 3455–3457, 2011.

[107] M. Blazek and W. Elsäßer, "Emission state hierarchy governed coherence and intensity noise properties of quantum dot superluminescent diodes," *IEEE J. Quantum Electron.*, vol. 48, p. 1578, 2012.

[108] G. A. Alphonse, D. B. Gilbert, M. G. Harvey, and M. Ettenberg, "High-power superluminescent diodes," *IEEE Journal of Quantum Electronics*, vol. 24, no. 12, pp. 2454–2457, 1988.

[109] H. A. M. Leymann, C. Hopfmann, F. Albert, A. Foerster, M. Khanbekyan, C. Schneider, S. Höfling, A. Forchel, M. Kamp, J. Wiersig, and S. Reitzenstein, "Intensity fluctuations in bimodal micropillar lasers enhanced by quantum-dot gain competition," *Phys. Rev. A*, vol. 87, p. 053819, 2013.

[110] M. Göppert-Mayer, "Über Elementarakte mit zwei Quantensprüngen," *Annalen der Physik*, vol. 401, no. 3, pp. 273–294, 1931.

[111] B. R. Mollow, "Two-photon absorption and field correlation functions," *Phys. Rev.*, vol. 175, pp. 1555–1563, 1968.

[112] F. Boitier, A. Godard, N. Dubreuil, P. Delaye, C. Fabre, and E. Rosencher, "Two-photon-counting interferometry," *Phys. Rev. A*, vol. 87, p. 013844, 2013.

[113] K. Mogi, K. Naganuma, and H. Yamada, "A novel real-time chirp measurement method for ultrashort optical pulses," *Jpn. J. Appl. Phys.*, vol. 27, no. 11R, p. 2078, 1988.

[114] L. Allen and G. I. Peters, "Amplified spontaneous emission I. The threshold condition," *Journal of Physics A: General Physics*, vol. 4, no. 2, p. 238, 1971.

[115] L. Allen and G. I. Peters, "Amplified spontaneous emission. II. The connection with laser theory," *J. Phys. A*, vol. 4, no. 3, p. 377, 1971.

[116] L. Allen and G. I. Peters, "Amplified spontaneous emission III. Intensity and saturation," *J. Phys. A*, vol. 4, no. 4, p. 564, 1971.

[117] L. Allen and G. I. Peters, "Amplified spontaneous emission. IV. Beam divergence and spatial coherence," *J. Phys. A*, vol. 5, no. 4, p. 546, 1972.

[118] A. Uskov, T. Berg, and J. Mørk, "Theory of pulse-train amplification without patterning effects in quantum-dot semiconductor optical amplifiers," *IEEE J. Quantum Electron.*, vol. 40, no. 3, pp. 306–320, 2004.

[119] M. Rossetti, P. Bardella, and I. Montrosset, "Time-domain travelling-wave model for quantum dot passively mode-locked lasers," *IEEE J. Quantum Electron.*, vol. 47, no. 2, pp. 139–150, 2011.

[120] M. Gioannini, P. Bardella, and I. Montrosset, "A fast time domain travelling wave method for simulation of quantum dot lasers and amplifiers," *23. CLEO Europe 2013, Munich, CB_3.2 Mon*, p. 1, 2013.

[121] S. Hartmann, A. Molitor, M. Blazek, and W. Elsäßer, "Tailored first- and second-order coherence properties of quantum dot superluminescent diodes via optical feedback," *Opt. Lett.*, vol. 38, no. 8, pp. 1334–1336, 2013.

[122] S. Hartmann, F. Friedrich, A. Molitor, M. Reichert, W. Elsäßer, and R. Walser, "Tailored quantum statistics from broadband states of light," *New Journal of Physics*, vol. 17, no. 4, p. 043039, 2015.

[123] Z. Y. Zhang, I. J. Luxmoore, C. Y. Jin, H. Y. Liu, Q. Jiang, K. M. Groom, D. T. Childs, M. Hopkinson, A. G. Cullis, and R. A. Hogg, "Effect of facet angle on effective facet reflectivity and operating characteristics of quantum dot edge emitting lasers and superluminescent light-emitting diodes," *Appl. Phys. Lett.*, vol. 91, no. 8, p. 081112, 2007.

[124] R. R. Puri, *Mathematical methods of quantum optics*. Springer, 2001.

[125] H. Gross, *Radiometry, handbook of optical systems, fundamentals of technical optics, vol. 1*. Wiley-VCH, Weinheim, 2005.

[126] T. Heil, I. Fischer, W. Elsäßer, B. Krauskopf, K. Green, and A. Gavrielides, "Delay dynamics of semiconductor lasers with short external cavities: Bifurcation scenarios and mechanisms," *Phys. Rev. E*, vol. 67, p. 066214, 2003.

[127] F. Albert, C. Hopfmann, S. Reitzenstein, C. Schneider, S. Höfling, L. Worschech, M. Kamp, W. Kinzel, A. Forchel, and I. Kanter, "Observing chaos for quantum-dot microlasers with external feedback," *Nature communications*, vol. 2, p. 366, 2011.

[128] J. A. Wheeler, "On the mathematical description of light nuclei by the method of resonating group structure," *Phys. Rev.*, vol. 52, pp. 1107–1122, 1937.

[129] P. Sudhakar, M. O. Scully, and W. Martienssen, "A quantum description of the beam splitter," *Opt. Commun.*, vol. 62, pp. 139–145, 1987.

[130] H. Fearn and R. Loudon, "Quantum theory of the lossless beam splitter," *Opt. Commun.*, vol. 64, pp. 485–490, 1987.

[131] R. A. Campos, B. E. A. Saleh, and M. C. Teich, "Quantum-mechanical lossless beam splitter: SU(2) symmetry and photon statistics," *Phys. Rev. A*, vol. 40, pp. 1371–1384, 1989.

[132] G. Lindblad, "On the generators of quantum dynamical semigroups," *Comm. Math. Phys.*, vol. 48, no. 2, pp. 119–130, 1976.

[133] L. Tian and H. J. Carmichael, "Incoherent excitation of the Jaynes-Cummings system," *Quantum Optics: Journal of the European Optical Society Part B*, vol. 4, no. 2, p. 131, 1992.

[134] T. Tawara, H. Kamada, T. Tanabe, T. Sogawa, H. Okamoto, P. Yao, P. K. Pathak, and S. Hughes, "Cavity-qed assisted attraction between a cavity mode and an exciton mode in a planar photonic-crystal cavity," *Opt. Express*, vol. 18, no. 3, pp. 2719–2728, 2010.

[135] M. R. Sturm, B. Rein, T. Walther, and R. Walser, "Feasibility of UV lasing without inversion in mercury vapor," *J. Opt. Soc. Am. B*, vol. 31, no. 8, pp. 1964–1974, 2014.

[136] N. B. Delone, *Basics of interaction of laser radiation with matter*. Editions Frontières, 1993.

[137] R. Kubo, "Statistical-mechanical theory of irreversible processes. I. general theory and simple applications to magnetic and conduction problems," *Journal of the Physical Society of Japan*, vol. 12, no. 6, pp. 570–586, 1957.

[138] P. Meystre and M. Sargent III, *Elements of quantum optics*. Berlin: Springer, 1990.

[139] C. Gardiner and P. Zoller, *The quantum world of ultra-cold atoms and light book II: The physics of quantum-optical devices*. World Scientific, 2015.

[140] C. W. Gardiner, "Driving a quantum system with the output field from another driven quantum system," *Phys. Rev. Lett.*, vol. 70, pp. 2269–2272, 1993.

[141] H. J. Carmichael, "Quantum trajectory theory for cascaded open systems," *Phys. Rev. Lett.*, vol. 70, pp. 2273–2276, 1993.

[142] M. I. Kolobov and I. V. Sokolov, "Quantum theory of light interaction with an optical amplifier," *Opt. Spektrosk.*, vol. 62, p. 112, 1987.

[143] G. S. Agarwal, *Quantum optics*. Cambridge University Press, 2013.

[144] C. W. Gardiner and M. J. Collett, "Input and output in damped quantum systems: Quantum stochastic differential equations and the master equation," *Phys. Rev. A*, vol. 31, pp. 3761–3774, 1985.

[145] B. Yurke and J. S. Denker, "Quantum network theory," *Phys. Rev. A*, vol. 29, pp. 1419–1437, 1984.

[146] M. Ley and R. Loudon, "Quantum theory of high-resolution length measurement with a Fabry-Perot interferometer," *Journal of Modern Optics*, vol. 34, no. 2, pp. 227–255, 1987.

[147] M. J. Collett and C. W. Gardiner, "Squeezing of intracavity and traveling-wave light fields produced in parametric amplification," *Phys. Rev. A*, vol. 30, pp. 1386–1391, 1984.

[148] P. Langevin, "Sur la theorie du mouvement brownien," *Comptes Rendus*, vol. 146, p. 530, 1906.

[149] M. Khanbekyan, L. Knöll, A. A. Semenov, W. Vogel, and D.-G. Welsch, "Quantum-state extraction from high-Q cavities," *Phys. Rev. A*, vol. 69, p. 043807, 2004.

[150] L. Knöll, W. Vogel, and D.-G. Welsch, "Resonators in quantum optics: A first-principles approach," *Phys. Rev. A*, vol. 43, pp. 543–553, 1991.

[151] J. Gough and M. R. James, "Quantum feedback networks: Hamiltonian formulation," *Communications in Mathematical Physics*, vol. 287, no. 3, pp. 1109–1132, 2009.

[152] J. Gough and M. R. James, "The series product and its application to quantum feedforward and feedback networks," *IEEE Transactions on Automatic Control*, vol. 54, no. 11, pp. 2530–2544, 2009.

[153] J. Combes, J. Kerckhoff, and M. Sarovar, "The SLH framework for modeling quantum input-output networks," *Advances in Physics: X*, vol. 2, no. 3, pp. 784–888, 2017.

[154] F. Constantinescu, J. E. G. Farina, and G. H. Fullerton, *Distributions and their applications in physics: International series in natural philosophy*. Elsevier Science, 2017.

[155] S. M. Barnett and P. M. Radmore, *Methods in theoretical quantum optics*. Oxford Series in Optical and Imaging Sciences, Clarendon Press, 2002.

[156] J. H. Eberly, "Atomic relaxation in the presence of intense partially coherent radiation fields," *Phys. Rev. Lett.*, vol. 37, pp. 1387–1390, 1976.

[157] H. Haken, *Synergetics: An introduction: Nonequilibrium phase transitions and self-organization in physics, chemistry and biology*. Springer series in synergetics, Springer, 1978.

[158] S. H. Strogatz, *Nonlinear dynamics and chaos: With applications to physics, biology, chemistry, and engineering*. Studies in Nonlinearity, Avalon Publishing, 2014.

[159] P. R. Berman, E. Arimondo, and C. C. Lin, *Advances in atomic, molecular, and optical physics*. No. Bd. 60 in Advances In Atomic, Molecular, and Optical Physics, Elsevier Science, 2011.

[160] I. Protsenko, P. Domokos, V. Lefèvre-Seguin, J. Hare, J. M. Raimond, and L. Davidovich, "Quantum theory of a thresholdless laser," *Phys. Rev. A*, vol. 59, pp. 1667–1682, 1999.

[161] S. Münch, S. Reitzenstein, P. Franeck, A. Löffler, T. Heindel, S. Höfling, L. Worschech, and A. Forchel, "The role of optical excitation power on the emission spectra of a strongly coupled quantum dot-micropillar system," *Opt. Express*, vol. 17, no. 15, pp. 12821–12828, 2009.

[162] A. Laucht, N. Hauke, J. M. Villas-Bôas, F. Hofbauer, G. Böhm, M. Kaniber, and J. J. Finley, "Dephasing of exciton polaritons in photoexcited InGaAs quantum dots in GaAs nanocavities," *Phys. Rev. Lett.*, vol. 103, p. 087405, 2009.

[163] P. Yao, P. K. Pathak, E. Illes, S. Hughes, S. Münch, S. Reitzenstein, P. Franeck, A. Löffler, T. Heindel, S. Höfling, L. Worschech, and A. Forchel, "Nonlinear photoluminescence spectra from a quantum-dot–cavity system: Interplay of pump-induced stimulated emission and anharmonic cavity QED," *Phys. Rev. B*, vol. 81, p. 033309, 2010.

[164] C. Z. Ning, "What is laser threshold," *IEEE J Sel Top Quantum Electron*, vol. 19, 2013.

[165] K. J. McNeil and D. F. Walls, "Quantum theory of multiphoton lasers. I. Systems in detailed balance," *Journal of Physics A: Mathematical and General*, vol. 8, no. 1, p. 104, 1975.

[166] F. C. Pampel, *Logistic regression: A primer*. SAGE Publications, 2000.

[167] A. Galántai, "The theory of Newton's method," *Journal of Computational and Applied Mathematics*, vol. 124, no. 1, pp. 25 – 44, 2000.

[168] E. Grilli, M. Guzzi, R. Zamboni, and L. Pavesi, "High-precision determination of the temperature dependence of the fundamental energy gap in gallium arsenide," *Phys. Rev. B*, vol. 45, pp. 1638–1644, 1992.

[169] K. H. Madsen, S. Ates, T. Lund-Hansen, A. Löffler, S. Reitzenstein, A. Forchel, and P. Lodahl, "Observation of non-Markovian dynamics of a single quantum dot in a micropillar cavity," *Phys. Rev. Lett.*, vol. 106, p. 233601, 2011.

[170] K. H. Madsen and P. Lodahl, "Quantitative analysis of quantum dot dynamics and emission spectra in cavity quantum electrodynamics," *New Journal of Physics*, vol. 15, no. 2, p. 025013, 2013.

[171] E. Gallardo, L. J. Martínez, A. K. Nowak, H. P. van der Meulen, J. M. Calleja, C. Tejedor, I. Prieto, D. Granados, A. G. Taboada, J. M. García, and P. A. Postigo, "Emission polarization control in semiconductor quantum dots coupled to a photonic crystal microcavity," *Opt. Express*, vol. 18, no. 12, pp. 13301–13308, 2010.

[172] A. Kiraz, P. Michler, C. Becher, B. Gayral, A. Imamoğlu, L. Zhang, E. Hu, W. V. Schoenfeld, and P. M. Petroff, "Cavity-quantum electrodynamics using a single InAs quantum dot in a microdisk structure," *Applied Physics Letters*, vol. 78, no. 25, pp. 3932–3934, 2001.

[173] J. W. Goodman, *Statistical optics*. Wiley, 2015.

[174] R. Boyd, *Contemporary nonlinear optics*. Quantum Electronics–Principles and Applications, Elsevier Science, 2012.

[175] M. Gaudin, "Une démonstration simplifiée du théorème de Wick en mécanique statistique," *Nuclear Physics*, vol. 15, pp. 89 – 91, 1960.

[176] W. H. Louisell, *Quantum statistical properties of radiation*. Wiley, 1990.

[177] E. T. Whittaker and G. N. Watson, *A course of modern analysis*. Cambridge university press, 1927.

[178] M. Abramowitz and I. A. Stegun, *Handbook of mathematical functions with formulas, graphs, and mathematical tables*. Dover, 1964.

[179] H. Carmichael, *Statistical methods in quantum optics 1: Master equations and Fokker-Planck equations*. Springer, 1999.

[180] A. Auffèves, D. Gerace, M. Richard, L. C. Kwek, S. Portolan, M. F. Santos, and C. Miniatura, *Strong light-matter coupling: From atoms to solid-state systems*. World Scientific, 2013.

[181] C. Gardiner, *Stochastic methods - A handbook for the natural and social sciences*. Springer Berlin Heidelberg, 2009.

LIST OF PUBLICATIONS

- S. Hartmann, F. Friedrich, A. Molitor, M. Reichert, W. Elsäßer and R. Walser,
  Tailored quantum statistics from broadband states of light,
  New J. Phys. **17**, 043039 (2015)

- F. Friedrich and R. Walser,
  Emission spectrum of broadband quantum dot superluminescent diodes,
  to be published

- F. Friedrich and R. Walser,
  Silent white light: Photon statistics of light emitting quantum dot superluminescent diodes,
  to be published

CONFERENCES, WORKSHOPS & SEMINARS

CONFERENCE CONTRIBUTIONS

- **Talk (Q 20.2)**,
  Emission properties and photon statistics of quantum-dot superluminescent diodes,
  DPG Frühjahrstagung 2018, Erlangen, Germany, 2018
- **Poster (EA-P.28)**,
  Hybrid coherent light: modeling quantum-dot superluminescent diodes,
  CLEO Europe 2017, München, Germany, 2017
- **Poster (Q 40.61)**,
  From incoherent to coherent: modeling quantum-dot superluminescent diodes,
  DPG Frühjahrstagung 2017, Mainz, Germany, 2017
- **Talk**,
  Emission spectrum of quantum-dot superluminescent diodes,
  Matariki Workshop on Quantum Science, Dunedin, New Zealand, 2016
- **Poster (Q 58.35)**,
  Photon statistics of QDSLDs,
  DPG Frühjahrstagung 2016, Hannover, Germany, 2016
- **Poster**,
  Photon statistics of QDSLDs,
  Frontiers of Quantum Optics: 600 Willhelm & Else Heraeus-Seminar, Bad Honnef, Germany, 2015
- **Poster (EA-P.16)**,
  Coherence of broadband light emitted by quantum-dot superluminescent diodes,
  CLEO Europe 2015, München, Germany, 2015
- **Talk (Q 8.4)**,
  Coherence studies of light emitting quantum-dot superluminescent diodes,
  DPG Frühjahrstagung 2015, Heidelberg, Germany, 2015
- **Poster (Q 30.70)**,
  Light characteristics of quantum dot SLEDs,
  DPG Frühjahrstagung 2014, Berlin, Germany, 2014
- **Poster (Q 35.98)**,
  Hybrid coherent light: modeling quantum dot superluminescent diodes,
  DPG Frühjahrstagung 2013, Hannover, Germany, 2013
- **Poster**,
  Amplified spontaneous emission in superluminescent diodes,
  Highlights of quantum optics: 500 Willhelm & Else Heraeus-Seminar, Bad Honnef, Germany, 2012

WORKSHOPS, SEMINARS & PROGRAMMING COURSES

- **Project Management basics**,
  Ingenium-Seminar, TU Darmstadt, Germany, 2016
- **Fortran for Scientific Computing**,
  Programming course, HLRS, University of Stuttgart, Germany, 2013
- **ZKI-Tagung Supercomputing**,
  TU Darmstadt, Germany, 2013

DANKSAGUNG

Die letzten Zeilen möchte ich nutzen, um mich bei einigen Menschen zu bedanken.

Insbesondere möchte ich mich bei meinem Doktorvater Herrn Prof. Dr. Reinhold Walser bedanken, der mir die Möglichkeit bot innerhalb seiner Arbeitsgruppe an dem Thema meiner Dissertation zu forschen. Ich habe seine Anmerkungen und die gemeinsamen Diskussionen immer sehr geschätzt. Auch seine Unterstützung bzgl. Workshops und Konferenzen haben mich nicht nur auf wissenschaftlicher Basis vorangebracht sondern auch in meiner Persönlichkeit positiv beeinflusst. Vielen Dank für die nette, hilfsbereite und kompetente Betreuung.

Ein großer Dank gilt auch Herrn Prof. Dr. Wolfgang Elsäßer, aus dessen Forschung sich die Fragestellung ergab, die letztlich zu dem Thema meiner Dissertation führte und mir somit eine direkte Zusammenarbeit zwischen Theorie und Experiment ermöglichte. Vielen Dank für die Diskussionen und der Gelegenheit, einen etwas tieferen Einblick in die experimentelle Forschung zu gewinnen.

Bei Herrn Prof. Dr. Gernot Alber und Herrn Prof. Dr. Robert Roth bedanke ich mich dafür, dass sie sich als Prüfer bei meiner Disputation zur Verfügung stellen.

Besonderer Dank geht an Sébastien Blumenstein für die gute Zusammenarbeit zwischen Theorie und Experiment. Auch für seine generelle Hilfsbereitschaft bei experimentellen Fragen möchte ich danke sagen.

Ein großer Dank geht an Antje Neumann, Polina Mironova, Jan Teske und Martin Sturm für das Korrekturlesen meiner Arbeit und die interessanten Gespräche. Vielen Dank für die aufmunternden Worte gegen Ende der Abgabefrist und für die Freundschaften, die entstanden sind.

Natürlich möchte ich mich noch beim gesamten Sekretariat, Christine Schütze und Dagmar Kutschera, sowie bei allen noch nicht genannten AG Walser Mitarbeitern Oliver Gabel, Kai Hansmann, Bastian Zapf und Florian Grewe für das sehr angenehme Arbeitsklima bedanken.

Abschließend bedanke ich mich noch bei meinen Eltern Rita und Helmut Friedrich, meiner Schwester Yvonne Partsch und meinem Schwager Florian Partsch sowie meinem Freund Marius Dommermuth für die jahrelange Unterstützung und ihren bedingungslosen Beistand, was ich ihnen über die gesamte Zeit sicherlich nicht immer leicht gemacht habe.

LEBENSLAUF

Franziska Friedrich
geboren am 17. Juni 1986 in Darmstadt
Email: FranziskaFriedrich1@gmx.de

Hochschullaufbahn

06.2013 bis heute	Doktorand/wissenschaftliche Mitarbeiterin AG theoretische Quantendynamik Prof. Dr. Reinhold Walser Institut für Angewandte Physik, TU Darmstadt
10.2010 bis 03.2013	Masterstudium Physik, TU Darmstadt
10.2005 bis 04.2010	Bachelorstudium Physik, TU Darmstadt

Schulbildung

08.2002 bis 06.2005	Gymnasiale Oberstufe Bertolt-Brecht-Schule, Darmstadt
09.1996 bis 06.2002	Gymnasialzweig Hessenwaldschule, Weiterstadt
08.1992 bis 07.1996	Grundschule Schloss-Schule, Gräfenhausen

DECLARATION

Hiermit versichere ich, dass ich die vorliegende Dissertation selbstständig angefertigt und keine anderen als die angegebenen Quellen und Hilfsmittel verwendet habe. Alle wörtlichen und paraphrasierten Zitate wurden angemessen kenntlich gemacht. Die Arbeit hat bisher noch nicht zu Prüfungszwecken gedient.

Darmstadt, 17. Dezember 2018

Franziska Friedrich